Author:
Jellett, Adam

Title:
Dissecting the molecular and functional interactions of retromer

Dissecting the molecular and functional interactions of retromer

Adam Patrick Jellett

A dissertation submitted to the University of Bristol in accordance with the requirements for award of degree of PhD in the Faculty of Life Sciences.

School of Biochemistry

University of Bristol

December 2018

Word count: 44,523

Table of contents

Table of contents ..... *i*

List of Figures ..... *vi*

List of Tables ..... *x*

Abstract ..... *xi*

Acknowledgments ..... *xii*

Authors declaration ..... *xiii*

Abbreviations ..... *xiv*

Publications ..... *xvii*

Chapter 1: Introduction *1*

1.1 Overview of membrane trafficking **2**

1.1.1 The principles of membrane trafficking 2

1.1.2 Membrane identity 2

1.1.2.1 Phosphoinositides 3

1.1.2.2 Rab GTPases 5

1.2 The endolysosomal pathway **6**

1.2.1 Endocytosis 7

1.2.2 The structure and organisation of the endosomal network 8

1.2.3 Endosomal maturation 11

1.2.3.1 Endosomal Rab conversion 11

1.2.3.2 Endosomal phosphoinositide conversion 12

1.2.3.3 The promotion of membrane fusions in the endolysosomal pathway 13

1.3 Endosomal cargo sorting **13**

1.3.1 ESCRT-mediated degradative cargo sorting 14

1.3.2 Endosomal retrieval and recycling 17

1.3.2.1 Sequence-dependent vs sequence-independent retrieval and recycling 17

1.3.2.2 Avoiding the degradative fate 18

1.4 Endosomal retrieval and recycling complexes **19**

1.4.1 The retromer complex 19

1.4.2 Cargo recycling by the SNX-BAR complex 22

1.4.3 Cargo recognition by retromer 23

1.4.3.1 SNX3-retromer 24

1.4.3.2 SNX27-retromer 25

1.4.4 Spatiotemporal control of retromer 26

1.4.5 The WASH complex 27

1.4.6 Retromer-independent endosomal retrieval 29

1.5 Endosomal cargo retrieval and recycling is neuroprotective **32**

1.5.1 Associations between endosomal retrieval complexes and neurological disorders .. 34

1.6 Aims 35

Chapter 2: Materials and Methods 37

2.1 Materials 38

2.1.1 List of suppliers 38

2.1.2 Sterilised water 38

2.1.3 Cell lines used in this study 38

2.1.4 Reagents for cell culture 39

2.1.5 Bacterial cell strains 40

2.1.6 Bacterial growth media and antibiotics 40

2.1.7 Buffers and solutions 41

2.1.8 Plasmid vectors 41

2.1.9 Oligonucleotides 44

2.1.10 Antibodies 48

2.2 Methods 51

2.2.1 Bacterial cell culture 51

2.2.1.1 Bacterial colony growth 51
2.2.1.2 Transformation of competent *E. coli* 51
2.2.1.3 Bacterial liquid cultures 51

2.2.2 Molecular biology methods 52

2.2.2.1 Small scale purification of plasmid DNA (Miniprep) 52
2.2.2.2 Large-scale purification of DNA (Maxiprep) 52
2.2.2.3 Nucleic acid quantification 53
2.2.2.4 DNA sequencing 53
2.2.2.5 Polymerase Chain Reaction (PCR) for gene amplification 53
2.2.2.6 Polymerase Chain Reaction (PCR) Site-Directed mutagenesis (SDM) 54
2.2.2.7 RNA extraction and quantitative-reverse transcriptase PCR 55
2.2.2.8 DNA analysis with agarose gel electrophoresis 56
2.2.2.9 Purification of PCR and restriction digest products 56
2.2.2.10 Restriction enzyme digestion 57
2.2.2.11 Ligations 57

2.2.3 Mammalian cell culture 58

2.2.3.1 Culturing mammalian cells 58
2.2.3.2 Passaging mammalian cells 58
2.2.3.3 HA antibody uptake (Wntless) assay 58
2.2.3.4 Transfection of DNA using PEI 59
2.2.3.5 Transfection of DNA using FuGENE 59
2.2.3.6 Transfection of siRNA using DharmaFECT 59
2.2.3.7 Lentiviral particle preparation 60
2.2.3.8 Transduction of cells using lentivirus 60

2.2.4 GFP- or RFP-nanotrap immunoprecipitations 60

2.2.5 Protein biochemistry 61

2.2.5.1 Cell lysis and sample preparation 61
2.2.5.2 Sodium dodecyl sulphate polyacrylamide gel electrophoresis (SDS PAGE) 61
2.2.5.3 Transfer of proteins onto a membrane 61
2.2.5.4 Immunoblotting 62

2.2.6 Proteomics 62

2.2.6.1 Stable isotope labelling of amino acids in culture (SILAC)-based proteomics ... 62
2.2.6.2 Tandem mass tagging (TMT) labelling and High pH reversed-phase chromatography ... 63
2.2.6.3 Nano-LC Mass Spectrometry ... 64
2.2.7 Microscopy ... 65
2.2.7.1 Fixing and permeabilising cells for immunofluorescence-based imaging ... 65
2.2.7.2 Staining fixed cells for immunofluorescence ... 65
2.2.7.3 Confocal microscopes ... 66
2.2.8 Software ... 66

Chapter 3: SNX3-retromer requires an evolutionary conserved MON2:DOPEY2:ATP9A complex to mediate Wntless sorting and Wnt secretion ... 67

3.1 Introduction ... 68
3.1.1 The intracellular trafficking of Wnt morphogens depend on their association with Wntless ... 68
3.1.2 Aims ... 69

3.2 Results ... 70
3.2.1 Identification of the SNX3:VPS35 binding surface ... 70
3.2.2 Heat repeat-domain containing SNX3-interactors associate independently of VPS35 ... 73
3.2.3 The association between VPS35 and SNX3 is required for the secretion of Wnt morphogens in *C. elegans* ... 75
3.2.4 SNX3, but not SNX1, associates with MON2 ... 77
3.2.5 MON2 and DOPEY2 share some features of their *S. cerevisiae* homologues ... 77
3.2.6 The MON2:DOPEY:ATP9A complex co-localise with SNX3-retromer and Wntless ... 79
3.2.7 Establishment of an *in vitro* cell culture-based system to study Wntless retrieval ... 80
3.2.8 The retrieval of HA-Wntless is dependent on MON2 and ATP9A ... 84
3.2.9 RNAi of *mon-2 and pad-1* cause a loss of *mig-14* levels and an EGL-20 secretion defect in *C. elegans* ... 87
3.2.10 Tat-5 flippase activity is necessary for the EGL-20-dependet posterior migration of the QL. neuroblast descendants in *C. elegans* ... 88

3.3 Discussion ... 91
3.3.1 The SNX3-retromer binding interface ... 91
3.3.2 The role of aminophospholipid translocases in membrane traffic ... 93
3.3.3 The role of MON2/DOPEY/ATP9A in Wntless recycling and Wnt secretion ... 96
3.3.4 Phopholipid flippase activity of ATP9A ... 98

Chapter 4: Analysis of rare Parkinsonism-associated retromer mutations ... 100

4.1 Introduction ... 101
4.1.1 Mutations in the retromer complex are associated with Parkinsonism disorders ... 101
4.1.2 Aims ... 104

4.2 Results.....105
4.2.1 Initial bioinformatic analysis of the VPS26A Parkinsonism-linked mutations..... 105
4.2.2 Creation of stably expressing GFP-VPS26A RPE-1 cell lines..... 108
4.2.3 The VPS26A variants retain the ability to form the retromer complex..... 108
4.2.4 The Parkinsonism-linked mutations do not perturb GFP-VPS26A localisation with the WASH complex, EEA1 or LAMP1..... 113
4.2.5 SILAC-based proteomics reveal changes in the interactome of VPS26A(p.K297X)113
4.2.6 VPS26A(p.K297X) fails to retrieve the SNX27-depedent cargo, GLUT1, away from lysosomal degradation..... 118
4.2.7 Initial bioinformatic analysis of the VPS35 N-terminal Parkinsonism-linked mutations..... 120
4.2.8 Generation of C-terminal VPS35-GFP construct..... 121
4.2.9 The Parkinsonism-linked VPS35 mutations do not perturb retromer complex association..... 127
4.2.10 The Parkinsonism-linked VPS35 mutations do not perturb VPS35 localisation.... 128
4.2.11 The Parkinsonism-linked VPS35 mutations do not perturb the ability of VPS35 to bind to candidate proteins..... 132
4.2.12 Tandem-mass tagging (TMT)-based proteomic analysis reveals no significant differences between the interactomes of VPS35-GFP compared to VPS35(p.R32S)-GFP or VPS35(p.G51S)-GFP..... 134
4.2.13 VPS35-GFP, VPS35(p.R32S)-GFP and VPS35(p.G51S)-GFP transduction rescues lysosomal GLUT1 degradation..... 137

4.3 Discussion 141
4.3.1 The VPS26A(p.K297X) truncation mutation uncouples SNX27 from the retromer complex..... 141
4.3.2 Investigations of the other Parkinsonism-linked retromer mutations..... 142

Chapter 5: FAM21 binds to areas of basic charge on the carboxyl-terminus of VPS35 145

5.1 Introduction.....146
5.1.1 The WASH complex binds to retromer through a series of acidic motifs in FAM21 146
5.1.2 Aims..... 147

5.2 Results.....148
5.2.1 Bioinformatic search to identify candidate residues in VPS35 that may mediate its interaction with FAM21..... 148
5.2.2 Immunoprecipitation screen to identify VPS35 mutations which perturb FAM21 binding..... 151
5.2.3 Introduction of VPS35(p.K555E, K556E, K559E)-GFP causes a loss in endosomal WASH complex association..... 157
5.2.4 Investigating the functional significance of the VPS35:FAM21 interaction..... 160

5.2.5 The retromer-WASH complex interaction contributes to the maintenance of endosomal subdomains 169
5.2.6 TMT-based proteomics do not reveal novel changes in the VPS35(p.K555E, K556E, K559E)-GFP interactome 171
5.2.7 The mechanism of VPS35-independent endosomal association of FAM21 is not dependent on VPS34 173

5.3 Discussion 177
5.3.1 Mechanism of endosomal WASH complex recruitment 177
5.3.2 Mechanism of the VPS35:FAM21 association 177
5.3.3 Functional significance of the WASH-retromer complexes interaction 181

Chapter 6: General discussion 184

6.1 Cargo recognition by retromer 185
6.1.1 Retromer cargo adaptors 185
6.1.2 Retromer dimerization and the formation of retromer coats 186

6.2 Endosomal subdomains 187
6.2.1 The mechanism of cargo leakage into the degradative pathway following retrieval complex perturbation 187
6.2.2 Coordination of the endosomal retrieval complexes 188

6.3 Neuroprotection by retromer 189
6.3.1 Retromer promotes microglial health 189
6.3.2 Neurodegeneration and aberrant Wnt signalling 190

Chapter 7: References 191

List of Figures

Figure 1.1 The principles of membrane trafficking 3
Figure 1.2 Phosphoinositides and Rab GTPases impart membrane identity..... 4
Figure 1.3 The endolysosomal pathway 9
Figure 1.4 Endosomal retrieval and degradative subdomains are segregated.....14
Figure 1.5 ESCRT-mediated inclusion of degradative cargo into intralumenal vesicles. 15
Figure 1.6 The structure of the retromer complex.....21
Figure 1.7 Retromer associated with various accessory proteins 24
Figure 1.8 Retromer-independent endosomal cargo retrieval. 31
Figure 1.9 Neuronal distribution of the endolysosomal pathway 33
Figure 3.1 Bioinformatic analysis to identify residues in SNX3 important for VPS35 binding. 70
Figure 3.2 Immunoprecipitation screen identify GFP-SNX3 constructs with perturbed VPS35 binding. 71
Figure 3.3 GFP-SNX3 constructs retain their endosomal association.....72
Figure 3.4 Model showing the identified residues in SNX3 important for the binding of VPS35.....73
Figure 3.5 SNX3 can bind to various HEAT-repeat domain-containing proteins independently of its ability to bind to the retromer complex.....74
Figure 3.6 The SNX3:VPS35 interaction is necessary for Wnt secretion and morphogenic gradient formation. 75
Figure 3.7 MON2, DOPEY1, DOPEY2 and ATP9A associate biochemically. 76
Figure 3.8 ATP9A localises to the TGN and SNX3-retromer positive endosomes. 78
Figure 3.9 ATP9A colocalises with MON2, DOPEY2 and Wntless. 80
Figure 3.10 Validation of the HA-WLS construct.....81
Figure 3.11 HA-WLS whole-cell levels are dependent on SNX3-retromer-mediated retrieval away from lysosomal degradation.....84
Figure 3.12 Inhibition of MON2 or ATP9A, but not DOPEY1/DOPEY2, cause the whole-cell level decrease of HA-WLS due to lysosomal degradation. 85
Figure 3.13 Inhibition of vps-35, mon-2 or pad-1 (DOPEY orthologue) causes a whole-cell level decrease of MIG-14 (Wntless) and its colocalisation with late endosomes/lysosomes in *C. elegans* L1 larvae.....86

Figure 3.14 Inhibition of vps-35, mon-2 or pad-1 (DOPEY orthologue) causes a loss of the EGL-20 (Wnt) gradient and a perturbation of the posterior migration of QL neuroblast decedents. 87
Figure 3.15 Suppressing tat-5 (ATP9A homologue), or inhibiting the ATPase activity of tat-5, perturbs the posterior migration of the QL neuroblast descendants in L1 larvae. 90
Figure 3.16 Modelling of the residues identified in SNX3 which causes a perturbation in VPS35 binding onto the SNX3:VPS35:VPS26A crystal structure 92
Figure 3.17 Flippases, floppases and scramblases mediate phospholipid transfers across the lipid bilayer. 94
Figure 3.18 Working model of the coordination of SNX3-retromer with the MON2:DOPEY1/2:ATP9A complex. 98
Figure 4.1 Bioinformatic alignment of VPS26 homologues and human paralogues. ..107
Figure 4.2 Model showing the location of the Parkinsonism-associated VPS26A mutations. 107
Figure 4.3 Lentivirally transduced GFP-VPS26A constructs are expressed at near endogenous levels. 107
Figure 4.4 The Parkinsonism-associated VPS26A mutations do not affect colocalisation with VPS35....110
Figure 4.5 The VPS26A Parkinsonism-associated mutations do not perturb assembly of the retromer complex. 110
Figure 4.6 The VPS26A Parkinsonism-associated mutations do not change the localisation of the GFP-VPS26A constructs in relation to early or late endosomes. ...113
Figure 4.7 The VPS26A Parkinsonism-associated mutations do not change the localisation of the GFP-VPS26A constructs in relation to the retromer-interacting FAM21. 114
Figure 4.8 SILAC-based proteomics reveals the interactome of the Parkinsonism-linked GFP-VPS26A constructs....115
Figure 4.9 The VPS26A(p.K297X) mutation abrogates binding to SNX27 and enhances binding to DENND4C and PKD2. 116
Figure 4.10 The binding of VPS26A(p.K297X) is severely perturbed SNX27.....118
Figure 4.11 VPS26A(p.K297X) missorts the SNX27-dependent cargo GLUT1.....119
Figure 4.12 Bioinformatic alignment of VPS35 homologues, highlighting the N-terminal Parkinson's disease associated mutations. 120
Figure 4.13 The VPS35-GFP construct is more endosomal compared to the GFP-VPS35 construct. 121
Figure 4.14 The C-terminal GFP tag enhances binding to the WASH complex and does not perturb retromer complex assembly. 122

Figure 4.15 SILAC-based proteomics reveal the VPS35-GFP interactome.....126
Figure 4.16 The Parkinsonism-linked VPS35(p.R32S) and VPS35(p.G51S) do not perturb retromer complex assembly. 127
Figure 4.17 Creation of stably transduced VPS35-GFP lines in VPS35 knockout HeLa cells.....128
Figure 4.18 N-terminal VPS35 Parkinsonism-associated mutations do not perturb endosomal association.....129
Figure 4.19 N-terminal VPS35 Parkinsonism-associated mutant constructs do not have altered early or late endosome localisation.....130
Figure 4.20 Parkinsonism-linked VPS35(p.R32S) and VPS35(p.G51S) rescue the localisation of FAM21 in VPS35 knockout HeLa cells.....132
Figure 4.21 The Parkinsonism-linked VPS35(p.R32S) and VPS35(p.G51S) do not impair association with the WASH complex or SNX27. 132
Figure 4.22 The Parkinsonism-linked VPS35(p.R32S) has a mild impairment in its ability to associate with SNX3. 133
Figure 4.23 Proteomic analysis using tandem mass tag spectrometry reveals slight changes in the interactome of the Parkinsonism-linked VPS35(p.R32S) and VPS35(p.G51S) mutations. 135
Figure 4.24 Parkinsonism-linked VPS35(p.R32S) and VPS35(p.G51S) rescue the localisation of GLUT1 in VPS35 knockout HeLa cells.....140
Figure 5.25 The VPS35 ARG32 and GLY51 residues are not in close proximity to the SNX3-retromer binding site 143
Figure 5.1 FAM21 binds to VPS35 through its extended carboxyl-terminus. 148
Figure 5.2 Bioinformatic analysis to identify candidate residues in VPS35 which may be important for FAM21 association.....149
Figure 5.3 The C-terminal half of VPS35 contain two patches enriched in basic residues. 150
Figure 5.4 Screen of VPS35-GFP variants reveal residues important for FAM21 binding (area 1). 152
Figure 5.5 Screen of VPS35-GFP variants reveal residues important for FAM21 binding (area 2). 153
Figure 5.6 Model of residues in VPS35 that are implicated in FAM21 association. 154
Figure 5.7 Lentiviral transduction of VPS35-GFP constructs into VPS35 knockout HeLa cells.....154
Figure 5.8 VPS35-GFP constructs with severely perturbed FAM21 association rescue the endosomal localisation of FAM21.....155

Figure 5.9 The VPS35(p.K555E, K556E, K559E)-GFP variant loses affinity for the WASH complex but retains the ability to assemble into the retromer complex. 156
Figure 5.10 Lentiviral transduction of VPS35(p.K555E, K556E, K559E)-GFP into VPS35 knockout HeLa cells. 157
Figure 5.11 Introduction of VPS35(p.K555E, K556E, K559E)-GFP does not rescue the endosomal localisation of FAM21. 158
Figure 5.12 Introduction of VPS35(p.K555E, K556E, K559E)-GFP does not rescue the endosomal localisation of WASH1. 159
Figure 5.13 Introduction of VPS35(p.K555E, K556E, K559E)-GFP does rescue the GLUT1 trafficking defect. 161
Figure 5.14 Knock-down of FAM21 in HeLa cells do not cause a significant increase in GLUT1 colocalisation with LAMP1 or TGN46. 162
Figure 5.15 Knock-down of FAM21 in RPE-1 cells causes a significant increase in GLUT1 colocalisation with LAMP1 and TGN46. 164
Figure 5.16 Overexpression of VPS35-GFP variants in RPE-1 cells outcompetes endogenous VPS35 for assembly into the retromer complex. 165
Figure 5.17 Overexpressing VPS35(p.K555E,K556E,K559E)-GFP in RPE-1 cells causes a decrease in endosomal association of FAM21. 166
Figure 5.18 Overexpressing VPS35(p.K555E,K556E,K559E)-GFP in RPE-1 cells does not increase the TGN localisation of GLUT1 167
Figure 5.19 Reintroducing VPS35(p.K555E,K556E,K559E)-GFP into VPS35 knockout HeLa cells causes a mild enlargement of the overlap between retrieval and degradative subdomains on enlarged endosomes. 168
Figure 5.20 FAM21 suppression causes a mild enlargement of the overlap between retrieval and degradative subdomains on enlarged endosomes. 171
Figure 5.21 VPS34 inhibition causes swelling of the early endosomal compartment. 174
Figure 5.22 VPS34 inhibition causes the dissociation of SNX1 from endosomes but not FAM21. 176
Figure 5.23 Modelling of the hydrophobicity surface of VPS35 178
Figure 5.24 Modelling of the identified residues which affect FAM21 binding onto the retromer dimer interface 180

List of Tables

Table 1.1 The subunits of the metazoan endosomal sorting complex required for transport (ESCRT) complexes....17
Table 1.2 Sorting motifs in endosomal cargo adapters....19
Table 1.3 Summary of the main endosomal retrieval complexes and how they associate with the endosomal membrane....32
Table 2.1 SILAC amino acids....40
Table 2.2 List of plasmids used in this study....41
Table 2.3 List of DNA oligonucleotides used for cloning....44
Table 2.4 List of primers for RT-qPCR....47
Table 2.5 siRNA duplexes used for knockdowns....47
Table 2.6 Primary antibodies....48
Table 2.7 Secondary antibodies....49
Table 3.1 P4-ATPases in *S. cerevisiae*, *C. elegans* and *H. sapiens*....95
Table 4.1 Mutations in the retromer complex linked to Parkinsonism disorders....103
Table 4.2 VPS35-GFP interactome....125
Table 4.3 GFP-VPS35 interactome members not present in VPS35-GFP interactome....126
Table 4.4 Comparison of VPS35-GFP interactors identified through SILAC-based proteomics compared to two runs of TMT-based proteomics....137
Table 4.5 Changes in the VPS35(p.R32S)-GFP interactome compared to VPS35-GFP interactome....139
Table 4.6 Changes in the VPS35(p.G51S)-GFP interactome compared to VPS35-GFP interactome....139
Table 5.1 VPS35-GFP variants created through site-directed mutagenesis....151
Table 5.2 Average change in the VPS35(p.K555E, K556E, K559E)-GFP interactome (TRIP) compared to the VPS35-GFP interactome (WT)....172

Abstract

The endosomal network is a central sorting station for transmembrane proteins (cargoes) which enter from the cell surface or the biosynthetic pathway. Here, cargoes are subject to a major fate decision: degradation versus retrieval and recycling. For cargoes fated to be degraded, they are retained within the endosomal limiting membrane and sorted into intraluminal vesicles, where they will eventually be degraded once late endosomes fuse with the lysosomes. To be reused, cargoes are retrieved from this degradative fate and recycled to other cellular compartments, such as the plasma membrane or the trans-Golgi network.

Retromer, a heterotrimeric complex of VPS35:VPS29:VPS26 (VPS26A and VPS26B are expressed in mammals), is the best-characterised endosome-localised cargo retrieval complex and is responsible for the retrieval of hundreds of different cargoes away from the degradative fate. The dysfunction of retromer has been implicated in diseases such as Alzheimer's disease and Parkinson's disease. To function correctly, retromer relies on its association with various proteins and multiprotein complexes. It is therefore not surprising that the most common Parkinson's disease-causing variant of retromer, VPS35(p.D620N), exhibits a reduced association with one of its most significant interactors: the WASH complex.

In this thesis I investigated some of retromer's interactions to gain insight into their functional significance. I firstly showed that retromer's interaction with SNX3, a major retromer cargo adaptor, is vital for the establishment of Wnt morphogenic gradients. I also identified that SNX3-retromer couples to an evolutionary-conserved flippase complex to link cargo recognition with membrane deformation. Secondly, by investigating whether other Parkinsonism-associated retromer variants also exhibit reduced interactor associations, I showed that the VPS26A(p.K297X) variant causes a severe perturbation in retromer's assembly with another cargo adaptor: SNX27. Finally, I identified that retromer couples to the WASH complex through a series of basic amino acids located on the carboxyl-terminus of VPS35 in proximity to the ASP620 residue. By creating retromer variants which have largely lost the ability to associate with the WASH complex, I showed that this interaction appears to be important for the segregation of the endosomal retrieval and degradative subdomains.

Acknowledgments

After getting lost in the building on my first day, I eventually found the lab and Pete's office. The first thing Pete said to me was: welcome home. Indeed, for the remaining years of my PhD the lab has felt like a home and a family. I'd love to firstly thank Pete for all your encouragement, support and good humour. In so doing, you have been a brilliant supervisor.

A massive thank you must also go to members, past and present, of the Cullen and Tavare labs: Boris, Kerrie, Kirsty, Rachel, Frances, Neil, Matt, Chris, Paul, James, Molly, Ash, Sharon, Elaine, Linda, Ian, Lesley and OJ. My time in this lab has been memorable in numerous ways: from great scientific discussions to entertaining political chats, from a 12 o'clock lunch regime to coma-inducing chilli nachos, from 'amazing' conference hostels to lab camping, from lively lab meetings to animated pub sessions, from Spiegeltent to the escape rooms. The list could go on for a long time. You have all made the last few years unforgettable and I feel very lucky to have worked with you.

I especially want to thank Kirsty for looking after me at the beginning of my PhD and for all your work and help in the K297X project. I also need to thank the Collins lab for their work on that project. I'd like to thank Ian and also the Korswagen lab for their roles in the Wntless project. Thanks also to Kate Heesom for all of her proteomics work.

There are many people that I'd like to thank for their friendship since coming to Bristol. In particular, I'd like to thank my gin and beer drinking, boardgame-playing, politics-discussing, all-round general friendship group: Dylan, Neil, Silvia, Scott, Elena and Boris. My bromance with Boris is no secret – he even asked me to marry him when Brexit begun to loom (even if he subsequently broke his plastic ring). Although not quite the "merry-go-round of my life", I am particularly grateful to have you as a friend.

I would not have gotten anywhere in life without the love, backing and belief of my family, especially my mum. I'd like to dedicate this thesis to my grandad who saw the start of my PhD but could not be here to see the end.

Authors declaration

I declare that the work in this dissertation was carried out in accordance with the requirements of the University's *Regulations and Code of Practice for Research Degree Programmes* and that it has not been submitted for any other academic award. Except where indicated by specific reference in the text, the work is the candidate's own work. Work done in collaboration with, or with the assistance of, others, is indicated as such. Any views expressed in the dissertation are those of the author.

SIGNED: ..... DATE: .....

Abbreviations

ALP	Alkaline phosphatase
AMSH	STAM-binding protein
AP	AP Adaptor protein
APP	Amyloid precursor protein
aq	In aqeous solution
Arp2/3	Actin-related protein 2/3
Aß	Amyloid β
ATP7A	ATPase, Cu2+ transporting, alpha polypeptide
BAR	Bin/Amphiphysin/Rvs
C16orf62	Open reading frame 62 on chromosome16
CCDC	Coiled-coil domain containing
CIMPR	Cation-independent mannose 6-phosphate receptor
CLASPS	Clathrin associated sorting proteins
CME	Clathrin-mediated endocytosis
COMMD	Copper metabolism and MUR domain containing protein
CRISPR	Clustered regularly interspersed short palindromic repeats
DAG	1 stearoyl 2-arachidonoyl diacylglycerol
DAPI	4’,6-diamidino-2-phenylindole
DENN	Differentially expressed in neoplastic versus normal cells
DMEM	Dulbecco’s Modified Eagle’s Medium
DNAJC	DnaJ homologue sub-family C member
DUBs	Deubiquitylating enzymes
DUIM	Double-sided ubiquitin-interaction motif
EDTA	Ethylenediaminetetraacetic acid
EEA1	Early endosomal antigen 1
EGFP	Enhanced green fluorescent protein
ER	Endoplasmic reticulum
ESCRT	Endosomal sorting complex required for transport
FAM	Family with sequence similarity
FBS	Foetal bovine serum
FERM	Protein 4.1/Ezrin/Radixin/Moesin
FYVE	Fab1-YOTB-Vac(vacuolated appearance)1-EEA1
g	Grams
x g	G-force
GAP	GTPase activating protein
GARP	Golgi associated retrograde transport
GDP	Guanosine diphosphate
GEF	Guanine nucleotide exchange factor
GGA	Golgi-localized γ-ear-containing ARF-binding protein
GLUE	GRAM-like ubiquitin binding in EAP45
GLUT	Glucose transporter
GPCR	G-protein coupled receptor
GTP	Guanosine triphosphate

HEAT	Huntingtin/EF3/PP2A/TOR1
HEK293T	Human embryonic kidney 293 large T antigen
HeLa	Henrietta Lacks
HPLC	High performance liquid chromatography
HRS	Hepatocyte growth factor-regulated tyrosine kinase substrate
hTERT	Human telomerase reverse transcriptase
ILV	Intra-lumenal vesicle
Kd	Dissociation constant
kDa	Kilodaltons
LAMP1	Lysosomal-associated membrane protein 1
LB	Luria-Bertani
LC-MS/MS	Liquid chromatography – tandem mass spectrometry
LDL(R)	Low density lipoprotein (receptor)
LFa	Leucine phenylalanine acidic
LRP	LDLR related protein
mCherry	Monomeric cherry protein
MEFs	Mouse embryonic fibroblasts
ml	Millilitres
MPR	Mannose 6-phosphate receptor
MVB	Multivesicular body
NMDA	N-methyl-D-aspartate
NPF	Nucleation promoting factor
PBS	Phosphate buffered saline
PCP	Planar cell polarity
PCR	Polymerase chain reaction
PDZ	Postsynaptic density 95 – Disc large – ZO1
PEI	Polyethylenimine
PFA	Paraformaldehyde
PH	Pleckstrin homology
PI	Phosphatidylinositol
PI(3,4)P2	Phosphatidylinositol 3,4-bisphosphate
PI(3,4,5)P3	Phosphatidylinositol 3,4,5-triphosphate
PI(3,5)P2	Phosphatidylinositol 3,5-bisphosphate
PI(4,5)P2	Phosphatidylinositol 4,5-bisphosphate
PI3K	Phosphatidylinositol 3-phosphate kinase
PI3P	Phosphatidylinositol 3-phosphate
PI4P	Phosphatidylinositol 4-phosphate
PI5P	Phosphatidylinositol 5-phosphate
PKD	Polycystic kidney disease
PTB	Phospho-tyrosine binding
PtdIns	Phosphatidylinositol
PTHR	Parathyroid hormone receptor
PX	Phox homology
Rab	Ras associated binding
RE	Recycling endosome
RME8	Receptor-mediated endocytosis

RPE	Retinal pigment epithelial
SDM	Site-directed mutagenesis
SDS	Sodium dodecyl sulphate
SILAC	Stable isotope labeling of amino acids in culture
siRNA	Short interfering ribose nucleic acid
SLC	Solute carrier family member
SNARE	Soluble NSF attachment receptor
SNpc	Substantia nigra pars compacta
SNX	Sorting nexin
SOC	Super-optimal broth with catabolite repression
SorCS	Sortilin-related VPS10 domain-containing receptor
SorLa	Sortilin related receptor with A-type repeats
SOUBA	Solenoid of overlapping ubiquitin-associated
STAM	Signal transducing adaptor molecule
STxB	Shiga toxin sub-unit B
SWIP	Strumpellin and WASH interacting protein
TAE	Tris/Acetic acid/EDTA
TBC1D	Tre2-BUB2p-Cdc16p1 domain family member
TBS	Tris-buffered saline
Tf(R)	Transferrin (receptor)
TGN	trans-Golgi network
Trem2	Triggering receptor expressed on myeloid cells 2
TSG101	tumour susceptibility gene 101 protein
UBAP1	ubiquitin-associated protein 1
UBM	ubiquitin binding domain
UEV	ubiquitin-conjugating enzyme E2 variant
UIM	ubiquitin-interaction motif
UV	Ultraviolet
VAMP	Vesicle associated membrane protein
VARP	Vps9 domain ankyrin repeat protein
VCA	Verprolin homology connector acidic domain
VPS	Vacuole protein sorting
WASH	Wiskott-Aldirch syndrome protein and SCAR homologue
WASP	Wiskott-Aldrich syndrome protein
WAVE	WASP family verprolin homologue
WHAMM	WASP homologue associated with actin, membranes and microtubules
WLS	Wntless
Wnt	Wingless and int-1

Publications

McGough IJ*, de Groot REA*, **Jellett AP***, Betist MC, Varandas KC, Danson CM, Heesom KJ, Korswagen HC and Cullen PJ. SNX3-retromer requires an evolutionary conserved MON2:DOPEY2:ATP9A complex to mediate Wntless sorting and Wnt secretion. Nat Communications. 2018;9(1):3737.

McMillan KJ, Gallon M*, **Jellett AP***, Clairfeuille T, Tilley FC, McGough IJ, Danson CM, Heesom KJ, Wilkinson KA, Collins BM and Cullen PJ. Atypical parkinsonism-associated retromer mutant alters endosomal sorting of specific cargo proteins. Journal of Cell Biology. 2016;214(4):389-99.

* These authors contributed equally

Chapter 1

Introduction

1.1 Overview of membrane trafficking

1.1.1 The principles of membrane trafficking

Eukaryotic cells are organised into a series of phospholipid bilayer-bound organelles. These organelles dynamically communicate, maintain and regulate each other through the process of membrane trafficking. Membrane trafficking allows the exchange of lipid and protein cargoes from a 'donor' compartment to an 'acceptor' compartment **(Figure 1.1)**. This process is spatiotemporally regulated by various multiprotein complexes and in principle relies on six steps **(Figure 1.1)**. The cargoes to be transferred are captured on the donor compartment by a coat complex, which forms on the cytosolic side of the donor membrane. The capture of these cargoes often relies on their sequence-dependent binding by the coat complexes and their accessory proteins. A budding process then takes place through the deformation of the membrane, allowing the creation of a cargo-enriched carrier (Hurley et al., 2010). These carriers can be vesicular or tubular in nature. Fission of tubulovesicular carriers must then occur for their separation from the donor membrane (Campelo and Malhotra, 2012). Motor proteins then transport the carriers along cytoskeletal fibres to the acceptor membrane (Ross et al., 2008). The carriers are uncoated and are recognised by tethers located on the acceptor membrane (Kummel and Ungermann, 2014). Lastly, the membrane carrier must fuse with the acceptor membrane in a process which is facilitated by the soluble NSF attachment protein receptor (SNARE) family of proteins (Han et al., 2017).

1.1.2 Membrane identity

Membrane trafficking events **(Section 1.1.1)** rely on the distinction and recognition of different cellular compartments for targeted membrane transfer. Following membrane acceptance at the acceptor compartment, the 'donor membrane' identity must dynamically reorientate into the acceptor membrane's identity. This process ensures the maintenance of organelle identity despite constant membrane flux. Key elements in defining organelle identity are phosphoinositides **(Section 1.1.2.1)** and Rab GTPases **(Section 1.1.2.2)**.

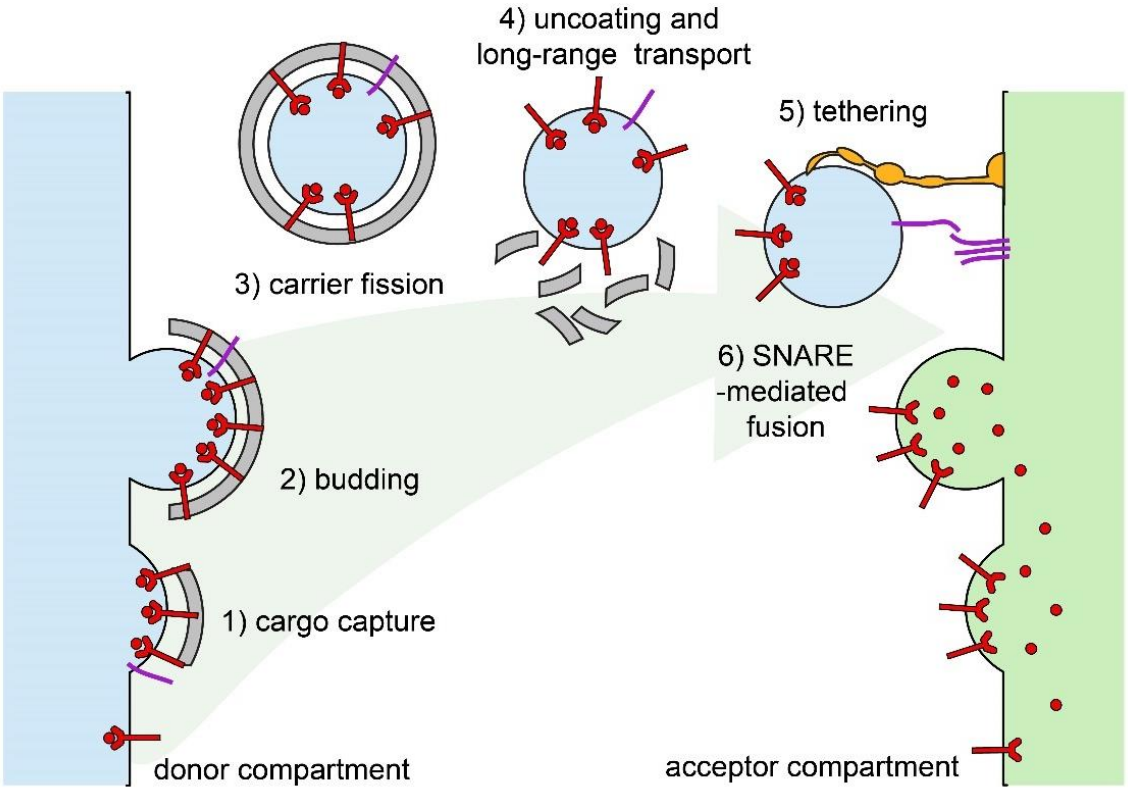

Figure 1.1 The principles of membrane trafficking

In general, membrane trafficking falls into 6 steps. 1) A membrane coat and its accessory proteins are recruited onto a donor compartment and captures luminal and transmembrane cargoes. 2) Through membrane deformation, a budding process occurs around the coat complex which forms a nascent vesicle. 3) The nascent vesicle is pinched off from the donor compartment in a fission process. 4) The coat complex disassociates from the vesicle while it is transported to an acceptor compartment. 5) Membrane tethers on the acceptor compartment recognise and capture the membrane vesicle. 6) The vesicle fuses with the acceptor compartment through SNARE-mediated fusion. Image from the thesis of Boris Simonetti; adapted from (Behnia and Munro, 2005).

1.1.2.1 Phosphoinositides

Phosphoinositides, although a relatively minor component of lipid bilayers, play a disproportionately important role in cell signalling, membrane identity and the regulation of membrane trafficking (Schink et al., 2016). Phosphoinositides are phosphorylated forms of phosphoinositol, which consists of a membrane-embedded diacylglycerol group linked to a cytosolic-facing inositol head at the D1 hydroxy group (Cullen, 2011) **(Figure 1.2A)**. Only the D3, D4 and D5 hydroxy groups are phosphorylated and form mono- bis- or tris-phosphorylated phosphoinositides **(Figure 1.2A)** (Cullen, 2011).

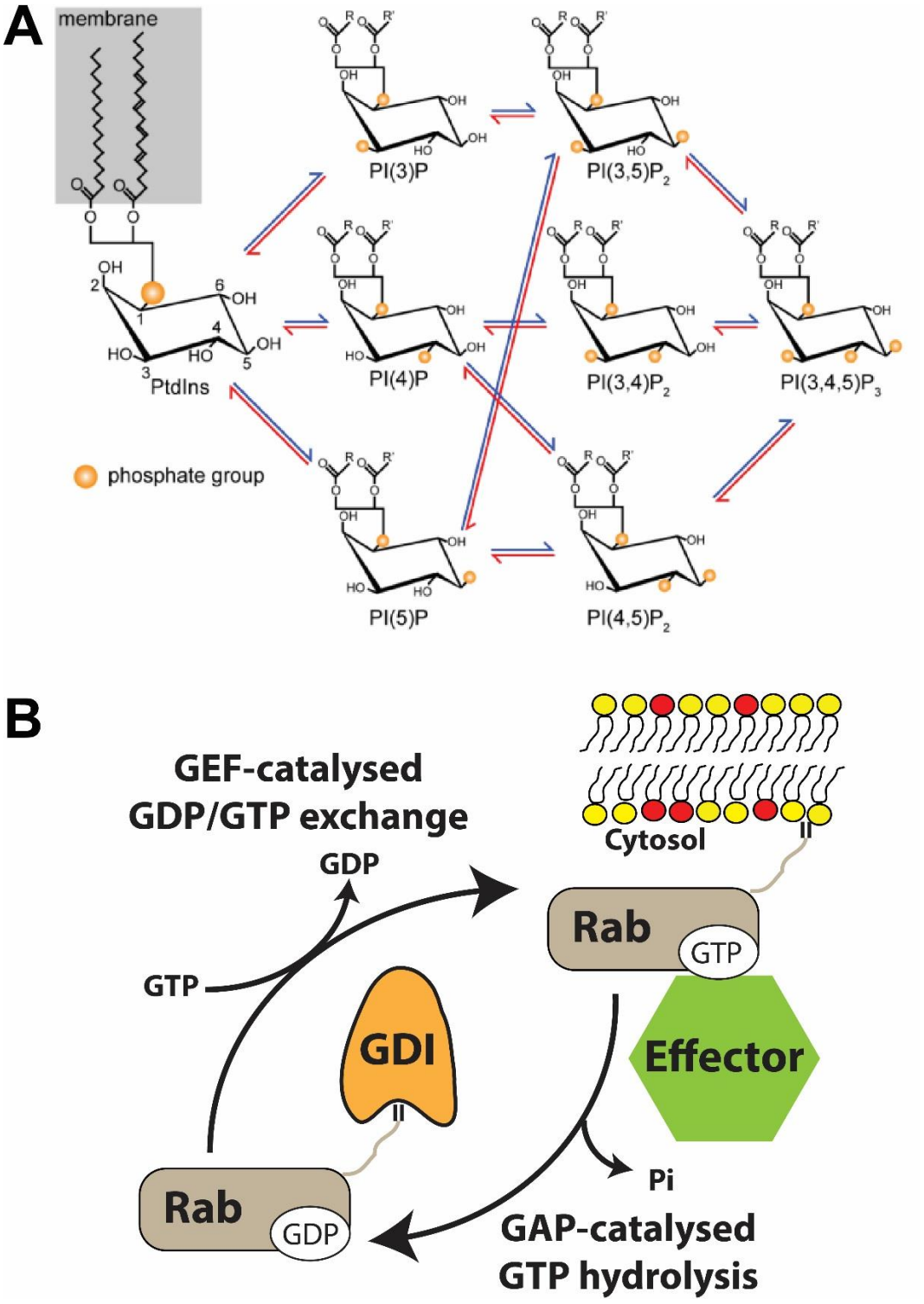

Figure 1.2 Phosphoinositides and Rab GTPases impart membrane identity.

(A) D-myo-inositol has a six-carbon ring with hydroxy groups on each carbon atom. Diacylglycerol is attached to the D1 carbon to enable membrane association. Phosphate groups can be added to or taken away from the other hydroxy groups on the six-carbon ring, by kinases (blue arrow) or phosphatases (red) arrow respectively, to form phosphoinositides. Image from the thesis of Matt Gallon; adapted from (Cullen, 2011). **(B)** The Rab-GTPase cycle. Rab-GTP, attached to a lipid bilayer by its two geranylgeranyl groups on its carboxyl-terminus, binds to effector proteins. GTPase activating proteins (GAPs) hydrolase GTP into GDP. Guanine nucleotide displacement inhibitors (GDIs) extract Rab-GDP from the membrane until guanine nucleotide exchange factors (GEFs) induce GDP/GTP exchange.

The functions of phosphoinositides depend on their nonuniform distribution throughout cellular compartments. Generally speaking, the Golgi apparatus is enriched in PI4P; early endosomes in PI3P; late endosomes and lysosomes in $PI(3,5)P_2$; and the plasma membrane in $PI(4,5)P_2$ and $PI(3,4,5)P_3$ (Schink et al., 2016). Although these are the major phosphoinositides on these membranes, the picture of minority proportions is more complex, with PI4P having been reported on endosomes and the plasma membrane, $PI(4,5)P_2$ reported on endosomes and lysosomes, and PI3P having been found also on the plasma membrane (Schink et al., 2016).

The phosphoinositide-mediated recruitment of effector proteins is critical in many cellular processes. The role of $PI(4,5)P_2$ in the process of endocytosis is discussed in **Section 1.2.1**. Effectors of endosomal PI3P are also discussed in relation to endosomal maturation **(Section 1.2.3)**, ESCRT-mediated cargo degradation **(Section 1.3.1)**, and endosomal cargo retrieval and recycling **(Section 1.4)**.

The interconversion of different phosphoinositide species, through the action of kinases and phosphatases, is a dynamic process and highly regulated. For example, although the endoplasmic reticulum is not particularly enriched in any one phosphoinositide species, PI4P is generated at endoplasmic reticulum exit sites during the formation of COP-II vesicles and is required for the fusion of these vesicles with the Golgi membrane (Blumental-Perry et al., 2006; Lorente-Rodriguez and Barlowe, 2011; Schink et al., 2016). The switch from PI3P to $PI(3,5)P_2$ as early endosomes mature into late endosomes, as well as the interconversion between plasma membrane and endosomal phosphoinositide identity, is discussed in **Section 1.2.3.2**.

1.1.2.2 Rab GTPases

The Rab family of small GTPases are instrumental regulators of vesicular trafficking and impart membrane identity. They and their effectors are involved in cargo sorting, the formation and transport of transport vesicles and membrane tethering and fusion. Rabs undergo reversible cycles of GTP loading and GTP hydrolysis into GDP **(Figure 1.2B)**. This switch in nucleotide binding induces a conformational change which has been described as a ‘loaded spring’, where the GTP-bound form causes the stabilisation of two ‘switch’ loops in the GTPase domain which can be recognised by Rab effectors (Vetter and Wittinghofer, 2001). Following GTP hydrolysis, the loops spring back into the GDP-loaded conformation (Vetter and Wittinghofer, 2001). It is therefore the ‘activated’ Rab-GTP which recruits effectors to impart and regulate

membrane identity. The roles of Rab5 and Rab7 (and their effectors) in early and late (respectively) endosome identity will be discussed in **Section 1.2.3.3**. The role of Rab7 in the endosomal recruitment of the retromer complex will also be discussed in **Section 1.4.1**.

Guanine nucleotide exchange factors (GEFs) 'activate' Rabs by promoting GDP dissociation which induces nucleotide exchange **(Figure 1.2B)** (Muller and Goody, 2018). Concentration of cytosolic GTP is approximately 10-fold higher than GDP and consequently, nucleotide exchange promotes GTP loading of the Rab (Traut, 1994; Muller and Goody, 2018). Conversely, Rab GTPase activating proteins (GAPs) promote an inactive GDP-bound Rab by the hydrolysis of GTP into GDP **(Figure 1.2B)**. Rab proteins intrinsically have GTPase activity, but it is very low (Muller and Goody, 2018). The role of GAPs is to catalyse this reaction spatiotemporally. The activation and inactivation of Rab5 and Rab7 will be discussed in **Section 1.2.3.1**.

The addition of two geranylgeranyl lipid groups is required for the reversible membrane association of Rab proteins (Muller and Goody, 2018). An inactive Rab is extracted from a membrane by guanine nucleotide displacement inhibitors (GDI), which bind to one of the 'switch' loops in the GDP-bound Rab conformation, stabilising the lipidated carboxyl-terminus of Rabs in a hydrophobic cavity (Sasaki et al., 1990; Pylypenko et al., 2006). GDI dissociation factors may displace the GDI from the Rab allowing membrane reinsertion (Dirac-Svejstrup et al., 1997), although more evidence is required to substantiate this model. The GTP-loading of Rabs and effector binding are also thought to induce a Rab conformation which is resistant to GDI, therefore stabilising it on a target membrane (Barr, 2013).

1.2 The endolysosomal pathway

The endosomal network is a series of interconnected membranous compartments and the sorting hub of numerous endocytic and biosynthetic cargoes (transmembrane proteins). Following endocytosis **(Section 1.2.1)** cargoes are delivered to the early endosomes **(Section 1.2.2)**, where they will subsequently be sorted for either degradation **(Section 1.3.1)** or retrieval and recycling **(Section 1.3.2)**. The endosomes undergo a maturation process characterised by changes in the enrichment of Rab-GTPases **(Section 1.2.3.1)** and phosphoinositide species **(Section 1.2.3.2)**, which ultimately leaves them competent to fuse with lysosomes **(Section 1.2.3.3)**.

1.2.1 Endocytosis

At the plasma membrane, to internalise cargo (transmembrane proteins) and their ligands, a process termed endocytosis occurs. There are various mechanisms of endocytosis including: clathrin-mediated endocytosis, caveolin-dependent endocytosis, the RhoA-dependent pathway, flotillin-dependent endocytosis, Cdc42-dependent endocytosis, the Arf6-associated pathway, fast endophilin A2-dependent endocytosis, macropinocytosis and phagocytosis (Mayor et al., 2014; Boucrot et al., 2015). Although results vary between studies depending on cell-types and experimental conditions (Ferreira and Boucrot, 2018), reports have suggested that in general clathrin-independent mechanisms have a much lower contribution to cargo internalisation compared to clathrin-mediated endocytosis (Bitsikas et al., 2014). Here, I will limit my description of endocytosis to clathrin-mediated endocytosis.

Clathrin-mediated endocytosis is thought to be initiated on the plasma membrane at both random (Ehrlich et al., 2004) and non-random sites (such as being concentrated at synapses or repeatably being initiated in a specific site) (Nunez et al., 2011; Kaksonen and Roux, 2018). Local enrichment in $PI(4,5)P_2$ or cargo (including cargo ubiquitination status) may also contribute to the probability of the formation of a clathrin-coated pit (Liu et al., 2010; Henry et al., 2012; Kaksonen and Roux, 2018). Although clathrin is the defining protein involved in clathrin-mediated endocytosis, over 50 cytosolic proteins act cooperatively in its orchestration (Kaksonen and Roux, 2018). An initial 'pioneer module', composed of the adaptor proteins (FCHO1/2, AP2), which are partly targeted to the plasma membrane through $PI(4,5)P_2$ binding, and scaffold proteins (EPS15, EPS15R and intersectins 1 and 2) which cluster the adaptor proteins, is thought to initiate clathrin-mediated endocytosis (Kaksonen and Roux, 2018).

Specific cargoes are recruited to the endocytic site through direct interactions with members of the clathrin coat complex. These direct interactions require specific sorting motifs in the cytosolic domains of cargo (the concept of sorting motifs will reappear in **Section 1.4**). For the AP-2 complex (a heterotetramer of α-adaptin, β2-adaptin, μ2-adaptin and a σ2-chain) sorting motifs include: YxxØ (Ø indicates amino acids with bulky hydrophobic side chains and 'x' indicates any amino acid) via its μ2-adaptin subunit (Collawn et al., 1990; Owen and Evans, 1998) and (D/E)xxx(L/I) via its β2-adaptin subunit (Letourneur and Klausner, 1992; Kelly et al., 2008). Additional cargo selective elements include clathrin associated sorting proteins (CLASPS), which can bind to clathrin as well as AP-2 (Traub, 2009). Sorting signals include: [FY]xNPx[YF] (recognised by phosphotyrosine-binding domain-containing CLASPS), ubiquitin

moieties (recognised by ubiquitin binding domain-containing CLASPS) and phosphorylated G protein-coupled receptors (recognised by β-arrestins) (Traub, 2009).

The clathrin triskelia is recruited by AP-2 and other adaptor proteins (Kirchhausen et al., 2014). The simultaneous binding of AP-2 to $PI(4,5)P_2$ and cargo (with tyrosine-based sorting motifs) has been shown to cause a conformational change in AP-2 which reveals a binding site for clathrin (Kelly et al., 2014; Kadlecova et al., 2017). Clathrin triskelia polymerise into a cage-like lattice structure which coats the membrane and leads to membrane remodelling. It has been proposed that clathrin polymerises onto an existing membrane bud, increasingly forming a spherical shape which forms the nascent clathrin-coated vesicle (Kaksonen and Roux, 2018).

The scission of the nascent vesicle is promoted by the large GTPase dynamin (Hinshaw and Schmid, 1995; Antonny et al., 2016). Dynamin is recruited by the SH3 domain of sorting nexin-9 (amongst others such as amphiphysin) (Lundmark and Carlsson, 2004), which also contains a BAR domain able to sense membrane curvature **(see Section 1.4.2)** (Kaksonen and Roux, 2018). Dynamin oligomerises around the neck of the nascent clathrin-coated vesicles and its GTPase activity induces scission (Antonny et al., 2016). Following this scission from the plasma membrane, the clathrin coat is disassembled, partly through the dephosphorylation of $PI(4,5)P_2$ (see **Section 1.2.3.2**).The endocytic carriers will subsequently fuse with the early endosomes (see **Section 1.2.2** and **Section 1.2.3.3)**.

1.2.2 The structure and organisation of the endosomal network

The endosomal network is a series of interconnected membranous compartments which continuously fuse with each other **(Figure 1.3)** (it should be noted that the endosomal network is more complex than **Figure 1.3** suggests and contains: APPL1, early, late and recycling compartments). Cargo-enriched endocytic carriers fuse (see **Section 1.2.3.3**) with the early endosomes within 1-5 minutes of internalisation (Klumperman and Raposo, 2014). Early endosomes are pleiomorphic in structure, being composed of a vacuolar section with 2-7 tubules emanating from it **(Figure 1.3)** (Geuze et al., 1983; Klumperman and Raposo, 2014). Cargoes, having entered the endosomal network, are either enriched into tubulovesicular carriers for their recycling, or within the limiting endosomal membrane for their eventual degradation (Geuze et al., 1983). A simplified model of endosomes, proposed by (Klumperman and Raposo, 2014), is their division into two domains: a sorting domain and a recycling domain **(Figure 1.3)**.

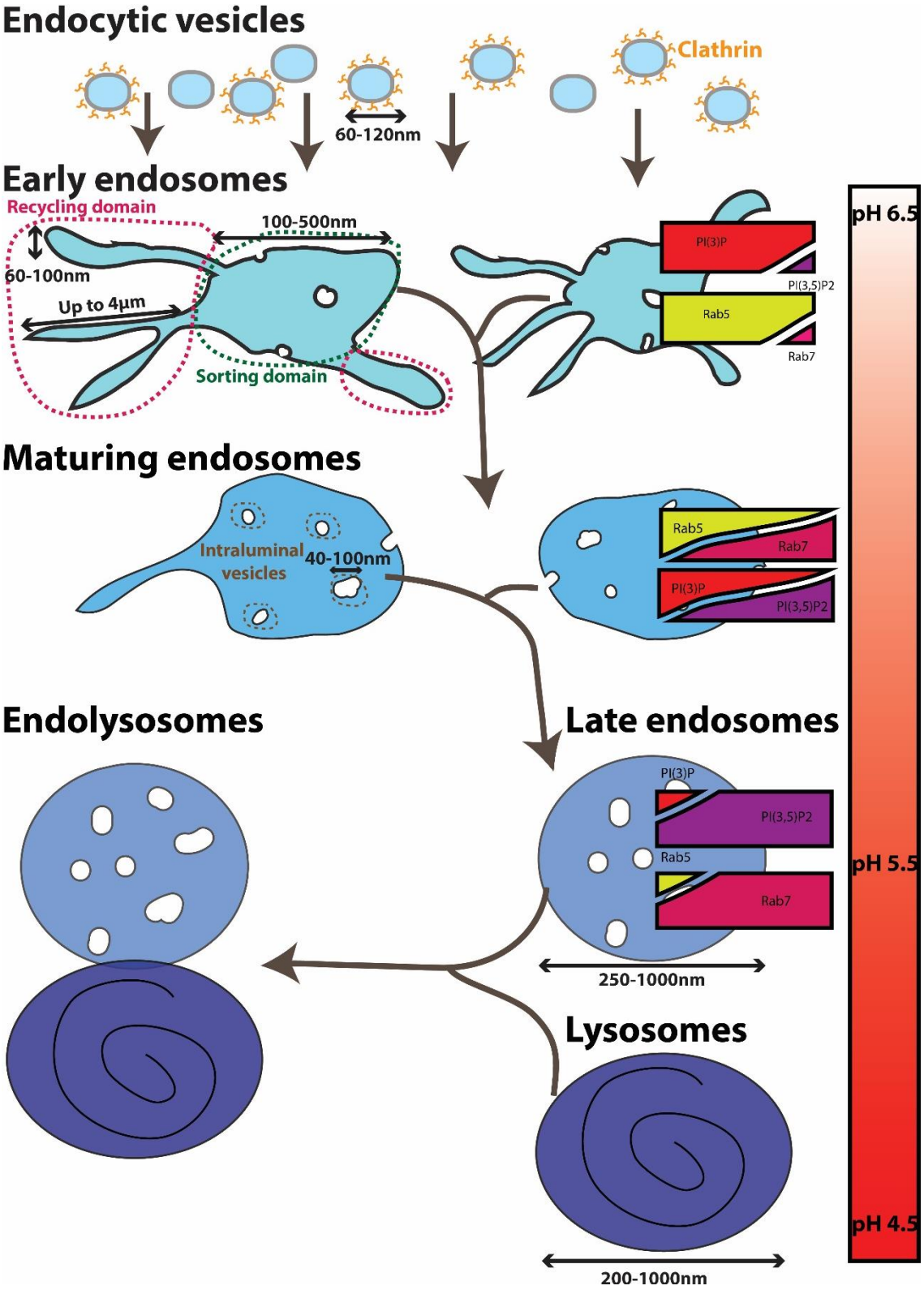

Figure 1.3 The endolysosomal pathway

A schematic which represents the endolysosomal pathway. Endocytic vesicles fuse onto the early endosomal compartment, which eventually matures into late endosomes. Late endosomes fuse with lysosomes to form endolysosomes. The maturation of the endolysosomal pathway is associated with a change in phosphoinositides, Rab GTPases and pH. The molecular dimensions were informed through (Klumperman and Raposo, 2014).

The sorting domain consists of the vacuolar portion of the early endosome. This is also the portion of the early endosomes which will mature down the endolysosomal pathway, becoming late endosomes which will eventually fuse with lysosomes. In the sorting domain, a major fate decision occurs: cargoes are sorted for either degradation **(Section 1.3.1)** or recycling **(Section 1.3.2)**. Briefly, for cargo recycling, the cargoes must be retrieved away from the vacuolar portion of sorting endosomes, into nascent tubulovesicular carriers, which detach and are recycled to an acceptor membrane (at the cell surface, the TGN or other specialised compartments). To ensure a cargo's degradation, it is actively sequestered into intralumenal vesicles (ILVs) within and unconnected to the endosomal limiting membrane (Murk et al., 2003) **(Section 1.3.1)**.

The loss and replenishment of endosomal membrane is key to understanding the morphological changes from early to late endosomes. Endosomal membrane is continuously lost as cargo-enriched recycling tubules and transport carriers detach, destined for various acceptor membranes. The formation of ILVs is another process by which the endosomal limiting membrane surface is lost. Alongside this process, membrane and cargo are continuously added to endosomes through the fusion of incoming endocytic and biosynthetic vesicles. The continuous fusion events of the endosomes **(Section 1.2.3.3)** is a major process by which sufficient membrane is made available for the generation of tubulovesicular carriers for cargo recycling.

As endosomes mature, the vacuolar portion of the limiting membrane enlarges and ILVs accumulate **(Figure 1.3)**. Typically, once the endosome accumulates 5 or more ILVs, they are morphologically considered late endosomes or multivesicular bodies; they can contain up to 30 ILVs (Huotari and Helenius, 2011; Klumperman and Raposo, 2014). They are also no longer 'competent' to fuse with the early endosomes (Klumperman and Raposo, 2014). Instead, they become able to fuse to lysosomes to form endolysosomes **(Section 1.2.3.3) (Figure 1.3)** (Klumperman and Raposo, 2014). The contents within the limiting membrane will be degraded by acid hydrolase activity, promoted by the pH change imparted by vacuolar ATPases which pump protons into the endosomal lumen (Maxfield and Yamashiro, 1987; Huotari and Helenius, 2011). Glycoproteins, such as LAMP1 and LAMP2, that line the limiting membrane of the late endosomes and lysosomes, are resistant to the degradative capacity of acid hydrolases (Huotari and Helenius, 2011). Most degradation is thought to occur in endolysosomes (Bright et al., 2016).

1.2.3 Endosomal maturation

As discussed in **Section 1.1.2**, the main imparters and regulators of membrane identity are Rab-GTPases and phosphoinositides. Early endosomes are identified by the presence of Rab5 and PI3P whereas late endosomes are identified by Rab7 and $PI(3,5)P_2$. The processes of endosomal Rab and phosphoinositide conversion are respectively discussed in **Section 1.2.3.1** and **Section 1.2.3.2**. How the interplay between Rabs and phosphoinositides promote endosomal maturation through endosomal and lysosomal membrane fusions is discussed in **Section 1.2.3.3**.

1.2.3.1 Endosomal Rab conversion

The major Rab proteins imparting membrane identity in the endosomal system include Rab5, which marks early endosomes, and Rab7, which marks late endosomes and lysosomes (Langemeyer et al., 2018). In recycling pathways, Rab4, Rab11 and Rab14 are required at early endosomes and Rab9 is required between lysosomes and the Golgi (Langemeyer et al., 2018). Here, I will focus on the central endosomal Rabs: Rab5 and Rab7.

On endocytic vesicles, ubiquitinylated cargoes recruit the Rab5 GEF Rabex5, which promotes the GTP-loading of Rab5 **(Section 1.1.2.2)** (Mattera and Bonifacino, 2008). The Vps9 domain of Rabex-5 has only a basal nucleotide exchange activity towards Rab5 and is only strongly activated upon formation of a complex with the Rab5 effector Rabaptin5 (Lippe et al., 2001). The formation of this complex is necessary for the Rab5-dependent fusion of early endosomes (Lippe et al., 2001). One recent study has suggested that Rabaptin5 is instead a Rab4-GTP effector which acts in a feed-forward mechanism to promote Rab5 activation. The inclusion of ubiquitinated cargo into intralumenal vesicles may promote Rabex5 membrane dissociation, therefore negatively regulating Rab5 activation (Kalin et al., 2016). PI3P synthesis, Rab5 and Rabex-5 are thought to recruit the Mon1-Ccz-1 complex, which is also thought to promote displacement of Rabex-5 (Poteryaev et al., 2010). Concurrently, the Rab5 GAP, RabGAP5, induces hydrolysis of Rab5-GTP to Rab5-GDP and therefore its membrane extraction by GDI (Haas et al., 2005) **(Section 1.1.2.2)**. The Mon1-Ccz1 complex also a Rab7 GEF and promotes its activation (Poteryaev et al., 2010). It is thought to activate late endosomal Rab7; the mechanism of Rab7 activation on lysosomes is unclear (Yasuda et al., 2016). The VPS34/p150 complex (see **Section 1.2.3.2**), which is a Rab5 and Rab7 effector, has been reported to recruit the GAP

TBC-2, acting as a negative feedback mechanism for both Rab5 and Rab7 (Law and Rocheleau, 2017).

1.2.3.2 Endosomal phosphoinositide conversion

Both Rab5-GTP and Rab7-GTP have been reported to recruit the VPS34/p150 class III PI3-kinase complex (Murray et al., 2002; Law and Rocheleau, 2017). VPS34/p150 recruitment promotes the synthesis of PI3P, the characteristic early endosomal phosphoinositide (Schu et al., 1993). In turn, the accumulation of PI3P onto early endosomes promotes the recruitment of a cohort of FYVE domain and PX domain containing endosomal effectors which play a variety of roles on the endosomal membrane, including in promoting a degradative **(Section 1.3.1)** or recycling **(Section 1.3.2)** fate for cargoes.

The Rab5 to Rab7 switch **(Section 1.2.3.1)** promotes a phosphoinositide conversion from PI3P to $PI3,5P_2$. Firstly, the Rab7-GTP interaction with WDR91 downregulates the activity of the PI3K complex, negatively regulating the generation of PI3P (Liu et al., 2017). The FYVE domain-containing phosphatidylinositol 3-phosphate 5-kinase, PIKfyve (Kim et al., 2014), is recruited to its substrate, PI3P, via its FYVE domain (Sbrissa et al., 2002). The generation of $PI3,5P_2$ has been reported to be essential for sorting cargo into the degradative fate (Odorizzi et al., 1998; Kim et al., 2014), modulating Ca^{2+} release (Dong et al., 2010) and v-ATPase activation (Li et al., 2014).

Constant membrane flux between the plasma membrane and the endosomal network requires continuous interconversion of phosphoinositide identity. Following endocytosis **(Section 1.2.1)**, phosphoinositides must be converted from a plasma membrane identity into an endosomal identity, through the dephosphorylation of the D4- and D5-positions on the inositol head group. Synaptojanin, INPP4A/B and OCRL are the phosphatases reported to promote this (Schink et al., 2016). Conversely, in endosome-to-plasma membrane trafficking, PI3P is converted into PI4P. This is accomplished though hydrolysis of the 3-position phosphate by the phosphatase MTM1 and subsequently, the phosphorylation of the D4 hydroxy group on the inositol ring by the PI4-kinase PI4Kα (Ketel et al., 2016). This process exemplifies the interconnectivity between PIs and Rabs: initial PI3P generation activates Rab11, which then recruits MTM1 to promote PI conversion (Campa et al., 2018).

1.2.3.3 The promotion of membrane fusions in the endolysosomal pathway

EEA1 contains a Rab5 binding site on one end and a PI3P-binding FYVE domain at the other. These two domains at either end of the 200nm coiled coil allows EEA1 to function as a tether to bring incoming endocytic vesicles into close proximity to early endosomes in a process known as 'entropic collapse' (Murray et al., 2016). The dimeric coiled-coil is stiff until it is bound to Rab5-GTP. Once flexibility is induced, EEA1 is thought to collapse, bringing a tethered vesicle close to an endosome. This process is coordinated with another Rab5-effector and coiled-coil tether rabenosyn-5, SNAREs and Vps45 (a member of the Sec1p/Munc-18 family) to couple membrane tethering to membrane fusion (Nielsen et al., 2000).

As well as promoting the endosomal fusion with incoming endocytic vesicles, Rab5-GTP promotes fusion of Rab5-GTP decorated endosomes. The Rab5-effector and multiprotein complex tether, the CORVET (Class C core vacuole/ endosome tethering) complex is thought to mediate this fusion (Balderhaar et al., 2013). It contains 6 subunits, including at either end Vps3 and Vps8, which can bind to Rab5, which is thought to enable multiple Rab5-containing endosomes to be connected for fusion (Balderhaar et al., 2013). In yeast, the CORVET subunit, Vps33, has been shown to bind to the syntaxin-like Pep12 protein, which suggests a mechanism for the coupling of membrane tethering with fusion (Subramanian et al., 2004).

Like Rab5, Rab7 promotes membrane tethering by associating with a multiprotein tethering complex: the HOPS complex. Rab7-GTP also promotes UVRAG to activate the HOPS complex (Sun et al., 2010). The HOPS complex shares four of six subunits of the CORVET complex: Vps33, Vps16, Vps18 and Vps11 (Langemeyer et al., 2018). The two unique subunits, Vps41 and Vps39, are Rab7-GTP binding which is thought to promote the fusion of Rab7-GTP decorated organelles (Langemeyer et al., 2018). This includes the fusion of Rab7-decorated endosomes and the heterotypic fusion of organelles such as late endosomes and lysosomes.

1.3 Endosomal cargo sorting

At sorting endosomes, a major fate decision occurs. Cargoes destined for degradation are sequestered within the endosomal limiting membrane into intralumenal vesicles, where they will eventually be degraded by acid hydrolases once late endosomes have fused with lysosomes **(Section 1.2.3.3)**. This process is largely mediated by the 'endosomal sorting complex required for transport' complexes **(Section 1.3.1)**. Cargoes which are to be recycled avoid this degradative fate either through sequence-

independent or sequence-dependent mechanisms **(Section 1.3.2)**. This thesis is largely concerned with the sequence-dependent retrieval of cargo by multiprotein retrieval complexes **(Section 1.4)**. Interestingly these fate decisions occur on the sorting endosomes in segregated retrieval and degradative subdomains **(Figure 1.4)** (McNally et al., 2017; Norris et al., 2017; Cullen and Steinberg, 2018).

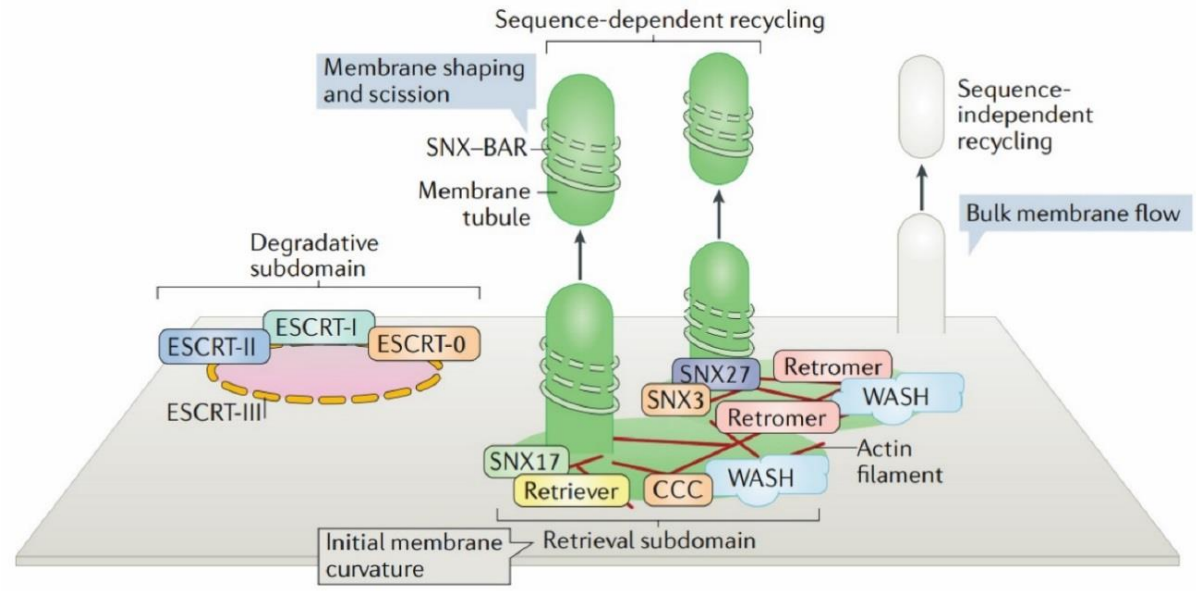

Figure 1.4 Endosomal retrieval and degradative subdomains are segregated

On the sorting endosomes, recycling and degradative subdomains are thought to be segregated. The degradative subdomain is thought to be marked by the endosomal sorting complex required for transport (ESCRT) complexes, which mediates degradative cargo recognition and inclusion into intralumenal vesicles. The recycling endosome is marked by retrieval and recycling complexes such as retromer, retriever and the WASH complex. The WASH complex is thought to polymerise branched actin filaments onto the retrieval subdomain. Sequence independent recycling also occurs. Figure adapted from (Cullen and Steinberg, 2018).

1.3.1 ESCRT-mediated degradative cargo sorting

To be degraded, transmembrane cargoes are actively sequestered into intralumenal vesicles (ILVs) within the endosomal limiting membrane. This process requires cargo to have an identifier to mark it for the degradative pathway. The best characterised mechanism for this is the monoubiquitination or polyubiquitination of the cytosolic-facing domains of the cargo (Katzmann et al., 2001; Bishop et al., 2002). This process is dependent on a series of four complexes **(Table 1.1)** known as the endosomal

sorting complex required for transport (ESCRT), (ESCRT-0, ESCRT-1, ESCRT-II and ESCRT-III).

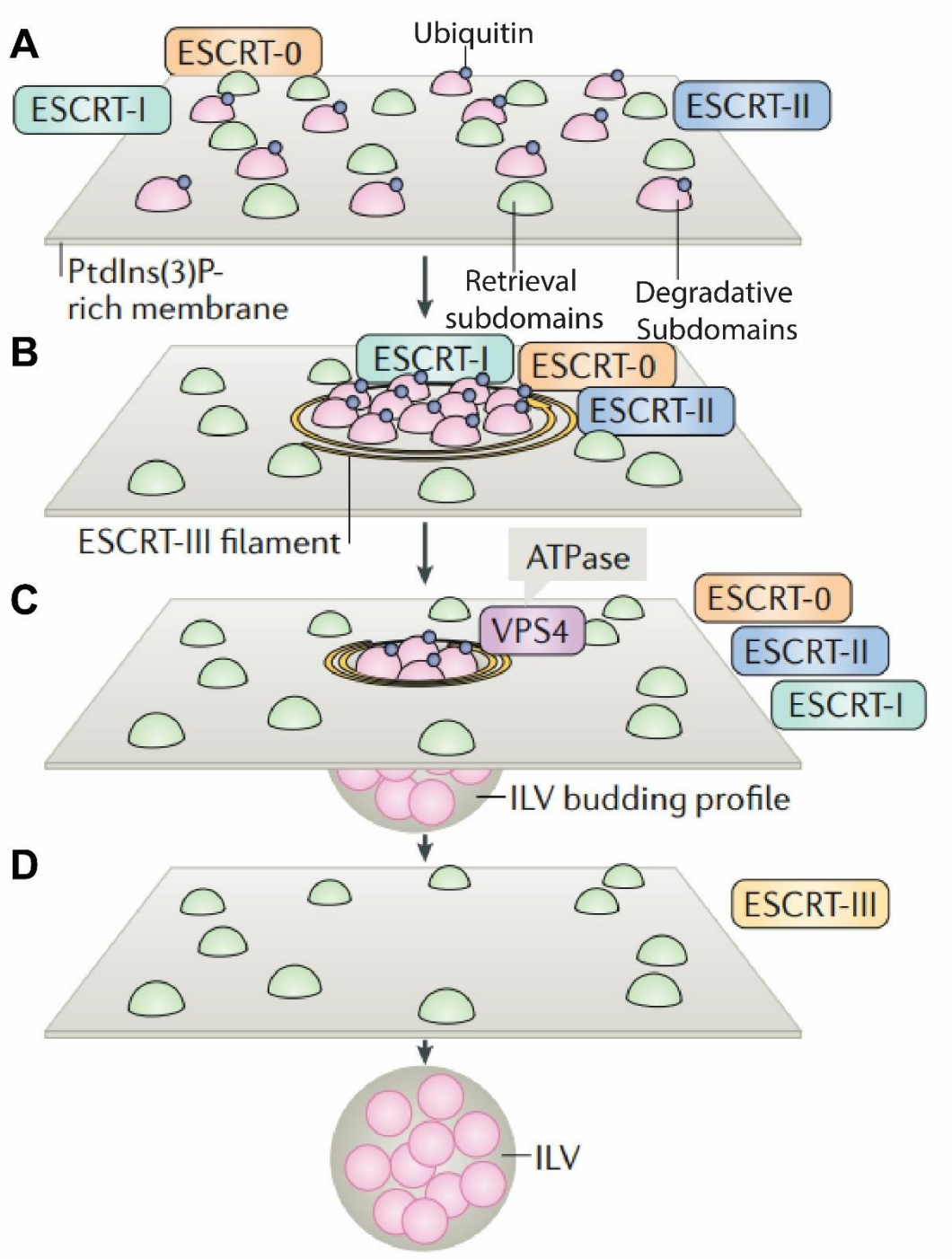

Figure 1.5 ESCRT-mediated inclusion of degradative cargo into intralumenal vesicles.

(A) The endosomal sorting complex required for transport (ESCRT) complexes ESCRT-0, ESCRT-I and ESCRT-II bind to ubiquitinated cargoes and segregate them in endosomal degradative subdomains. **(B)** ESCRT-III is recruited to the degradative subdomains and induces membrane deformation towards the endosomal lumen. **(C)** VPS4, as well as deubiquitinating

enzymes, are recruited to the degradative subdomain. **(D)** The degradative cargoes, having been deubiquitinated, are sequestered within the endosomal limiting membrane in intralumenal vesicles (ILVs) following a fission process. Adapted from (Cullen and Steinberg, 2018)

Through multiple low-affinity interactions (70-500 nM) with ubiquitin moieties, ubiquitin binding domains (UBDs) within ESCRT-0, ESCRT-I and ESCRT-II **(Table 1.1)** are thought to establish the selectivity of the degradative pathway (Frankel and Audhya, 2018). These low affinity interactions are amplified through the concentration of cargo, increasing the avidity and the ability of the UBDs to 'sense' ubiquitinated cargo and may contribute to the rapid transfer of the proteins between the ESCRT complexes (Frankel and Audhya, 2018).

ESCRT-0 components HGF-regulated tyrosine kinase substrate (HRS) and signal transducing adaptor molecule (STAM) are thought to provide the initial recognition of ubiquitinated cargoes (Bishop et al., 2002; Raiborg et al., 2002; Bache et al., 2003). ESCRT-0 self-associates on membranes through the PI3P-binding FYVE domain of HRS and interacts with clathrin (Raiborg et al., 2001a; Raiborg et al., 2001b). ESCRT-0 is thought to mediate the establishment of degradative subdomains, decorated with flat clathrin lattices, on the sorting endosome to segregate ubiquitinated cargoes from those which are destined to be recycled (Murk et al., 2003; Cullen and Steinberg, 2018) **(Figure 1.5A)**. ESCRT-I and ESCRT-II are subsequently sequentially recruited and also contribute to cargo selectivity through UBDs (Frankel and Audhya, 2018) **(Table 1.1)**.

ESCRT-III is recruited to the nascent ILV by sensing the density of ESCRT-II (Chiaruttini and Roux, 2017) **(Figure 1.5B)**. In an alternative pathway, ESCRT-III can also be recruited by ALG-2-interacting protein X (ALIX), which can sense ubiquitinated cargoes (Dowlatshahi et al., 2012; Keren-Kaplan et al., 2013; Pashkova et al., 2013), but has also been shown to bind cargoes, such as protease-activated receptor 1 and the $P2Y_1$ purinergic receptor, in a sequence-dependent manner (using a $YPX_{(3)}L$ sorting motif) (Dores et al., 2012; Dores et al., 2016).

Once recruited, ESCRT-III generates negative membrane curvature **(Figure 1.5B)** (Schoneberg et al., 2017). How this occurs is not fully understood, but it is thought to oligomerise into filaments formed from structures with varying curvatures, varying these structures dynamically to drive membrane constriction, and a 'release' of the imposed stress to buckle the membrane (Chiaruttini and Roux, 2017). Deubiquitinating enzymes are recruited by ESCRT-III (and STAM) to remove the ubiquitin moieties on

degradative cargoes **(Figure 1.5C)** (McCullough et al., 2006; Kyuuma et al., 2007). The scission of the nascent ILV is thought to also require the AAA ATPase, VPS4, which is also thought to drive ESCRT-III disassembly **(Figure 1.5D)** (Babst et al., 1998; Bishop and Woodman, 2000; Chiaruttini and Roux, 2017; Mierzwa et al., 2017).

Complex	Subunit	Ubiquitin-binding domain?
ESCRT-0	Hrs	Yes (DUIM, VHS)
	STAM1,2	Yes (UIM, VHS)
ESCRT-I	TGS101	Yes (UEV)
	VPS28	No
	VPS37 A, B, C, D	No
	MAV12 A, B,	No
	UBAP1	Yes (SOUBA)
ESCRT-II	EAP30	No
	EAP20	No
	EAP46	Yes (GLUE)
ESCRT-III	CHMP1A, B	No
	CHMP2A, B	No
	CHMP3	No
	CHMP4A, B, C	No
	CHMP5	No
	CHMP6	No
	CHMP7	No
	IST1	No

Table 1.1 The subunits of the metazoan endosomal sorting complex required for transport (ESCRT) complexes

1.3.2 Endosomal retrieval and recycling

1.3.2.1 Sequence-dependent vs sequence-independent retrieval and recycling

As discussed in **Section 1.3.1** cargo not destined for degradation are sorted away from sequestration within ILVs to be retrieved and recycled. Historically, it was believed that the high surface-area-to-volume ratio of recycling tubules compared to the vacuolar sorting domain **(Section 1.2.2)** preferentially sorts membrane-embedded cargo into a recycling route; in the absence of targeting signals for sequestration into ILVs, cargo would be recycled (Mayor et al., 1993; Maxfield and McGraw, 2004). This is termed ‘geometry-based sorting’ or ‘bulk flow’, where transmembrane cargo would be enriched in recycling tubules and the relatively high luminal content of the sorting domain would cause the enrichment of soluble proteins (Maxfield and McGraw, 2004).

In recent years, with the discovery of cargo adaptors which recognise specific sequences in the cytosolic-facing domains of cargoes **(Table 1.2)**, this model has been evolved to include sequence-dependent mechanisms of cargo retrieval and recycling (Dai et al., 2004; Cullen and Steinberg, 2018). The sequence-dependent retrieval and recycling of cargoes depend on several evolutionary-conserved multiprotein complexes. These complexes include: retromer **(Section 1.4.1)**, retriever **(Section 1.4.6)**, the CCC complex **(Section 1.4.6)**, the WASH complex **(Section 1.4.5)** and the SNX-BAR complex **(Section 1.4.2)** (Cullen and Steinberg, 2018). All these complexes are thought to be located on an endosomal retrieval subdomain, which is separated from the degradative subdomain discussed in **Section 1.3.1 (Figure 1.4)** (Cullen and Steinberg, 2018).

1.3.2.2 Avoiding the degradative fate

Generally speaking, the perturbation of endosomal retrieval complexes leads to cargo (whose recycling depend on specific sorting motifs; see **Table 1.2)**, by default, to enter the degradative pathway to be degraded (Seaman et al., 1998; Steinberg et al., 2012; Steinberg et al., 2013b; Kvainickas et al., 2017a; McNally et al., 2017; Simonetti et al., 2017; Cullen and Steinberg, 2018). Conversely, inclusion of transmembrane cargo into ILVs for degradation is a highly selective process: for ESCRT-mediated inclusion it depends on the ubiquitylation of cargo **(Section 1.3.1)**.

The retrieval complexes may therefore be required for restricting the lateral mobility of cargo away from endosomal degradative subdomains. Perturbation of retrieval complexes may cause cargo to 'leak' into degradative subdomains and be included into ILVs. Experimental evidence of this is lacking however and would require an active signal to cause the inclusion of the cargo into intralumenal vesicles.

Cargo adaptor	Sorting motif	Example cargo	Reference	See section
Retromer	FANSHY	SorLA	(Fjorback et al., 2012)	1.4.3
SNX3-retromer	Φ-X-[L/M/V]	DMT1-II	(Lucas et al., 2016)	1.4.3.1
SNX27 (PDZ domain)	$[E/D]^{-5}$ x $^{-4}[E/D]^{-3}[S/T]^{-2}$ x $^{-1}\Phi^{0}$	GLUT1	(Clairfeuille et al., 2016)	1.4.3.2

	$[ED/pSpT]^{-6}[E/D]^{-5}$ x $^{-4}[E/D]^{-3}[S/T]^{-2}$ x $^{-1}\Phi^{0}$ $[ED/pSpT]^{-5}$ x $^{-4}[E/D]^{-3}[S/T]^{-2}$ x $^{-1}\Phi^{0}$ $[ED/pSpT]^{-6}[ED/pSpT]^{-5}$ x $^{-4}[pS/pT]^{-3}[S/T]^{-2}$ x $^{-1}\Phi^{0}$ $[ED/pSpT]^{-6}$ x $^{-5}$ x $^{-4}[pS/pT]^{-3}[S/T]^{-2}$ x $^{-1}\Phi^{0}$ $[E/D]^{-3}[S/T]^{-2}$ x $^{-1}\Phi^{0}$ $[pS/pT]^{-3}[S/T]^{-2}$ x $^{-1}\Phi^{0}$			
SNX27 (FERM domain)	ΦxNPxpY ΦxNxxpY	P-selectin	(Ghai et al., 2013)	1.4.3.2
SNX17 (FERM domain)	ΦxNPx[F/Y] ΦxNxx[F/Y]	β1-integrin	(Bottcher et al., 2012)	1.4.6
COMMD1	NPxY	LDLR	(Bartuzi et al., 2016)	1.4.6
SNX-BAR complex	Hydrophobic motif	CIMPR	(Kvainickas et al., 2017a; Simonetti et al., 2017)	1.4.6

Table 1.2 Sorting motifs in endosomal cargo adapters

Adapted from (Cullen and Steinberg, 2018). (Φ indicates an aromatic residue; x indicates any amino acid; pS indicates phosphoserine; pT indicates phosphotyrosine).

1.4 Endosomal retrieval and recycling complexes

1.4.1 The retromer complex

S. cerevisiae has proved a powerful genetic tool in the identification of genes which affect specific processes of interest (Forsburg, 2001). Genetic screens identified more than 40 ‘vacuolar protein sorting’ (VPS) genes required for the efficient lysosomal delivery of acid hydrolases (Bankaitis et al., 1986; Rothman and Stevens, 1986; Robinson et al., 1988). Several Vps proteins (Vps29, Vps26, Vps35, Vps5 and Vps17) were subsequently shown to form a multiprotein complex and have a role in the retrograde transport of the transmembrane protein Vps10p from the endosomes to the Golgi; their perturbation resulted in the accumulation of Vps10p in the vacuole (the

yeast equivalent of lysosomes) (Horazdovsky et al., 1997; Seaman et al., 1997; Seaman et al., 1998). This complex was named 'retromer' (Seaman et al., 1998).

The heteropentameric yeast retromer is formed of two subcomplexes: a heterotrimer of Vps35, Vps26 and Vps29 and a heterodimer of Vps5 and Vps17 (Horazdovsky et al., 1997; Seaman et al., 1998). The highly conserved and ubiquitously-expressed mammalian homologues of the Vps35/Vps26/Vps29 heterotrimer are VPS35, VPS26A/VPS26B and VPS29 respectively (Haft et al., 2000; Koumandou et al., 2011). The differential incorporation of VPS26A or VPS26B into the retromer complex likely allows differential cargo sorting abilities, although negligible interactome differences have been detected (Bugarcic et al., 2011; McMillan et al., 2016). DSCR3 (Downs syndrome critical region 3), also known as VPS26C, is a third VPS26 paralogue but does not assemble into the retromer complex (see **Section 1.4.6**) (Koumandou et al., 2011; McNally et al., 2017). The VPS35:VPS26:VPS29 subcomplex mediates cargo retrieval (Cullen and Steinberg, 2018). How this complex recognises cargo is discussed in **Section 1.4.3**.

The ancestral Vps5 and Vps17 genes have undergone gene duplication in higher metazoans: mammals have two Vps5 homologues, sorting nexin (SNX)-1 and SNX2 (Horazdovsky et al., 1997; Carlton et al., 2004), while Vps17 has three homologues, SNX5, SNX6 and SNX32 (Wassmer et al., 2007; Wassmer et al., 2009; Koumandou et al., 2011). Common to Vps5/17 and SNX1/2/5/6/32 are a Phox-homology (PX) domain and a Bin/Amphiphysin/Rvs (BAR) domain (Cullen, 2008). They belong to the 'SNX-BAR' family of sorting nexins (Carlton et al., 2004). The SNX-BAR-containing subcomplex (discussed in greater detail in **Section 1.4.2**) is responsible for membrane remodelling to promote cargo recycling and has been referred to as the 'membrane deformation complex' (van Weering et al., 2010; Burd and Cullen, 2014a).

In contrast to fungal retromer, the metazoan VPS35:VPS26:VPS29 heterotrimer and the SNX1/2:SNX5/6/32 heterodimer have not been shown to form a stable complex (Norwood et al., 2011). Although these two complexes are thought to cooperate in the sorting of many retromer-dependent cargo, they also have independent activities (Harterink et al., 2011; Zhang et al., 2011; Kvainickas et al., 2017a; Simonetti et al., 2017; Cullen and Steinberg, 2018). To distinguish between the two complexes, I will henceforth use the term 'retromer' for the VPS35:VPS26:VPS29 heterotrimer and 'SNX-BAR complex' for the SNX1/2:SNX5/6/32 heterodimer. I will discuss in greater detail SNX-BAR complex-dependent recycling in **Section 1.4.2** and will subsequently discuss cargo retrieval via different retromers, such as the SNX3-retromer **(Section 1.4.3.1)** and the SNX27-retromer **(Section 1.4.3.2)**.

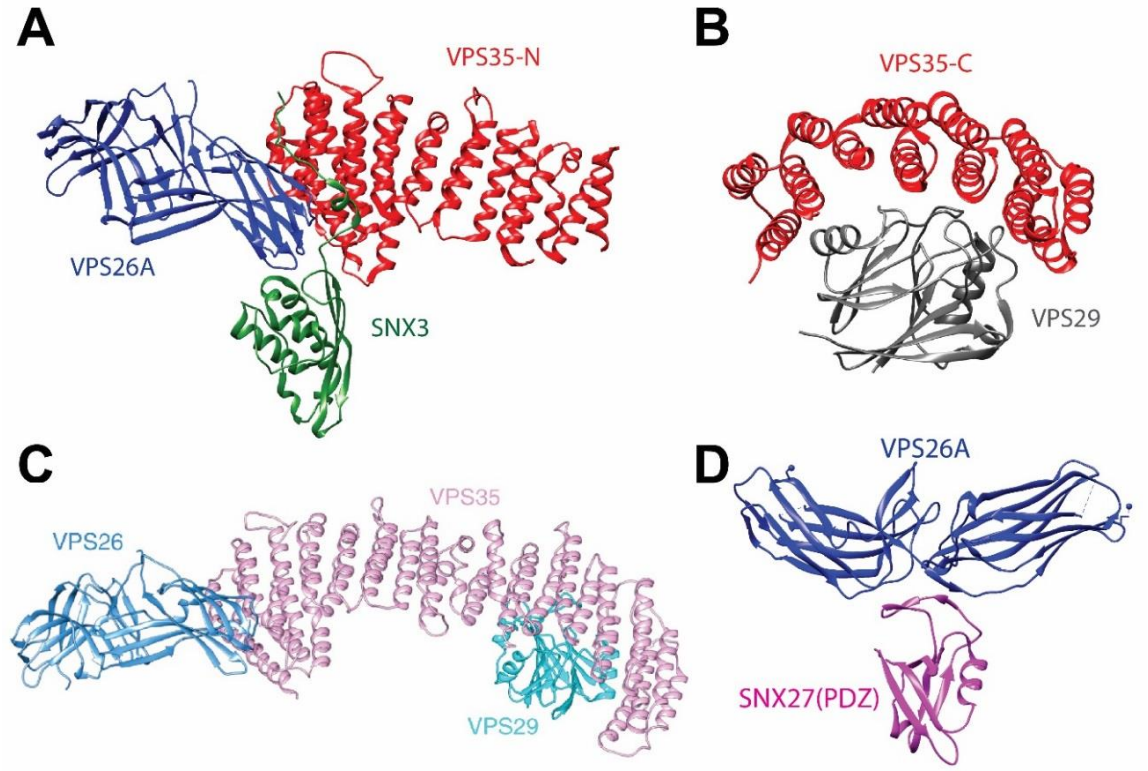

Figure 1.6 The structure of the retromer complex

(A) Model of the amino-terminus of VPS35 (red) bound to VPS26A (blue) and SNX3 (green) (Lucas et al., 2016). **(B)** Model of the carboxyl-terminus of VPS35 (red) bound to VPS35 (grey) (Hierro et al., 2007). **(C)** Predicted model of the entire VPS35 (pink): VPS26A(blue): VPS29 (cyan) heterotrimer derived from (Gershlick and Lucas, 2017). **(D)** Model of VPS26A (blue) bound to the SNX27 PDZ-domain (pink) (Gallon et al., 2014a).

Structural studies have been invaluable for understanding of how the multiprotein complex assembles and functions. The VPS35, VPS26, VPS29 heterotrimer assembles in a 1:1:1 ratio (Norwood et al., 2011). A high-resolution structure of mammalian retromer has not been solved in isolation, but partial structures are available: the N-terminal region of VPS35 in complex to SNX3 and VPS26A (Lucas et al., 2016) **(Figure 1.6A)** and the C-terminal region of VPS35 in complex to VPS29 (Hierro et al., 2007) **(Figure 1.6B)**. Through modelling, it has been possible to combine the available structures to reveal the overall architecture of retromer (Lucas et al., 2016) **(Figure 1.6C)**. VPS35 has a curved α-helical solenoid structure that is formed from 33 α-helices, organised into 16 anti-parallel α-helices (known as HEAT [Huntingtin/EF3/PP2A/TOR1] repeat domains) **(Figure 1.6C)**. VPS26A has an arrestin-like fold, consisting of antiparallel β-strands forming paired β-sandwich subdomains (Gallon et al., 2014a). VPS26A and VPS26B are structurally very similar and compete for the same site on the N-terminus of VPS35 (Collins et al., 2008). VPS29 binds to the

C-terminus of VPS35 and adopts a phosphoesterase-like fold (it can bind to divalent metals but has no *in vitro* enzymatic activity) (Collins et al., 2005; Hierro et al., 2007; Swarbrick et al., 2011) **(Figure 1.6C)**. Recently, the assembly of the fungal *C. thermophilium* retromer bound to the BAR-domain containing Vps5 on a membrane tubule was solved. This will be discussed in greater detail in **Section 5.3.2** and **Section 6.1.2**.

1.4.2 Cargo recycling by the SNX-BAR complex

As described earlier **(Section 1.4.1)**, the retromer pathway must couple with the SNX-BAR complex to link cargo retrieval with membrane deformation and cargo enrichment into tubular recycling carriers. The SNX-BAR complex (as defined in this thesis) is composed of a heterodimer of SNX1 or SNX2 complexed with SNX5, SNX6 or SNX32 (Cozier et al., 2002; Carlton et al., 2004; Wassmer et al., 2007; Wassmer et al., 2009). The formation of tubules has been observed: emanating from endosomes when SNX1 or SNX2 are overexpressed in cells (Carlton et al., 2004), or when SNX1 or SNX2 were purified and incubated with liposomes *in vitro* (van Weering et al., 2012). SNX5, SNX6 and SNX32 incorporate into a heterodimeric complex with SNX1 or SNX2 to promote tubule formation (van Weering et al., 2012).

As described in **Section 1.4.1**, in addition to a PX-domain, the SNX-BAR complex members contain BAR domains. BAR domains contain a hydrophobic dimerization interface containing charged residues which add specificity to which SNX-BARs can dimerise together (Dislich et al., 2011; van Weering et al., 2012). Furthermore, on the surface of BAR domain's concave surface there are positively charged residues which can electrostatically interact with lipid bilayers (Gallop and McMahon, 2005).

The SNX-BAR complex is initially recruited to the endosomal membrane through the PX-domain 'coincidence detection' of endosomal phosphoinositides and membrane curvature sensing through the BAR domain (Carlton et al., 2004; van Weering et al., 2012). Additionally, the SNX-BARs contain amphipathic helices which can be inserted into lipid bilayers to robustly associate the complex to the membrane and also induce membrane curvature (Pylypenko et al., 2007; Bhatia et al., 2009; van Weering et al., 2012). Tubule extension is promoted by the dimerization and formation of higher-order tubular lattices composed of SNX-BAR complexes (Frost et al., 2008; Mim et al., 2012).

1.4.3 Cargo recognition by retromer

Having first been identified in *S. cerevisiae* as a multiprotein trafficking complex required for the retrograde transport of Vps10p **(Section 1.4.1)**, the mammalian retromer has subsequently been shown to sort hundreds of transmembrane cargo away from a degradative fate in the lysosomes (Cullen and Steinberg, 2018). In terms of endosome-to-TGN cargo sorting, many mammalian functional homologues of Vps10p have been identified as being retromer cargoes, including: sortilin (Mari et al., 2008), SorLA (Fjorback et al., 2012) and SorCS1 (Lane et al., 2010). In recent years, the role of retromer in endosome-to-plasma membrane sorting has increasingly become appreciated.

Surface biotinylation of transmembrane proteins and their isolation, coupled to unbiased quantitative proteomics, has elucidated hundreds of cargoes which rely on retromer for their cell-surface localisation (Steinberg et al., 2013b). The development of global and unbiased quantitative proteomic techniques for examining the localisation of transmembrane proteins at other intracellular compartments, such as the TGN, will be instrumental in uncovering more retromer-dependent cargo. Although retromer has been described as 'cargo-selective', most cargoes are thought to be retrieved and recycled through the formation of larger multiprotein complexes in addition to retromer. The concept of retromer as a scaffolding hub for the recruitment of various accessory proteins to promote cargo retrieval and recycling, is increasingly being recognised **(Figure 1.7)** (Burd and Cullen, 2014a). The concept of sorting nexin-3 as a cargo adaptor is discussed in **Section 1.4.3.1** and sorting nexin-27 as a cargo adaptor in **Section 1.4.3.2**. Retromer also binds to the WASH complex **(Section 1.4.5)**, which promotes the formation of branched actin networks (Derivery et al., 2009; Gomez and Billadeau, 2009; Harbour et al., 2012; Jia et al., 2012).

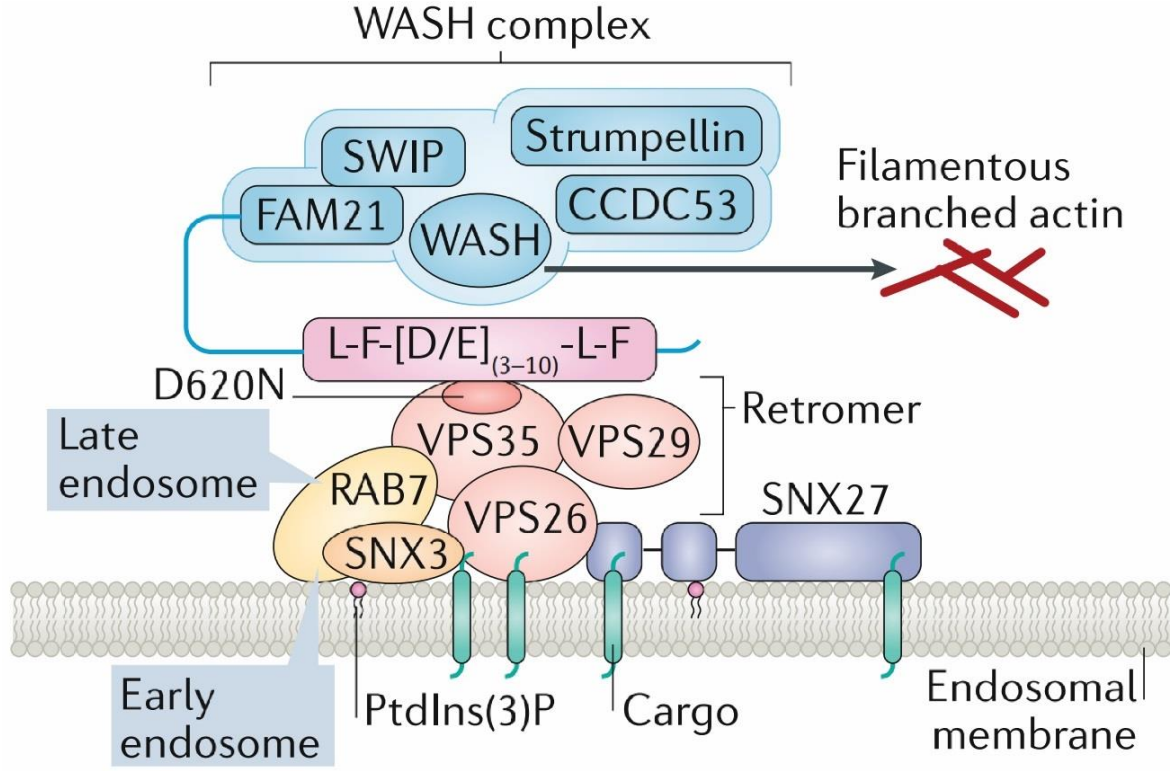

Figure 1.7 Retromer associated with various accessory proteins

Retromer, a heterotrimer of VPS35:VPS29:VPS26 (in mammals, VPS26A and VPS26B is expressed), is recruited to endosomal membrane by Rab7 and the PI3P-binding SNX3. SNX3 and SNX27 act as retromer cargo adapters to increase retromer's repertoire of cargoes. The WASH complex, associated with retromer via an L-F-[D/E]$_{(3-10)}$-L-F motif, induces the polymerisation of filamentous branched actin. The Parkinson's disease causing retromer variant, VPS35(p.D620N), reduces retromer's association with the WASH complex. Adapted from (Cullen and Steinberg, 2018).

1.4.3.1 SNX3-retromer

'Golgi retention defective', or 'grd' proteins, were identified in a *S. cerevisiae* genetic screen for mutants which resulted in the vacuolar mislocalisation of A-ALP (Nothwehr et al., 1996). One of these, 'Grd19p', contained a PX domain and is also required for the localisation of A-ALP and Kex2p (Voos and Stevens, 1998). Due to the homology of its PX domain with SNX1 (Ponting, 1996), it was categorised into the sorting nexin family as 'sorting nexin-3' (SNX3) (Haft et al., 1998). SNX3 associates with endosomes via its PX-domain, which directly interacts with PI3P (Xu et al., 2001; Zhou et al., 2003) and SNX3 does not contain a BAR domain (Cullen and Korswagen, 2012).

SNX3 recruits retromer to early endosomes via a direct interaction (Harterink et al., 2011). Through the formation of the SNX3-retromer, where SNX3 jointly binds to VPS35 and to VPS26, SNX3 acts as a retromer cargo adapter (Strochlic et al., 2007; Lucas et al., 2016) **(Figure 1.6A)**. Metazoan SNX3-retromer cargoes include: Wntless

(Belenkaya et al., 2008; Franch-Marro et al., 2008; Pan et al., 2008; Yang et al., 2008; Harterink et al., 2011; Zhang et al., 2011), transferrin receptor (Xu et al., 2001; Chen et al., 2013), DMT1-II (Lucas et al., 2016), polycystin-2 (Feng et al., 2017) and the *C. elegans* bone morphogenic protein type I receptor SMA-6 (Gleason et al., 2014). Interestingly, electron microscopy has revealed that the membrane carriers positive for SNX3 are vesicular, rather than tubular, and are decorated with clathrin (Harterink et al., 2011). Furthermore, at least for the SNX3-retromer-dependent sorting of Wntless, the SNX-BAR complex is not required (Harterink et al., 2011; Zhang et al., 2011). The question of how SNX3-retromer couples to a membrane deformation complex to facilitate Wntless recycling is examined in **Chapter 3**.

The Lucas et al. (2016) crystal structure of a SNX3:VPS26A:VPS35 complex bound to the DMT1-II recycling signal defined the structural basic of SNX3-retromer cargo recognition. The direct association of SNX3 to retromer causes a conformational change in VPS26, revealing a binding site at the SNX3:VPS26 interface for cargo with a Ø-X-[L/M/V] motif (Ø indicates an aromatic residue) (Lucas et al., 2016) (**Table 1.2**) . This Ø-X-[L/M/V] motif is present in several known retromer cargoes, including Wntless, DMT1-II, CIMPR and sortilin; this motif has previously been shown to be important for the endosomal retrieval of Wntless and CIMPR (Seaman, 2007; Lucas et al., 2016; Varandas et al., 2016).

1.4.3.2 SNX27-retromer

Another member of the PX-domain containing sorting nexin family is sorting nexin-27 (SNX27), which also contains a postsynaptic density 95/discs large/zonula occludens-1 (PDZ)-domain and band 4.1/ezrin/radixin/moesin (FERM)-domain. SNX27 is predominantly expressed in the brain and in testes; it was originally identified as an upregulated gene following methamphetamine injection in rodents and also in a proteomic screen for interactors of 5-hydroxytryptamine type 4 receptors (Kajii et al., 2003; Joubert et al., 2004). Global unbiased cell-surface proteomics have revealed hundreds of cargoes which rely on SNX27 for their endosomal retrieval and recycling to the plasma membrane (Steinberg et al., 2013b). Some of the identified cargoes include: N-methyl-D-aspartate (NMDA) receptors (Wang et al., 2013), α-amino-3-hydroxy-5-methyl-4-isoxazolepropionic acid (AMPA) receptors (Hussain et al., 2014; Loo et al., 2014), the β2-adrenergic receptor (Temkin et al., 2011), the parathyroid hormone receptor (Chan et al., 2016), the inwardly rectifying potassium channel 3.3 (Kir3.3) (Balana et al., 2011) and glucose transporter 1 (GLUT1) (Steinberg et al., 2013b).

The SNX27 PDZ domain recognises cargoes with a type I PDZ binding motif: [S/T]-x-Φ (in which Φ represents any hydrophobic residue) (Hung and Sheng, 2002). SNX27 has been shown to engage PDZ binding motifs with either high or low affinity; high affinity binders require the presence of acidic residues located upstream of the PDZ binding motif which can be substituted by conserved phosphorylation sites (see **Table 1.2** for full sorting motifs) (Clairfeuille et al., 2016). Building on this information, bioinformatic screening for potential SNX27-depenent cargoes identified over 400 potential binders of SNX27 with appropriate PDZ binding motifs (Clairfeuille et al., 2016).

The SNX27 FERM-domain is thought to bind numerous NPxY or NxxY binding motif-containing cargoes, with a preference for those which are phosphorylated at position 'Y_0' (i.e. the tyrosine at the end of the motif; see **Table 1.2**) (Ghai et al., 2013). Validated SNX27-dependent cargoes with NPxY/NxxY binding motifs include the amyloid precursor protein and P-selectin; a peptide array has also suggested that various activated (i.e. Y_0-phosphorylated) receptor tyrosine kinases are SNX27 cargo too (Ghai et al., 2011; Ghai et al., 2013).

By directly binding to retromer (Steinberg et al., 2013b; Gallon et al., 2014a), SNX27 acts as a retromer cargo adapter (Burd and Cullen, 2014a). A hydrophobic pocket within VPS26 is contacted by Leu67 and Leu74 within the β3-β4 loop of SNX27's PDZ domain, an area distant from the site of PDZ binding motif recognition, explaining SNX27's simultaneous association with retromer and cargo (Gallon et al., 2014a) **(Figure 1.6D)**. The formation of the SNX27-retromer allosterically enhances the affinity of SNX27 for PDZ binding motifs (Gallon et al., 2014a). SNX27-retromer dependent retrieval and recycling is thought to occur on Rab4-positive early endosomes and requires the SNX-BAR complex **(Section 1.4.2)** (Temkin et al., 2011; Steinberg et al., 2013b).

1.4.4 Spatiotemporal control of retromer

Retromer does not have any intrinsic membrane-binding ability and relies on protein:protein interactions to associate with the cytosolic surface of endosomal membranes. As previously outlined (**Section 1.4.3.1)**, retromer associates with early endosomes via SNX3 (Harterink et al., 2011; Harrison et al., 2014b; Lucas et al., 2016). A recent study has suggested a mechanism for the regulation of the ability of SNX3 to associate with PI3P: phosphorylation of Ser72 on the PI3P binding site which prevents membrane association (Lenoir et al., 2018). How this is regulated is currently unclear, but this phosphorylation is thought to extend to other sorting nexins, including

SNX1, and may be a general mechanism for controlling the membrane association of PX-domain containing proteins (Lenoir et al., 2018).

In addition, retromer is recruited to maturing endosomes through its interaction with Rab7-GTP (Nakada-Tsukui et al., 2005; Rojas et al., 2008). Together with the Rab7 GAP TBC1D5 (which directly binds to VPS29 of retromer), retromer negatively regulates Rab7 activity and localisation; concurrently, by promoting Rab7-GTP hydrolysis, retromer initiates a negative feedback loop which promotes retromer dissociation from the endosomal membrane (Seaman et al., 2009; Jia et al., 2016; Jimenez-Orgaz et al., 2018).

Due to its profound role in maintaining and modulating transmembrane protein localisation, it is likely that the function and activity of retromer is regulated transcriptionally and post-translationally. Evidence for the transcriptional control of retromer is currently lacking. A phosphorylation-dependent mechanism for modulating assembly of Vps35:Vps26:Vps29 into retromer has been described for *S. cerevisiae* Vps26; its relevance for mammalian retromer has not yet been proven (Cui et al., 2017). Retromer has also been described to undergo Parkin-mediated polyubiquitylation, although the functional consequence of this is currently unknown (Williams et al., 2018). It is likely that as the molecular details of retromer cargo recognition become increasingly understood, research focus will turn towards the question of the regulation and modulation of retromer activity.

1.4.5 The WASH complex

Correct endosomal organisation and function is dependent on the polymerisation of branched actin networks (Puthenveedu et al., 2010; Ohashi et al., 2011; Derivery et al., 2012; Gomez et al., 2012). Branched actin polymerisation is promoted by the actin-related protein 2/3 (Arp2/3) complex-dependent nucleation of monomeric actin; however, without being engaged by nucleation-promoting factor (NPF) proteins, it possesses little biochemical activity (Goley and Welch, 2006). On endosomes, the principle NPF is WASP and SCAR homologue 1 (WASH1), which incorporates into the heteropentameric WASH complex (Derivery et al., 2009; Gomez and Billadeau, 2009; Jia et al., 2010).

The WASH complex is composed of: WASH1, Family with sequence similarity 21 (FAM21), Strumpellin, Coiled-coil domain containing 53 (CCDC53), and Strumpellin and WASH-interacting protein (SWIP). There is no high-resolution structure available of the WASH complex, but it is thought to be analogous to another heteropentameric NPF

complex, the WASP family verprolin homolog isoforms (WAVE) complex, based on an electron microscopy-solved 20 Å structure and immunoprecipitation experiments (Jia et al., 2010).

WASH1 knockout mouse embryonic fibroblasts (MEFs) show a 'collapsed' endolysosomal network, where endosomes coalesce into the juxta-nuclear region and are devoid of filamentous endosomal actin (Gomez et al., 2012). Importantly, this phenotype could not be rescued with a WASH mutant devoid of its Arp2/3 complex-activating domain (Gomez et al., 2012). This 'collapsed' endolysosomal phenotype has subsequently been reproduced for Strumpellin knockouts in mouse melanocytes (Tyrrell et al., 2016). Although elongated endosomal tubules have been reported when WASH complex components have been depleted (Derivery et al., 2009; Gomez and Billadeau, 2009; Duleh and Welch, 2010), this is not phenocopied in the WASH1 knockout MEFs or when actin polymerisation or the Arp2/3 complex is suppressed, where endosomes become swollen, aggregated and devoid of tubules (Gomez et al., 2012). It is hypothesised that these contradictory phenotypes may represent two distinct roles of the WASH complex (Gautreau et al., 2014).

There is increasing evidence that some cargo may directly interact with actin to facilitate their endosomal sorting. The fusion of an actin-binding domain was able to overcome the addition of a ubiquitin degradative signal in a transferrin receptor chimeric protein (MacDonald et al., 2018) and replacing the PDZ binding motif of the β2-adrenergic receptor (a SNX27-retromer cargo) with an actin binding domain permitted functional recycling (Puthenveedu et al., 2010). As actin has a role in endosomal recycling, it is therefore not surprising that various cargo, including the transferrin receptor (Derivery et al., 2009), CIMPR (Gomez and Billadeau, 2009), the β2-adrenergic receptor (Puthenveedu et al., 2010), α5β1 integrin (Zech et al., 2011), T-cell receptor (Piotrowski et al., 2013), GLUT1 (Lee et al., 2016), LDLR (Bartuzi et al., 2016) and GLUT2 (Ding et al., 2018) have been shown to require the WASH complex for either their endosome-to-plasma membrane or endosome-to-TGN recycling. Many of these cargoes also require retromer or retriever for their sorting (see **Section 1.4.1** and **Section 1.4.6)**.

The WASH complex localises to retromer-positive endosomes, dependent on the ~1100 amino acid unstructured and flexible 'tail' of FAM21 (Derivery et al., 2009; Gomez and Billadeau, 2009). A large portion of the endosomal association of the WASH complex is dependent on its direct association with retromer (Harbour et al., 2012; Jia et al., 2012; McNally et al., 2017). This direct interaction has been shown to be dependent on a series of approximately 21 L-F-$[D/E]_{3-10}$-L-F (so-called 'LFa') motifs

(Jia et al., 2012). It has been proposed that the binding of multiple retromers by FAM21 allows the density of endosomal retromer to be sensed, thereby coordinating cargo recognition and clustering with the endosomal recruitment of the WASH complex and therefore the polymerisation of filamentous actin (Jia et al., 2012; Cullen and Steinberg, 2018).

The mechanism of retromer-independent endosomal WASH complex recruitment is undetermined. However, FAM21 binds to other endosome-localised proteins, including RME-8 (Freeman et al., 2014) and SNX27 (Steinberg et al., 2013b). It has also been shown to bind promiscuously to lipids *in vitro*, including PI3P and PI(3,5)P_2 (Derivery et al., 2009).

1.4.6 Retromer-independent endosomal retrieval

In recent years, it has become increasingly clear that retromer, although responsible for the retrieval and recycling of hundreds of transmembrane proteins, is not involved in all sequence-dependent endosomal cargo sorting (McNally and Cullen, 2018). Hundreds of transmembrane proteins have been identified as being dependent on the SNX27-retromer for their cell-surface localisation (see **Section 1.4.3.2**) (Steinberg et al., 2013b). However, there were around 40 transmembrane proteins which were lost from the cell surface in a SNX27-dependent but retromer-independent fashion, suggesting retromer-independent SNX27 cargo retrieval and recycling (Steinberg et al., 2013b).

Sorting nexin-17 (SNX17) is another FERM-domain containing (but not PDZ-domain containing) sorting nexin (Ghai et al., 2011). SNX17 does not associate with retromer (Steinberg et al., 2012). Consistent with this, a global cell-surface proteomic study revealed that SNX17 regulates the cell-surface localisation of hundreds of ΦxNPx[F/Y]- or ΦxNxx[F/Y]-motif containing cargo **(Table 1.2)**, independently of retromer (McNally et al., 2017). SNX17-dependent cargoes include β1-integrin (Bottcher et al., 2012; Steinberg et al., 2012), low-density lipoprotein receptor-related protein 1 (LRP1) (van Kerkhof et al., 2005) and P-selectin (Florian et al., 2001). Upon perturbation of SNX17, these cargoes undergo lysosomal-mediated cargo degradation.

Further molecular insight into SNX17-dependent cargo retrieval came from the discovery that SNX17 requires the evolutionary-conserved, retromer-like, ‘retriever’ complex to mediate endosomal cargo retrieval and recycling (McNally et al., 2017). The retriever complex is thought to be structurally homologous to retromer, being a heterotrimer of VPS29, chromosome 16 open reading frame 62 (C16orf62 but now known as VPS35L; predicted to contain HEAT-repeats similar to VPS35) and VPS26C

(see **Section 1.4.1**) (McNally et al., 2017). Interestingly, the copy number (in HeLa cells) of C16orf62 and DSCR3 is much lower compared to VPS35 and VPS26A/VPS26B (Kulak et al., 2014; McNally and Cullen, 2018).

The endosomal association of retriever is not dependent on SNX3 or Rab7, but another evolutionary conserved, multiprotein endosomal sorting complex: the CCC complex (McNally et al., 2017). The CCC complex is composed of coiled-coil domain-containing protein 22 (CCDC22), coiled-coil domain-containing protein 93 (CCDC93) and (at least) one of ten copper metabolism MURR1 domain (COMMD) proteins (Starokadomskyy et al., 2013; Phillips-Krawczak et al., 2015). COMMD proteins are thought to recognise cargo (Li et al., 2015). They can also homo- and hetero-dimerize (Burstein et al., 2005), suggesting that different COMMD-combinations assembled into the CCC complex may enable the recognition of different cargo. For example, COMMD1 has been implicated in the retrieval and recycling of ATP7A (Phillips-Krawczak et al., 2015) and LDLR **(Table 1.2)** (Bartuzi et al., 2016), whereas the plasma-membrane retrieval and recycling of Notch2 requires a heterodimer of COMMD9:COMMD5/COMMD10 (Li et al., 2015). The degree of cross-over between cargo retrieval of the CCC complex and retriever is currently unclear. It is also unclear how SNX17:retriever:CCC complex couples cargo recognition to membrane deformation.

To add an extra layer of complication, the endosomal association of the CCC complex is dependent on its interaction with the FAM21 subunit of the WASH complex (Phillips-Krawczak et al., 2015) (see **Section 1.4.5**). Therefore, retriever is dependent on both the CCC and WASH complexes for its endosomal localisation **(Figure 1.8)** (McNally et al., 2017). Perturbation of SNX17, retriever, the CCC complex, or the WASH complex results in the lysosomal missorting of β1-integrin (Zech et al., 2011; Steinberg et al., 2012; McNally et al., 2017). As stated before, a large proportion of the WASH complex associated with endosomes requires an interaction with retromer (Harbour et al., 2012; Jia et al., 2012). Retromer knockout results in a mild β1-integrin trafficking defect, likely due to the loss of the endosomal association of the WASH complex (McNally et al., 2017).

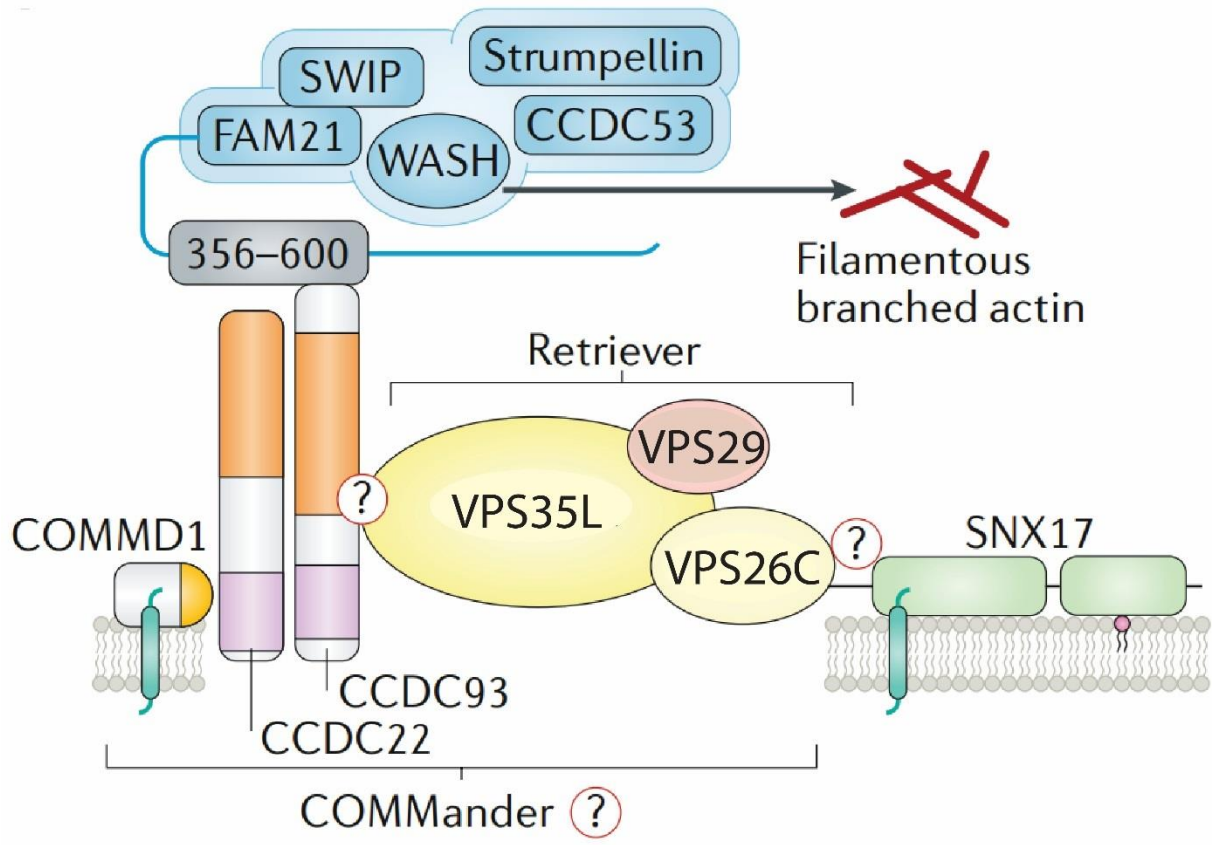

Figure 1.8 Retromer-independent endosomal cargo retrieval.

Retriever, a heterotrimeric complex of VPS35L:VPS26C:VPS29, is recruited to the endosomal membrane by its interactions with the CCC complex (CCDC22:CCDC93:COMMD), which is recruited to endosomes through its interactions with the WASH complex. It is hypothesised that this forms a higher order complex called 'COMMander', although experimental evidence for this is currently lacking. SNX17 and COMMD proteins are thought to act as cargo adaptors for the COMMander complex. Adapted from (Cullen and Steinberg, 2018).

Although the SNX-BAR complex has traditionally been thought of as the membrane deformation element to which the cargo-selective retromer couples (see **Section 1.4.2**), two recent papers independently described SNX-BAR complex-dependent, retromer-independent recognition of the CI-MPR and insulin-like growth factor 1 receptor (IGF1R), challenging the dogma of the field (Kvainickas et al., 2017a; Simonetti et al., 2017). All of the endosomal retrieval complexes are thought to coexist on the same retrieval subdomains (McNally et al., 2017; Cullen and Steinberg, 2018) (**Figure 1.4**). A summary of the retrieval complexes is shown in **Table 1.3**.

Endosomal retrieval complex	Components	How does it associate with endosomes?	Reference(s)
Retromer	VPS35; VPS26A/VPS26B; VPS29	Through interactions with Rab7 and SNX3	(Seaman et al., 1998; Rojas et al., 2008; Harterink et al., 2011; Harrison et al., 2014b)
The WASH complex	WASH1; FAM21; CCDC53; Strumpellin; SWIP	Through retromer-dependent and -independent mechanisms	(Derivery et al., 2009; Gomez and Billadeau, 2009; Harbour et al., 2012; Jia et al., 2012; McNally et al., 2017)
The CCC complex	CCDC22; CCDC93; COMMD1-10	Through the WASH complex	(Phillips-Krawczak et al., 2015)
Retriever	VPS35L (C16orf62); VPS26C (DSCR3); VPS29	Through the WASH and CCC complexes	(McNally et al., 2017)
SNX-BAR complex	SNX1/SNX2; SNX5/SNX6/SNX32	Through their PX and BAR domains	(Kvainickas et al., 2017a; Simonetti et al., 2017)

Table 1.3 Summary of the main endosomal retrieval complexes and how they associate with the endosomal membrane.

1.5 Endosomal cargo retrieval and recycling is neuroprotective

As endosomal cargo retrieval and recycling plays such a major role in the maintenance and modulation of the cell surface proteome (and of other intracellular compartments), it is not surprising that the deletion of various components of this pathway, including VPS35, VPS26A (but not VPS26B), FAM21, CCDC53, WASH1, Strumpellin, SNX3, COMMD1, COMMD9 and a combination of SNX1 and SNX2, result in embryonic lethality in mice (Lee et al., 1992; Schwarz et al., 2002; van de Sluis et al., 2007; Kim et al., 2010; Wen et al., 2011; Gomez et al., 2012; Jahic et al., 2015; Li et al., 2015) (the lethality of SNX3, FAM21 and CCDC53 knockouts were identified by the International Mouse Phenotyping Consortium). Furthermore, dysfunction of many of these components have also been implicated in human neurological diseases **(Section 1.5.1)**. A growing body of evidence also suggest that the enhancement of the best-

characterised endosomal retrieval complex, retromer, is neuroprotective in a range of disease models (Bi et al., 2013; MacLeod et al., 2013; Linhart et al., 2014; Mecozzi et al., 2014; Dhungel et al., 2015; Follett et al., 2016; McMillan et al., 2017).

Why are neurons particularly sensitive to disruptions in the endosomal cargo sorting machinery? Their 'extreme' morphology and polarisation, with elaborate branched dendritic projections and long axonal extensions (of up to 1m in length) **Figure 1.9)**, makes the endolysosomal pathway and retrograde transport a logistical challenge (Jin et al., 2018). Most degradative lysosomes are located close to the cell body meaning that cargoes may have to travel long distances to be degraded (**Figure 1.9)** (Kulkarni and Maday, 2018). Neuronal synaptic and postsynaptic biology, including the synaptic vesicle cycle and the modulation of cell-surface transmembrane proteins, is also heavily dependent on an efficient endosomal system (Jin et al., 2018). Furthermore, neurons are post-mitotic, long-lived and not easily replaced if this system becomes dysfunctional (Schreij et al., 2016).

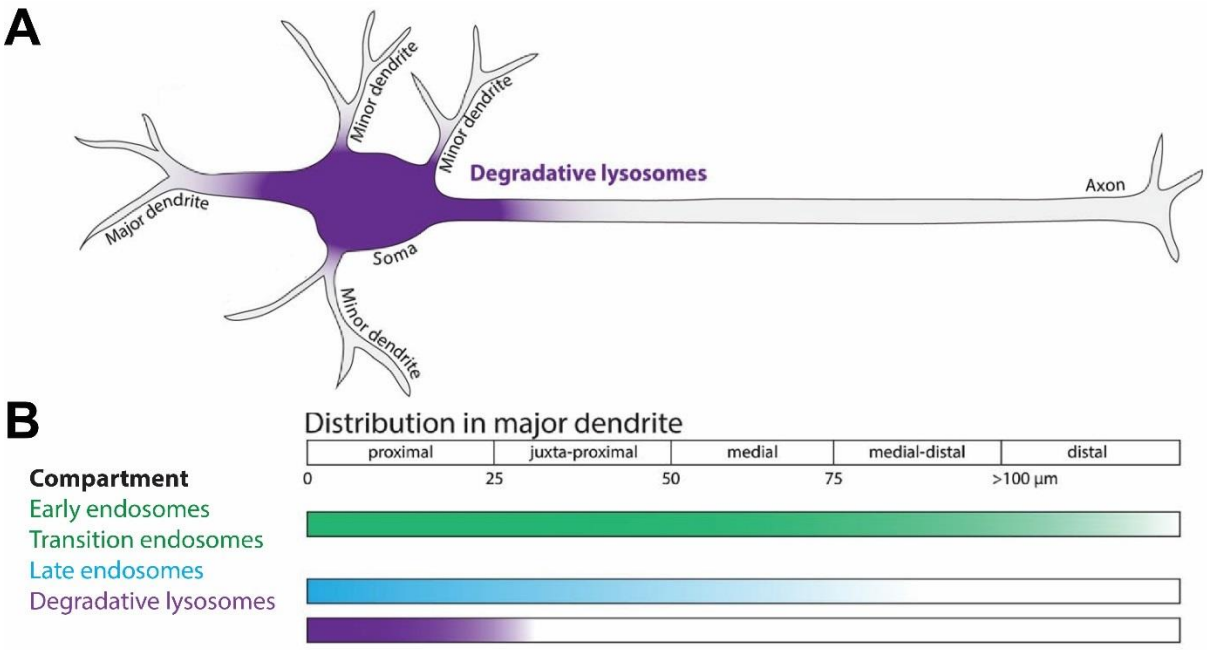

Figure 1.9 Neuronal distribution of the endolysosomal pathway

(A) A cartoon representing the morphology of neuronal cells. The degradative lysosomes are distributed in proximity to the soma. **(B)** The distribution of early, transition and late endosomes, as well as degradative lysosomes, in major dendrites. Adapted from (Kulkarni and Maday, 2018)

1.5.1 Associations between endosomal retrieval complexes and neurological disorders

In Alzheimer's disease (AD), the protein levels of VPS35 and VPS26 of retromer were shown to be decreased in the hippocampal tissue of patients with AD (Small et al., 2005). Depletion of retromer components in human tissue culture or using *in vivo* models results in the pathogenic processing of amyloid precursor protein (APP) into amyloid-β (a hallmark of AD pathology) (Small et al., 2005; Muhammad et al., 2008; Lane et al., 2010; Vieira et al., 2010; Wen et al., 2011; Bhalla et al., 2012; Fjorback et al., 2012; Mecozzi et al., 2014). Conversely, an AD mouse model (which overexpresses a variant of APP which causes early-onset AD), displayed reduced levels of retromer components (Chu and Pratico, 2017). Mechanistically, retromer has been implicated in AD pathology through influencing the processing of the APP: the trafficking of APP is dependent on the retromer cargo SorLA (and other VPS10-containing proteins). The depletion of retromer increases the time APP spends in endosomes where it can be processed into amyloid-β (Small and Petsko, 2015). *In vivo* models depleting retromer components displayed Alzheimer's disease phenotypes, such as impaired cognition, synaptic dysfunction and defective long-term potentiation (Muhammad et al., 2008; Wen et al., 2011). Non-synonymous *de novo* variants of VPS35 were also identified associated with sporadic early-onset AD (Rovelet-Lecrux et al., 2015). Likewise, other endosome-associated proteins including SNX3, SWIP, Rab7A and SNX1 have been genetically linked to AD (Vardarajan et al., 2012).

Rare mutations in various subunits of retromer have been implicated in familial Parkinsonism disorders (McMillan et al., 2017). The best characterised and most common of these is the autosomal dominant VPS35(p.D620N) mutation, which has been identified in both familial and sporadic forms of the disease (Vilarino-Guell et al., 2011; Zimprich et al., 2011; Ando et al., 2012; Kumar et al., 2012; Lesage et al., 2012; Sharma et al., 2012; Sheerin et al., 2012; Chen et al., 2017; McMillan et al., 2017; Bentley et al., 2018). This mutation causes a decrease in retromer's association with the WASH complex (McGough et al., 2014b; Zavodszky et al., 2014) and functionally has been implicated in perturbing: lysosomal health (Follett et al., 2014; McGough et al., 2014b; Zavodszky et al., 2014); mitochondrial health (Tang et al., 2015b; Wang et al., 2016b; Wang et al., 2017); synaptic plasticity (Munsie et al., 2014); and dopamine transport and signalling (Wang et al., 2016a; Wu et al., 2017; Cataldi et al., 2018). Furthermore, in samples of sporadic Parkinson's disease patients' substantia nigra pars compacta (the brain area which displays prominent dopaminergic neuronal death in Parkinson's disease), the mRNA levels of VPS35 were reduced (MacLeod et al.,

2013). A more detailed consideration of retromer's association with Parkinson's disease will be explored in **Chapter 4**.

The retromer-associated cargo adapter SNX27 has also been linked to neurological disorders. Patients harbouring a homozygous deletion mutation of SNX27 die within 2 years of birth and exhibit intractable monoclinic epilepsy and psychomotor defects (Damseh et al., 2015). In Down's syndrome, the trisomic chromosome 21 causes the overexpression of a negative regulator of SNX27, miR-155, leading to a decreased expression of SNX27. Interestingly, synaptic and cognitive phenotypes exhibited in a mouse model of Down's syndrome can be rescued through SNX27 overexpression (Wang et al., 2013). Other neurodevelopmental disorders implicated with endosomal sorting complexes include: X-linked recessive intellectual disability, which can be caused by mutations in CCDC22 (Kolanczyk et al., 2015; Bartuzi et al., 2016); and autosomal recessive intellectual disease, which can be caused by a mutation in SWIP (Ropers et al., 2011). Various mutations in Strumpellin have also been identified which cause hereditary spastic paraplegia (Valdmanis et al., 2007; Bettencourt et al., 2013; de Bot et al., 2013; Ishiura et al., 2014; Wang et al., 2014; Ichinose et al., 2016) and Ritscher-Schinzel/3C syndrome (Elliott et al., 2013).

1.6 Aims

Once transmembrane protein cargoes enter the endosomal network, a fundamental fate decision occurs: cargoes are either sorted for degradation or they undergo retrieval and recycling. The process of endosomal retrieval and recycling has been highlighted by its association with several neurological diseases **(Section 1.5.1)**. Our understanding of the process of retrieval and recycling has greatly improved in recent years and we now understand retromer, retriever, the WASH complex, the CCC complex and the SNX-BAR complex to be fundamental orchestrators, together with their various interactors **(Figure 1.4)** (Cullen and Steinberg, 2018). The general aim of my thesis was to dissect key molecular and functional interactions of the best characterised of these complexes: retromer.

Global and unbiased proteomic studies have increasingly mapped the interactors of retromer **(Section 1.4.1)** and the retromer cargo adaptors SNX3 **(Section 1.4.3.1)** and SNX27 **(Section 1.4.3.2)**. Notably, a detailed understanding of the mechanism by which some of these interactions occur and their functional significance is lacking.

In **Chapter 3**, I will describe research aimed at defining the residues in SNX3 which allow the formation of the SNX3-retromer. Through a collaboration with the Rik

Korswagen lab, I aimed to identify the importance of the physical association between SNX3 and retromer in the formation of Wnt morphogenetic gradients. In addition, I provide new insight into the fundamental question of how SNX3-retromer couples to a membrane deformation complex in order to couple cargo enrichment with membrane carrier formation.

In **Chapter 4**, I examine retromer's role in the pathogenesis of familial Parkinson's disease. The most common mutation in retromer which causes Parkinson's disease, VPS35(p.D620N), has set a precedent that disease-causing mutations in retromer may affect its molecular interactions. Taking forward this precedent, I describe whether other Parkinsonism-associated retromer mutations affect its interactome.

Lastly, in **Chapter 5**, I aim to increase our understanding of one of the more enigmatic of the retromer interactions: the retromer-WASH complex association. Both retromer and the WASH complex are fundamental players in endosomal biology and much has been inferred from their interaction. However, much of this speculation is not based upon experimental evidence. I will describe research that has defined the retromer residues which are critical for this interaction and aim to elucidate its functional importance.

Chapter 2

Materials and Methods

2.1 Materials

2.1.1 List of suppliers

Abcam, Cambridge, UK. AbD Serotec, Raleigh, NC, USA. Adobe Systems, Uxbridge, UK. Amersham, Little Chalfont, UK. Apollo Scientific, Denton, UK. BD Biosciences, San Jose, CA, USA. Beckman Coulter, High Wycombe, UK. Bio-Rad, Hemel Hempstead, UK. Calbiochem, San Diego, CA, USA. Cell Signaling Technology (CST), Beverley, MA, USA. Corning, Corning, NY, USA. Covance, Princeton, NJ, USA. Dharmacon, Lafeyette, CO, USA. Elga Labwater, High Wycombe, UK. Eppendorf, Hamburg, Germany. Eurofins MWG Operon, Ebersberg, Germany. GE Healthcare, Piscataway, NJ, USA. Hamamatsu Photonics, Hamamatsu, Japan. Improvision, Coventry, UK. Jackson ImmunoResearch, West Grove, PA, USA. Leica Microsystems, Milton Keynes, UK. Life Technologies, Carlsbad, CA, USA. Lonza, Basel, Switzerland. Microsoft, Redmond, WA, USA. Millipore, Watford, UK. Molecular Devices, Sunnydale, CA, USA. Molecular Probes, Cambridge, UK. New England Biolabs, Hitchin, UK. Novagen, Madison, WI, USA Olympus Microscopes, London, UK. PerkinElmer Life Sciences, Waltham, MA, USA. Pierce, Rockford, IL, USA. Promega, Southampton, UK. Qiagen, Crawley, UK. Roche Applied Science, Lewes, UK. Santa Cruz Biotechnology, CA, USA. Sigma-Aldrich (UK), Poole, UK. Solent Scientific, Segensworth, UK. Stratagene, La Jolla, CA, USA. ThermoScientific UK.

2.1.2 Sterilised water

All water used in the preparation of reagents or in experiments was sterilised using a PURELAB Option system (Elga Labwater). Nuclease-free water was purchased from Promega (cat. # P1193).

2.1.3 Cell lines used in this study

HEK 293: a human embryonic kidney cell line, immortalised by transformation with sheared human adenovirus type 5 DNA and stably transfected with the large T antigen of SV40 (Graham et al., 1977). This cell line was used for transient transfections and biochemical GFP/RFP trap experiments.

hTERT-RPE-1: a human retinal pigment epithelial cell line immortalised through stable transfection of human telomerase reverse transcriptase (hTERT) (Bodnar et al., 1998). This cell line was used in stable transductions and transient transfections for confocal imaging.

HeLa: human cervical adenocarcinoma cell line (Scherer et al., 1953). This cell line was used in stable transduction and transient transfections for confocal imaging.

2.1.4 Reagents for cell culture

Media for culturing HEK 293, HeLa and RPE-1 cells: Dulbecco's Modified Eagle's Medium (DMEM) with 4.5 g L^{-1} glucose/L, L-glutamine, $NaHCO_3$ and pyridoxine (Sigma, cat. # D5796), supplemented with 10% (v/v) foetal bovine serum (Sigma, cat. # F7524). Cells were grown without antibiotics.

Media for cell line transfection: OptiMEM® reduced serum media with GlutaMAX™ supplement (ThermoScientific, Gibco, cat. # 51985034) for transfecting siRNA oligonucleotides; OptiMEM® reduced serum media (ThermoScientific, Gibco, cat. # 31985062) for transfecting plasmid DNA.

For washing cells: cell culture-grade phosphate buffered saline (PBS) with 170 mM NaCl, 1 mM Na_2HPO_4, 3 mM KCl, 1.8 mM KH_2PO_4, pH 7.4. (Lonza, cat. # 17-516F).

For detaching cells from tissue culture plate: trypsin-EDTA solution, with 0.2 g/L EDTA, 0.5 g/L porcine trypsin in Hank's balance salt solution (Sigma, cat. **#** T3924).

Inhibitors used: VPS34-IN1 ($C_{21}H_{24}ClN_7O$), a VPS34 inhibitor (Calbiochem®, cat. # 532628). Bafilomycin A1 ($C_{35}H_{58}O_9$), a lysosomal acidification inhibitor (Sigma, cat. # B1793).

For culturing cell lines for a SILAC experiment: Dulbecco's Modified Eagle's Medium (DMEM) with 1000mg/L D-glucose, L-glutamine, and sodium bicarbonate, without arginine, leucine, lysine, sodium pyruvate, and phenol red (Sigma, cat. # D9443), supplemented with 10% (v/v) dialysed foetal bovine serum (Sigma, cat. # F0392). This media was supplemented with SILAC amino acids **(Table 2.1)**.

Table 2.1 SILAC amino acids

SILAC amino acids	Composition	Source	Catalogue number
R0 (light arginine)	L-arginine monohydrochloride	Sigma	A6969
K0 (light lysine)	L-lysine monohydrochloride	Sigma	L8662
R6 (medium arginine)	L-arginine -$^{13}C_6$ hydrochloride	Silantes	201204302
K4 (medium lysine)	L-lysine-2HCl, 4, 4, 5, 5-D4	Silantes	211204302

2.1.5 Bacterial cell strains

XL-Blue competent *E. coli,* genotype: recA1, endA1, gyrA96, thi^{-1}, hsdR17, supE44, relA1 lac [F' proAB laclq ZΔM15 Tn10(Tetr)] were purchased from Stratagene (cat. # 200236). Used in the transformation of constructs generated by restriction enzyme digestion followed by ligation.

XL10-Gold ultracompetent *E. coli*, genotype: TetrD(mcrA)183, D(mcrCB-hsdSMR-mrr)173, endA1, supE44, thi^{-1}, recA1, gyrA96, relA1, lac were purchased from Stratagene (cat. # 200314). Used in the transformation of constructs generated by site-directed mutagenesis.

2.1.6 Bacterial growth media and antibiotics

Luria-Bertani (LB) media (10 g NaCl, 10 g Tryptone, 5 g yeast extract in 1 L sterilised water). Purchased from Sigma (cat. # L3022).

Super Optimal broth with Catabolite repression (SOC) media (20 g Tryptone, 5 g yeast extract in 1 L sterilised water). Purchased from Sigma (cat. # S1797).

LB agar (20 g agar, 10 g NaCl, 10 g Tryptone, 5 g yeast extract in 1 L sterilised water). Purchased from Sigma (cat. #L2897).

Ampicillin: Working concentration 100 µg ml^{-1} (*aq*). Purchased from Sigma (cat. # A9518) in salt form.

Kanamycin: Working concentration 50 µg ml^{-1} (*aq*). Purchased from Sigma (cat. # B5264) in salt form.

2.1.7 Buffers and solutions

Phosphate buffered saline (PBS): PBS tablets (Oxoid™, cat. # BR0014G) were dissolved in laboratory grade purified water (1 tablet per 100 ml).

Lysis buffer: PBS, 5 mM ethylenediaminetetraacetic acid (EDTA), 1% (v/v) Triton X-100 (Sigma, cat. # T8787) and 1x complete protease inhibitor (Roche, cat. 04693124001).

GFP/RFP nanotrap buffer: 20 mM Tris/HCl, pH 7.4, 0.5% (v/v) Igepal (NP-40) (Sigma, cat. # I8896) and 1x complete protease inhibitor (Roche, cat. 04693124001).

Sample buffer: NuPAGE SDS sample buffer (4x) (ThermoScientific, Invitrogen cat. # NP0007) supplemented with 2.5% β-mercaptoethanol (Sigma, cat. # M6250).

2.1.8 Plasmid vectors

pEGFP-C1, pEGFP-N1, pmCherry-C1 were purchased from Clontech and used for transient transfection of mammalian cells.

pcDNA3.1 was purchased from Invitrogen and used for the transient transfection of mammalian cells.

pXLG3 was derived from pHR9SINSEW (Demaison et al., 2002) and modified by Dr Florian Steinberg. pMDG2 (VSV-G lentivirus envelope plasmid) was derived from (Ory et al., 1996). pCMV_R8.91 (lentivirus packaging construct) was derived from (Zufferey et al., 1997). These plasmids were used for the generation of lentiviral particles.

Other plasmids used in this study are listed in **Table 2.2**.

Table 2.2 List of plasmids used in this study

Plasmid name	Vector type	Origin
GFP-SNX3	pEGFP-C1	from the lab
GFP-SNX3 (p. 9,10 RR-AA)	pEGFP-C1	SDM of GFP-SNX3

GFP-SNX3 (p.Δ22-28)	pEGFP-C1	SDM of GFP-SNX3
GFP-SNX3 (p EID-TIR)	pEGFP-C1	SDM of GFP-SNX3
GFP-SNX3 (p. E50K)	pEGFP-C1	SDM of GFP-SNX3
GFP-SNX3 (p. E75A)	pEGFP-C1	SDM of GFP-SNX3
GFP-SNX3 (p. ESK(84-86)NAG)	pEGFP-C1	SDM of GFP-SNX3
GFP-SNX3 (p.Δ99-110)	pEGFP-C1	SDM of GFP-SNX3
GFP-SNX3 (p. Y154A)	pEGFP-C1	SDM of GFP-SNX3
GFP-SNX3 (p. P156A)	pEGFP-C1	SDM of GFP-SNX3
GFP-SNX3 (p. R160A)	pEGFP-C1	SDM of GFP-SNX3
GFP-SNX3 (p.Y22A)	pEGFP-C1	SDM of GFP-SNX3
GFP-SNX11	pEGFP-C1	from the lab
GFP-SNX12	pEGFP-C1	from the lab
GFP-SNX1	pEGFP-C1	from the lab
GFP-MON2	pcDNA3.1	cloned by Dr Ian McGough
MON2-GFP	pEGFP-N1	cloned by Dr Ian McGough
MON2-flag	pcDNA3.1	cloned by Dr Ian McGough
DOPEY2-GFP	pEGFP-N1	cloned by Dr Ian McGough
Flag-DOPEY2	pcDNA3.1	cloned by Dr Ian McGough
ATP9A-HA	pcDNA3.1	cloned by Dr Ian McGough
HA-Wntless-HA	pIRESneo3	a gift from Dr Katherine Varandas
HA-Wntless-HA	pXLG3	cloned by PCR
GFP-VPS26A	pEGFP-C1	from the lab
GFP-VPS26A (p.K93E)	pEGFP-C1	SDM of GFP-VPS26A
GFP-VPS26A (p.M112V)	pEGFP-C1	SDM of GFP-VPS26A
GFP-VPS26A (p.K297X)	pEGFP-C1	SDM of GFP-VPS26A
GFP-VPS26A	pXLG3	from the lab
GFP-VPS26A (p.K93E)	pXLG3	subcloning
GFP-VPS26A (p.M112v)	pXLG3	subcloning
GFP-VPS26A (p.K297X)	pXLG3	subcloning
GFP-VPS35	pEGFP-C1	from the lab
GFP-VPS35	pXLG3	from the lab
VPS35-GFP	pEGFP-C1	cloned by PCR
VPS35-GFP	pXLG3	subcloning
VPS35 (p.R32S)-GFP	pEGFP-C1	SDM of VPS35-GFP

VPS35 (p.R32S)-GFP	pXLG3	subcloning
VPS35 (p.G51S)-GFP	pEGFP-C1	SDM of VPS35-GFP
VPS35 (p.G51S)-GFP	pXLG3	subcloning
mCherry-SNX3	pmCherry-C1	from the lab
mCherry-Rab7 (p.Q67L)	pmCherry-C1	from the lab
GFP-FAM21 (1-220)	pEGFP-C1	from the lab
GFP-FAM21 (Δ1-220)	pEGFP-C1	from the lab
VPS35 (p.D620N)-GFP	pEGFP-N1	SDM of VPS35-GFP
VPS35 (p.K552H)-GFP	pEGFP-N1	SDM of VPS35-GFP
VPS35 (p.K559Q)-GFP	pEGFP-N1	SDM of VPS35-GFP
VPS35 (p.K573N)-GFP	pEGFP-N1	SDM of VPS35-GFP
VPS35 (p.R650E)-GFP	pEGFP-N1	SDM of VPS35-GFP
VPS35 (p.K659E)-GFP	pEGFP-N1	SDM of VPS35-GFP
VPS35 (p.K663E)-GFP	pEGFP-N1	SDM of VPS35-GFP
VPS35 (p.K694E)-GFP	pEGFP-N1	SDM of VPS35-GFP
VPS35 (p.R695E)-GFP	pEGFP-N1	SDM of VPS35-GFP
VPS35 (p.K701E)-GFP	pEGFP-N1	SDM of VPS35-GFP
VPS35 (p.K705E)-GFP	pEGFP-N1	SDM of VPS35-GFP
VPS35 (p.K552H, K555N, K556L)-GFP	pEGFP-N1	SDM of VPS35-GFP
VPS35 (p.K555N, K556L, K559Q)-GFP	pEGFP-N1	SDM of VPS35-GFP
VPS35 (p.K555E, K556E, K559E)-GFP	pEGFP-N1	SDM of VPS35-GFP
VPS35 (p.D620N)-GFP	pXLG3	subcloning
VPS35 (p.K559Q)-GFP	pXLG3	subcloning
VPS35 (p.K555N, K556L, K559Q)-GFP	pXLG3	subcloning
VPS35 (p.K555E, K556E, K559E)-GFP	pXLG3	subcloning
BFP-Rab5(p.Q79L)	BFP-C1	from the lab

SDM indicates ‘site-directed mutagenesis’.

2.1.9 Oligonucleotides

The PCR primers used to amplify genes or to create site directed mutations in contructs are listed in Table 2.2. The primers used for RT-qPCR are listed in Table 2.4. The siRNA duplexes used for knockdowns are listed in Table 2.5.

Table 2.3 List of DNA oligonucleotides used for cloning

Primer name	Sequence, 5'-3'
SNX3 SDM (9,10 RR-AA) F	accgtggctgacaccgcggcgctgatcaccaagcc
SNX3 SDM (9,10 RR-AA) R	ggcttggtgatcagcgccgcggtgtcagccacggt
SNX3 SDM (Δ22-28) F	gaacctgaatgacgccctcgagatcgatgtga
SNX3 SDM (Δ22-28) R	tcacatcgatctcgagggcgtcattcaggttc
SNX3 SDM (30-32 EID-TIR) F	ccccccagcaacttcctcacgatccgtgtgagcaacccgcaaac
SNX3 SDM (30-32 EID-TIR) R	gtttgcgggttgctcacacggatcgtgaggaagttgctgggggg
SNX3 SDM (E50K) F	gccgcttcaccacttacaaaatcagggtcaagaca
SNX3 SDM (E50K) R	tgtcttgaccctgattttgtaagtggtgaagcggc
SNX3 SDM (84-86 ESK-NAG) F	tgactttgaatggctgcgaagtgaattagaaagaaatgccctagtcgtagttcccccgctccctgg
SNX3 SDM (84-86 ESK-NAG) R	ccagggagcgggggaactacgactagggcatttctttctaattcacttcgcagccattcaaagtca
SNX3 SDM (Δ99-110) F	gggaaagcgtttttgcgtcaggatgacaattttattgaggaa
SNX3 SDM (Δ99-110) R	ttcctcaataaaattgtcatcctgacgcaaaaacgctttccc
SNX3 SDM (Y154A) F	ttttacaagatgaaataatagataaaagcgctactccatctaaaataagacatgcctgag
SNX3 SDM (Y154A) R	ctcaggcatgtcttattttagatggagtagcgcttttatctattatttcatcttgtaaaa
SNX3 SDM (P156A) F	gaaataatagataaaagctatactgcatctaaaataagacatgcctgag

SNX3 SDM (P156A) R	ctcaggcatgtcttattttagatgcagtatagcttttatctattatttc
SNX3 SDM (R160A) F	ataatagataaaagctatactccatctaaaatagcacatgcctgaggatcca
SNX3 SDM (R160A) R	tggatcctcaggcatgtgctattttagatggagtatagcttttatctattat
VPS26A SDM (K93E) F	gttctccaggtaaggctagttcctccactaggtttacaaattcatga
VPS26A SDM (K93E) R	tcatgaatttgtaaacctagtggaggaactagccttacctggagaac
VPS26A SDM (M112V) F	gactcagagcagaagttatgattttgaatttgtgcaagttgaaaagcc
VPS26A SDM (M112V) R	ggcttttcaacttgcacaaattcaaaatcataacttctgctctgagtc
VPS26A SDM (K297X) F	gaagtccggagttcactaagcatattagaagcatgttttag
VPS26A SDM (K297X) R	ctaaaacatgcttctaatatgcttagtgaactccggacttc
VPS35 SDM (D620N) F	gtatgaagatgaaatcagcaattccaaagcacagctagc
VPS35 SDM (D620N) R	gctagctgtgctttggaattgctgatttcatcttcatac
VPS35 SDM (K515S) F	gatttccaccagctccaaaatggcttcgtgctgtgttcaaaatcaa
VPS35 SDM (K515S) R	ttgattttgaacacagcacgaagccattttggagctggtggaaatc
VPS35 SDM (K552H) F	aatcttctggcatttcttttcccaatggtcatccactttagaattctcttt
VPS35 SDM (K552H) R	aaagagaattctaaagtggatgaccattgggaaaagaaatgccagaagatt
VPS35 SDM (K559Q) F	ggtgggcaaatgaaaaaatctgctggcatttcttttcccattt
VPS35 SDM (K559Q) R	aaatgggaaaagaaatgccagcagatttttttcatttgcccacc
VPS35 SDM (K573N) F	ctgccagctctgcattgatcaaagcactgatagt
VPS35 SDM (K573N) R	actatcagtgctttgatcaatgcagagctggcag
VPS35 SDM (R650E) F	gcaagggcacactgagtctccagaggttcatgattctc
VPS35 SDM (R650E) R	gagaatcatgaacctctggagactcagtgtgcccttgc
VPS35 SDM (K659E) F	gatcaggtttctttagaagctcggatgcagcaagggcacac

VPS35 SDM (K659E) R	gtgtgcccttgctgcatccgagcttctaaagaaacctgatc
VPS35 SDM (K663E) F	gctcggccctgatcaggctcctttagaagtttggatgcagc
VPS35 SDM (K663E) R	gctgcatccaaacttctaaaggagcctgatcagggccgagc
VPS35 SDM (K694E) F	actccattaccctctcgcctccgtgaagctc
VPS35 SDM (K694E) R	gagcttcacggaggcgagagggtaatggagt
VPS35 SDM (R695E) F	tttaggcactccattacctccttgcctccgtgaagctc
VPS35 SDM (R695E) R	gagcttcacggaggcaaggaggtaatggagtgcctaaa
VPS35 SDM (K701E) F	gcaagagggtaatggagtgcctagagaaagctctaaaaatagcaaatca
VPS35 SDM (K701E) R	tgatttgctatttttagagctttctctaggcactccattaccctcttgc
VPS35 SDM (K705E) F	ggtccatgcactgatttgctatctctagagctttttttaggcactcc
VPS35 SDM (K705E) R	ggagtgcctaaaaaaagctctagagatagcaaatcagtgcatggacc
VPS35 SDM (K552H, K555N, K556L) F	tggtgggcaaatgaaaaaatcttctggcataaattttcccaatggtcatccactttagaattctctttatatcg
VPS35 SDM (K552H, K555N, K556L) R	cgatataaagagaattctaaagtggatgaccattgggaaaatttatgccagaagatttttttcatttgcccacca
VPS35 SDM (K555N, K556L, K559Q) F	ctggtgggcaaatgaaaaaatctgctggcataaattttcccatttgtcatccactttagaattct
VPS35 SDM (K555N, K556L, K559Q) R	agaattctaaagtggatgacaaatgggaaaatttatgccagcagatttttttcatttgcccaccag
HA-Wntless-HA primer (Spe1) F	tatactagtcgccaccatggctggggcaattata
HA-Wntless-HA primer (Kpn1) R	atgatgttccagattacgcttagggtaccatag
VPS35-GFP primer (Spe1) F	ataagaactagtcgccaccatgcctaca

VPS35-GFP primer (BamH1) R	cctatggatccttacttgtacagctcgtcc

Abbreviations: SDM (site directed mutagenesis), F (forward/sense primer), R (reverse/antisense primer).

Table 2.4 List of primers for RT-qPCR

Primer name	**Sequence, 5'-3'**
β-actin left	agagctacgagctgcctgac
β-actin right	cgtggatgccacaggact
ATP9A left	gcctcaccaagatcctctttgg
ATP9A right	ggttcacgcgcaaactaatggg

Table 2.5 siRNA duplexes used for knockdowns

siRNA target	**5'-3' sequence**	**Supplier**
ON-TARGET plus nontargeting control pool	ugguuuacaugucgacuaa, ugguuuacauguuguguga, ugguuuacauguuuucuga, ugguuuacauguuuuccua	GE Healthcare
ON-TARGET plus human SNX27 siRNA pool	caaauuagcugcacguaua, gaguauagauuccggcuca, ggaauaugguugauuagau, gaguacaaaacgugagaau	GE Healthcare
MON2	caugcagauaauguauccagcuatt	Eurofins MWG operon
SNX3	aacaagggcuggagcaguyyatt	Eurofins MWG operon
DOPEY2	uuggcaaacucaacaaggcucuutt	Eurofins MWG operon
VPS35	guuguuaugugcuuagua; aaauaccacuugacacuua	Eurofins MWG operon
SNX1	aagaacaagaccaagagccac	Eurofins MWG operon
SNX2	aaguccaucaucuccagaacc	Eurofins MWG operon
ATP9A	gaaggugaagaguucuaacautt	Eurofins MWG operon
ON-TARGET plus human DOPEY1 siRNA pool	ggguauacaucaacgagaa, gaugaaaaggagcggguua, cagcaguacaaacuu	GE Healthcare
VPS26A	gcuagaacaccaaggaauu	Eurofins MWG operon

VPS26B	gaaguucucugugcgcuau	Eurofins MWG operon
ON-TARGET plus human FAM21 smartpool	Unknown (cat. # l-029678-01)	GE Healthcare

Oligonucleotides were modified with a 3'dTdT overhang.

2.1.10 Antibodies

The primary antibodies used in this study are listed in **Table 2.6** and the secondary antibodies are listed in **Table 2.7**.

Table 2.6 Primary antibodies

Primary antibody	Species	Dilution	Supplier	Catalogue number
GFP	Mouse	1:2000 (IB) 1:1000 (IF)	Roche	11814460001
VPS35	Rabbit	1:2000 (IB)	Abcam	Ab157220
VPS35	Rabbit	1:200 (IF)	Abcam	Ab97545
VPS35	Goat	1:200 (IF)	Abcam	Ab10099
VPS26A	Rabbit	1:1000 (IB)	Abcam	Ab137447
VPS26A	Rabbit	1:200 (IF)	Abcam	Ab23892
VPS29	Rabbit	1:1000 (IB)	Abcam	Ab98929
SNX27	Mouse	1:500 (IB)	Abcam	Ab77799
SNX3	Rabbit	1:500 (IB) 1:100 (IF)	Proteintech	10772-1-AP
FAM21	Rabbit	1:1000 (IB) 1:500 (IF)	Gift from Billideau	N/A
Strumpellin	Rabbit	1:500 (IB)	Santa Cruz	Sc-87442
WASH1	Rabbit	1:1000 (IB) 1:500 (IF)	Gift from Billideau	N/A
SWIP	Rabbit	1:1000 (IB)	Proteintech	S1101-1-AP
CDC53	Rabbit	1:1000 (IB)	Temecula	ABT69
Ankrd50	Rabbit	1:1000 (IB)	Abcam	Ab108219
mTOR	Rabbit	1:1000 (IB)	Cell signalling	2983P
ATM	Rabbit	1:500 (IB)	Abcam	Ab32420
MON2	Rabbit	1:500 (IB)	Gift from Wantanabe	N/A

DOPEY1	Rabbit	1:500 (IB)	Abcam	Ab95458
DOPEY2	Rabbit	1:500 (IB)	Santa Cruz	Sc-83241
HA	Mouse	1:2000 (IB) 1:1000 (IF)	Proteintech	66006-1-1g
Tubulin	Mouse	1:2000 (IB)	Sigma	T9026
β-actin	Mouse	1:2000 (IB)	Sigma	A1978
GAPDH	Rabbit	1:2000 (IB)	sigma	G9545
GCN1	Rabbit	1:1000 (IB)	Abcam	Ab86139
EEA1	Mouse	1:200 (IF)	BD transduction laboratories	610456
EEA1	Goat	1:200 (IF)	Santa Cruz	Sc-6415
LAMP1	Rabbit	1:400 (IF)	Abcam	Ab24170
LAMP1	Mouse	1:400 (IF)	Developmental Studies Hybridoma Bank	H4A3
Rab7	Rabbit	1:1000 (IB)	Cell Signalling	93675
SNX1	Mouse	1:1000 (IB) 1:200 (IF)	BD transduction laboratories	611482
SNX2	Mouse	1:1000 (IB)	BD transduction laboratories	611308
SNX5	Rabbit	1:1000 (IB)	Proteintech	17918-1-AP
SNX6	Mouse	1:1000 (IB)	Santa cruz	S6324
mCherry	Rabbit	1:1000 (IB)	Abcam	Ab167453
GLUT1	Rabbit	1:1000 (IB) 1:150 (IF)	Abcam	Ab115730
TGN46	Sheep	1:400 (IF)	BioRad	AHP500GT
Hrs/Hrs-2	Mouse	1:200 (IF)	Enzo	ALX-804-382-C050

Abbreviations: IB (immunoblot), IF (immunofluorescence), N/A (not applicable)

Table 2.7 Secondary antibodies

Secondary antibody	**Species**	**Dilution**	**Supplier**	
Alexa 488 anti-mouse IgG	Donkey	IF 1:400	Molecular Probes	

Alexa 568 anti-mouse IgG	Donkey	IF 1:400	Molecular Probes	
Alexa 647 anti-mouse IgG	Donkey	IF 1:400	Molecular Probes	
Alexa 488 anti-rabbit IgG	Donkey	IF 1:400	Molecular Probes	
Alexa 568 anti-rabbit IgG	Donkey	IF 1:400	Molecular Probes	
Alexa 647 anti-rabbit IgG	Donkey	IF 1:400	Molecular Probes	
Alexa 488 anti- goat IgG	Donkey	IF 1:400	Molecular Probes	
Alexa 488 anti- goat IgG	Donkey	IF 1:400	Molecular Probes	
Alexa 488 anti- goat IgG	Donkey	IF 1:400	Molecular Probes	
Alexa 800 anti-rabbit IgG	Donkey	IB 1:20000	Life Technologies	
Alexa 680 anti-mouse IgG	Donkey	IB 1:20000	Life Technologies	

Abbreviations: IB (immunoblot), IF (immunofluorescence).

2.2 Methods

2.2.1 Bacterial cell culture

2.2.1.1 Bacterial colony growth

Bacterial colonies were grown through the inoculation of a 9 cm LB-agar (15 g Agar, 5 g NaCl, 10 g Tryptome, 5 g yeast extract in 1L H_20, pH 7.0 (aq), *Sigma*) plates containing the appropriate antibiotics. An ethanol sterilised spreader was used for inoculations under sterile conditions (flame). The plates were left for 16-20 hours at 37°C for colony growth to occur. Colonies were then picked under sterile conditions and grown in liquid cultures.

2.2.1.2 Transformation of competent *E. coli*

5-50 ng of DNA were mixed with 30 µl of thawed chemically competent *E. coli* in a 1.5 ml Eppendorf tube. The tubes were incubated on ice for 30 minutes prior to heat shock at 42°C for 45 seconds. 200 µl of SOC media (20 g Tryptone, 5 g yeast extract, 0.5 g NaCl, 20 mM glucose in 1 L H_20, *Sigma*) was added following a 2 minute incubation on ice. The tube was then incubated for 1 hour at 37°C with shaking at 180 rpm. 100 µl of the sample was then used to inoculate agar plates containing the appropriate antibiotic for colony growth and incubated for 12-16 hours at 37°C.

2.2.1.3 Bacterial liquid cultures

Bacterial liquid cultures were grown in suspension in LB broth (10 g NaCl, 10 g Tryptome, 5 g yeast extract in 1L H_20, pH 7.0 (aq), Sigma) in appropriate antibiotics for 16-20 hours at 37°C, with shaking at 180 rpm. For small scale DNA purification (minipreps), cultures were grown in 5 ml of LB broth in a 20 ml universal tube. For large scale DNA purification (maxipreps), cultures were grown in 500 ml of LB broth in a 1 L conical flask.

2.2.2 Molecular biology methods

2.2.2.1 Small scale purification of plasmid DNA (Miniprep)

The 'QIAprep Spin Miniprep Kit' (Qiagen, cat. # 27106) was used for the small-scale purifications of plasmid DNA from liquid cultures. Purifications were performed according to the manufacturer's instructions and at room temperature. 4 ml of liquid bacterial culture were pelleted in centrifuge tubes at 6,800 x g for 3 min at room temperature. The pellets were resuspended in 250 µl P1 buffer (50 mM Tris-Cl, 10 mM EDTA, 100 µg ml^{-1} RNase, pH 8.0 (*aq*)) before mixing with 250 µl of P2 buffer (200 mM NaOH, 1 % (w/v) SDS (*aq*)) through inversion to lyse the cells. 350 µl of N3 buffer (contents not disclosed) was then added and thoroughly mixed to neutralise the solution before centrifugation at 17,900 x g for 10 minutes; this step took place within 5 minutes of the addition of the P2 buffer. The supernatants were then added to a QIAprep spin column before a 1 minute centrifugation step at 16,000 x g. The flow through was discarded. The QIAprep spin column was then washed with 500 µl of PB buffer (contents not disclosed) and then subsequently with 750 µl of PE buffer (contents not disclosed, contains 80 % (v/v) ethanol). Residual wash buffer was then removed with a further centrifugation step at 16,000 x g for 1 minute. 50 µl of RNAse free water was then incubated onto the column for 1 minute before the DNA was eluted through centrifugation at 16,000 x g for 1 minute. The DNA samples were then stored at -20°C.

2.2.2.2 Large-scale purification of DNA (Maxiprep)

The 'HiSpeed Plasmid Maxi Kit' (Qiagen cat. # 12662) was used for large-scale purification of plasmid DNA from liquid cultures (buffer contents undisclosed by the manufacturer). 500 ml of bacterial liquid culture was pelleted through centrifugation at 4,000 x g for 10 minutes at 4°C and resuspended in 10 ml of Buffer P1. The bacterial suspension was then lysed through the addition of 10 ml Buffer P2, thoroughly mixed and incubated for 5 minutes at room temperature. 10 ml of Buffer P3 was then added to neutralise the solution before the lysate was poured into a QIAfilter Cartridge and incubated at room temperature for 10 minutes. A plunger was then inserted into the QIAfilter Cartridge to filter the cell lysate into a HiSpeed Tip which had been equilibrated with Buffer QBT. The HiSpeed Tip was then washed with 60 ml of Buffer QC following the lysate entering. The DNA was then eluted using Buffer QF and

precipitated through the addition of 10.5 ml isopropanol, mixed and incubated at room temperature 5 minutes. The Buffer QF/isopropanol mixture was then placed into a syringe and filtered through a QIAprecipitator. The sample was then washed with 70% ethanol and dried. 1ml of DNAase-free water was then used to elute the DNA into a 1.5 ml Eppendorf tube. The DNA samples were then stored at 20°C

2.2.2.3 Nucleic acid quantification

Purified DNA and RNA concentrations were determined through absorbance measurements from a ND-1000 NanoDrop spectrophotometer.

2.2.2.4 DNA sequencing

DNA samples, 50-100 ng/µl, were sent to Eurofins MWG Operon, who performed all DNA sequencing reactions.

2.2.2.5 Polymerase Chain Reaction (PCR) for gene amplification

To amplify a gene of interest from a purified plasmid, the following reaction mix was prepared:

Step	**Temperature**	**Time**
Initial denaturation	98°C	30 seconds
35 cycles of: Denaturation	98°C	20 seconds
Annealing	50-72°C*	30 seconds
Extension	72°C	30 seconds /kb
Final extension	72°C	2-10 minutes **
Hold	4°C	Until stopped

*value dependent of Tm of primers; **dependent on length of DNA

Once completed, the PCR products were stored at -4°C.

2.2.2.6 Polymerase Chain Reaction (PCR) Site-Directed mutagenesis (SDM)

To introduce mutation(s) in a target construct, primers containing complementary DNA as well as specific nucleotide changes were designed using the Agilent QuikChange® Primer design tool (https://www.agilent.com/store/primerDesignProgram.jsp).

The following mix was prepared in a PCR tube:

Component	**Amount**
Pfu buffer (+$MgSO_4$)	5 µl
PCR enhancer	5 µl
10 mM dNTPs	0.5 µl
10 µM sense primer	0.75 µl
10 µM antisense primer	0.75 µl
Template DNA	Up to 50 ng
Pfu polymerase**	1 µl
Nuclease-free water	To 50 µl (final volume)

*Pfu DNA polymerase (Thermo Scientific, cat. # EP0501).

The PCR mixture was then transferred to a T100 Thermal Cycler machine (Bio-Rad) and the following programme was performed:

Step	**Temperature**	**Time**
Initial denaturation	95°C	30 seconds
18 cycles of: Denaturation	95°C	30 seconds
Annealing	55°C	30 seconds
Extension	72°C	1 minute per kb
Final extension	72°C	10 minutes
Hold	4°C	Until stopped

Following the PCR reaction, the methylated DNA, i.e. non-mutated template DNA, was digested using 1 µl of the restriction enzyme Dpn1 (New England Biolabs, cat. # R0176) per 30 µl of PCR products and incubated at 37°C for 1 hour. The sample was then transformed into XL10-Gold ultracompetent *E. coli*.

2.2.2.7 RNA extraction and quantitative-reverse transcriptase PCR

The RNeasy kit (Qiagen, cat. # 74134) was used to extract cellular RNA. Cells in a confluent 6-well tray were washed twice in ice-cold PBS. Using a cell scraper, cells were lysed with 350 µl of ice-cold RLT buffer (contents undisclosed), supplemented with 1% (v/v) β-mercaptoethanol, and transferred to an ice-cold Eppendorf tube. 350 µl of 70% ethanol was added to the lysate before transferring to a RNeasy column. Following centrifugation at 8000 x g for 15 seconds, the flow through was discarded. Three wash steps were performed (including centrifugation at 8000 x g for 60 seconds and the discarding of the flow through), once with 700 µl RW1 buffer and twice with 500 µl RPE buffer. The RNA was eluted using 30 µl of RNase-free water and stored at -80°C.

For q-RT PCR analysis, to analyse gene expression following RNAi-mediated suppression, a SuperScript III Platinum SYBR Green One-Step qRT-PCR kit (Invitrogen, cat. # 11736059) was utilised. Each primer reaction was performed in triplicate. The sense and antisense q-RT PCR primers (100 µM stock) were diluted with RNase-free water to 0.1 µM.

For each well required, the following mix was prepared in an RNase-free Eppendorf (added in the order of H20, RNA, 2x SYBR® Mix, SuperScript III Reverse Transcriptase):

	RNA sample	2x SYBR® Mix	SuperScript III RT	RNase-free water
1 well sample	0.1 µg	10 µl	0.4 µl	To 16 µl (total volume
1 well blank	0 µg	10 µl	0.4 µl	To 16 µl (total volume

Following thorough mixing, 16 µl of the mix was added to each well, followed by 4 µl of each primer. The plate was then centrifuged at 2000 x g for 4 minutes. Thermo cycling was performed in an Opticon2 system (MJ Research) using the following programme:

Step	**Temperature**	**Time**
cDNA synthesis	50°C	3 minutes
Initial denaturation	95°C	5 minutes
40 cycles	95°C 60°C	15 seconds 30 seconds
Final extension	40°C	1 minutes

Hold	4°C	Until stopped

The fluorescence threshold was set manually. The Cycle threshold (C_T) value (the number of cycles required to cross the threshold) was calculated by the Opticon2 software. The change in gene expression was determined through: $x=2^{-\Delta\Delta CT}$ (ΔC_T = difference in C_T values between gene of interest and the control gene [β-actin]; $\Delta\Delta C_T$ = difference between ΔC_T of the experimental sample [targeting siRNA] and the control sample [non-targeting siRNA]).

2.2.2.8 DNA analysis with agarose gel electrophoresis

To analyse the size of PCR products and restriction digests, the DNA samples were loaded onto a 1% agarose gel for electrophoresis. Agarose gels were made by mixing the required w/v mass of agarose with tris-acetate-EDTA (TAE) buffer (20 mM EDTA, 0.8 M Tris-acetate, pH 7.8). The solution was heated in a conical flask using a microwave until the agarose was dissolved, left to cool for 2 minutes and added to a casting tank which contained ethidium bromide (6 µl of 10mg/ml stock per 100 ml of the agarose-TAE mixture). A comb was inserted into the buffer. Once set, the comb was removed and the gel was transferred to a gel running tank and submerged in TAE buffer. The DNA samples were mixed with 6x gel loading due (NEB, cat. # B7024) and loaded onto the gel with a 2-log DNA ladder (NEB, cat. # N3200) alongside, before a voltage of 100 V was applied for an appropriate time. The DNA was visualised using the ChemiDoc system (Bio-Rad) through UV light. DNA bands could be excised from the gel and then purified immediately.

2.2.2.9 Purification of PCR and restriction digest products

PCR or restriction digest products to be used in subsequent reactions were purified using the GFX PCR DNA and Gel Band purification kit (GE Healthcare, cat. # 28-9034-70). The buffer contents of the kit are not disclosed by the manufacturer.

For DNA purification from agarose gels, the DNA band was excised from the gel using a clean scalpel blade and transferred to an Eppendorf. 10 µl of Capture buffer was added for each 10 mg of agarose gel excised and incubated at 60°C. Once the agarose gel had dissolved, the mixture was transferred to a GFX MicroSpin Column, centrifuged at 16,000 x g and the flow through discarded. The column was washed

twice in 500 µl Wash buffer with 1 minute 16,000 x g centrifugation steps to discard any flow through. An appropriate volume of nuclease-free water was then incubated with the column for 1 minute and the DNA was eluted into a clean Eppendorf through a 1 minute 16,000 x g centrifugation step. The purified DNA could then be stored at -20°C.

If the DNA was being purified from a solution, the same protocol was carried out with two modifications: 500 µl of Capture buffer was added, which was not heated at 60°C.

2.2.2.10 Restriction enzyme digestion

Restriction digestions, from either plasmid vectors or PCR products, were performed using high-fidelity restriction enzymes from New England Biolabs. The following mixtures were prepared:

Component	**Amount (plasmid vector)**	**Amount (PCR product)**
DNA	1 µg	43 µl
Compatible NEB buffer (10x)	1 µl	5 µl
Restriction enzyme 1	1 µl	1 µl
Restriction enzyme 2	1 µl	1 µl
Nuclease-free water	To 10 µl (final volume)	N/A

The digests were incubated at 37°C for at least 1 hour prior to the purification of the DNA.

2.2.2.11 Ligations

Digested PCR products and the digested vector were mixed in an insert/vector molar ratio of 3:1 and the following mix was prepared in a PCR tube:

Component	**Volume**
Purified digested vector DNA	Variable
Purified digested insert DNA	Variable
T4 DNA ligase*	1 µl
10x T4 ligase buffer	1.5 µl
Nuclease-free water	To 15 µl (final volume)

*T4 DNA ligase (ThermoScientific, cat. # EL0014).

The ligation mixture was incubated at room temperature for 1 hour. 2 µl of ligation mixture was used to transform XL-Blue competent *E. coli*.

2.2.3 Mammalian cell culture

2.2.3.1 Culturing mammalian cells

Human cell lines were cultured in humidified incubators at a constant temperature of 37°C with 5% CO_2. All cell-based experiments, including passaging, seeding, transfections, transductions and RNAi-based suppressions were performed in sterile class II vertical laminar flow cabinets (Holten Laminair, Thermo Fisher). All disposable materials used for cell based experiments were purchased as sterile items. Non-disposable materials were sterilised using 70% ethanol before use. Glass coverslips used for the seeding of cells for imaging were flame sterilised using 100% ethanol.

2.2.3.2 Passaging mammalian cells

Tissue-cultured cell lines were regularly passaged to prevent the cell density (confluency) becoming too high. DMEM was removed through aspiration before the cells were washed in sterile PBS. The cells were then incubated in Tryspin-EDTA solution for 5 minutes at 37°C to detach them from the plate. With the addition of DMEM, the cell suspension was centrifuged at 3000 x g for 2 minutes in sterile tubes to pellet the cells. The supernatant was then removed before the cells were resuspended in 1 ml of DMEM. An appropriate proportion of the cells were then seeded into a cell culture dish containing an appropriate volume of growth media.

2.2.3.3 HA antibody uptake (Wntless) assay

RPE-1 cells stably expressing HA-Wntless-HA were plated onto coverslips to achieve appropriate confluency for the following day. Cells were then placed on ice and washed in ice-cold PBS and labelled with α-HA antibodies (Roche 11867423001) diluted in ice-cold PBS (1:1000) for 30 minutes on ice. The cells were then washed with room temperature PBS. Cells for the 0 minute time point were immediately fixed using 4% paraformaldehyde. For the other time points, 37°C DMEM was added to the cells to induce trafficking and were placed in a 37°C incubator for set time points. Following

completion of each time point, the cells were washed in PBS and fixed in 4% paraformaldehyde.

2.2.3.4 Transfection of DNA using PEI

The PEI (polyethlenimine) method of transfection was used for HEK293 cells for GFP/RFP trap experiments or the production of lentivirus. Cells were grown in tissue culture dishes to a confluency of 80-90%. For 15 cm dishes, 5 ml (2.5 ml for a 10 cm dish) of OptiMEM was aliquoted into 2 separate sterile tubes. 15 µg (or 10 µg for a 10 cm dish) of DNA was added to one of these tubes and left to incubate for 5 minutes. To the second tube, 4.5 µl (or 3 µl for a 10 cm dish) of PEI was added and thoroughly mixed with the OptiMEM through vortexing, and filter sterilised using a 0.2 µm filter. The two Opti-MEM containing mixtures were then mixed and incubated at room temperature for 20 minutes.

The HEK 29T cells were then washed twice in sterile PBS before being incubated with the OptiMEM/DNA/PEI mixture for 4 hours at 37°C. The OptiMEM was then removed and exchanged for normal serum-containing DMEM and incubated for 48 hours at 37°C prior to experimental use.

2.2.3.5 Transfection of DNA using FuGENE

The FuGENE transfection protocol was used for RPE-1 cells or HeLa cells for subsequent confocal imaging experiments. Cells were seeded onto coverslips in a 12-well tray at a density of 3.5×10^4 per well and left for 16 hours. For each well, 1 µg of DNA and 3 µl of FuGENE 6 (Promega, cat. # E2691) were added to 100 µl of Opti-MEM in a sterile 1.5 ml Eppendorf. The mixture was then mixed through pipetting and left to incubate at room temperature for 20 minutes. The mixture was then added drop-wise to the well. Cells were then incubated at 37°C for 24 hours before fixation.

2.2.3.6 Transfection of siRNA using DharmaFECT

DharmaFECT (Dharmacon, cat. # T-2001) was used to transfect siRNA to knockdown genes. All knockdown experiments involved the transfection of siRNA twice in order to achieve adequate levels of gene suppression. The transfections were performed on cells, at approximately 80% confluency, adhered to 6-well plates. 200 µl of OptiMEM

was aliquoted into two different sterile Eppendorf tubes. 3 µl of siRNA (20 µM) was diluted in one of the tubes and 6 µl of DharmaFECT was diluted in the other. Following a 5 minute incubation at room temperature, the contents of the two tubes were mixed and a further room temperature incubation was performed for 20 minutes. The mixture was then added dropwise to cells in a 6-well plate. The cells were then left at 37°C until the next day, when they were split to be approximately 80% confluent the day after, when a second transfection (as already described) was completed. The cells were then incubated for a further 48 hours before subsequent protocols.

2.2.3.7 Lentiviral particle preparation

Genes of interest were packaged into lentiviral particles which could then be harvested and used to transduce cells. 40 µg of pXLG3 vector containing the gene of interest, 10 µg of pMDG2 envelope plasmid and 30 µg of pCMV_R8.91 packing construct were transfected into HEK293T cells in a 15 cm cell culture plate using the PEI method of transfection. The virus was left to proliferate for 3 days, in which time viral particles accumulated in the media. The media was pipetted into sterile tubes and centrifuged for 10 minutes at 4000 x g. The supernatants were then filtered through 0.45 µm filters before being aliquoted into 1.5 ml cryovials and stored at -80°C.

2.2.3.8 Transduction of cells using lentivirus

Viral transduction allows the creation of cells stably expressing a gene of interest. In a 12-well tray, 79,000 cells (RPE-1s) were seeded per well. A quantity of virus was then added to each well (the viral supernatants were titrated and supplemented with DMEM to give a final volume of 1 ml per well) before being incubated for 2 days at 37°C.

2.2.4 GFP- or RFP-nanotrap immunoprecipitations

Cells were transfected or transduced to express GFP-tagged or mCherry-tagged proteins and were grown to full confluency in a cell culture dish and washed twice in ice-cold PBS. Cells were lysed in GFP/RFP nanotrap buffer and the lysate was cleared by centrifugation at 13,000 x g at 4°C for 10 minutes. The resulting supernatant was incubated with 20 µl of GFP-nanotrap (Chromotek, cat. # gta-20) or RFP-nanotrap (Chromotek, cat. # rta-20) beads in a 1.5 ml microcentrifuge tube and incubated at 4°C on a rocker for 1 hour. Following incubation with the lysates, the beads were

centrifuged at 2000 x g for 10 seconds at 4°C and washed by resuspension in GFP/RFP nanotrap buffer. This washing process was repeated three times. The beads were then resuspended in 2x sample buffer, heated at 95°C for 5 minutes, and resolved using SDS-PAGE and immunoblotting.

2.2.5 Protein biochemistry

2.2.5.1 Cell lysis and sample preparation

When ready for lysis, cell culture dishes were placed on ice before being washed twice in ice-cold PBS. An appropriate amount of lysis buffer (approximately 100 µl for a 12-well tray, 150 µl for a 6-well tray) was added to the cells before a cell scraper was used to expose the cells to the lysis buffer. The lysed cells were transferred into 1.5 ml microcentrifuge tubes and centrifuged at 13,000 x g for 10 minutes at 4°C. The supernatant was added to an ice-cold microcentrifuge tube and mixed with 4x sample buffer supplemented with 2.5% (v/v) β-mercaptoethanol. The samples were then heated to 95°C for 5 minutes and resolved using SDS-PAGE and immunoblotting.

2.2.5.2 Sodium dodecyl sulphate polyacrylamide gel electrophoresis (SDS PAGE)

Proteins were resolved by SDS-PAGE using the NuPAGE® gel electrophoresis system by Invitrogen/Life Technologies. 500 ml of NuPAGE® MOPS running buffer (Invitrogen, cat. # NP0001) was added to the gel tank. Samples and the precision plus all blue standard (Bio-Rad, cat. #1610373) were loaded into the wells of a NuPAGE® 4-12% gradient Bris-Tris precast gels (Invitrogen, cat. # NP0322BOX). 150 V was applied to the system until the dye front had migrated to the required degree.

2.2.5.3 Transfer of proteins onto a membrane

The resolved proteins were subsequently transferred onto a polyvinylidene difluoride (PVDF) membrane (Immobilon-FL, pore size 0.45 um, Millipore, cat. # IPFL00010) using the Bio-Rad Mini Trans-Blot Electrophoretic Transfer cell (cat. # 170-3930). The membrane was soaked in methanol for 30 seconds. The components of the cassette (PVDF membrane, 2 foam pads, and 2 pieces of Whatman 3 mm filter blotting paper) were then soaked in transfer buffer (25 mM tris, 192 mM glycine, 10% methanol) before assembly. The gel and membrane were then sandwiched between

the foam pads and filter paper and braced into a blotting cassette and placed in a mini-Trans Blot Cell (Biorad) electrophoretic transfer cell and submerged in transfer buffer. 100 V was applied to the cassette for 1 hour to transfer the protein samples onto the PVDF membrane.

2.2.5.4 Immunoblotting

Following protein transfer onto the PVDF membrane, the membrane was removed from the transfer cassette and a blocking step proceeded in order to prevent unspecific antibody binding to the membrane. The membrane was incubated for 1 hour at room temperature in 5% (w/v) milk powder in TBS 0.1% (v/v) Tween-20 (TBST) on a rocker. The membrane was then incubated with the primary antibody, diluted in 2% (w/v) Bovine Serum Albumin (BSA) in PBS, overnight at 4°C.

The membrane was then washed 3 times in TBST for 10 minutes each. The membrane was then incubated with fluorophore-conjugated secondary antibodies, diluted in 5% (w/v) powdered milk in TBST, for 1 hour at room temperature in darkness. Following secondary antibody incubation, the membrane was washed 3 times for 10 minutes, twice in TBST and then once in TBST supplemented with 0.1% (w/v) sodium dodecyl sulphate (SDS). Fluorescence was detected using an Fc Odyssey scanner (LI-COR).

2.2.6 Proteomics

2.2.6.1 Stable isotope labelling of amino acids in culture (SILAC)-based proteomics

SILAC was used in this study to identify a protein of interest's interactors through mass spectrometry, an 'interactome', and to compare this interactome with a mutant form of the same protein, therefore distinguishing any changes in the interactome caused by the mutation.

This was accomplished by the differential incorporation of labelled essential amino acids. Cells were grown in culture media deficient in the amino acids arginine and lysine, supplemented with arginine and lysine with heavy isotopes of hydrogen, carbon and nitrogen (^{2}H, ^{13}C and ^{15}N). This media was also supplemented with dialysed FBS (to avoid any growth factors with 'normal' amino acids).

Cells could be labelled with the following amino acids: R0K0 (light media), R6K4 (medium media) and R10K8 (heavy media). In the medium media, cells are labelled with lysine residues containing four heavy isotopes, making the lysine residues 4 Da heavier (hence the 'K4' label) compared to lysine residues in the light media (referred to as 'K0'). In the heavy media, the arginine residues contain ten heavy isotopes, making them 10 Da heavier (hence the R10) compared to arginine residues in the light media (R0) and 4 Da heavier compared to arginine residues in the medium media (R6).

In this study, the three conditions (labelled with either light, medium or heavy media) were: GFP-only, GFP chimera with a protein of interest, and a GFP chimera with a mutant protein of interest. To sufficiently label and incorporate the isotope-labelled amino acids within the cellular proteome, the cells were cultured for at least 6 doublings. The cells were then subjected to a GFP-trap experiment according to **Section 2.2.4**. Following the washing steps, all the GFP-trap beads were combined and combined with sample buffer and heated to 95°C and the sample was run on an SDS-PAGE gel and stained with SimplyBlue SafeStain (Invitrogen, cat. # LC6060). Stained gels were then given to the proteomics facility in the Faculty of Life Sciences at the University of Bristol to carry out Nano-LC Mass Spectrometry analysis using an Orbitrap Fusion Tribrid mass spectrometer (Thermo Scientific).

2.2.6.2 Tandem mass tagging (TMT) labelling and High pH reversed-phase chromatography

TMT-based proteomics was used in this study in a similar experimental design to the SILAC-based proteomics: comparison of a protein of interest's interactors through mass spectrometry to generate an 'interactome' and its comparison with the interactome of a mutant form of the same protein. A GFP-trap experiment was carried out and following the wash steps, the GFP-trap beads were sent to the proteomics facility in the Faculty of Life Sciences at the University of Bristol to carry out TMT labelling.

Samples were digested with trypsin (2.5 µg trypsin; 37°C, overnight), labelled with Tandem Mass Tag (TMT) ten plex reagents according to the manufacturer's protocol (Thermo Fisher Scientific, Loughborough, LE11 5RG, UK) and the labelled samples pooled. The pooled sample was then evaporated to dryness, resuspended in 5% formic acid and then desalted using a SepPak cartridge according to the manufacturer's instructions (Waters, Milford, Massachusetts, USA). Eluate from the SepPak cartridge was again evaporated to dryness and resuspended in buffer A (20 mM ammonium

hydroxide, pH 10) prior to fractionation by high pH reversed-phase chromatography using an Ultimate 3000 liquid chromatography system (Thermo Scientific). In brief, the sample was loaded onto an XBridge BEH C18 Column (130Å, 3.5 µm, 2.1 mm X 150 mm, Waters, UK) in buffer A and peptides eluted with an increasing gradient of buffer B (20 mM Ammonium Hydroxide in acetonitrile, pH 10) from 0-95% over 60 minutes. The resulting fractions were evaporated to dryness and resuspended in 1% formic acid prior to analysis by nano-LC MSMS using an Orbitrap Fusion Tribrid mass spectrometer (Thermo Scientific).

2.2.6.3 Nano-LC Mass Spectrometry

High pH RP fractions were further fractionated using an Ultimate 3000 nano-LC system in line with an Orbitrap Fusion Tribrid mass spectrometer (Thermo Scientific). In brief, peptides in 1% (v/v) formic acid were injected onto an Acclaim PepMap C18 nano-trap column (Thermo Scientific). After washing with 0.5% (v/v) acetonitrile 0.1% (v/v) formic acid peptides were resolved on a 250 mm × 75 µm Acclaim PepMap C18 reverse phase analytical column (Thermo Scientific) over a 150 minute organic gradient, using 7 gradient segments (1-6% solvent B over 1 minute, 6-15% B over 58 minute, 15-32% B over 58 minutes, 32-40%B over 5 minutes, 40-90%B over 1minutes, held at 90%B for 6 minutes and then reduced to 1%B over 1 minute) with a flow rate of 300 nl min^{-1}. Solvent A was 0.1% formic acid and Solvent B was aqueous 80% acetonitrile in 0.1% formic acid. Peptides were ionized by nano-electrospray ionization at 2.0kV using a stainless steel emitter with an internal diameter of 30 µm (Thermo Scientific) and a capillary temperature of 275°C.

All spectra were acquired using an Orbitrap Fusion Tribrid mass spectrometer controlled by Xcalibur 2.0 software (Thermo Scientific) and operated in data-dependent acquisition mode using an SPS-MS3 workflow. FTMS1 spectra were collected at a resolution of 120 000, with an automatic gain control (AGC) target of 200 000 and a max injection time of 50 ms. Precursors were filtered with an intensity threshold of 5000, according to charge state (to include charge states 2-7) and with monoisotopic precursor selection. Previously interrogated precursors were excluded using a dynamic window (60s +/-10 ppm). The MS2 precursors were isolated with a quadrupole mass filter set to a width of 1.2m/z. ITMS2 spectra were collected with an AGC target of 10 000, max injection time of 70ms and CID collision energy of 35%.

For FTMS3 analysis, the Orbitrap was operated at 50 000 resolution with an AGC target of 50 000 and a max injection time of 105 ms. Precursors were fragmented by

high energy collision dissociation (HCD) at a normalised collision energy of 60% to ensure maximal TMT reporter ion yield. Synchronous Precursor Selection (SPS) was enabled to include up to 5 MS2 fragment ions in the FTMS3 scan.

The raw data files were then processed and quantified using Proteome Discoverer software v2.1 (Thermo Scientific) and searched against the UniProt Human database (downloaded 14-09-17: 140000 sequences) using the SEQUEST algorithm. Peptide precursor mass tolerance was set at 10 ppm, and MS/MS tolerance was set at 0.6 Da. Search criteria included oxidation of methionine (+15.9949) as a variable modification and carbamidomethylation of cysteine (+57.0214) and the addition of the TMT mass tag (+229.163) to peptide N-termini and lysine as fixed modifications. Searches were performed with full tryptic digestion and a maximum of 2 missed cleavages were allowed. The reverse database search option was enabled and the data was filtered to satisfy false discovery rate (FDR) of 5%.

2.2.7 Microscopy

2.2.7.1 Fixing and permeabilising cells for immunofluorescence-based imaging

Cells were seeded onto sterile 13 mm glass coverslips. Once at an appropriate confluency, the DMEM was removed through aspiration and then washed twice in PBS. The cells were then incubated with 4% (w/v) paraformaldehyde (Pierce, 16% Formaldehyde, cat. # 28906, diluted in PBS) for 20 minutes at room temperature. The PFA was then removed before three further PBS washes.

The PBS was removed before incubating the fixed cells with 0.1% (v/w) Triton X-100 (Sigma, cat. # T8787) in PBS for 5 minutes at room temperature to permeabilise the cells. The cells were then washed three times in PBS. For LAMP1 staining, 0.1% (w/v) Saponin in PBS replaced Triton X as a cell permeabiliser.

2.2.7.2 Staining fixed cells for immunofluorescence

Following permeabilization of cells, the PBS was replaced with 1% (w/v) BSA in PBS and incubated for 15 minutes at room temperature to block non-specific antibody binding. Primary antibodies were diluted in 1% (w/v) BSA in PBS and were aliquoted into 60 µl spots onto Parafilm. Coverslips were placed cell-side down onto the antibody-containing spots and incubated for 1 hour at room temperature (in darkness if

the cells had expressed GFP-tagged proteins). The coverslips were then washed 3 times in PBS before being placed onto 60 µl spots of Alexafluor-conjugated secondary antibodies diluted in 1% (w/v) BSA in PBS containing 4′,6-Diamidino-2-phenylindole dihydrochloride (DAPI) (0.5 µg per ml) for 1 hour at room temperature in darkness. The coverslips were then washed a further 3 times in PBS before being dried and mounted cell-side down onto Fluoromount-G (Invitrogen, cat. # 00-4958-02) on glass slides. The Fluoromount-G was left to dry for at least 4 hours at room temperature in darkness.

2.2.7.3 Confocal microscopes

Microscopy images were collected using a confocal laser-scanning microscope (SP5 AOBS; Leica Microsystems) attached to an inverted epifluorescence microscope (DMI6000; Thermo Fisher Scientific). A 63x CX PL APO lambda blue UV oil-immersion lens was used to take all images. Leica Application Suite AF software (version 2.7.3.9723) was used to acquire the images.

2.2.8 Software

Colocalisation analysis was performed using Volocity 6.3 Software (PerkinElmer). Pearson's correlation coefficient (PCC), which measures the correlation in the variation between two channels) and Overlap coefficient (measuring the degree to which the corresponding channel overlaps with the other channel) were measured using automatic thresholding using the Costes method (Costes et al., 2004).

Protein fluorescent band intensity from Western blots were measured using an Odyssey Fc imaging system from LI-COR.

Statistical analyses were performed using GraphPad Prism 7 software (La Jolla, CA). All quantified Western blot and colocalisation analysis data were the result of at least 3 independent experiments.

3D-modelling of protein structures were performed using UCSF Chimera (version 1.13).

Chapter 3

SNX3-retromer requires an evolutionary conserved MON2:DOPEY2:ATP9A complex to mediate Wntless sorting and Wnt secretion

3.1 Introduction

3.1.1 The intracellular trafficking of Wnt morphogens depend on their association with Wntless

Wnt proteins are a family of secreted glycoproteins which act as morphogens (Langton et al., 2016). Wnts are synthesised in and secreted from 'Wnt-producing' cells and activate Wnt signalling in 'Wnt-receiving' cells. This can initiate several downstream signal transduction pathways, including canonical signalling, where target gene expression is regulated, and the non-canonical planar cell polarity pathway (Sokol, 2015). Not only is it essential for stem and progenitor cell proliferation and differentiation during embryonic development and adult tissue homeostasis (Steinhart and Angers, 2018), but aberrant Wnt signalling has been implicated in a variety of diseases, including various cancers (Zhan et al., 2017), neurodegenerative disorders (Libro et al., 2016) and osteoporosis (Baron and Kneissel, 2013).

Wnts associate with an intracellular chaperone called 'Wntless', which mediates their intracellular transport from the endoplasmic reticulum to the cell surface (Banziger et al., 2006; Bartscherer et al., 2006; Goodman et al., 2006). Once synthesised in the ER, Wnts are lipidated, which facilitates their binding to Wntless (Herr and Basler, 2012). The Wnt:Wntless complex is then transported to the Golgi before the Wnts are secreted. There is controversy in the literature regarding the mechanism of Wnt secretion: whether the Wnt:Wntless complex is trafficked straight from the Golgi to the cell surface or from the Golgi to an endosomal compartment before arriving at the cell surface; it is also unclear whether the Wnt:Wntless complex dissociates in the acidic endosomal environment or once at the cell surface (Langton et al., 2016). How the Wnts reach the Wnt-receiving cells is also uncertain, models include: their incorporation into exosomes or lipoprotein particles, and direct cell:cell transfers (Langton et al., 2016).

After the Wnt morphogen dissociates from Wntless, the unbound Wntless is endocytosed through an AP-2-dependent mechanism (Pan et al., 2008; Port et al., 2008; Yang et al., 2008; Gasnereau et al., 2011). Once delivered to the endosomes, retromer (Coudreuse et al., 2006; Prasad and Clark, 2006; Franch-Marro et al., 2008; Pan et al., 2008; Yang et al., 2008) and sorting nexin-3 (SNX3) (Harterink et al., 2011; Zhang et al., 2011) **(see Section 1.4.3.1)** mediate the endosomal retrieval of Wntless to the Golgi, preventing its lysosomal degradation. SNX3 and retromer directly interact (Harterink et al., 2011; Zhang et al., 2011; Vardarajan et al., 2012; Harrison et al., 2014b), but whether or not this physical interaction is required for the sorting of Wntless

(and other cargo) back to the Golgi is unknown. Once retrieved and subsequently recycled to the Golgi, Wntless is retrogradely transported back to the ER through a COPI-mediated mechanism, where it undergoes further cycles of Wnt trafficking (Yu et al., 2014). The functional consequence of blocking the endosomal retrieval of Wntless is defective Wnt signalling, as the decrease in whole-cell quantities of Wntless perturbs the trafficking and therefore the secretion of Wnt morphogens (Belenkaya et al., 2008; Franch-Marro et al., 2008; Pan et al., 2008; Yang et al., 2008; Harterink et al., 2011; Zhang et al., 2011).

Intriguingly, the endosomal retrieval of Wntless has been shown to be independent of the classical retromer membrane remodelling complex: the SNX-BAR complex composed of SNX1/2 and SNX5/SNX6/SNX32 (Harterink et al., 2011; Zhang et al., 2011). This has been shown in the context of *D. melanogaster*, *C. elegans* and *in vitro* human cell culture (Harterink et al., 2011; Zhang et al., 2011). One study reported that SNX1 suppression increased Wntless colocalisation with lysosomes (Shi et al., 2009), but their analyses were limited to intensity measurements from immunofluorescence data and did include a biochemical or functional assessment. Without associating with the SNX-BAR complex, how the SNX3-retromer couples Wntless cargo recognition with membrane deformation and carrier formation is unclear.

3.1.2 Aims

In this chapter I aim to progress our molecular understanding of the SNX3-retromer mediated endosomal sorting of the Wnt chaperone, Wntless. To explore whether the physical interaction between VPS35 and SNX3 is necessary for Wntless sorting, I sought to identify SNX3 mutants unable to bind to retromer. The functional consequences of perturbing this interaction was then explored *in vivo* through a collaboration with the Korswagen lab. To identify how the SNX3-retromer coordinates Wntless enrichment with endosomal membrane deformation and carrier formation, I sought to investigate two proteins enriched in the SNX3 interactome: MON2 and DOPEY2. The *S. cerevisiae* homologues of these proteins form a complex with the putative aminophospholipid translocase, Neo1p, which is proposed to generate membrane curvature and to be involved in membrane trafficking within the endosomal network (Barbosa et al., 2010).

3.2 Results

3.2.1 Identification of the SNX3:VPS35 binding surface

To investigate the functional importance of the SNX3 interaction with the retromer complex, I first sought to identify residues in SNX3 critical for its association with the core retromer component: VPS35. To establish candidate binding-residues in SNX3, I performed a bioinformatics sequence alignment. SNX3 and its paralogue, SNX12, can immunoprecipitate VPS35 (Pons et al., 2012); SNX11, a closely related sorting nexin, cannot **(Figure 3.1A)**. I aligned the sequences of the VPS35-binding sorting nexins (SNX3 and SNX12) with the non-VPS35 binder (SNX11) to identify residues conserved between SNX3 and SNX12, but not conserved in SNX11 **(Figure 3.1B)**. From this, I identified several residues that may be critical for VPS35 association. I therefore generated several mutant GFP-SNX3 constructs through site directed mutagenesis **(Figure 3.1B)**.

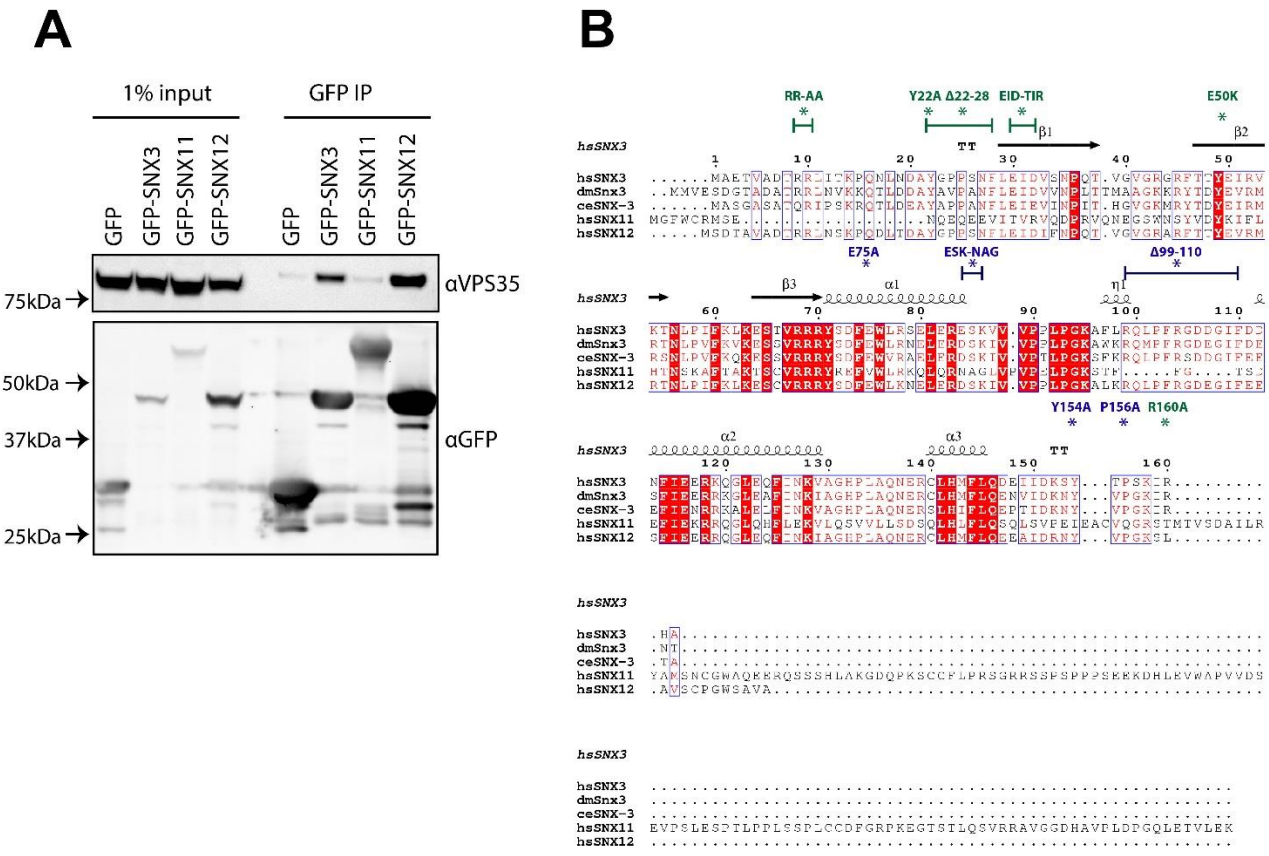

Figure 3.1 Bioinformatic analysis to identify residues in SNX3 important for VPS35 binding.

(A) SNX3 and SNX12 but not SNX11 can bind to VPS35. HEK293T cells were transfected with GFP-tagged SNX3, SNX12 and SNX11 constructs and subjected to a GFP-trap before immuno-blotting for VPS35. **(B)** Sequence alignment comparing the retromer associating SNX3 and

SNX12 with the non-retromer binding SNX11. *H. sapiens*, *D. melanogaster* and *C. elegans* SNX3 homologues were aligned against H. sapiens SNX12 and SNX11. SNX3 residues identified as candidates for VPS35 association are marked on the alignment.

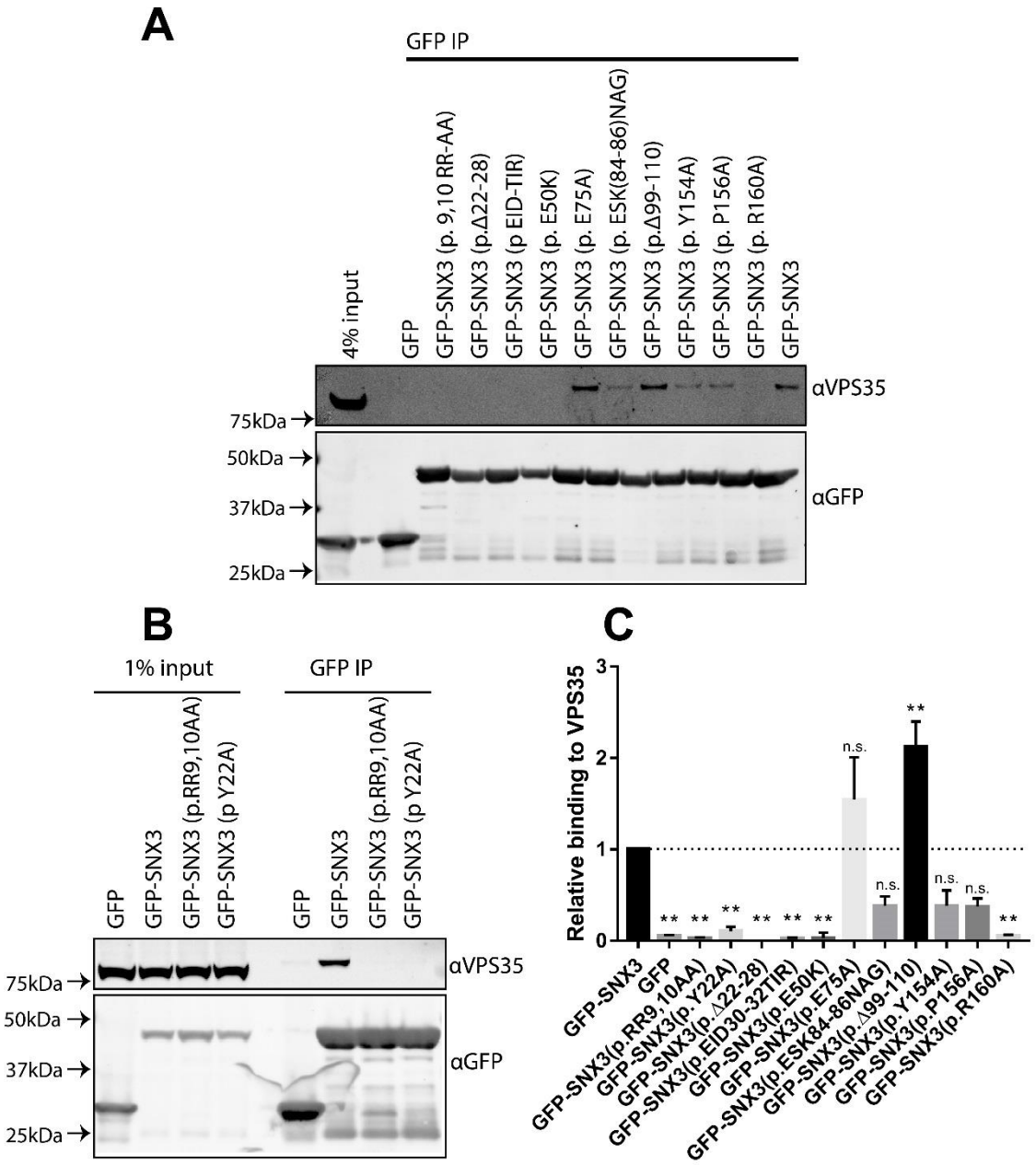

Figure 3.2 Immunoprecipitation screen identify GFP-SNX3 constructs with perturbed VPS35 binding.

(A-B) HEK293T cells were transfected with the indicated GFP-SNX3 constructs and subjected to a GFP-trap before immuno-blotting for VPS35. HEK293T cells were transfected with the indicated GFP-SNX3 constructs and subjected to a GFP-trap immunoprecipitation. The immuno-precipitates were then immuno-blotted for VPS35. **(C)** Quantifications show the mean of 3 independent experiments ± s.e.m. of the relative binding to VPS35 of the various GFP-SNX3 constructs relative to wild-type GFP-SNX3. Data were analysed using a one-way ANOVA followed by a Dunnett's test, comparing the various GFP-SNX3 constructs to the wild-type; ** P ≤ 0.01.

To screen for mutations which perturb SNX3's association with VPS35, I transiently transfected HEK293T cells with the GFP-SNX3 constructs. I then performed GFP-nanotrap immuno-precipitations and immuno-blotted for VPS35 **(Figure 3.2A)**. When the immuno-precipitated VPS35 was quantified over 3 independent experiments, several of these SNX3 mutations were revealed to diminish VPS35 binding **(Figure 3.2C)**. Building on the drastic loss of VPS35 association in the ∆22-28 mutation, I generated a single point mutation, Y22A, which also caused perturbed VPS35 association **(Figure 3.2B)**. To show that this loss of VPS35 association was not due to a loss of endosomal association, I transiently transfected the mutant GFP-SNX3 constructs into HeLa cells. All GFP-SNX3 variants colocalised on endosomal puncta positive for VPS35 **(Figure 3.3).**

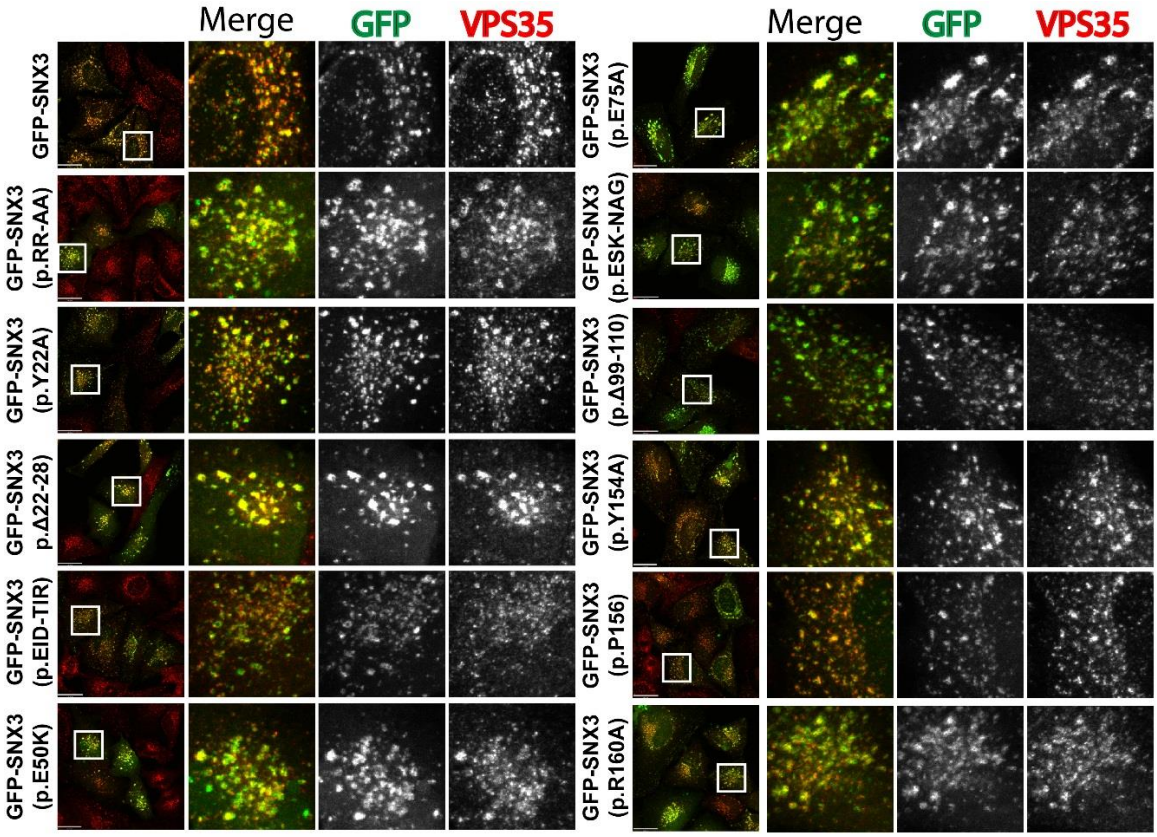

Figure 3.3 GFP-SNX3 constructs retain their endosomal association.

HeLa cells were transfected with the indicated GFP-SNX3 constructs and were stained for endogenous VPS35 before being imaged on a confocal microscope. Scale bars indicate 23 µm.

I then identified the spatial distribution of the SNX3 residues important for VPS35 binding using a model of the NMR-solved SNX3 solution structure (Overduin et al., 2015) **(Figure 3.4)**. This revealed a potential binding surface consisting of the N- and C-termini of SNX3, as well as the anti-parallel *β-sheet,* which may be essential for VPS35 association. It should be noted that the N- and C-termini of SNX3 are thought to be intrinsically disordered (Overduin et al., 2015).

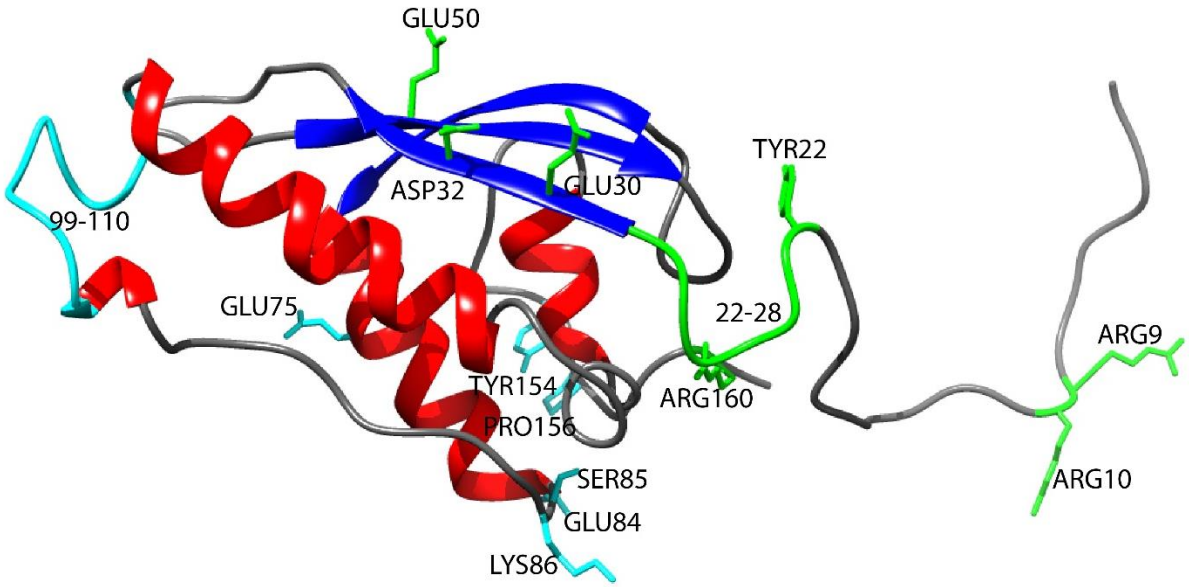

Figure 3.4 Model showing the identified residues in SNX3 important for the binding of VPS35.

Model of the NMR-resolved SNX3 structure from Overduin et al., 2015. The residues which, when mutated, caused a loss of association between SNX3 and VPS35 are shown in green. The residues which, when mutated, did not cause a dramatic loss of VPS35 associated are shown in blue. Note that the N- and C-termini of SNX3 are intrinsically disordered.

3.2.2 Heat repeat-domain containing SNX3-interactors associate independently of VPS35

Several proteins in the SNX3 interactome, including VPS35, contain a similar tertiary structure composed of a series of HEAT (Huntingtin, elongation factor 3, protein phosphatase 2A and TOR1) repeat domains (McGough et al., 2018). This raised the possibility that these interactors may bind to SNX3 through the same mechanism as VPS35. I therefore utilised the SNX3 variants which have severely perturbed VPS35 association and determined whether other HEAT-repeat containing SNX3-interactors could bind. Following transient transfection, into HEK293T cells, of GFP, GFP-SNX3 or

one of two mutant GFP-SNX3 variants (9,10 RR-AA and R160A) with perturbed VPS35 association, I performed a GFP-nanotrap experiment. I subsequently immuno-blotted for various HEAT repeat containing SNX3 interactors (MON2, GCN1, mTOR and ATM) **(Figure 3.5A)**. Although VPS35 and VPS26A of the retromer complex consistently lost association with the mutant GFP-SNX3 variants, the other interactors did not **(Figure 3.5B).** The mechanism of VPS35 association to SNX3 is therefore independent from other HEAT repeat domain-containing interactors.

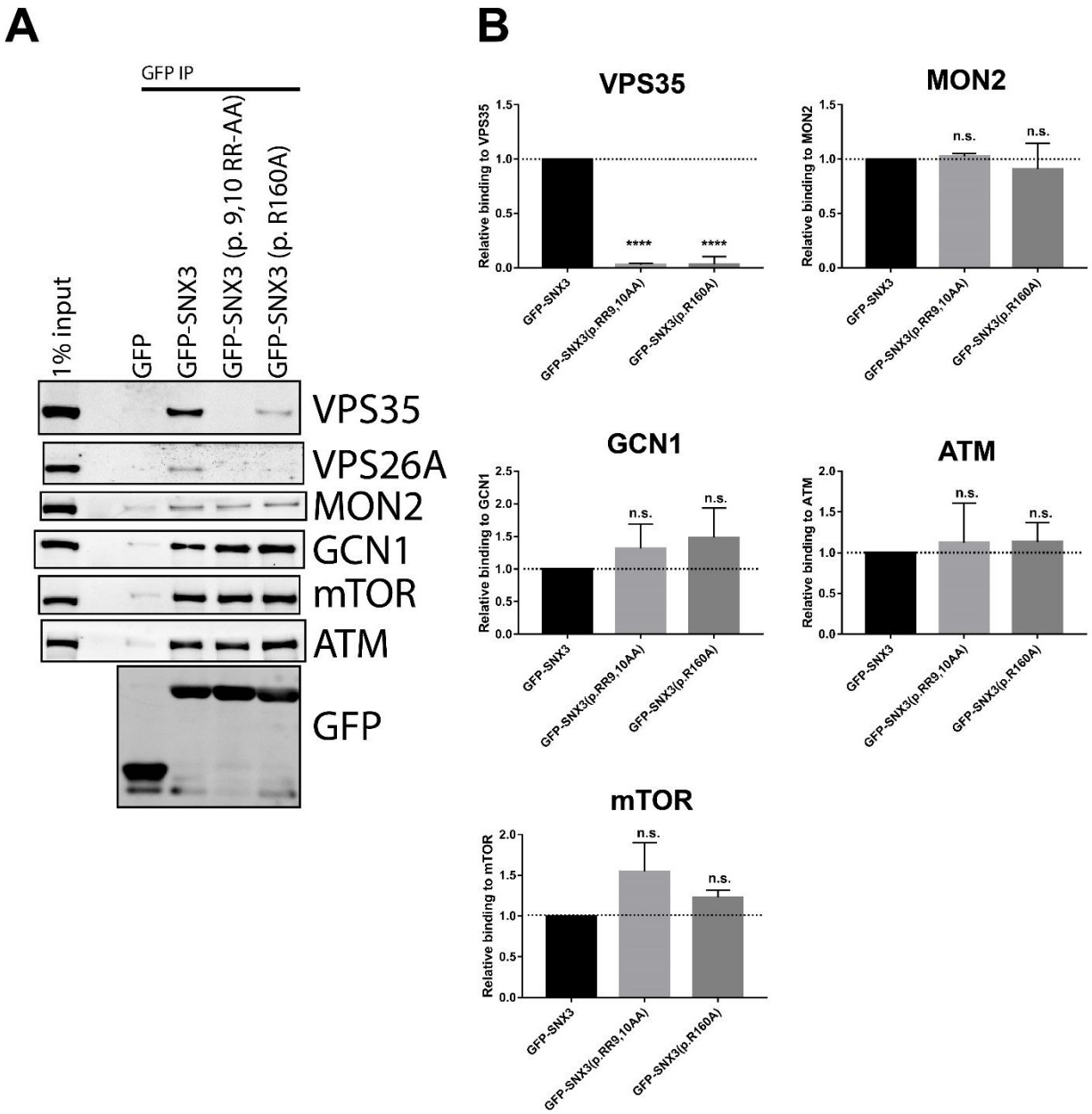

Figure 3.5 SNX3 can bind to various HEAT-repeat domain-containing proteins independently of its ability to bind to the retromer complex.

(A) HEK293T cells were transfected with the indicated GFP-SNX3 construct and subjected to a GFP trap. The immuno-precipitate was resolved using SDS-PAGE before immuno-blotting for

the indicated antibodies. **(B)** Quantification of the GFP-SNX3 constructs' ability to bind to VPS35, MON2, GCN1, mTOR and ATM. The binding is shown relative to the wild-type GFP-SNX3 construct. Data were analysed using a one-way ANOVA with a post-hoc Dunnetts test, comparing the mutant constructs to the wild-type; **** $p \geq 0.0001$..

3.2.3 The association between VPS35 and SNX3 is required for the secretion of Wnt morphogens in *C. elegans*

Having established point mutations in SNX3 which perturb VPS35 association, I wished to determine the functional importance of this interaction. The best characterised function of SNX3-retromer is the trafficking of Wntless, a Wnt chaperone (Banziger et al., 2006). Whether the physical interaction between SNX3 and VPS35 is required for Wntless retrieval, or whether these proteins act separately or sequentially, has never been explored.

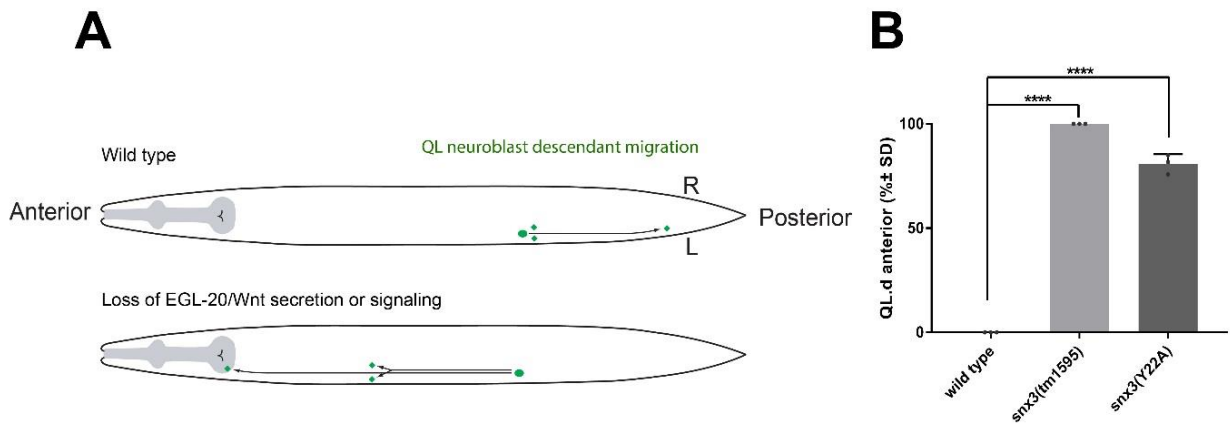

Figure 3.6 The SNX3:VPS35 interaction is necessary for Wnt secretion and morphogenic gradient formation.

(A) Schematic representation of the migration of the QL neuroblast descendants (QL.d) and the dependency of this migration on Wnt signalling. In wild type, the QL.d migrate to positions in the posterior part of the animal. In the absence of Wnt signalling, the QL.d migrate in the opposite, anterior, direction. **(B)** *C. elegans* CRISPR knock-in of snx-3(p.Y22A), which cannot bind to vps-35, causes a failure of the posterior migration of the QL neuroblast descendants. The percentage of *C. elegans* with an anterior migration of the QL.d are shown ± standard deviation. Significance was determined using a Student's t-test. *** $p < 0.0001$. Data from Dr Marco Betist.

To translate my *in vitro* biochemical data into an *in vivo* setting, I turned to a collaboration with the Rik Korswagen lab, who use *C. elegans* as a model to study Wnt signalling. In *C. elegans*, the EGL-20 (a Wnt homologue)-dependent migration of the QL neuroblast descendants (QL.d) is a well characterised assay for studying of Wnt

signalling defects (Maloof et al., 1999; Pan et al., 2008; Yang et al., 2008; Harterink et al., 2011). In wild-type *C. elegans*, the QL.d will migrate posteriorly. In a genetic context where EGL-20 cannot be secreted, such as in a snx-3 or vps-35 null *C. elegans*, or when there is a loss of EGL-20 signalling, the QL.d will migrate anteriorly **(Figure 3.6A)**. Building on my cell-culture based analysis of human SNX3 variants with perturbed VPS35 binding **(Figure 3.2)**, Dr Marco Betist generated *C. elegans* with CRISPR-mediated knock-in of snx-3(p.Y22A) and examined the migration of QL.d in these worms. The snx-3(p.Y22A) knock-in *C. elegans* had a 81 ± 4.7 % penetrant QL.d migration defect (n = 202) **(Figure 3.6B)**. This compares with snx-3 null *C. elegans* which have a fully penetrant QL.d migration defect and wild-type *C. elegans* which do not have a QL.d migration defect. This is the first evidence that the physical interaction between vps-35 and snx-3, and therefore assembly of the SNX3-retromer complex, is required for Wnt secretion and Wnt signalling.

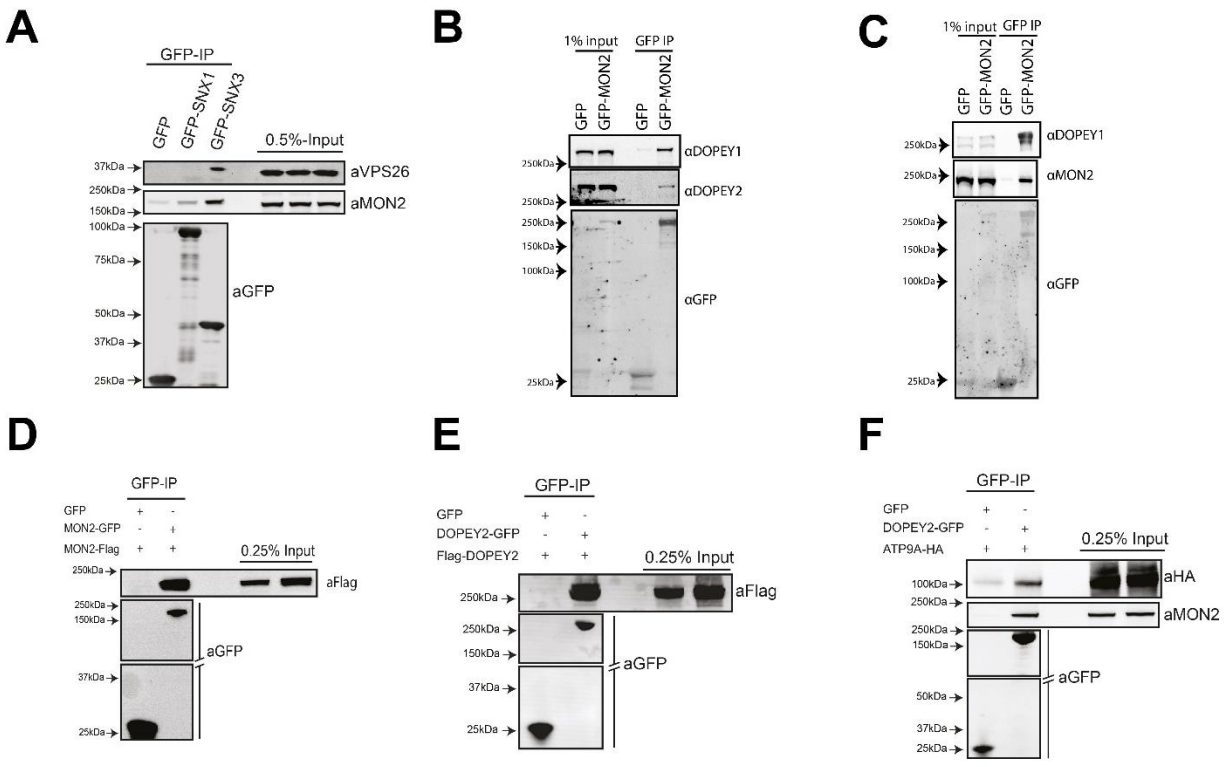

Figure 3.7 MON2, DOPEY1, DOPEY2 and ATP9A associate biochemically.

(A-F) HEK293T cells were transfected with the indicated construct and subjected to a GFP-trap. The immuno-lysates were then resolved using SDS-PAGE and immuno-blotted for the indicated antibodies. A, D, E and F were performed by Dr Ian McGough.

3.2.4 SNX3, but not SNX1, associates with MON2

The SNX3-retromer retrieval of Wntless is independent from the classic retromer-associated remodelling complex (the SNX-BAR complex) (Harterink et al., 2011; Zhang et al., 2011). One major interest in the generation of the SNX3 interactome was to identify potential membrane remodelling proteins. Two SNX3 interactome hits, MON2 and DOPEY2, have been shown in *S. cerevisiae* to interact with a putative phospholipid translocase, implicated in membrane remodelling (Hua and Graham, 2003; Wicky et al., 2004; Singer-Kruger et al., 2008; Barbosa et al., 2010). Dr Ian McGough therefore set up a GFP-trap immuno-precipitation experiment to compare the binding of MON2 to GFP-SNX3 and a member of SNX-BAR complex, GFP-SNX1 **(Figure 3.7A)**. As well as binding to the known SNX3-interactor, VPS26, SNX3 could immunoprecipitate endogenous MON2. The immunoprecipitation of MON2 was specific to SNX3 and therefore shows heterogeneity between SNX3-retromer and SNX-BAR-retromer.

3.2.5 MON2 and DOPEY2 share some features of their *S. cerevisiae* homologues

Very little is known about mammalian MON2 and DOPEY1/DOPEY2; however, there is some genetic and biochemical data from their yeast homologues. Mon2p and Dop1p (*S. cerevisiae* homologues of MON2 and DOPEY1/DOPEY2 respectively) have been shown to genetically and biochemically associate with each other (Efe et al., 2005; Gillingham et al., 2006; Barbosa et al., 2010). It is unknown whether their mammalian homologues do the same. To test this, I transfected GFP-tagged constructs into HEK293T cells followed by a GFP-trap experiment. GFP-MON2 could immuno-precipitate endogenous DOPEY1 and DOPEY2 **(Figure 3.7B)** and GFP-DOPEY2 could immuno-precipitate endogenous MON2 and endogenous DOPEY1 **(Figure 3.7C)**. The formation of a complex between MON2 and DOPEY1/DOPEY2 therefore seems to be conserved from yeast to humans.

Another feature of the *S. cerevisiae* proteins Mon2p and Dop1p, is their ability to form homomeric complexes, i.e. Mon2p can bind to Mon2p, and Dop1p can bind to Dop1p (Barbosa et al., 2010). To test whether this has been conserved in their mammalian homologues, Dr Ian McGough transiently transfected HEK293T cells and performed GFP-trap experiments. MON2-GFP could pull down Flag-tagged MON2 **(Figure 3.7D)**

and DOPEY2-GFP could pull-down Flag-tagged DOPEY2 **(Figure 3.7E)**. The divergence of Dop1p into the two human paralogues, DOPEY1 and DOPEY2, has not changed the ability of these proteins to associate with one another, as GFP-trap of DOPEY2-GFP could pull down endogenous DOPEY1 **(Figure 3.7C)**. The self-association properties of Mon2p and Dop1p are therefore conserved from yeast to humans.

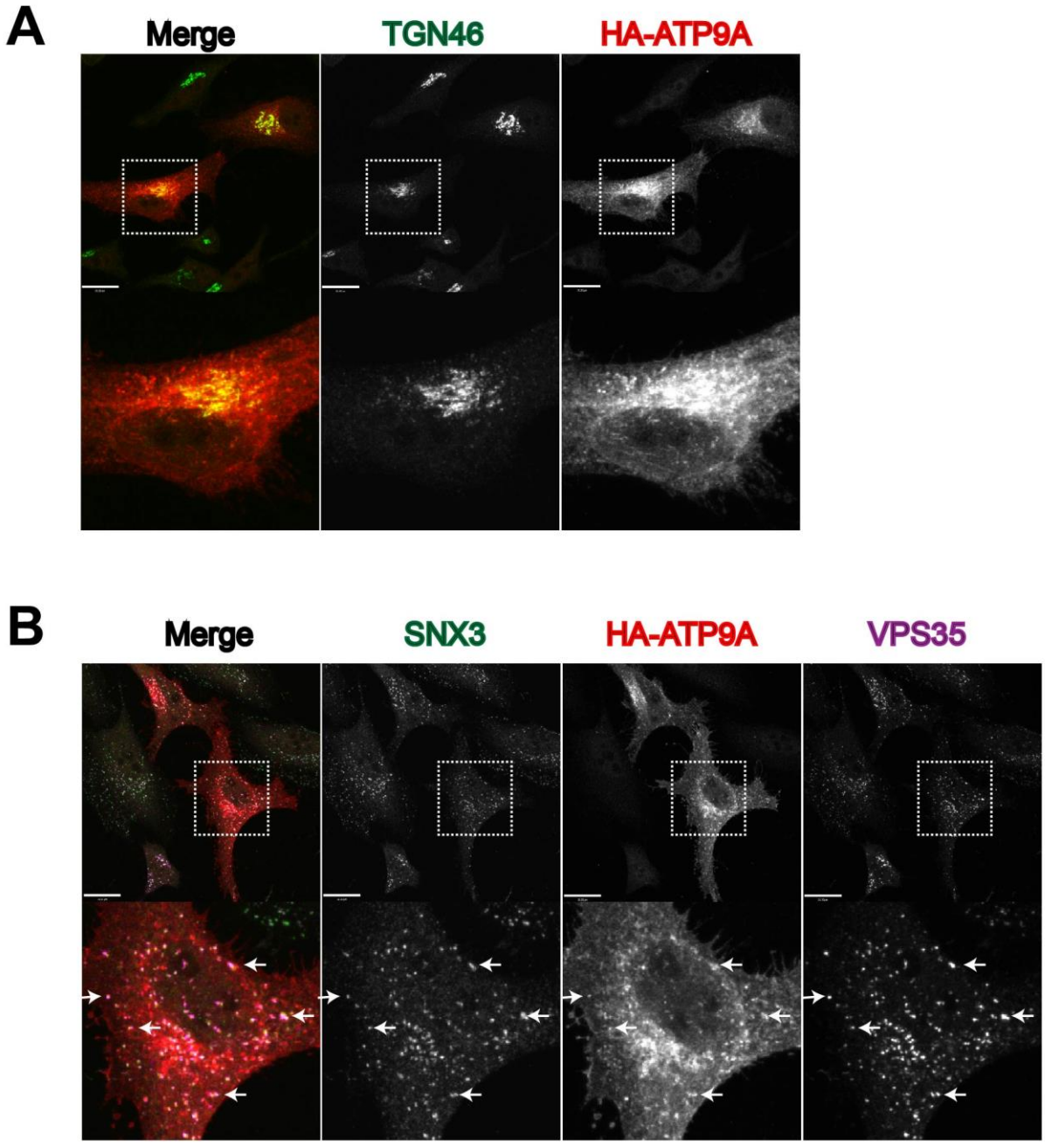

Figure 3.8 ATP9A localises to the TGN and SNX3-retromer positive endosomes.

(A) HeLa cells were transfected with ATP9A-HA and stained for HA and endogenous TGN46. Cells were imaged on a confocal microscope. Scale bar indicates 19 µm. **(B)** HeLa cells were transfected with ATP9A-HA and stained for HA and endogenous SNX3 and VPS35. Cells were imaged on a confocal microscope. Scale bar indicates 19 µm.

Mon2p and Dop1p interact genetically and biochemically with Neo1p, a putative aminophospholipid translocase (flippase) (Hua and Graham, 2003; Wicky et al., 2004; Singer-Kruger et al., 2008; Barbosa et al., 2010). Neo1p has two homologues in humans: ATP9A and ATP9B. ATP9A localises to the TGN and endosomal network whereas ATP9B localizes just to the TGN (Takatsu et al., 2011; Tanaka et al., 2016). To test whether ATP9A (the endosome-localised paralogue) could bind to the MON2-DOPEY1/2 complex, Dr Ian McGough co-expressed DOPEY2-GFP and ATP9A-HA (an endogenous ATP9A antibody could not be validated) in HEK293T cells and performed a GFP-trap experiment. ATP9A-HA and endogenous MON2 could be pulled down by DOPEY2-GFP **(Figure 3.7F)**. The formation of a Mon2p:Dop1p:Neo1p complex therefore seems to be conserved from yeast to humans.

3.2.6 The MON2:DOPEY:ATP9A complex co-localise with SNX3-retromer and Wntless

To examine the localisation of MON2, DOPEY2 and ATP9A in cells, I turned to confocal microscopy. Following the transient transfection of ATP9A-HA into HeLa cells, I observed that ATP9A localised to the TGN-marker TGN46 **(Figure 3.8A)** and to endogenous SNX3-retromer positive puncta **(Figure 3.8B)**. Dr Ian McGough also found extensive co-localisation of co-expressed ATP9A-HA, DOPEY2-GFP and MON2-Flag when transfected into HeLa cells **(Figure 3.9A)**.

Together, the biochemical and imaging-based data raise the possibility that MON2, DOPEY2 and ATP9A may support SNX3-retromer-mediated cargo-retrieval. We therefore tested whether the SNX3-retromer cargo protein Wntless co-localised with ATP9A and SNX3. To this end, Dr Ian McGough transiently expressed ATP9A-HA and Wntless-mCherry and stained for endogenous SNX3 in HeLa cells **(Figure 3.9B).** ATP9A co-localises with Wntless and SNX3-enriched endosomes. SNX3-retromer dependent retrieval of Wntless therefore seems to be taking place on endosomes enriched for ATP9A.

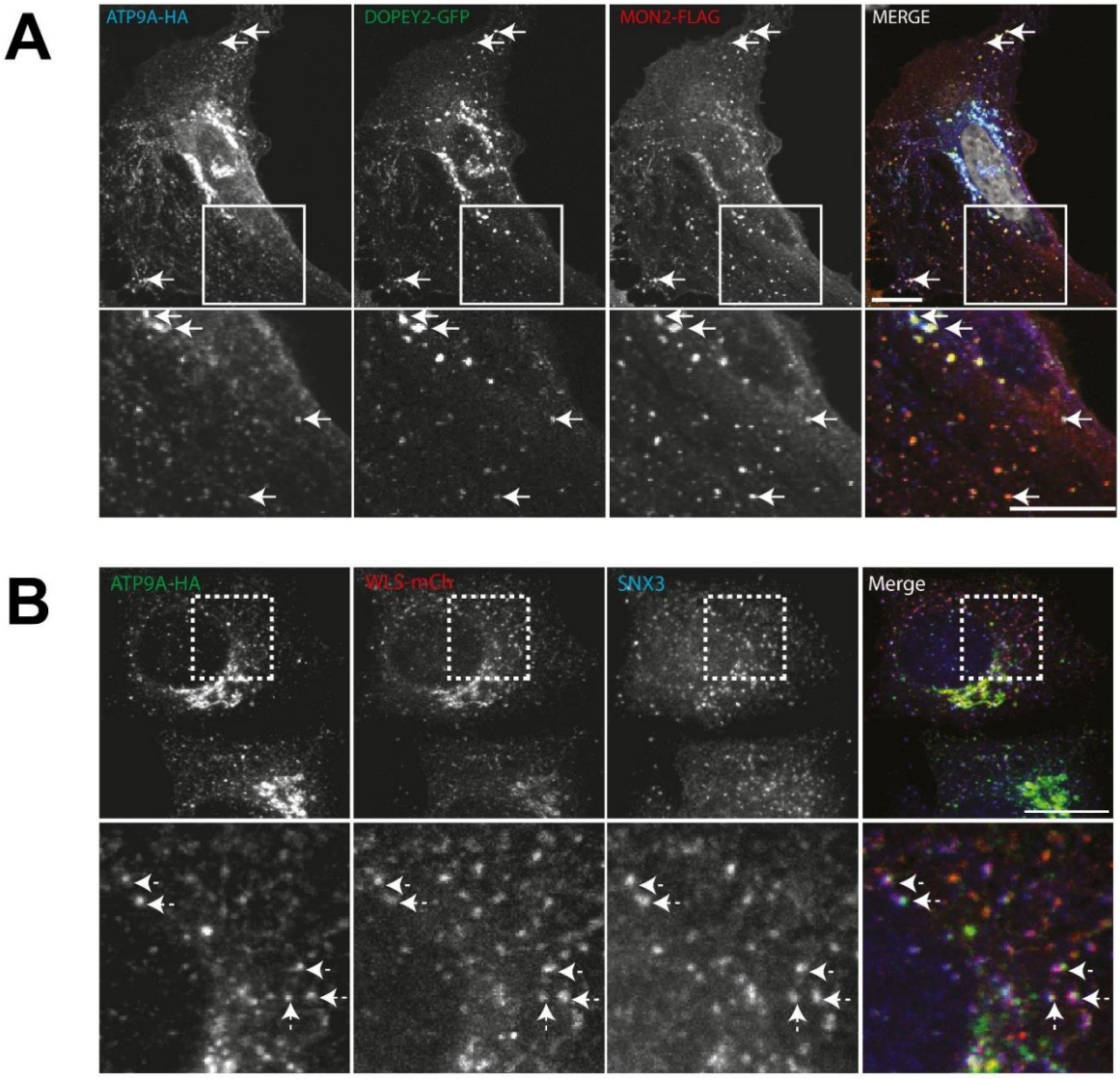

Figure 3.9 ATP9A colocalises with MON2, DOPEY2 and Wntless.

(A) Hela cells were transfected with ATP9A-HA, DOPEY2-GFP and MON2-Flag and imaged on a confocal microscope. Data from Dr Ian McGough. **(B)** Hela cells were transfected with ATP9A-HA and Wntless(WLS)-mCherry and stained for endogenous SNX3. Cells were imaged on a confocal microscope. Scale bars represents 10 μm. Data from Dr Ian McGough.

3.2.7 Establishment of an *in vitro* cell culture-based system to study Wntless retrieval

MON2, DOPEY1/2 and ATP9A associate biochemically and co-localise in cells with SNX3 and Wntless. These data raise the intriguing possibility that the MON2:DOPEY1/2:ATP9A complex may aid the retrieval of Wntless from the endosomes to the TGN. I therefore wanted to perform functional biochemistry experiments to test whether this is the case. To do this, I decided to create a cell-line

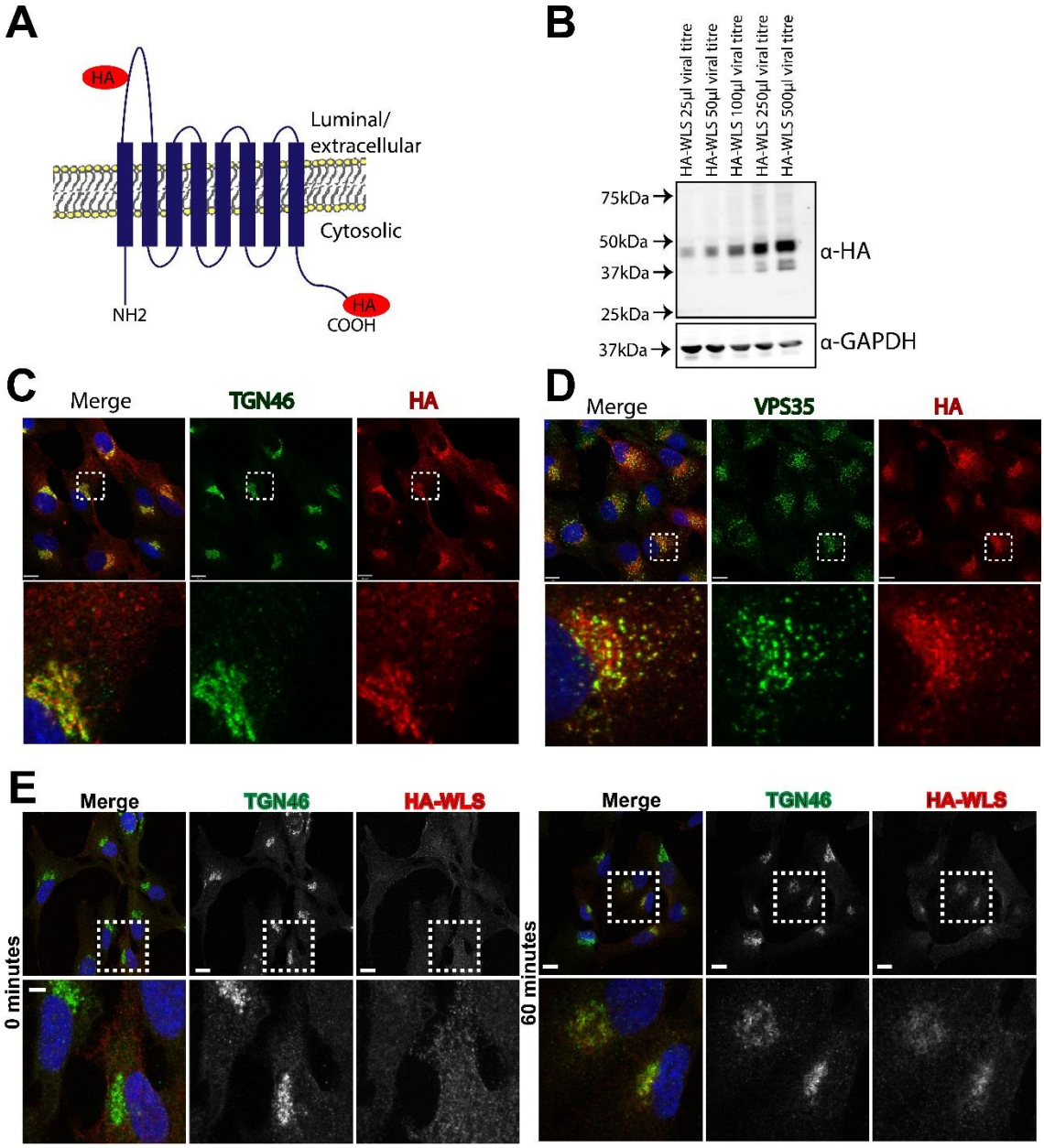

Figure 3.10 Validation of the HA-WLS construct.

(A) Schematic of the HA-WLS (HA-Wntless) construct. **(B)** RPE-1 cells, transduced with various titres of lentivirus to express HA-WLS, were lysed and immuno-blotted for the indicated antibodies. RPE-1 cells, transduced with HA-WLS, were stained for HA and endogenous: **(C)** TGN46 and **(D)** VPS35. Cells were imaged on a confocal microscope; the scale bar indicates 11 µm. **(E)** RPE-1 cells were transduced with HA-WLS. The HA-tag was then chased from the cell surface to the TGN. The cells were fixed at the indicated time points following incubation with an α-HA primary antibody to label cell-surface localised HA-WLS. Cells were imaged on a confocal microscope; the scale bar indicates 11 µm.

stably expressing a Wntless construct. I utilised a Wntless construct, recently published by the Von Zastrow lab (Varandas et al., 2016), in which the ER localisation signal is

masked using an HA-tag to optimise trafficking of the complex through the endosomal system (HA-WLS) **(Figure 3.10A)**.

To produce a stable population of HA-Wntless in a cell line, I cloned HA-Wntless into the XLG3 lentiviral vector and produced lentivirus. I then transduced RPE-1 cells to express HA-Wntless with various titres of lentivirus and tested the expression of HA-Wntless using western blotting **(Figure 3.10B**). I selected the 250 µl titre as it gave a strong signal by western blotting and showed extensive co-localisation between the TGN marker TGN46 **(Figure 3.10C)** and VPS35-positive endosomes **(Figure 3.10D)**.

At the cell surface, Wntless is endocytosed into the endosomes through an AP-2 and clathrin-dependant mechanism (Port et al., 2008; Yang et al., 2008; Gasnereau et al., 2011) and then retrieved to the Golgi via SNX3-retromer (Belenkaya et al., 2008; Franch-Marro et al., 2008; Pan et al., 2008; Yang et al., 2008; Harterink et al., 2011; Zhang et al., 2011). I therefore tested the functionality of the HA-Wntless construct's cell surface to Golgi trafficking. By labelling the cell surface with primary antibodies raised against the HA-tag, which bind to the HA-Wntless at the cell surface, I could follow the internalisation of the HA-Wntless. Consistent with functional HA-Wntless cycling between the Golgi and the cell surface, the cell-surface labelled HA-Wntless could be chased to the TGN after a 60-minute time point **(Figure 3.10E)**.

The endosome-to-Golgi retrieval of Wntless away from lysosomal degradation (and therefore the whole-cell proteins levels of Wntless) is dependent on SNX3-retromer but not the SNX-BAR complex (Harterink et al., 2011; Zhang et al., 2011). To further validate the HA-Wntless expressing RPE-1 line, I examined whether the whole-cell protein levels of HA-Wntless is dependent on the SNX3-retromer, rather than the SNX-BAR-retromer or the SNX27-retromer **(Figure 3.11A)**. The whole-cell level of HA-Wntless was significantly decreased following the suppression of VPS35 or SNX3 but not following SNX1/SNX2 or SNX27 suppression **(Figure 3.11B)**. To examine whether the decrease in HA-Wntless levels were due to lysosomal degradation, I treated the cells with Bafilomycin A1, a lysosomal acidification inhibitor (Yoshimori et al., 1991), for 16 hours prior to cell lysis **(Figure 3.11C)**. Bafilomycin A1 treatment rescued the whole-cell levels of HA-Wntless following SNX3 or retromer suppression **(Figure 3.11D)**. Furthermore, when HA-Wntless was transfected into VPS35-knockout HeLa cells, it co-localised with the late endosomal/ lysosomal marker LAMP1; however, when transfected into VPS35-knockout HeLa cells rescued with VPS35-GFP, its localisation was reminiscent of the TGN and endosomes **(Figure 3.11E)** which is similar to its

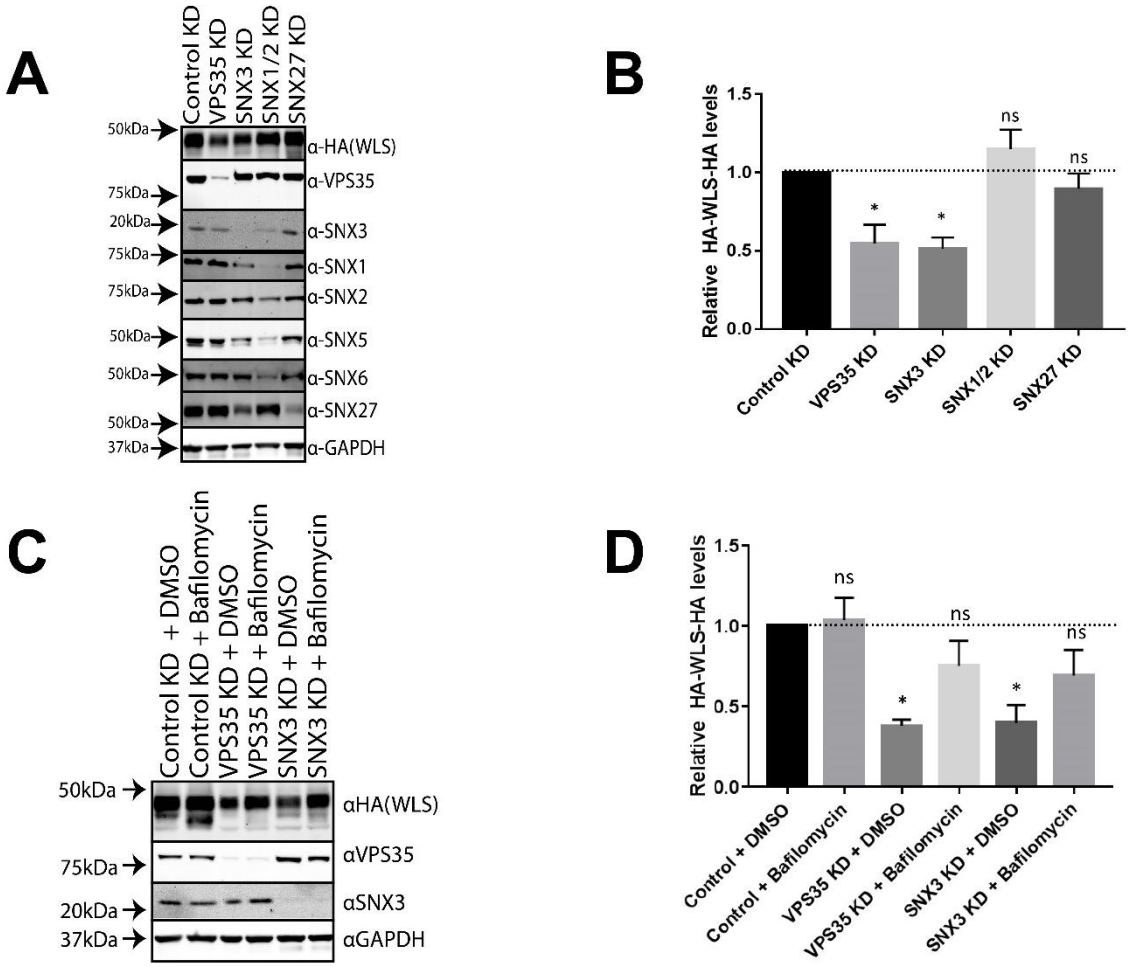
A
Control KD
VPS35 KD
SNX3 KD
SNX1/2 KD
SNX27 KD
50kDa
α-HA(WLS)
α-VPS35
75kDa
20kDa
α-SNX3
75kDa
α-SNX1
75kDa
α-SNX2
50kDa
α-SNX5
50kDa
α-SNX6
50kDa
α-SNX27
37kDa
α-GAPDH
B
Relative HA-WLS-HA levels
1.5
1.0
0.5
0.0
ns
ns
*
*
Control KD
VPS35 KD
SNX3 KD
SNX1/2 KD
SNX27 KD
C
Control KD + DMSO
Control KD + Bafilomycin
VPS35 KD + DMSO
VPS35 KD + Bafilomycin
SNX3 KD + DMSO
SNX3 KD + Bafilomycin
50kDa
αHA(WLS)
75kDa
αVPS35
20kDa
αSNX3
37kDa
αGAPDH
D
Relative HA-WLS-HA levels
1.5
1.0
0.5
0.0
ns
ns
ns
*
*
Control + DMSO
Control + Bafilomycin
VPS35 KD + DMSO
VPS35 KD + Bafilomycin
SNX3 KD + DMSO
SNX3 KD + Bafilomycin
E
Merge
VPS35
HA-WLS
LAMP1
VPS35 KO
VPS35 KO + VPS35-GFP

Figure 3.11 HA-WLS whole-cell levels are dependent on SNX3-retromer-mediated retrieval away from lysosomal degradation.

(A) RPE-1 cells, transduced with HA-Wntless(WLS), were suppressed with siRNA targeting the indicated protein(s). Cells were lysed, the lysates resolved using SDS-PAGE and immuno-blotted using the indicated antibodies. **(B and D)** The intensities of the fluorescent HA-WLS bands were quantified using a Licor Odyssey scanner. Data were normalised to the non-targeting control (with DMSO in D). Data shows the mean of 3 independent experiments ± s.e.m. Significance was determined by a one-way ANOVA with a post-hoc Dunnett's test comparing experimental conditions to the control knock-down. **(C)** Following suppression with non-targeting siRNA, VPS35 siRNA or SNX3 siRNA, RPE-1 cells, stably expressing HA-WLS, were treated with 100nM Bafilomycin or DMSO for 16 hours prior to cell lysis. The lysates were then resolved using SDS-PAGE and immuno-blotted with the indicated antibodies. **(E)** VPS35 knockout HeLa cells, supplied from Dr Florian Steinberg, were transduced with VPS35-GFP and transfected with HA-WLS. Once adhered onto coverslips, the cells were fixed with 4% paraformaldehyde and immuno-stained for HA, and endogenous LAMP1. Cells were imaged using a confocal microscope. The scale bar indicates 33 µm.

normal distribution **(Figure 3.10C-D)**. These data validate this *in vitro* cell culture-based system as a tool to study the endosomal-TGN retrieval of Wntless.

3.2.8 The retrieval of HA-Wntless is dependent on MON2 and ATP9A

Having validated the *in vitro* cell culture-based system to examine Wntless retrieval, I then examined whether MON2, DOPEY1/2 and ATP9A have a role in the retrieval of Wntless. I firstly examined whether MON2, DOPEY1, DOPEY2 or DOPEY1+DOPEY2 suppression would phenocopy VPS35 suppression in terms of decreasing the whole-cell levels of HA-Wntless **(Figure 3.12A)**. Although MON2 suppression caused a similar decrease in HA-Wntless levels as VPS35 suppression, knocking down DOPEY1, DOPEY2 or a combination of DOPEY1 and DOPEY2 did not **(Figure 3.12B)**. I then examined whether the decrease in HA-Wntless levels following MON2 suppression was due to lysosomal degradation **(Figure 3.12C)**. Inhibiting lysosomal acidification through Bafilomycin A1 increased the levels of HA-Wntless following MON2 knockdown compared to the DMSO-treated control, suggesting that the decrease in HA-Wntless levels following MON2 suppression is due to lysosomal degradation **(Figure 3.12D)**.

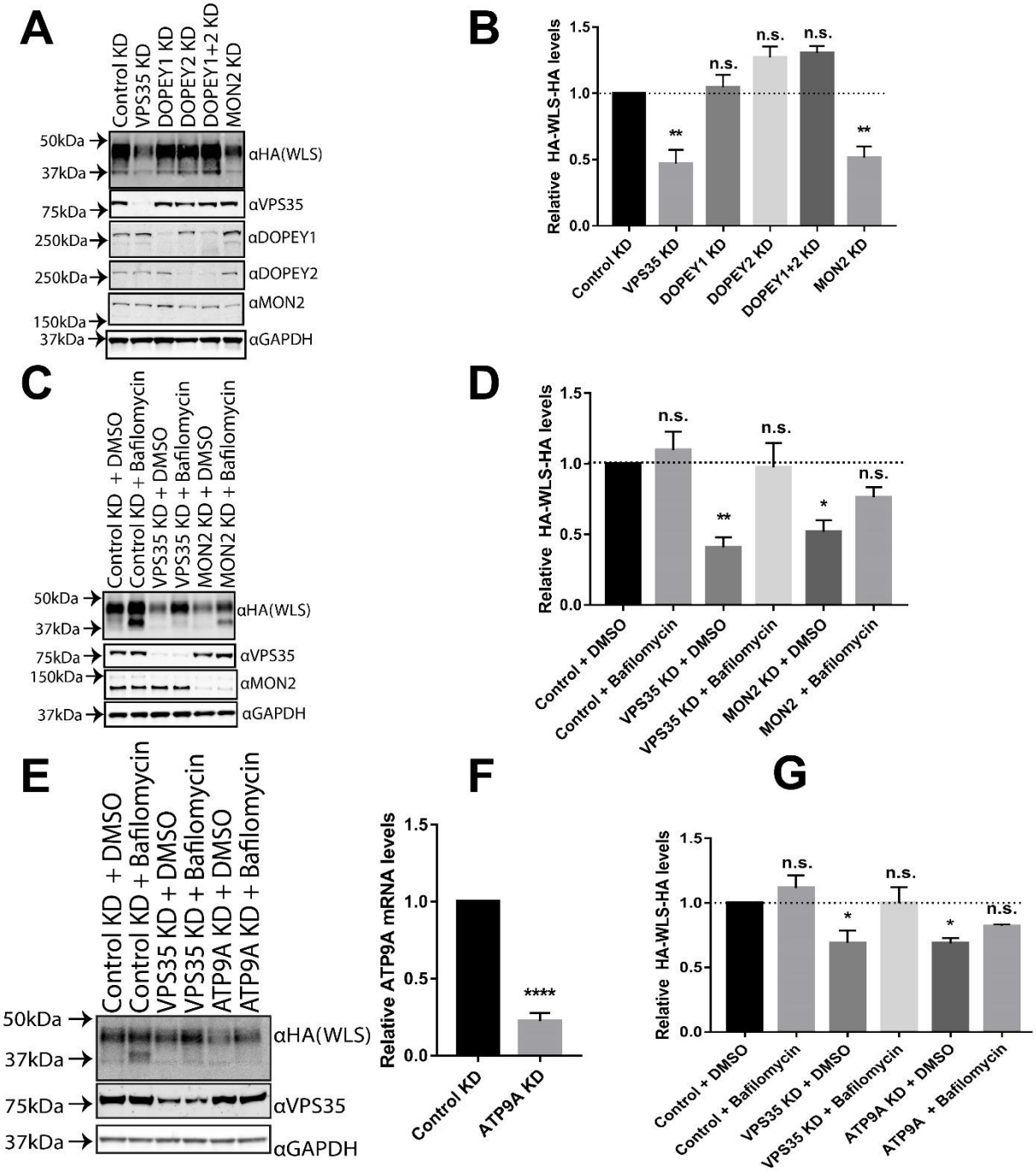

Figure 3.12 Inhibition of MON2 or ATP9A, but not DOPEY1/DOPEY2, cause the whole-cell level decrease of HA-WLS due to lysosomal degradation.

(A) RPE-1 cells, transduced with HA-Wntless(WLS), were suppressed with siRNA targeting the indicated protein(s). Cells were lysed, the lysates resolved using SDS-PAGE and immuno-blotted using the indicated antibodies. **(B, D and G)** The intensities of the fluorescent HA-WLS bands were quantified using a Licor Odyssey scanner. Data were first normalised to GAPDH before normalisation to the non-targeting control (with DMSO in D and G). Data is a mean from 3 (or 5 in G) individual experiments ± s.e.m. Significance was determined by a one-way ANOVA with a post-hoc Dunnett's test comparing experimental conditions to the control knock-down; *p ≤ 0.05; **p ≤ 0.01. **(C and E)** Following suppression with the indicated siRNAs, RPE-1 cells, stably expressing HA-WLS, were treated with 100nM Bafilomycin or DMSO for 16 hours prior to cell lysis. The lysates were then resolved using SDS-PAGE and immuno-blotted with the

indicated antibodies. **(F)** Knock-down of ATP9A was confirmed through RT-qPCR. Significance was determined using a student's t-test. Error bars indicate standard error; **** $p \leq 0.0001$.

I then examined the role of ATP9A in Wntless recycling via RNAi-mediated suppression **(Figure 3.12E)**. As no endogenous antibody for ATP9A could be verified, I used qRT-PCR to confirm an 80% suppression of ATP9A **(Figure 3.12F)**. ATP9A suppression phenocopies VPS35 suppression in terms of the decrease in the whole-cell levels of HA-Wntless **(Figure 3.12G)**. Furthermore, the inhibition of lysosomal acidification increased the levels of HA-Wntless compared to the DMSO-treated control **(Figure 3.12G).** The levels of HA-Wntless are therefore dependent on MON2 and ATP9A proteins, but not DOPEY1/2, in this *in vitro* cell culture system.

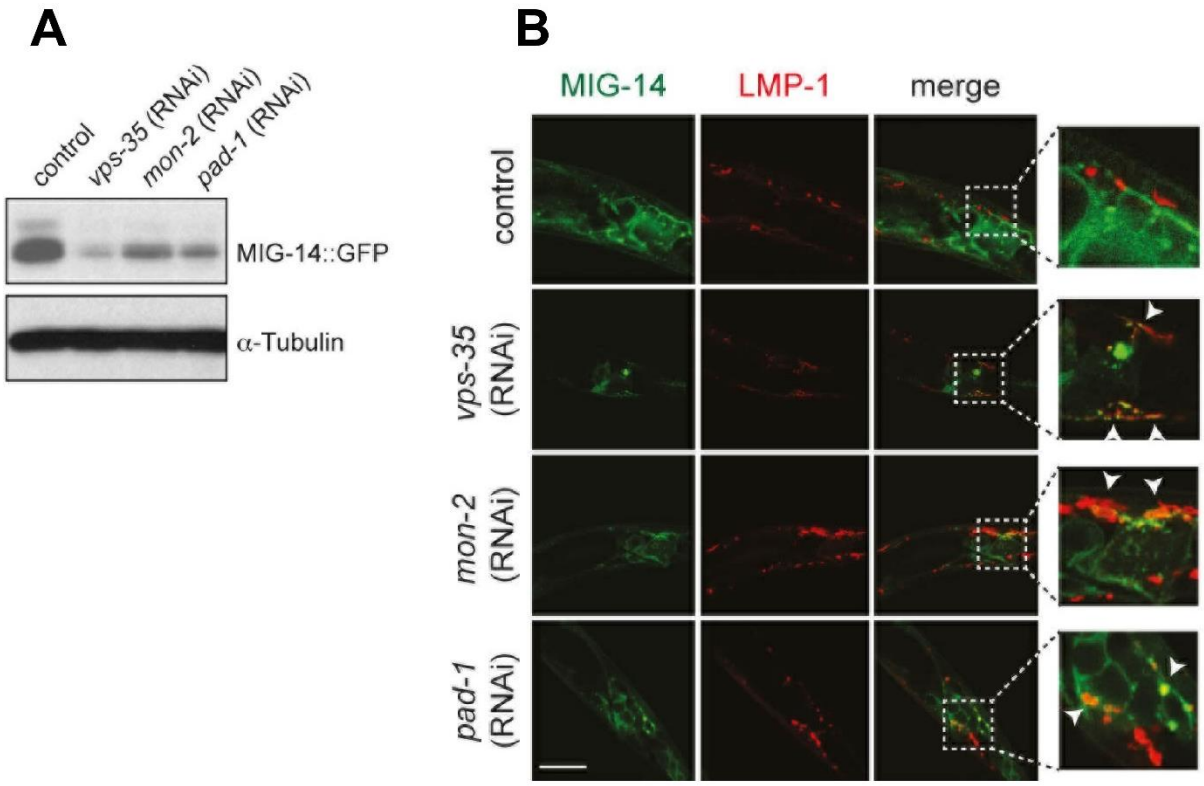

Figure 3.13 Inhibition of vps-35, mon-2 or pad-1 (DOPEY orthologue) causes a whole-cell level decrease of MIG-14 (Wntless) and its colocalisation with late endosomes/lysosomes in *C. elegans* L1 larvae.

(A) *C. elegans*, endogenously expressing MIG-14::GFP (huSi2), were treated with RNAi targeting vps-35, mon-2, pad-1 or non-targeting RNAi. The proteins were then resolved on an SDS-PAGE gel and immunoblotted for GFP or tubulin. **(B)** *C. elegans* L1 larvae were treated with the indicated RNAi and immuno-stained for MIG-14::GFP and the late endosomal and lysosomal marker LMP-1::mCherry. Arrows indicate colocalisation. The tail area is shown; anterior is left and dorsal is up. Images were taken on a confocal microscope and the scale bar is 10 µm. Data in this figure was collected by Dr Reinoud de Groot.

3.2.9 RNAi of *mon-2 and pad-1* cause a loss of *mig-14* levels and an EGL-20 secretion defect in *C. elegans*

Having presented biochemical evidence in a mammalian cell culture-based system that Wntless retrieval is dependent on MON2, but not DOPEY1/DOPEY2, we wanted to translate these finding into an *in vivo* setting. We therefore returned to the *C. elegans* model to study Wnt signalling *in vivo* (all further *C. elegans* experiments were performed by Dr Reinoud de Groot)*. C. elegans* were systemically fed dsRNA to suppress the orthologues of VPS35, MON2 and DOPEY1/DOPEY2 (vps-35, mon-2 and pad-1 respectively). Systemic knockdown of these proteins caused a decrease in the total levels of GFP-fused MIG-14 (the *C. elegans* orthologue of Wntless), as shown through immunoblotting for GFP **(Figure 3.13A)**. Furthermore, suppressing vps-35, mon-2 or pad-1 caused MIG-14 to co-localise with the late endosomal/lysosomal marker LMP-1 **(Figure 3.13B).** These data show that mon-2 and pad-1 are required for the maintenance of MIG-14 levels *in vivo*. This contrasts with the mammalian orthologues of pad-1 (DOPEY1/2), which, at least in my *in vitro* model of Wntless retrieval, does not cause a decrease in HA-Wntless levels at the level of suppression I achieved using siRNA **(Figure 3.12A)**.

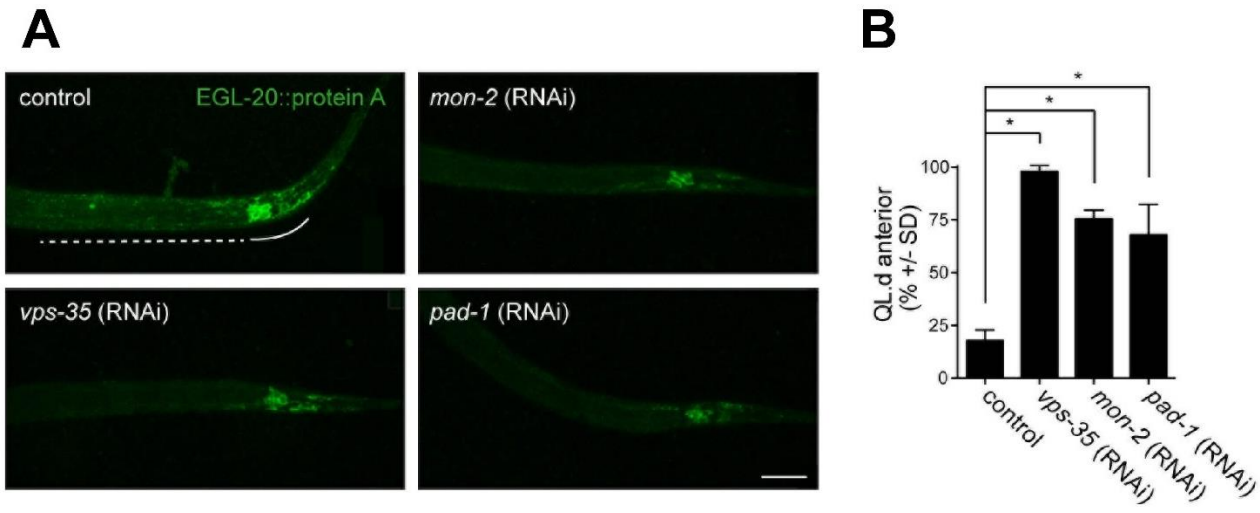

Figure 3.14 Inhibition of vps-35, mon-2 or pad-1 (DOPEY orthologue) causes a loss of the EGL-20 (Wnt) gradient and a perturbation of the posterior migration of QL neuroblast decedents.

(A) *C. elegans* L1 larvae were treated with RNAi targeting vps-35, mon-2, pad-1 or non-targeting RNAi were immuno-stained for EGL-20::protA. The EGL-20 producing cells are indicated with a solid line and the punctate gradient that is formed by EGL-20::protA is indicated with a dashed line. Anterior is left and dorsal is up. Images were obtained on a confocal microscope; scale bar is 10 µm. **(B)** Systemic knock-down of mon-2 or pad-1 interferes with the EGL-20/Wnt dependent posterior migration of the QL neuroblast descendants (QL.d) in a vps-29(tm1320) sensitized genetic background. The percentage of animals with anteriorly displaced

QL.d is shown (data are presented as mean +/- SD and include results from 4 experiments, with n≥25 per experiment) *p=1.158 x 10-6 for vps-35 RNAi, *p=1.44 x 10-5 for mon-2 RNAi and *p=0.0024 for pad-1 RNAi (Student's t-test). Data in this figure was collected by Dr Reinoud de Groot.

During *C. elegans* development, EGL-20 (a Wnt orthologue) is secreted in the posterior of the worm from Wnt secreting cells; this secretion forms a morphogenic gradient along the worm **(Figure 3.14A)** (Maloof et al., 1999). Suppressing vps-35 prevented EGL-20 secretion from the Wnt secreting cells and caused a loss of the EGL-20 gradient **(Figure 3.14A)**. Mon-2 and pad-1 suppression phenocopied vps-35 suppression in terms of the EGL-20 secretion defect **(Figure 3.14A)**. The secretion of MIG-14 is therefore dependent on mon-2 and pad-1 *in vivo*.

During *C. elegans* development, the QL. neuroblast descendants (QL.d) migrate towards the posterior of the worm, due to signalling cascades initiated by EGL-20 **(Figure 3.6A)**; this contrasts with the QR. neuroblast descendants, which do not encounter EGL-20 and migrate anteriorly (Lorenowicz et al., 2014). Reinoud de Groot took advantage of this EGL-20-dependent posterior migration of the QL.ds as an assay for Wnt secretion deficits. As QL.d migration is relatively insensitive to EGL-20 and the suppressions of mon-2 and pad-1 are only partial, a sensitised background (vps-29 mutant) was used to assay the effects of mon-2 and pad-1 suppression. Vps-35, mon-2 and pad-1 suppression caused a significant increase in the anterior migration of the QL.ds **(Figure 3.14B)**. These data show that that vps-35, mon-2 and pad-1 are necessary for EGL-20 secretion and the EGL-20-dependant posterior migration of the QL. neuroblast descendants.

3.2.10 Tat-5 flippase activity is necessary for the EGL-20-dependent posterior migration of the QL. neuroblast descendants in *C. elegans*

The suppression of tat-5 (the *C. elegans* ATP9A orthologue) *in vivo* is lethal (Wehman et al., 2011). To suppress tat-5 in *C. elegans*, the RNAi against tat-5 was expressed using a MIG-14 promoter (to suppress tat-5 only in the Wnt secreting cells). This method of suppression causes a poorer knock-down of the protein of interest compared to systemic feeding of dsRNA (personal communication from Professor Rik Korswagen), as shown by the lower penetrance of the QL.d anterior-migration phenotype when vps-35 suppressed using this method **(Figure 3.15A)** compared to

systemic feeding of dsRNA targeting vps-35 **(Figure 3.14B)**. Expression of the RNAi targeting tat-5 using the MIG-14 promotor resulted in an increase in the anterior migration of the QL.d, similar to what is seen with vps-35 suppression using the same method **(Figure 3.15B)**.

The *C. elegans* data presented so far indicate that mon-2, pad-1 or tat-5 suppression phenocopy vps-35 suppression in terms of their effect on the migration of QL.d. I have not yet presented any data which would indicate that the flippase activity of ATP9A/tat-5 is important for Wntless/MIG-14 retrieval and Wnt/EGL-20 secretion. The ability of aminophospholipids to flip lipids is dependent on the activity of the protein's ATPase cycle (Lenoir et al., 2009). A yeast Drs2(p.E342Q) mutation blocks its ATPase cycle at the E_2P conformation and inhibits phospholipid translocation across the lipid bilayer (Lenoir et al., 2009; Zhou and Graham, 2009). Dr Reinoud de Groot created a construct which would express the equivalent mutation **(Figure 3.15C)**, tat-5(E246Q), and overexpressed it under a heatshock promotor. This resulted in the increase in the QL.d migration defect **(Figure 3.15D)**. These data indicate that the ATPase-cycle and therefore the flippase activity of tat-5 is important for Wnt secretion *in vivo*.

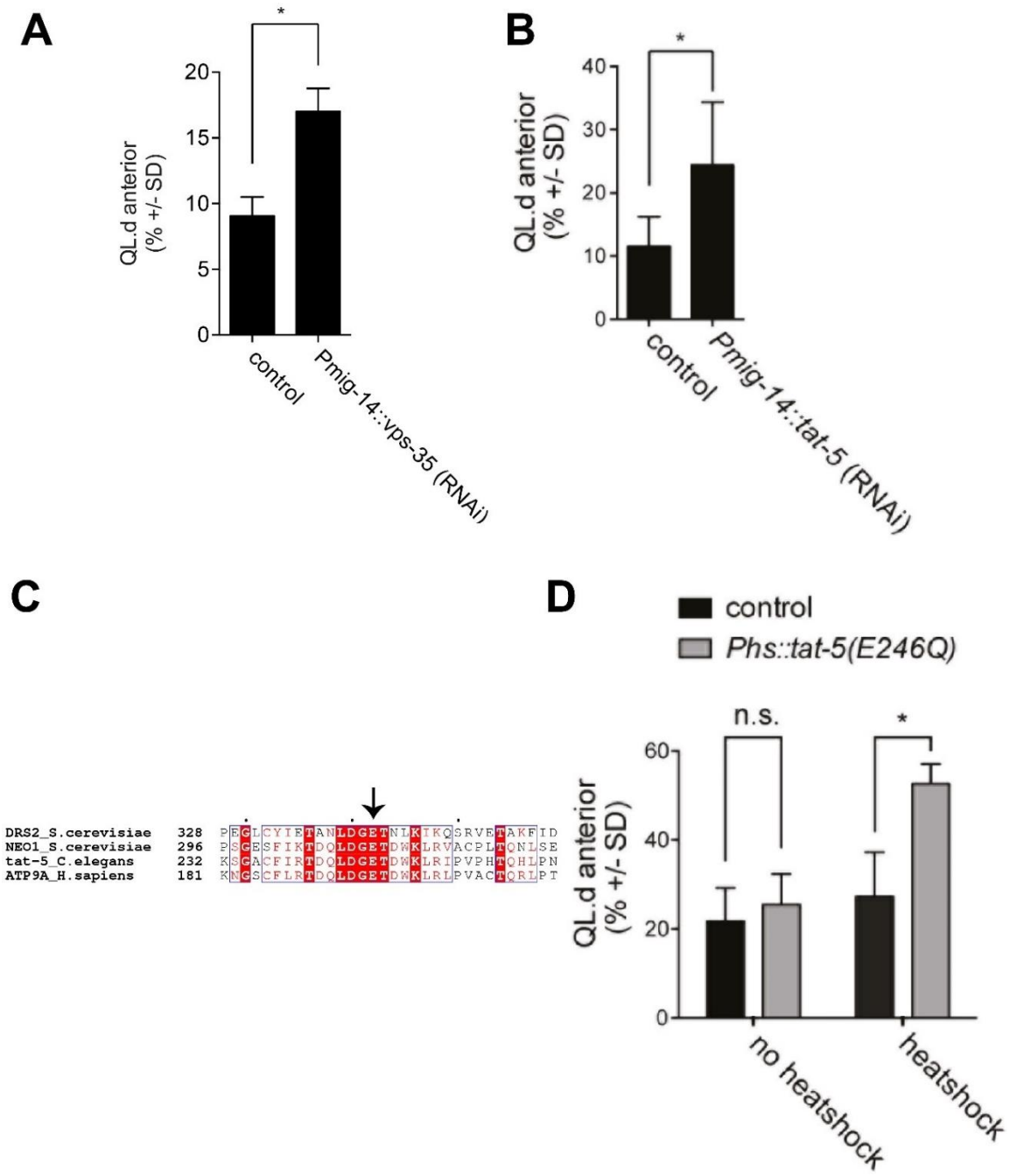

Figure 3.15 Suppressing tat-5 (ATP9A homologue), or inhibiting the ATPase activity of tat-5, perturbs the posterior migration of the QL neuroblast descendants in L1 larvae.

Tissue specific RNAi of vps-35 **(Ai)** or tat-5 **(Aii)** in Wnt producing cells (Pmig-14::tat-5 RNAi) in a *C. elegans* vps-29(tm1320) sensitized mutant background. The percentage of animals with anteriorly displaced QL.d is shown (data are presented as mean +/- SD and include results from 7 experiments, n≥24 per experiment) *p=0.013 (Student's t-test). **(Bi)** Sequence alignment of Drs2p with Neo1p homologues highlighting the conserved catalytic glutamic acid residue essential for ATPase activity. **(Bii)** Overexpression of catalytically inactive TAT-5(E246Q) in a vps-29(tm1320) sensitized mutant background. The percentage of animals with anteriorly displaced QL.d is shown (data are presented as mean +/- SD and include results from 3 experiments, n≥30 per experiment) *p=0.0089 (Student's t-test). Data in this figure was collected by Dr Reinoud de Groot.

3.3 Discussion

3.3.1 The SNX3-retromer binding interface

Previous work indicated that SNX3 associates with the retromer complex through the direct association with VPS35 (Harterink et al., 2011; Zhang et al., 2011; Vardarajan et al., 2012; Harrison et al., 2014b). To extend these findings, I undertook a biochemical screen, informed through a bioinformatic sequence alignment of similar PX-only sorting nexins, to identify candidate residues within SNX3 which may be important for retromer association. This approach identified several mutations of highly evolutionary-conserved residues within the termini of SNX3, as well as its anti-parallel β-sheet, which abrogate SNX3-retromer association, informing the mechanism of this association **(Figure 3.4)**.

Following my identification of the critical SNX3 residues essential for retromer association, a crystal structure of SNX3 bound to a VPS26/VPS35 interface was published (Lucas et al., 2016). This structure revealed that SNX3 directly associates not only with VPS35, but also to VPS26A; this induces a conformational change in VPS26A revealing a cargo-binding pocket (see section **1.4.1.2.1**) (Tabuchi et al., 2010; Lucas et al., 2016). Most of the residues I identified to be critical for retromer binding, when highlighted in the Lucas et al., (2016) structure, were located on the SNX3-retromer interface, therefore validating my results **(Figure 3.16)**. However, the Lucas et al., (2016) crystal structure reveals no interaction between the C-terminus of SNX3 and retromer. This contrasts with my findings, which identified that the C-terminal SNX3 residues mutations, Y154A and P156A, causes a partial loss of VPS35 association and most strikingly, R160A, which severely perturbs retromer binding **(Figure 3.2)**. The Lucas et al., (2016) crystal structure utilises a non-canonical SNX3 isoform lacking the final 3 amino acids (K158, I159 and R160). It may be the case that a crystal structure formed using full-length SNX3 may bind to retromer in a different conformation, with both termini of SNX3 engaging with retromer. Although the crystal structure indicates that the C-terminus of SNX3 is not essential for retromer binding in the *in vitro* crystallisation conditions, the perturbation of GFP-SNX3(p.R160A) binding to VPS35 **(Figure 3.2)** suggests that, *in vivo,* the C-terminus of SNX3 may be critical in stabilising the SNX3-retromer interaction. Furthermore, a recently published solution structure of full-length SNX3 has identified that its C-terminus is structured (interfacing with the α1, α3, and α4 helices of SNX3), facing away from the PI3P binding site with the N-

terminus; the authors hypothesise that the termini form a binding platform for interactions with the retromer complex (Lenoir et al., 2018).

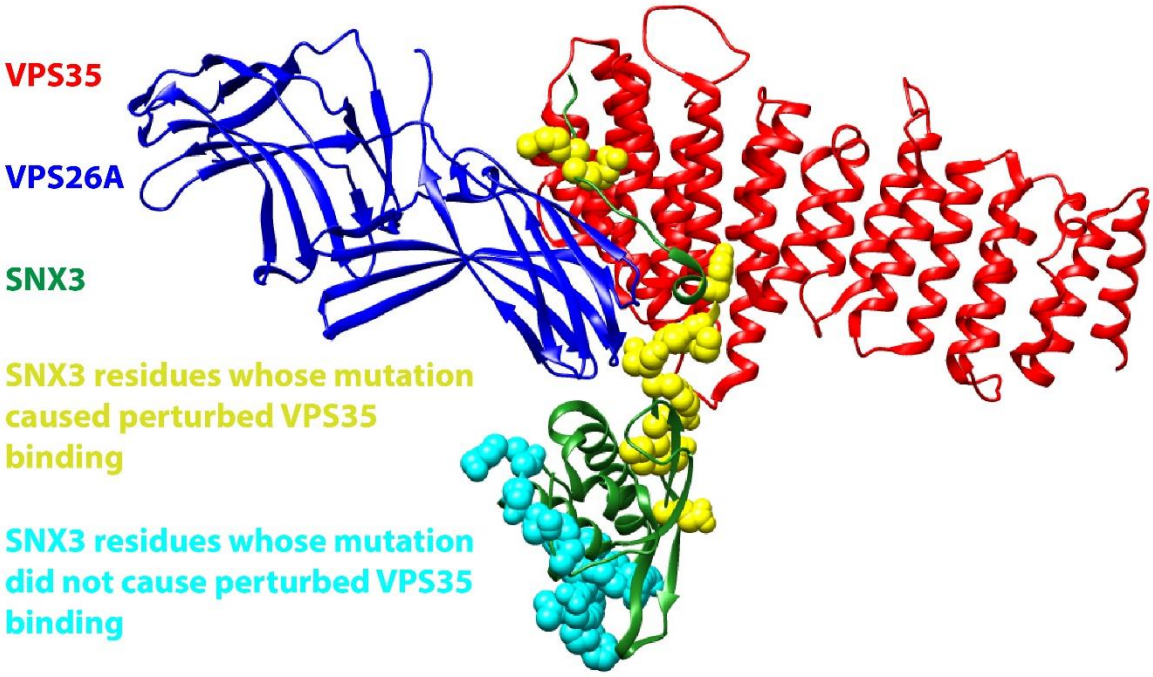

Figure 3.16 Modelling of the residues identified in SNX3 which causes a perturbation in VPS35 binding onto the SNX3:VPS35:VPS26A crystal structure

Model of the SNX3 (yellow):VPS35 (red):VPS26A (blue) crystal structure from Lucas et al., 2016. The residues which, when mutated, caused a loss of association between SNX3 and VPS35 are shown in yellow. The residues which, when mutated, did not cause a dramatic loss of VPS35 associated are shown in cyan. For clarity, a spherical representation of the highlighted residues is shown on the ribbon backbone.

The Lucas et al., (2016) structure revealed that the SNX3 binding to the VPS35/VPS26A interface induces a conformational change in VPS26A which opens-up a binding site for cargoes which contain a binding site for ØX(L/M/V) motifs (where Ø is an aromatic residue). The divalent iron transporter, DMT1-II, is the only cargo with structural evidence to prove this. However, several retromer cargoes, including Wntless, contain this motif, making it a probable mechanism for its binding (Lucas et al., 2016).

Both SNX3 and the retromer complex have previously been shown to be essential for the endosomal sorting of the Wnt chaperone, Wntless, and therefore Wnt secretion (Belenkaya et al., 2008; Franch-Marro et al., 2008; Pan et al., 2008; Yang et al., 2008; Harterink et al., 2011; Zhang et al., 2011). However, due to the lack of structural

information of how SNX3 associates with retromer, it had never been established whether the direct association between SNX3 and retromer is required for the endosomal sorting of Wntless. Here, data I gathered through a biochemical, site-directed mutagenesis screen, which identified specific SNX3 residues required for VPS35 association **(Figure 3.2)**, could be translated into an *in vivo C. elegans* setting through the CRISPR knock-in of SNX3(p.Y22A), which uncouples SNX3 from the retromer complex. Animals with SNX3(p.Y22A) exhibited a Wnt secretion defect, with the QL.d migrating in the anterior, rather than the posterior, direction **(Figure 3.6)**. These data reveal the necessity of the interaction between SNX3 and retromer for the endosomal sorting of Wntless and the maintenance of Wnt secretion. As it is probable that cargo bind to SNX3-retromer through the same binding mechanism (Lucas et al., 2016), the functional insight gained through uncoupling the SNX3-retromer interaction in the context of Wntless trafficking may also be relevant for other SNX3-retromer cargoes, such as DMT1-II and the Transferrin receptor (Tabuchi et al., 2010; Chen et al., 2013; Lucas et al., 2016).

The SNX3 interactome contain several proteins (such as VPS35, ATM kinase, GCN1 and mTOR) which have a similar tertiary structure: HEAT-repeat domains (Hierro et al., 2007; Knutson, 2010; Lau et al., 2016; Rakesh et al., 2017). It was therefore tempting to speculate that they all associate with SNX3 through the same mechanism. However, when I examined the ability of SNX3 variants unable to associate with VPS35, to bind to the other interactors, there was no difference in the binding **(Figure 3.5)**. This establishes that even though these other interactors have a similar tertiary structure to VPS35, that they do not associate using the same mechanism. The Lucas et al., (2016) SNX3-retromer crystal structure, which revealed that SNX3 associates with the VPS26A retromer subunit, which has an arrestin-like structure (Gallon et al., 2014b), as well as to VPS35, is consistent with the SNX3-retromer interaction being unique.

3.3.2 The role of aminophospholipid translocases in membrane traffic

Protein trafficking has received extensive research attention, but the trafficking of lipids is less well understood. The subcellular lipid organisation within cells is maintained through mechanisms which concentrate specific lipid species within specific organelles, and between the lipid bilayers within these organelles (Santos and Preta, 2018). Although there is rapid lipid lateral mobility within a membrane bilayer, the spontaneous translocation (or flip-flop) of lipids between one leaflet to another, due to the polar head

group crossing the hydrophobic membrane, faces high energetic barriers (Singer and Nicolson, 1972). The translocation of phospholipids is therefore coordinated via 3 protein families: scramblases, flippases and floppases **(Figure 3.17)**. Most phospholipid synthesis occurs in the ER (Bell et al., 1981; Blom et al., 2011). To maintain this lipid bilayer, some phospholipids must be redistributed, or flipped, onto the other leaflet. The ER membrane contains scramblases, which, in an energy-independent fashion, non-specifically redistributes the lipids across the bilayer. The identities of these ER-localised scramblases have remained elusive, but recent results, largely through studies on Opsin, suggest that GPCRs may be responsible (Menon et al., 2011; Goren et al., 2014); the evidence for this comes from *in vitro* reconstitution experiments, not in cells. Many cellular lipid bilayers tend to be asymmetric in their lipid composition; this is best characterised in the plasma membrane, where sphingomyelin and phosphatidylcholine are enriched in the extracellular leaflet, while phosphatidylethanolamine and phosphatidylserine are enriched to the cytosolic leaflet (Ingolfsson et al., 2014).

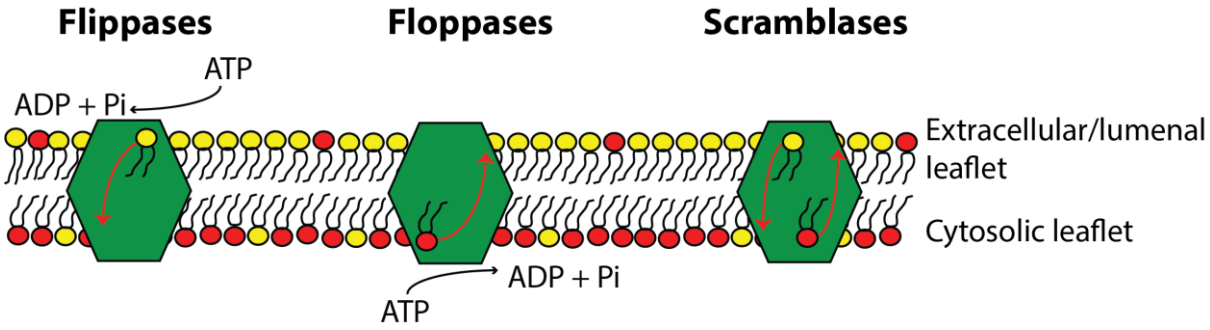

Figure 3.17 Flippases, floppases and scramblases mediate phospholipid transfers across the lipid bilayer.

A schematic depicting the protein families which mediate the transfer of phospholipids across lipid bilayers. Flippases use ATP hydrolysis to transfer phospholipids from the extracellular/luminal leaflet to the cytosolic leaflet. Floppases use ATP hydrolysis to transfer phospholipids from the cytosolic leaflet to the extracellular/luminal leaflet. Scramblases transfer phospholipids across the lipid bilayer in an energy-independent fashion.

This differential and asymmetric distribution of lipids creates unique membrane properties which can dynamically be exploited for numerous cellular applications. For example, exposure of phosphatidylserine on the outer plasma membrane lipid leaflet, mediated through a scramblase, serves as a trigger of apoptosis (Fadok et al., 2001). The active redistribution of lipids from one side of a leaflet to another induces membrane bending, which can be a trigger for vesicular budding in the endocytic and secretory pathways (Farge et al., 1999; Muthusamy et al., 2009; Takada et al., 2018). The deformation of membranes through cytosolic coat proteins **(Section 1.1.1)** is the

best-characterised mechanism for the generation of transport vesicles, but accessory proteins such as flippases are thought to aid the generation of membrane curvature (Shin et al., 2012; Takada et al., 2018). Not only are lipids, such as sterols and sphingolipids, segregated during the formation of secretory vesicles (Klemm et al., 2009; Deng et al., 2016), the action of flippases have been implicated in the formation of extracellular vesicles (Wehman et al., 2011), exocytic vesicles (Gall et al., 2002) and endocytic carriers (Pomorski et al., 2003).

Flippases (also known as P4 ATPases and aminophospholipid translocases) mediate the ATP-dependent translocation of aminophospholipids, such as phosphatidylserine and phosphatidylethanolamine, from the extracellular (or luminal) leaflet of the lipid bilayer, to the cytosolic leaflet **(Figure 3.17)**. In *S. cerevisiae*, there are 5 members of the flippase family: Drs2p, Dnf3p, Dnf1p, Dnf2p and Neo1p. The only essential gene in this family is NEO1 (Hua et al., 2002), but the best characterised is Drs2p, which is involved in the flipping of (predominantly) phosphatidylserine in the TGN compartment (Natarajan et al., 2004; Chen et al., 2006). *C. elegans* have 6 and humans have 14 P4-ATPases **(Table 3.1)**. Unlike cation transporter members of the P-ATPase family, which have a conserved acidic residues in their transmembrane segments, aminophospholipid translocases have a highly conserved lysine residue critical for their function (Coleman et al., 2012). Reconstitution assays have demonstrated the activity of several flippases (Coleman et al., 2009; Zhou and Graham, 2009; Takatsu et al., 2014; Yabas et al., 2016) but many of the others have phenotypes consistent with a role in flipping lipids.

Table 5.1 VPS35-GFP variants created through site-directed mutagenesis

P4-ATPases, class	***S. cerevisiae***	***C. elegans***	***H. sapiens***
1a	DRS2	tat-1	ATP8A1, ATP8A2
1b	N/A	tat-2	ATPB1, ATPB2, ATPB3, ATPB4
2	NEO1	tat-5, tat-6	ATP9A, ATP9B
3	DNF1, DNF2	N/A	N/A
4	DNF3	N/A	N/A
5	N/A	tat-3, tat-4	ATP10A, ATP10B, ATP10D
6	N/A	N/A	ATP11A, ATP11B, ATP11C

Table 3.1 P4-ATPases in *S. cerevisiae*, *C. elegans* and *H. sapiens*

3.3.3 The role of MON2/DOPEY/ATP9A in Wntless recycling and Wnt secretion

The SNX3-retromer-mediated retrieval of Wntless is independent from the SNX-BAR complex, the classical membrane deformation complex associated with retromer-mediated retrieval and recycling (Harterink et al., 2011; Zhang et al., 2011). The generation of the SNX3 interactome revealed candidate proteins for the SNX3-retromer-associated membrane-remodelling complex: MON2 and DOPEY2, which in *S. cerevisiae*, interact with the putative phospholipid translocase: neo1p (Hua and Graham, 2003; Wicky et al., 2004; Singer-Kruger et al., 2008; Barbosa et al., 2010). Some members of the MON2/DOPEY2/ATP9A complex and the retromer complex (or associated endosomal proteins) and have previously been linked together in the regulation of β-catenin asymmetry during *C. elegans* stem cell divisions (Kanamori et al., 2008), the regulation of extracellular vesicle budding in *C. elegans* (Beer et al., 2018) and cargo recycling in *S. cerevisiae* (Dalton et al., 2017). Furthermore, ATP9A has been linked to the endosomal recycling of GLUT1 and transferrin (Tanaka et al., 2016).

MON2 has been implicated in promoting cargo sorting (Avaro et al., 2002; Bonangelino et al., 2002; Efe et al., 2005; Gillingham et al., 2006) and reported to be required for correct Gag localisation during HIV-1 infection of mammalian cells (Tomita et al., 2011). The Sec7-like domain of MON2 resulted in it being proposed as a GEF for Arl1 (Wicky et al., 2004), but this was subsequently shown to be incorrect (Mahajan et al., 2013). Little is known about mammalian DOPEY1/2 beyond associations with Down's syndrome, Alzheimer's disease and breast cancer (Rachidi et al., 2009; Swaminathan et al., 2012; Lend et al., 2015). In *C. elegans* it is an essential gene required for embryonic patterning (Guipponi et al., 2000).

Here, I have further characterised human MON2 and DOPEY1/2 proteins and have established that they share many features of their yeast homologues (Mon2p and Dop1p respectively). This includes self-association properties (i.e. MON2 interacts with MON2 and DOPEY2 interacts with DOPEY2) (Barbosa et al., 2010), their association with each other (i.e. MON2 interacts with DOPEY2) (Gillingham et al., 2006) and the formation of a complex with the human equivalent of the putative phospholipid translocase neo1p: ATP9A (Barbosa et al., 2010) **(Figure 3.7B-F)**. I have also presented evidence that this putative flippase complex of MON2, DOPEY1/2 and

ATP9A can associate with SNX3-retromer **(Figure 3.7A)**, although whether this is a direct interaction or not will need further investigation.

In vivo, RNAi of the *C. elegans* homologues of MON2, DOPEY1/2 and ATP9A (mon-2, pad-1 and tat-5 respectively) all cause a Wnt-secretion phenotype, phenocopying the RNAi of vps-35 **(Figure 3.14B and Figure 3.15A-B)**. In my *in vitro* model of Wntless retrieval, the knock-down of MON2 or ATP9A phenocopy that of SNX3 or retromer in terms of the decrease in whole-cell levels of HA-Wntless **(Figure 3.12A-B)**. However, DOPEY1/2 knock-down did not recapitulate this phenotype **(Figure 3.12A-B)**. This suggests that in the human cell culture model, either the levels of suppression I achieved during siRNA-treatment were insufficient, the DOPEY proteins are not needed for Wntless retrieval, or that there is another factor in human cells that is redundant for these proteins. Performing a bioinformatic BLAST search on the SNX3 interactome did not reveal any other homologous interactors to DOPEY1/2. In the mammalian context, the role of DOPEY1 and DOPEY2 is therefore unclear. There is some evidence in *C. elegans* that mon-2 and pad-1 may have some differing functions, with tat-5/pad-1 maintaining PE asymmetry at the cell surface, and tat-5/mon-2 regulating endosomal trafficking (Beer et al., 2018). It is therefore possible that mammalian MON2 and DOPEY1/2 could have functions that relate together as well as separately in this pathway.

It is interesting to note that in both yeast and humans, Mon2p and MON2 respectively, can associate with and influence the localisation of the GGA (Golgi-localising, γ-adaptin ear domain homology, ARF-binding protein) adaptors via the GGA VHS domain (Singer-Kruger et al., 2008). As GGA adaptors have previously been linked to endosomal cargo recycling (Zhao and Keen, 2008; Parachoniak et al., 2011; Ratcliffe et al., 2016; Toh et al., 2018), it is tempting to link this interaction to the clathrin decoration of SNX3-positive transport carriers enriched with Wntless (Harterink et al., 2011). Future studies will need to investigate the importance of this connection for SNX3-retromer mediated cargo retrieval.

The data I have presented here are consistent with a model **(Figure 3.18)** in which the tat-5/mon-2/pad-1 and MON2/ATP9A (the role of mammalian DOPEY1/2 remains unclear) complexes couple with SNX3-retromer to combine Wntless cargo enrichment with endosomal membrane deformation and initial membrane bending and carrier formation. Membrane deformation, induced via the ATPase-dependent flippase activity of ATP9A, causes the enrichment of phospholipids in the cytosolic leaflet of the endosomal membrane, increasing its surface area compared to the luminal leaflet,

inducing bending into the cytosol. The oligomeric properties of MON2/DOPEY have previously been proposed to promote and stabilise membrane deformation by forming a meshwork, concentrating the flippase action of ATP9A in a diffusion-restricted membrane microdomain (Barbosa et al., 2010). The alteration of the membrane properties through the concentration of specific phospholipids species such as phosphatidylethanolamine may also promote the recruitment of accessory proteins to support membrane deformation and initial membrane bending, promoting carrier formation. This is the case in *S. cerevisiae*, where endosomal recycling is supported by the Drs2p-mediated flipping of phosphatidylserine to recruit the ARFGAP Gcs1 (Xu et al., 2013) and in mammalian cells, where EHD1 is recruited to recycling endosomes by the flippase ATP8A1 (Lee et al., 2015). The interaction between MON2 and GGA adapters (Singer-Kruger et al., 2008) may also be required for the observed clathrin-decoration of SNX3-positive vesicles (Harterink et al., 2011). Future studies will be required to test various aspects of this model.

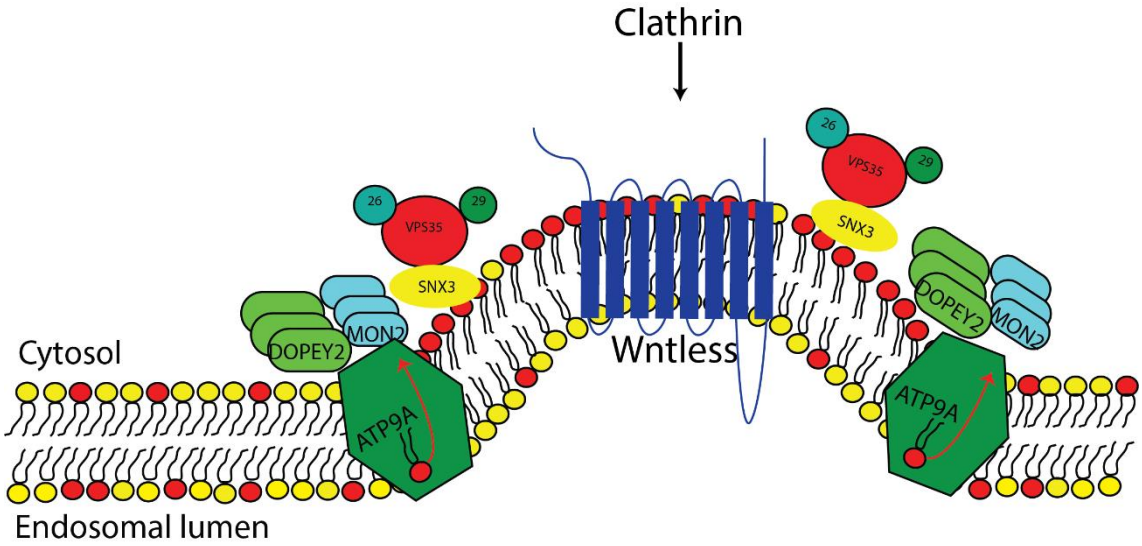

Figure 3.18 Working model of the coordination of SNX3-retromer with the MON2:DOPEY1/2:ATP9A complex.

SNX3-retromer enriches cargoes such as Wntless on the endosomal membrane. In tandem, SNX3 can (directly or indirectly) couple to the MON2:DOPEY1/2:ATP9A complex. ATP9A causes the translocation of aminophospholipids, such as phosphatidylethanolamine, from the luminal leaflet to the cytosolic leaflet of the lipid bilayer, inducing initial membrane bending and the formation of cargo-enriched nascent carriers. SNX3-positive carriers are clathrin-decorated, possibly induced by the MON2 interaction with GGA adaptors.

3.3.4 Phopholipid flippase activity of ATP9A

The class II members of the P4 ATPase family include Neo1p in *S. cerevisiae*, tat-5 in *C. elegans* and ATP9A/B in *H. sapiens*. Neo1p and tat-5 are the only members of the

aminophospholipid translocase family to be essential for survival and cannot be compensated for by overexpression of others (Hua et al., 2002; Lyssenko et al., 2008). It has not been possible, due to technical issues, to biochemically reconstitute and conclusively show that Neo1p/tat-5/ATP9A/ATP9B flip lipids across a membrane (Takar et al., 2016). Whether or not flippase activity is reconstituted is a significant question. This is due to their activity being implicated in protein trafficking pathways, which may raise the question of whether the phenotypes exhibited are caused by perturbed trafficking of other proteins, such as an uncharacterised lipid transporter. The class II flippases are distinct from others in that they do not associate with a Cdc50 family member (Saito et al., 2004; Takatsu et al., 2011), which are required for the flippase activity of other flippases such as Drs2p, (Lenoir et al., 2009). The purification of 10-pass transmembrane spanning proteins, with potentially critical (and undefined) accessory proteins, and the reconstitution of the lipid-flipping activity in proteoliposomes, is not trivial.

Disruption of neo1p, tat-5 and ATP9A all lead to phenotypes indicative of their role in phospholipid flipping (Wehman et al., 2011; Ansari et al., 2015; Takar et al., 2016; Tanaka et al., 2016; Wu et al., 2016; Dalton et al., 2017; Beer et al., 2018). Their lipid substrate has not been conclusively shown, but their disruption leads to the cell surface exposure of phosphatidylethanolamine, making it the most likely candidate (Wehman et al., 2011; Takar et al., 2016; Wu et al., 2016; Beer et al., 2018). A mutation in Neo1p, Neo1p(D503N), which blocks the ATPase cycle at the E1 stage, fails to complement the *neo1*∆ yeast strain (Takar et al., 2016), showing that the ATPase activity and therefore its putative flippase activity, is required for *S. cerevisiae* viability. The *drs2*∆ (a proven flippase) yeast strain displays growth deficits, which can be suppressed through overexpression of Neo1p, but not through the overexpression of Neo1p(D503N); Neo1p overexpression also suppresses the loss of PE and PS asymmetry in *drs2*∆ cells (Takar et al., 2016). Further evidence has be seen in *C. elegans*, where catalytically inactive tat-5(*E246Q)* failed to rescue the tat-5 mutant embryonic lethality phenotype (Wehman et al., 2011) and tat-5(*E246Q)* overexpression led to a Wnt secretion defect **(Figure 3.15D)**. These data are entirely consistent with Neo1p/tat-5/ATP9A/B acting as flippases. However, it will be necessary for future studies to demonstrate the biochemical reconstitution of the flippase activity.

Chapter 4

Analysis of rare Parkinsonism-associated retromer mutations

4.1 Introduction

4.1.1 Mutations in the retromer complex are associated with Parkinsonism disorders

Parkinson's disease (PD) is the second most common neurodegenerative disorder. In males over 40, the incidence rate is 61.21 per 100,000 person-years; for females over 40, the incidence rate is 37.55 per 100,000 person-years (Hirsch et al., 2016). The most recognised symptoms of PD are the motor dysfunctions, which include bradykinesia (slow movements), extrapyramidal rigidity (muscle stiffness), gait disturbance, postural instability (loss of balance) and tremors (Williams and Litvan, 2013). Non-motor systems include: impaired olfaction; cardiovascular, gastrointestinal and urinary abnormalities; and sleep disorders (Ferrer et al., 2011). The predominant pathology of PD is the progressive degeneration of dopaminergic neurons in the substantia nigra pars compacta (SNpc) which contain protein aggregates called Lewy bodies, enriched with α-synuclein (Dickson, 2012). It is now recognised that Parkinson's disease fits within a broader class of Parkinsonism disorders. Examples of other Parkinsonism disorders include: progressive supranuclear palsy, multiple system atrophy, and dementia with Parkinson's disease (Williams and Litvan, 2013).

PD is a multifactorial disease with a variety of risk factors including environmental and genetic, with age being the most dominant. The majority of cases are sporadic while <10% have a familial aetiology, where a specific disease-causing mutation is passed onto the next generation (Thomas and Beal, 2007). However, several PD disease-causing mutations sporadically form in patients with no family history; this may be explained by incomplete penetrance, early death of relatives before symptoms develop or inaccurate medical records (Zhang et al., 2018). Proteins which are associated with familial PD highlight the molecular pathways involved in disease progression; these include: defects in autophagy, mitophagy, lysosomal health, synaptic transmission and endosomal recycling (Lin and Farrer, 2014). A greater understanding of rare familial mutations may assist in our understanding of disease pathogenesis.

The retromer complex (composed of a VPS35:VPS26A/B:VPS29 heterotrimer) (**Section 1.4.1**), when dysfunctional, is implicated in several neurological diseases, including PD **(Section 1.5.1)**. The mRNA levels of the retromer complex components VPS35 and VPS26 were reduced in samples of sporadic PD patients' SNpc (MacLeod et al., 2013). However, it was originally implicated in familial PD when an autosomal dominant missense mutation in the retromer complex, VPS35(p.D620N), was identified in multiple family members in several ethnicities (Vilarino-Guell et al., 2011; Zimprich et

al., 2011). More incidences of this mutation have been reported worldwide (Vilarino-Guell et al., 2011; Zimprich et al., 2011; Ando et al., 2012; Kumar et al., 2012; Lesage et al., 2012; Sharma et al., 2012; Sheerin et al., 2012; Chen et al., 2017; McMillan et al., 2017; Bentley et al., 2018). It is currently thought to cause 1.3% of familial Parkinson's disease cases and 0.3% of sporadic Parkinson's disease, with symptoms similar to sporadic PD (Mohan and Mellick, 2017). Many other rarer mutations in the retromer complex have been identified to be associated with Parkinsonism disorders **(Table 4.1)**, but most are yet to be characterised.

Biochemically, the VPS35(p.D620N) variant does not affect the assembly of the retromer heterotrimer, but reduces association (by approximately 50%) with the WASH complex (McGough et al., 2014b; Zavodszky et al., 2014). Functionally, it has been reported to perturb CIMPR, ATG9 and LAMP2a trafficking, impacting lysosomal health, autophagy and chaperone-mediated autophagy (Follett et al., 2014; McGough et al., 2014b; Zavodszky et al., 2014; Tang et al., 2015a). These trafficking deficits are thought to partly explain the increased α-synuclein aggregates reported in cells and animal models (Miura et al., 2014; Dhungel et al., 2015; Tang et al., 2015a; Tang et al., 2015b).

VPS35(p.D620N) has also been implicated in perturbed endosome-to-plasma membrane trafficking. VPS35(p.D620N) has been reported to cause defects in the cell surface localisation of GLUT1 (Zavodszky et al., 2014), dopamine receptor-D1 (Wang et al., 2016a), the dopamine transporter (Wu et al., 2017; Cataldi et al., 2018) and AMPA receptors (Munsie et al., 2014). Impaired trafficking of these proteins is thought to contribute to the perturbed dopaminergic neurotransmission in the striatum of VPS35(p.D620N) knock-in mice (Ishizu et al., 2016), and the impaired excitatory neurotransmission in rat cortical neurons (carrying the mutation) and induced pluripotent stem cells (from human p.D620N carriers) differentiated into dopaminergic neuronal-like cells (Munsie et al., 2014). Furthermore, VPS35(p.D620N) has been reported to impair the trafficking of the mitochondrial fission regulator DLP1 and increase mitochondrial fragmentation and dysfunction (Wang et al., 2016b).

Gene	AA change	No. of patients	Found in controls?	Average AAO	Clinical diagnosis	Reference(s)
VPS35	D620N	Frequency of 1.3% (familial PD) and 0.3% (sporadic PD)	No	51.4	PD	Various* (Mohan and Mellick, 2017)
	L774M	2	Yes	62	PD	(Sharma et al., 2012)
	M607V	1	No	76	PD	(Verstraeten et al., 2012)
	H599R	1	No	54	PD	(Verstraeten et al., 2012)
	I560T	1	Yes	68	PD	(Verstraeten et al., 2012)
	R524W	1	No	37	PD	(Zimprich et al., 2011)
	P316S	2	Yes	53	PD	(Vilarino-Guell et al., 2011; Nuytemans et al., 2013)
	I241M	1	No	72	PD	(Zimprich et al., 2011)
	M57I	1	No	62	PD	(Zimprich et al., 2011)
	G51S	2	Yes	60.5	DPD/PD	(Sharma et al., 2012; Gustavsson et al., 2015)
	R32S	1	No	Unknown	PD	(Bandres-Ciga et al., 2016)
VPS26A	K297X	1	No	70	PDP	(Gustavsson et al., 2015)
	M112V	1	No	51	PSP	(Gustavsson et al., 2015)
	K93E	2	No	57	MSA/PD	(Shannon et al., 2014; Gustavsson et al., 2015)
	R127H	1	Yes	70	DPD	(Gustavsson et al., 2015)
	N308D	1	Yes	73	PSP	(Gustavsson et al., 2015)
VPS29	N72H	1	Yes	70	PD	(Shannon et al., 2014)

Table 4.1 Mutations in the retromer complex linked to Parkinsonism disorders

AA= amino acid; AAO= age-at-onset; PD= Parkinson's disease; DPD = dementia with Parkinson's disease; PSP= progressive supranuclear palsy; MSA= multiple system atrophy. *(Vilarino-Guell et al., 2011; Zimprich et al., 2011; Ando et al., 2012; Kumar et al., 2012; Lesage et al., 2012; Sharma et al., 2012; Sheerin et al., 2012; Chen et al., 2017; McMillan et al., 2017; Bentley et al., 2018). Table adapted from (McMillan et al., 2017).

4.1.2 Aims

In this chapter, I sought to characterise several other Parkinsonism-associated retromer complex mutations. I focused on several mutations in VPS26A [VPS26A(p.K93E), VPS26A(p.M112V) and VPS26A(p.K297X)] and mutations in the amino-terminus of VPS35 [VPS35(p.R32S) and VPS35(p.G51S)]. To this end, I analysed the retromer variants' localisation, ability to assemble into the retromer heterotrimer and whether the mutations impacted the interactome of retromer.

4.2 Results

4.2.1 Initial bioinformatic analysis of the VPS26A Parkinsonism-linked mutations

Genome Wide Association Studies (GWAS) have identified several Parkinsonism-linked mutations in the retromer subunit VPS26A (Gustavsson et al., 2015). Among them are VPS26A(p.K93E), VPS26A(p.M112V) and VPS26A(p.K297X) ('X' denotes a premature stop codon) (Gustavsson et al., 2015). To identify the conservation across species of the residues linked with the Parkinsonism disorders, I performed a sequence alignment of various homologues of human VPS26A and its paralogue VPS26B **(Figure 4.1)**. The K93 residue is largely conserved through the compared species – the biggest divergence identified was in *C. elegans*, where the lysine residue has diverged into the similar basic amino acid, arginine **(Figure 4.1)**. The M112 residue is not well conserved through evolution, or within the VPS26 human paralogues **(Figure 4.1)**. The K297 residue is completely conserved between the aligned VPS26A homologues and VPS26B; however, some of the residues following the K297 residue, which are all lost in the K297X truncation, are not well conserved **(Figure 4.1)**.

VPS26A has an arrestin-like fold – antiparallel β-strands forming paired β-sandwich subdomains – which binds to the β-hairpin in the SNX27 PDZ domain (Gallon et al., 2014a). To gain structural insight into the Parkinsonism-linked mutations, I analysed their location on the 3-dimentional VPS26A structure using the coordinates of the VPS26A:SNX27 crystal structure (Gallon et al., 2014a) **(Figure 4.2)**. The K93 and M112 residues of VPS26A are both exposed in a similar region of VPS26A, on one of the β-sandwich subdomains **(Figure 4.2)**. These are in close proximity to the SNX27 binding site, but no direct contacts are formed (Gallon et al., 2014a). The residues following K297 are on the opposite β-sandwich subdomains, again in proximity to, but not directly interacting with SNX27 **(Figure 4.2)**.

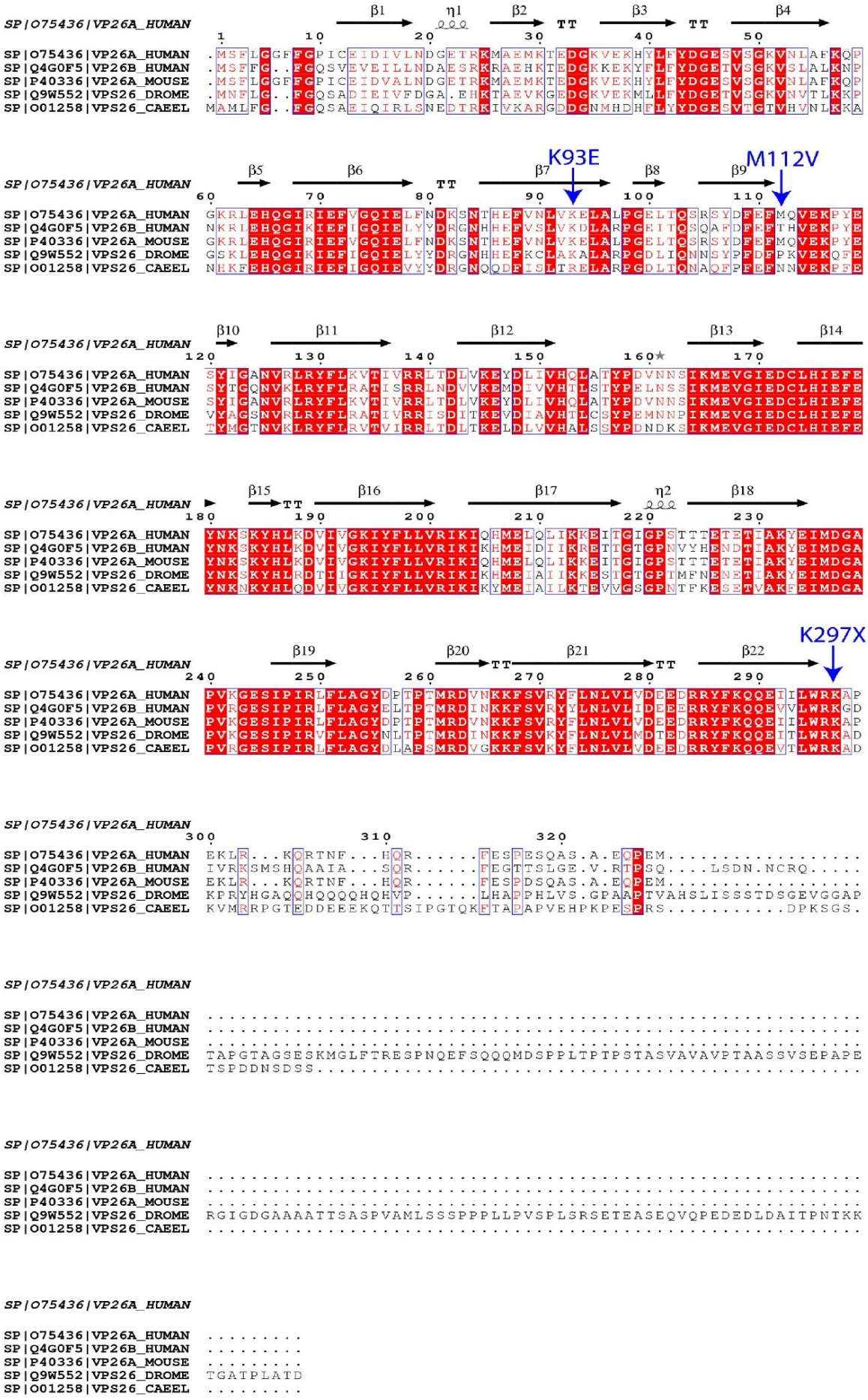
K93E
M112V
K297X
SP|O75436|VP26A_HUMAN
SP|Q4G0F5|VP26B_HUMAN
SP|P40336|VP26A_MOUSE
SP|Q9W552|VPS26_DROME
SP|O01258|VPS26_CAEEL

Figure 4.1 Bioinformatic alignment of VPS26 homologues and human paralogues.

Sequences of H. sapiens, M. musculus, D. melanogaster and C. elegans VPS26 homologues were aligned using ESPript 3.0 online software (Robert and Gouet, 2014). Secondary structural information was modelled in using the VPS26A crystal structure as a reference (Gallon et al., 2014). The Parkinsonism-associated mutations (K93E, M112V and K297X) are indicated with blue arrows.

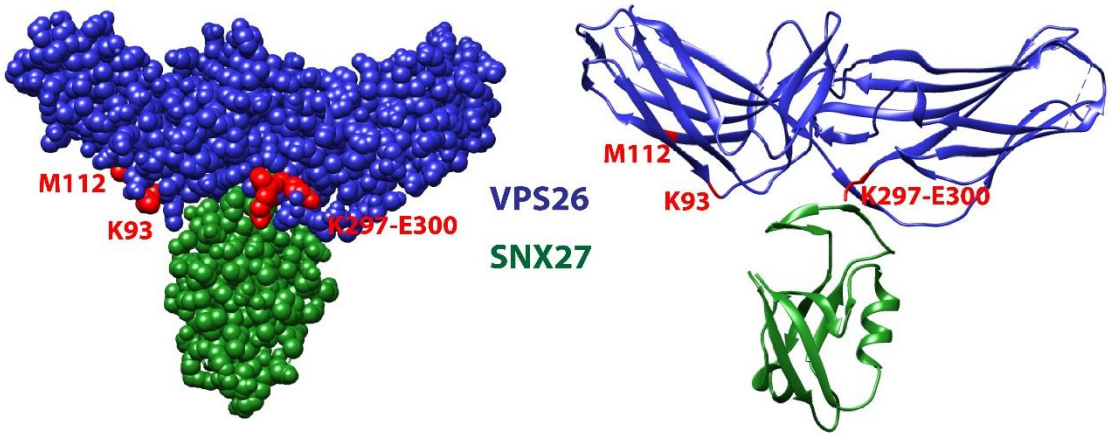

Figure 4.2 Model showing the location of the Parkinsonism-associated VPS26A mutations.

Modelling the VPS26A residues which have been associated with Parkinsonism-linked disorders (K93E, M112V and K297X) onto the structure of SNX27 bound to VPS26A (Gallon et al., 2014). VPS26A (blue), SNX27 (green). Modelling was performed using UCSF Chimera software.

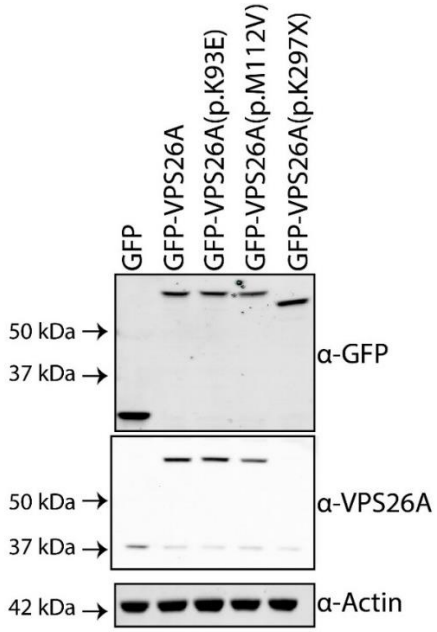

Figure 4.3 Lentivirally transduced GFP-VPS26A constructs are expressed at near endogenous levels.

RPE-1 cells, lentivirally transduced with the indicated GFP-VPS26A construct, were lysed. The lysates were resolved using SDS-PAGE and immuno-blotted for the indicated antibodies.

4.2.2 Creation of stably expressing GFP-VPS26A RPE-1 cell lines

To experimentally investigate the VPS26A Parkinsonism-associated mutations, I used site directed mutagenesis to introduce the 'K93E', 'M112V' and 'K297X' mutations into GFP-VPS26A XLG3 lentiviral constructs, which I then packaged into lentivirus. Lentiviral-mediated transduction of RPE-1 cells allowed the expression of the GFP-VPS26A variants at similar whole-cell protein levels compared to the endogenous VPS26A **(Figure 4.3)**. When the GFP-VPS26A variants were expressed, the whole-cell levels of endogenous VPS26A (at 37kDa on the immunoblot) were reduced **(Figure 4.3)**, presumably due to the outcompeting of the endogenous VPS26A for assembly into the stable retromer complex, causing the proteasomal-mediated degradation of the unbound VPS26 subunit. I created a number of cell lines which stably expressed GFP-VPS26A, GFP-VPS26A(p.K93E), GFP-VPS26A(p.M112V) and GFP-VPS26A(p.K297X), all at similar levels of expression with little endogenous VPS26A remaining in the cells **(Figure 4.3)**. When immunoblotting for the GFP-VPS26A(p.K297X), there was no band when blotting against VPS26A as the epitope of the monoclonal anti-VPS26A antibody is at the C-terminus of VPS26A, which is lost in this truncation **(Figure 4.3)**. I therefore used anti-GFP primary antibodies to visualise GFP-VPS26A(p.K297X) **(Figure 4.3)**. GFP-VPS26A(p.K297X) also has a lower molecular weight compared to GFP-VPS26A wild-type due to the truncation mutation **(Figure 4.3)**.

4.2.3 The VPS26A variants retain the ability to form the retromer complex

I then tested the GFP-VPS26A variants for their ability to localise to retromer-positive endosomes. All the GFP-VPS26A variants had a similar punctate localisation positive for VPS35 **(Figure 4.4A)**. Colocalisation analysis between the variants of GFP-VPS26A with endogenous VPS35 revealed no significant differences in the Pearson's colocalisation coefficient (PCC) or Overlap Coefficient (OC) **(Figure 4.4B)**. This is consistent with the Parkinsonism-linked variants retaining the ability to localise to endosomes and form the retromer complex. To extend this biochemically, Dr Kirsty McMillan transfected HEK293T cells with the various GFP-VPS26A variants and performed a GFP-trap immunoprecipitation experiment **(Figure 4.5A)**. No significant differences were found between the ability of the wild-type GFP-VPS26A and the Parkinsonism-linked GFP-VPS26A variants to associate with the other retromer components **(Figure 4.5B)**. Therefore, neither K93E, M112V or K297X mutations in VPS26A perturb retromer complex assembly.

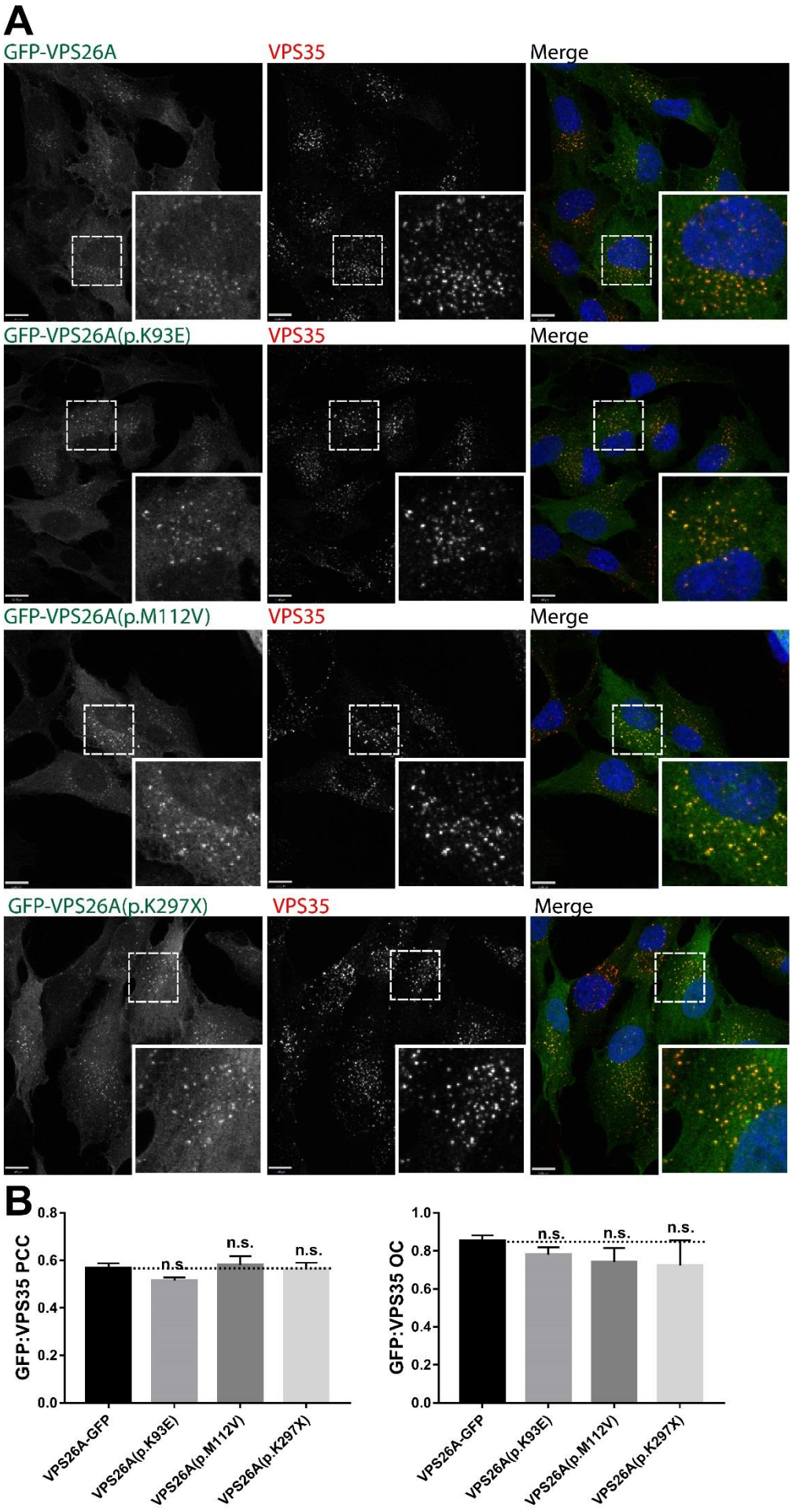
A
GFP-VPS26A
VPS35
Merge
GFP-VPS26A(p.K93E)
VPS35
Merge
GFP-VPS26A(p.M112V)
VPS35
Merge
GFP-VPS26A(p.K297X)
VPS35
Merge
B
GFP:VPS35 PCC
0.0
0.2
0.4
0.6
0.8
n.s.
n.s.
n.s.
VPS26A-GFP
VPS26A(p.K93E)
VPS26A(p.M112V)
VPS26A(p.K297X)
GFP:VPS35 OC
0.0
0.2
0.4
0.6
0.8
1.0
n.s.
n.s.
n.s.
VPS26A-GFP
VPS26A(p.K93E)
VPS26A(p.M112V)
VPS26A(p.K297X)

Figure 4.4 The Parkinsonism-associated VPS26A mutations do not affect colocalisation with VPS35.

(A) RPE-1 cells, stably expressing the indicated GFP-VPS26A constructs, were fixed with 4% paraformaldehyde, stained for endogenous VPS35 and imaged on a confocal microscope. Scale bar indicates 11 µm. **(B)** Graph showing the quantified Pearson's colocalisation coefficient (PCC) and Overlap coefficient (OC) from 3 independent experiments (at least 25 cells were quantified per experiment). Error bars indicate standard error; data were analysed using a one-way ANOVA and a Dunnett's post-hoc test comparing the mutant constructs to the wild-type VPS26A-GFP construct.

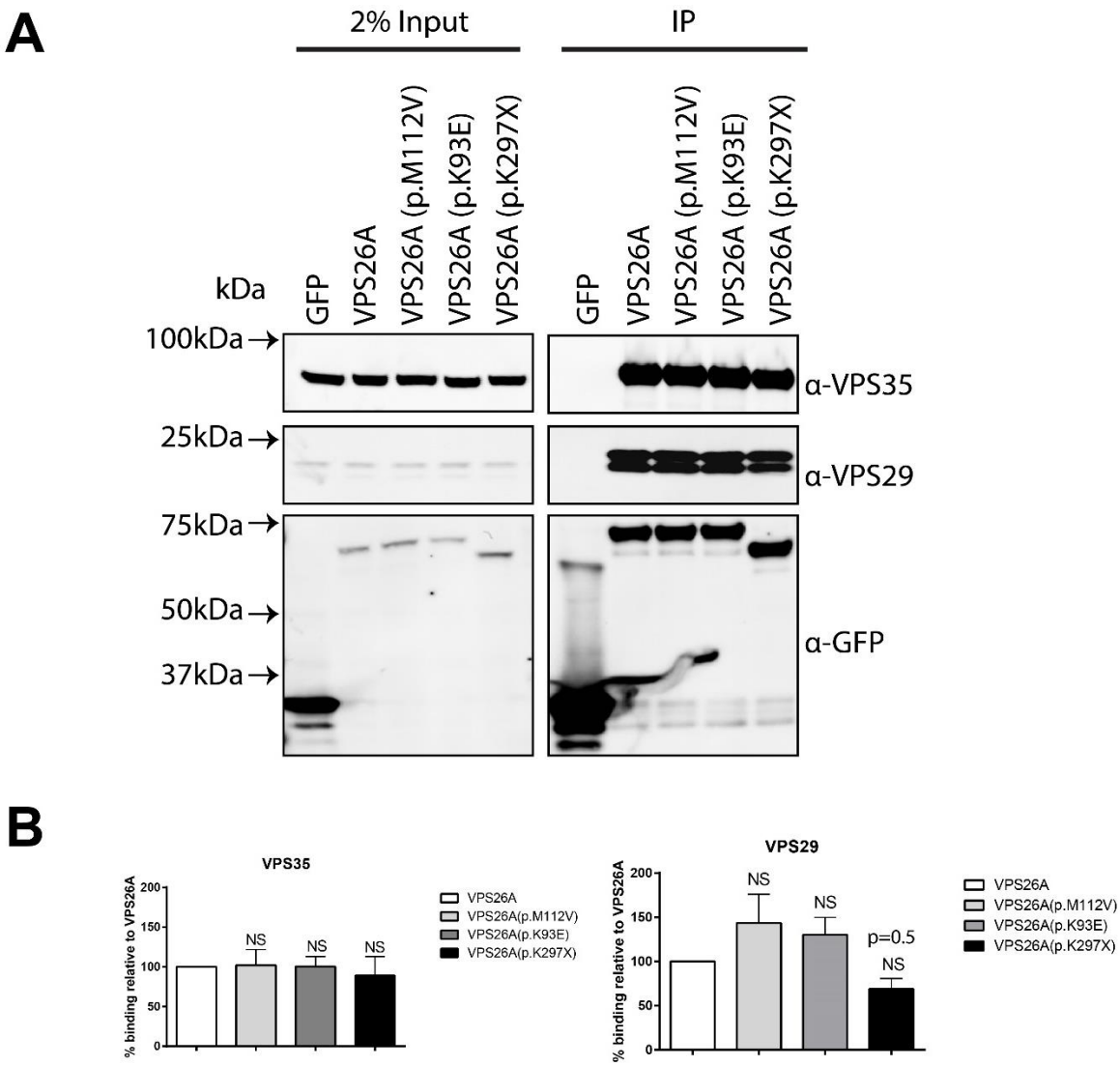

Figure 4.5 The VPS26A Parkinsonism-associated mutations do not perturb assembly of the retromer complex.

(A) HEK293T cells were transfected with the indicated GFP-VPS26A construct before subjecting the cells to a GFP-trap. The immuno-precipitates were then resolved using SDS-PAGE and immunoblotted using the indicated antibodies. **(B)** Quantification of the VPS26A constructs' relative biding to VPS35 and VPS29 from at least 3 independent experiments; error bars indicate s.e.m. Florescent bands were quantified using a Licor Odyssey scanner. Significance was determined through a one-way ANOVA followed by a Dunnett's post-hoc test. Data collected by Dr Kirsty McMillan.

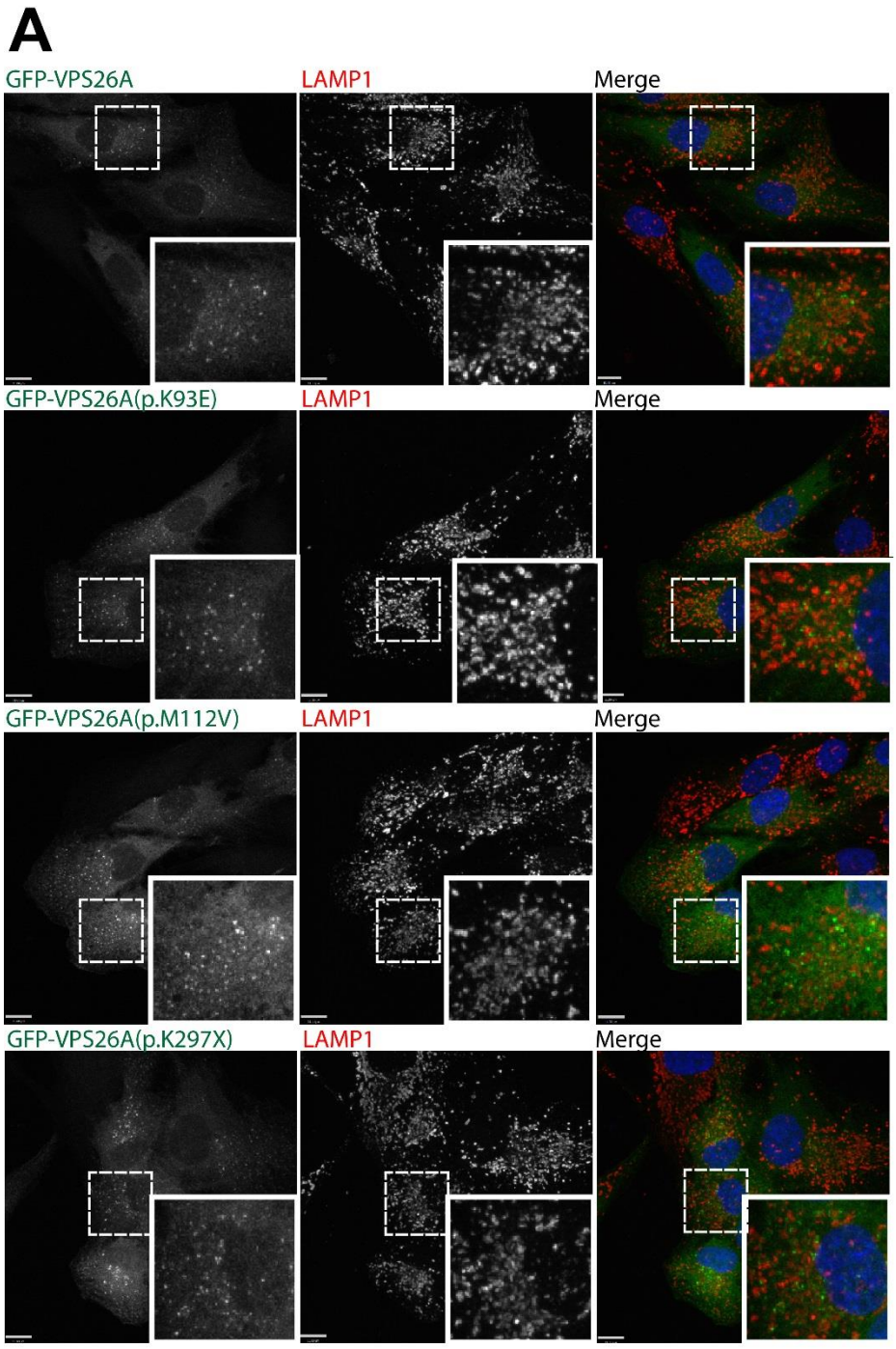
A
GFP-VPS26A
LAMP1
Merge
GFP-VPS26A(p.K93E)
LAMP1
Merge
GFP-VPS26A(p.M112V)
LAMP1
Merge
GFP-VPS26A(p.K297X)
LAMP1
Merge

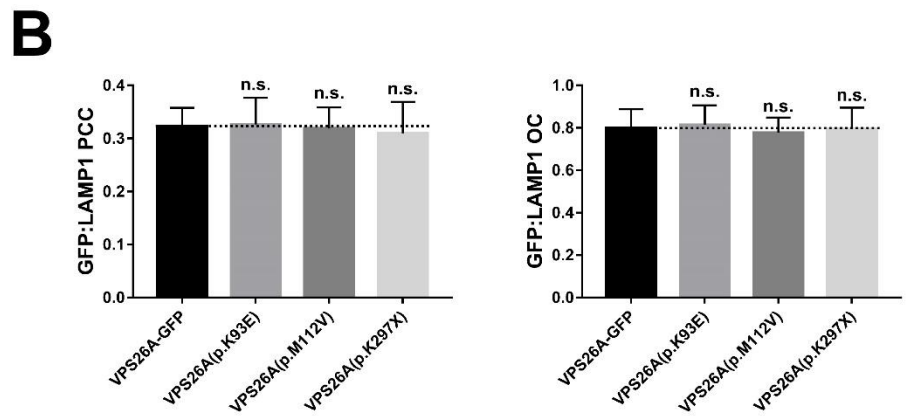
B
GFP:LAMP1 PCC
0.4
0.3
0.2
0.1
0.0
n.s.
n.s.
n.s.
VPS26A-GFP
VPS26A(p.K93E)
VPS26A(p.M112V)
VPS26A(p.K297X)
GFP:LAMP1 OC
1.0
0.8
0.6
0.4
0.2
0.0
n.s.
n.s.
n.s.
VPS26A-GFP
VPS26A(p.K93E)
VPS26A(p.M112V)
VPS26A(p.K297X)

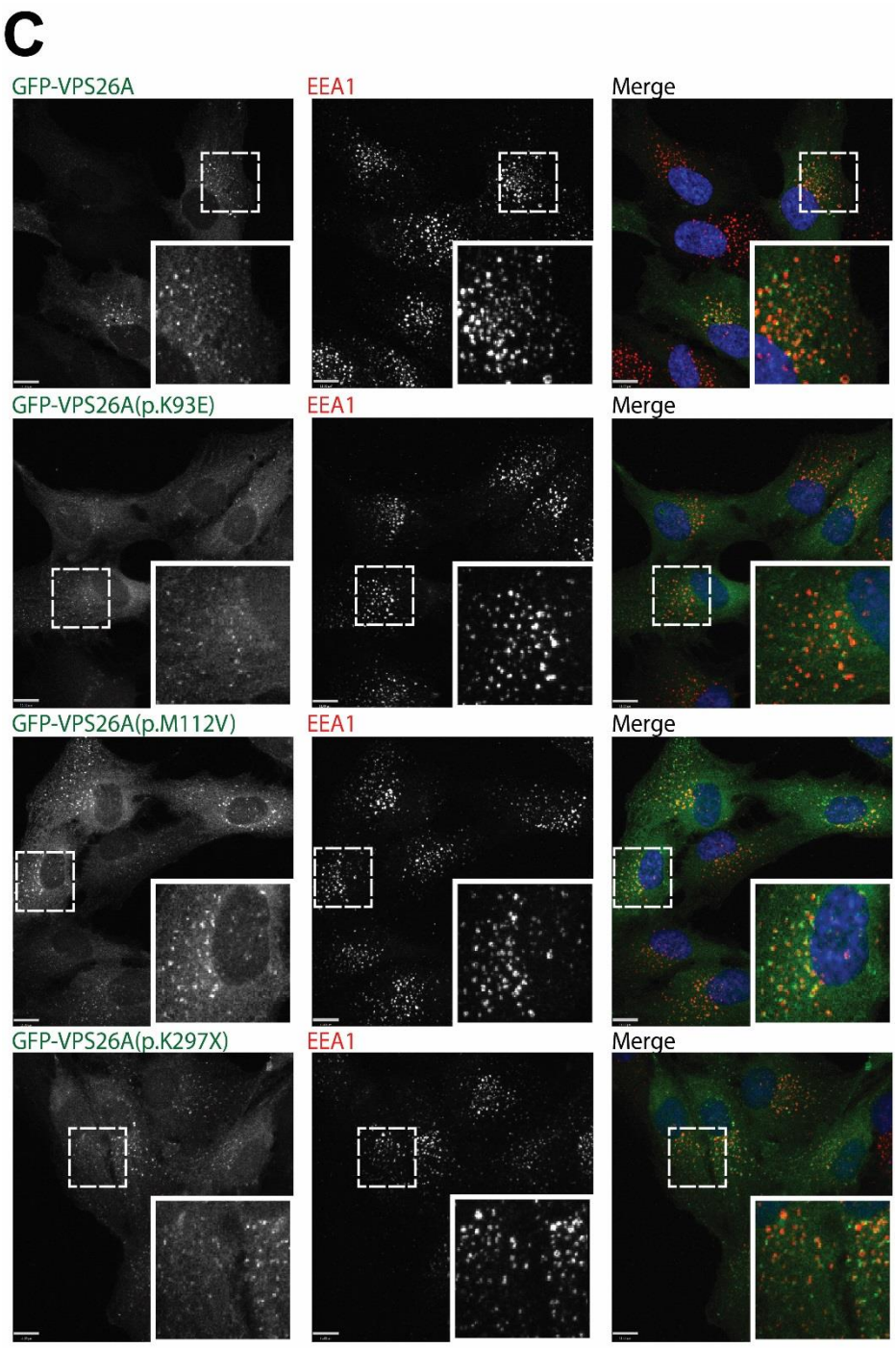
C
GFP-VPS26A
EEA1
Merge
GFP-VPS26A(p.K93E)
EEA1
Merge
GFP-VPS26A(p.M112V)
EEA1
Merge
GFP-VPS26A(p.K297X)
EEA1
Merge
D
GFP:EEA1 PCC
0.4
0.3
0.2
0.1
0.0
n.s.
n.s.
n.s.
VPS26A-GFP
VPS26A(p.K93E)
VPS26A(p.M112V)
VPS26A(p.K297X)
GFP:EEA1 OC
0.8
0.6
0.4
0.2
0.0
n.s.
n.s.
n.s.
VPS26A-GFP
VPS26A(p.K93E)
VPS26A(p.M112V)
VPS26A(p.K297X)

Figure 4.6 The VPS26A Parkinsonism-associated mutations do not change the localisation of the GFP-VPS26A constructs in relation to early or late endosomes.

RPE-1 cells, stably transduced with the indicated GFP-VPS26A constructs, were fixed with 4% paraformaldehyde and immuno-stained for endogenous **(A)** LAMP1 and **(C)** LAMP1. Cells were imaged on a confocal microscope. The scale bar indicates 11 μm. **(B and D)** Quantification of the pearson's colocalisation coefficient (PCC) and the overlap coefficient (OC) over 3 independent experiments, with at least 25 cells quantified per experiment. Error bars indicate standard error. Significance was determined using a one-way ANOVA followed by a post-hoc Dunnett's test, comparing the mutant constructs to wild-type VPS26A-GFP.

4.2.4 The Parkinsonism-linked mutations do not perturb GFP-VPS26A localisation with the WASH complex, EEA1 or LAMP1

I then sought to analyse the localisation of the GFP-VPS26A variants with further endosomal markers. The stably transduced RPE-1 GFP-VPS26A lines were fixed and stained with the late endosomal/lysosomal marker, LAMP1 **(Figure 4.6A)** and the early endosomal marker, EEA1 **(Figure 4.6C)**. No significant differences in colocalisation were detected within the GFP-VPS26A variants and LAMP1 **(Figure 4.6 B)** or EEA1 **(Figure 4.6D)**. I also analysed the colocalisation of the GFP-VPS26A variants with a known interactor of the retromer complex: FAM21 (**Figure 4.7A)**; no significant differences within the GFP-VPS26A variants and endogenous FAM21 were detected **(Figure 4.7B)**.

4.2.5 SILAC-based proteomics reveal changes in the interactome of VPS26A(p.K297X)

As the assembly and localisation of the retromer complex were not perturbed in the GFP-tagged VPS26A variants, I sought to use unbiased proteomics to determine whether the K93E, M112V or K297X mutations affect the interactome of VPS26A. In collaboration with Dr Kirsty McMillan, I used GFP-trap immunoprecipitation coupled with quantitative stable isotope labelling with amino acids in cell culture (SILAC)-based proteomics to directly compare the interactome of the wild-type and mutant GFP-VPS26A variants. I took advantage of the RPE-1 lines which were lentivirally transduced with near endogenous levels of GFP-VPS26A **(Figure 4.3)**. The RPE-1 line stably expressing GFP-VPS26A wild-type was grown in lysine- and arginine-deficient SILAC media, supplemented with 'light' isotopes of lysine and arginine (K0, R0). The GFP-VPS26A(p.K93E), GFP-VPS26A(p.M112V) or GFP-VPS26A(p.K297X) RPE-1 lines were supplemented with 'medium' isotopes of arginine and lysine (K4, R6). Following 8 doublings in the respective SILAC media (to ensure sufficient incorporation

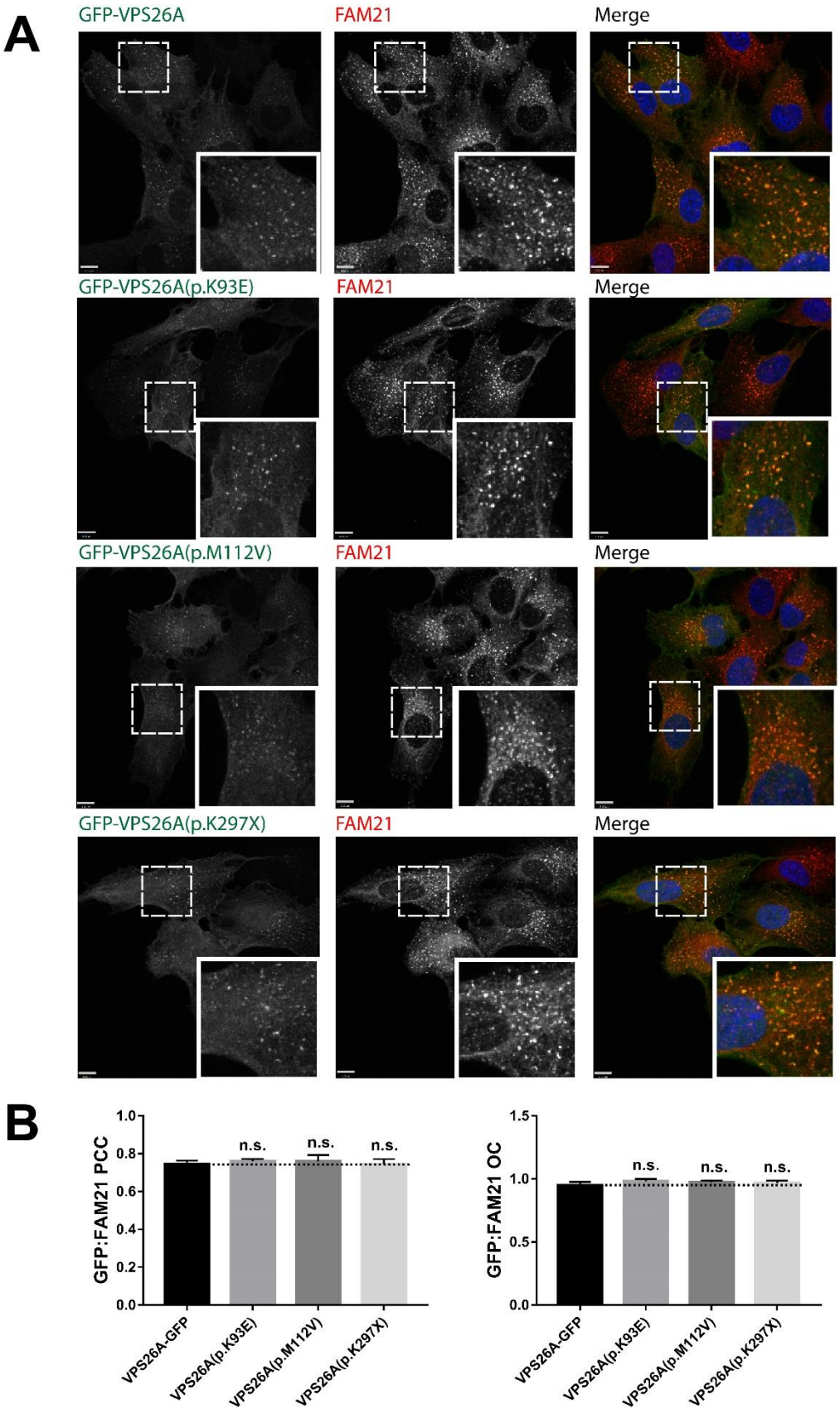

Figure 4.7 The VPS26A Parkinsonism-associated mutations do not change the localisation of the GFP-VPS26A constructs in relation to the retromer-interacting FAM21.

RPE-1 cells, stably transduced with the indicated GFP-VPS26A constructs, were fixed with 4% paraformaldehyde and immuno-stained for endogenous **(A)** FAM21. Cells were imaged on a confocal microscope. The scale bar indicates 9 µm **(B)** Quantification of the pearson's colocalisation coefficient (PCC) and the overlap coefficient (OC) over 3 independent experiments, with at least 25 cells quantified per experiment. Error bars indicate standard error. Significance was determined using a one-way ANOVA followed by a post-hoc Dunnett's test, comparing the mutant constructs to wild-type VPS26A-GFP.

of the new amino acids) the cells were lysed and immunoprecipitated using GFP-trap nanobeads. In each experiment, i.e. GFP-VPS26A(wild-type) vs GFP-VPS26A(mutant), the beads were combined and resolved using SDS-PAGE before being subjected to liquid chromatography-tandem mass spectrometry (LC-MS/MS) identification. Three independent experiments were performed for each of the mutations.

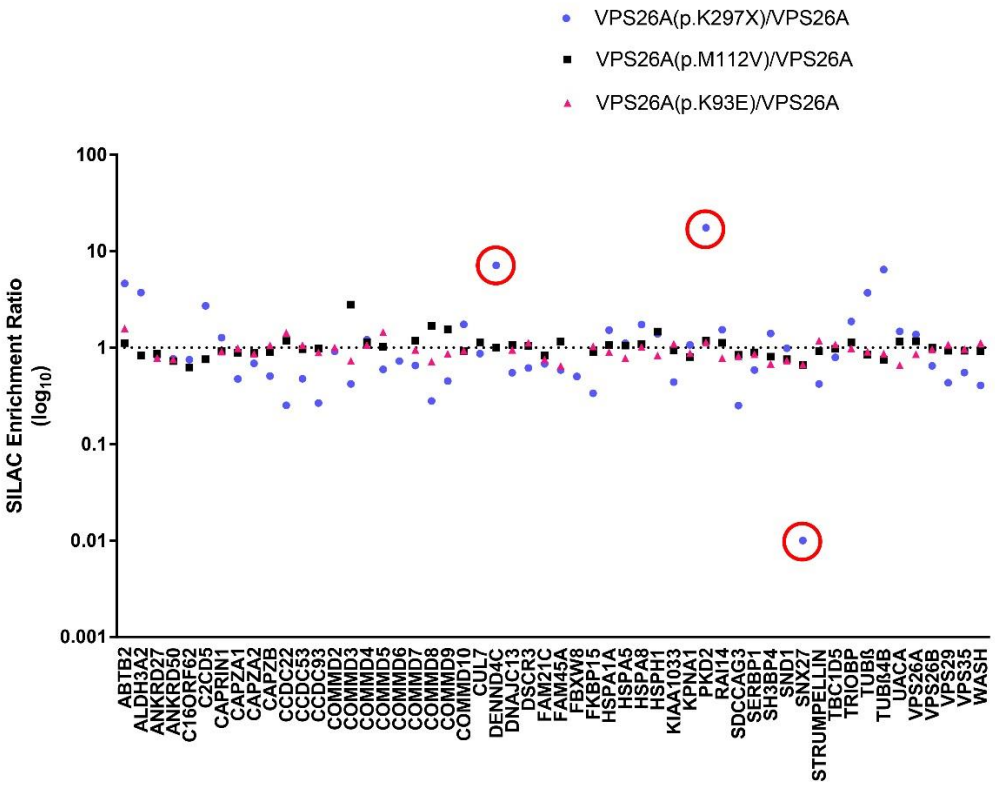

Figure 4.8 SILAC-based proteomics reveals the interactome of the Parkinsonism-linked GFP-VPS26A constructs

RPE-1 cells stably expressing GFP-only, wild-type GFP-VPS26 and Parkinsonism-linked GFP-VPS26A were grown in SILAC medium supplemented with light (R0 K0), medium (R6 K4) heavy (R10 K8) amino acids respectively for 8 doublings. The cells were then lysed and subjected to GFP-trap. The co-immunoprecipitated proteins were resolved using SDS-PAGE and identified using mass spectrometry. The relative enrichment of co-immunoprecipitated proteins of the Parkinsonism-linked VPS26A constructs compared to wild-type VPS26A is indicated in the graph. Data is an average of 3 independent experiments and collected in collaboration with Dr Kirsty McMillan.

There were no drastic changes in the interactome of the GFP-VPS26A compared to the VPS26A(p.K93E) or VPS26A(p.M112V) **(Figure 4.8)**. However, there were several changes in the interactome of VPS26A compared to VPS26A(p.K297X). Most strikingly, the K297X truncation caused a 100-fold loss in binding with SNX27 **(Figure 4.8)**. There was also an 8-fold increase in DENND4C binding and an 11-fold increase in PKD2 binding (**Figure 4.8)**. The mass spectrometry data indicated that VPS26A(p.K297X) had an enhanced binding to ABTB2, ALDH3A2 and TUBβ4B; however, immunoprecipitation experiments failed to validate their interactions with VPS26A(p.K297X) (Dr Kirsty McMillan, unpublished).

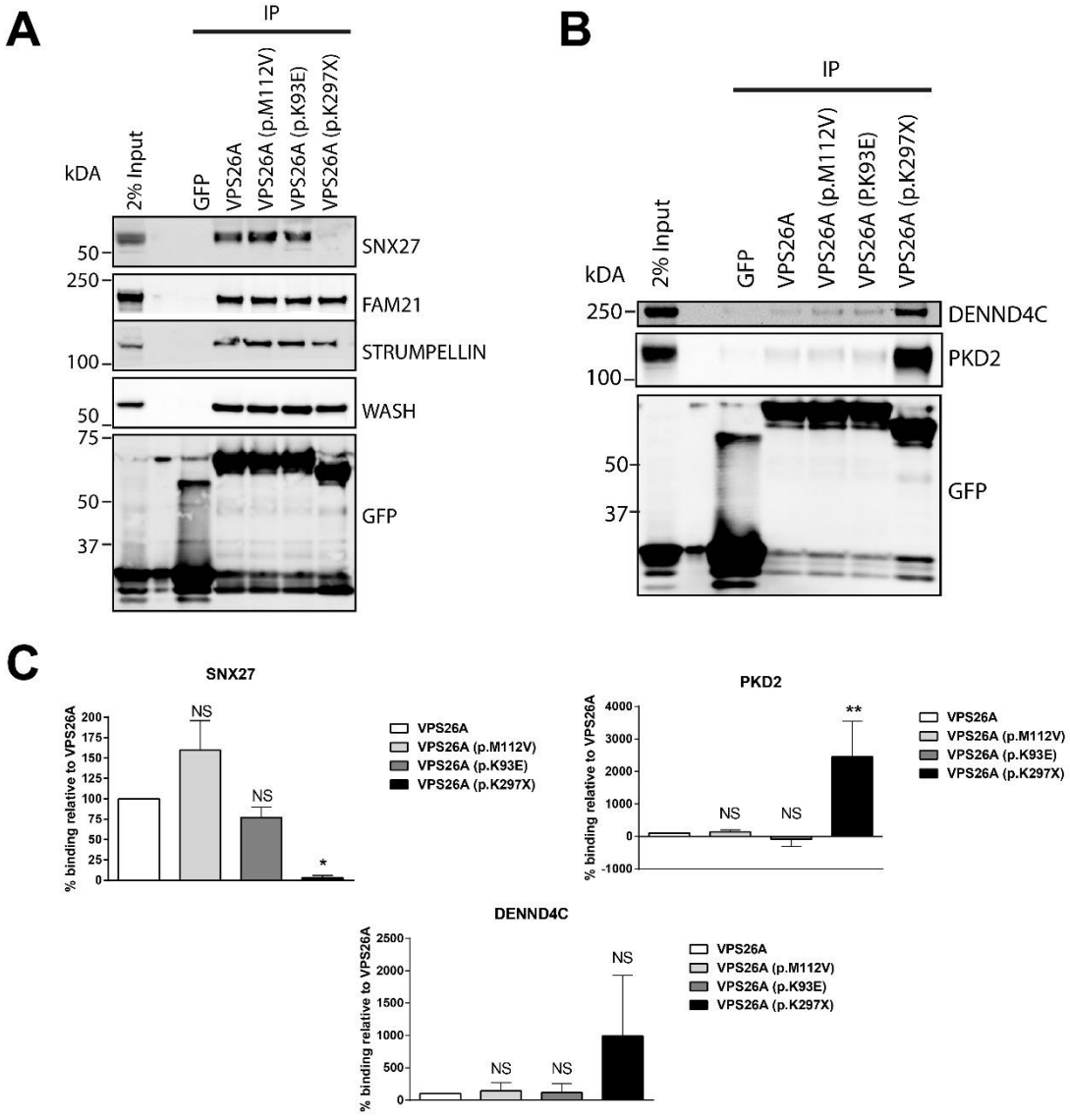

Figure 4.9 The VPS26A(p.K297X) mutation abrogates binding to SNX27 and enhances binding to DENND4C and PKD2.

(A-B) HEK293T cells were transfected with the indicated GFP-VPS26A construct and subjected to a GFP trap experiment. The immuno-precipitates were then resolved using SDS-PAGE and immuno-blotted with the indicated antibodies. **(C)** Relative binding of the VPS26A constructs

compared to wild-type VPS26A. The intensities of the fluorescent bands were quantified using a Licor Odyssey scanner over 3 independent experiments. Error bars indicate standard error; data analysed using a one-way ANOVA followed by a Dunnett's post hoc test; * P ≤ 0.05; ** P ≤ 0.01. Data in this figure was collected by Dr Kirsty McMillan and Dr Frances Tilley.

Dr Kirsty McMillan confirmed that the introduction of 'K297X' perturbed SNX27 association through GFP-trap immunoprecipitations of the GFP-VPS26A constructs **(Figure 4.9A and Figure 4.9C).** The gain of DENND4C and PKD2 associations were confirmed by Dr Frances Tilley, also through a GFP-trap immunoprecipitation **(Figure 4.9B and Figure 4.9C)**.

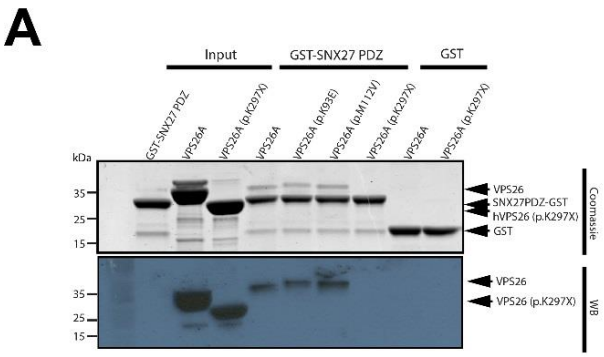

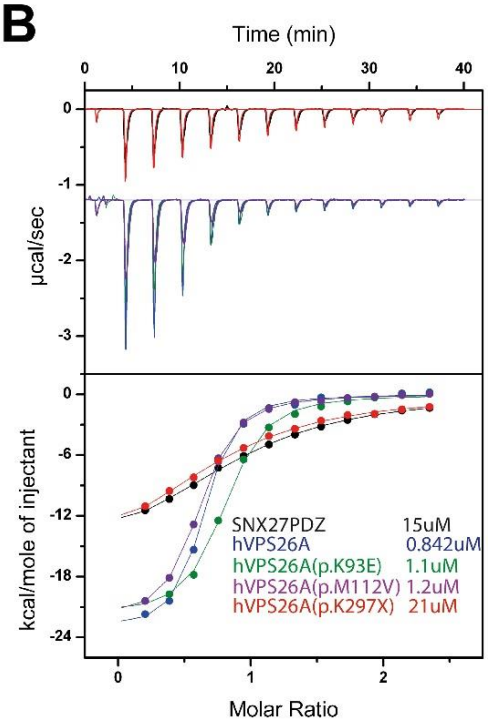

C

Protein	Kir3.3 Sequence	Kd (µM)	ΔH (kcal/mol)	TΔS (kcal/mol)	ΔG (kcal/mol)	Stoichiometry, N
SNX27PDZ	PPESESKV	15±2	-16.0±1.8	-9.4±1.7	-6.6±2.5	0.86±0.03
SNX27PDZ + VPS26	PPESESKV	0.84±0.05	-22.6±0.5	-14.2±0.5	-8.3±0.7	0.61±0.04
SNX27PDZ + VPS26(pK93E)	PPESESKV	1.05±0.01	-21.0±0.0	-12.9±0.0	-8.2±0.0	0.73±0.02
SNX27PDZ + VPS26(pM112V)	PPESESKV	1.21±0.01	-21.7±0.1	-13.7±0.1	-8.1±0.2	0.58±0.01
SNX27PDZ + VPS26(pK297X)	PPESESKV	21±5	-21.0±3.1	-14.6±3.2	-6.4±4.5	0.76±0.05

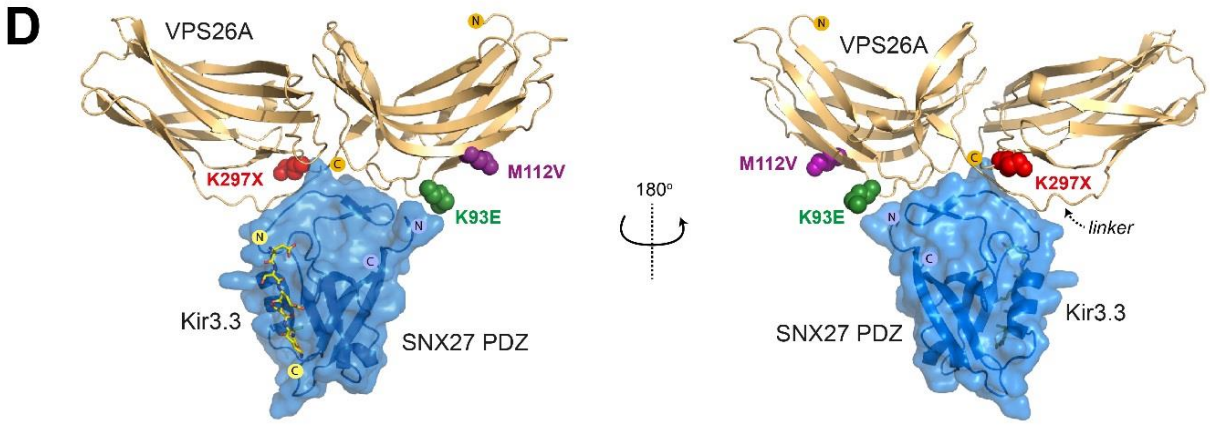

Figure 4.10 The binding of VPS26A(p.K297X) is severely perturbed SNX27.

(A) Recombinantly expressed GST-SNX27 PDZ domain and His-tagged human VPS26A constructs were purified via the GST-tag. The purified proteins were resolved on an SDS-PAGE and detected by Coomassie staining (top) or Western blotting using anti-His antibody (bottom). **(B)** Isothermal Titration Calorimetry (ITC) was used to calculate the binding affinity of the Kir3.3 peptide to the SNX27-binding domain alone, or in the presence of wild-type or mutant VPS26A (green). The raw data is shown at the top and the integrated and normalised data is shown at the bottom. **(C)** Table of the binding affinities of the Kir3.3 peptide (PPESESKV) to the SNX27 PDZ domain alone, or in the presence of VPS26A constructs. **(D)** Structural modelling of VPS26A (gold ribbon) complexed to SNX27 (blue ribbon) from Gallon et al., 2014. The Parkinsonism-associated mutations are indicated, as is the site of the Kir3.3 (yellow sticks) interaction (modelled based on the SNX27-Kir3.3 structure from Balana et al., 2011). Data in this figure was collected by Dr Thomas Clairefeuille.

The severe reduction of association between VPS26A(p.K297X) and SNX27 was further confirmed by Dr Thomas Clairefeuille through direct binding assays. The VPS26A variants were purified from *E. coli* and incubated with GST-tagged SNX27 PDZ domain. Immunoprecipitating the GST-SNX27 PDZ could pull-down VPS26A, VPS26A(p.K93E) and VPS26A(p.M112V) but not VPS26A(p.K297X) **(Figure 4.10A)**. Dr Thomas Clairefeuille then used isothermal titration calorimetry to measure the binding affinity of the tail of the SNX27-dependent cargo, Kir3.3 (including its PDZ ligand) (Balana et al., 2011), to the SNX27 PDZ domain. On its own, the SNX27 PDZ domain has a low affinity for Kir3.3 (a Kd of 15 ± 2 μM) **(Figure 4.10B-C)**. When VPS26, VPS26A(p.K93E) or VPS26A(p.M112V) was added with the SNX27 PDZ domain, the formation of SNX27-retromer allosterically increased its affinity for Kir3.3 (Kds of 0.84 ± 0.05 μM, 1.05 ± 0.01 μM and 1.21 ± 0.01 μM respectively) **(Figure 4.10B-C)**. However, when VPS26A(p.K297X) was added with the SNX27 PDZ domain, the affinity was not enhanced (a Kd of 21 ± 5 μM) **(Figure 4.10B-C)**. Therefore, VPS26A(p.K297X) fails to form the SNX27-retromer and the allosteric enhancement of Kir3.3 affinity did not occur.

4.2.6 VPS26A(p.K297X) fails to retrieve the SNX27-depedent cargo, GLUT1, away from lysosomal degradation

Having established that the VPS26A K297X mutation perturbs SNX27 binding and the formation of the SNX27-retromer, Dr Kirsty McMillan examined the trafficking of the well-characterised SNX27-dependent cargo, GLUT1 (Steinberg et al., 2013b). The steady-state localisation of GLUT1 is at the cell surface; RNAi against VPS26A and VPS26B in HeLa cells caused GLUT1 to be rerouted to the lysosomes and colocalise with LAMP1 (Gallon et al., 2014a) **(Figure 4.11A).** When siRNA-resistant GFP-VPS26A

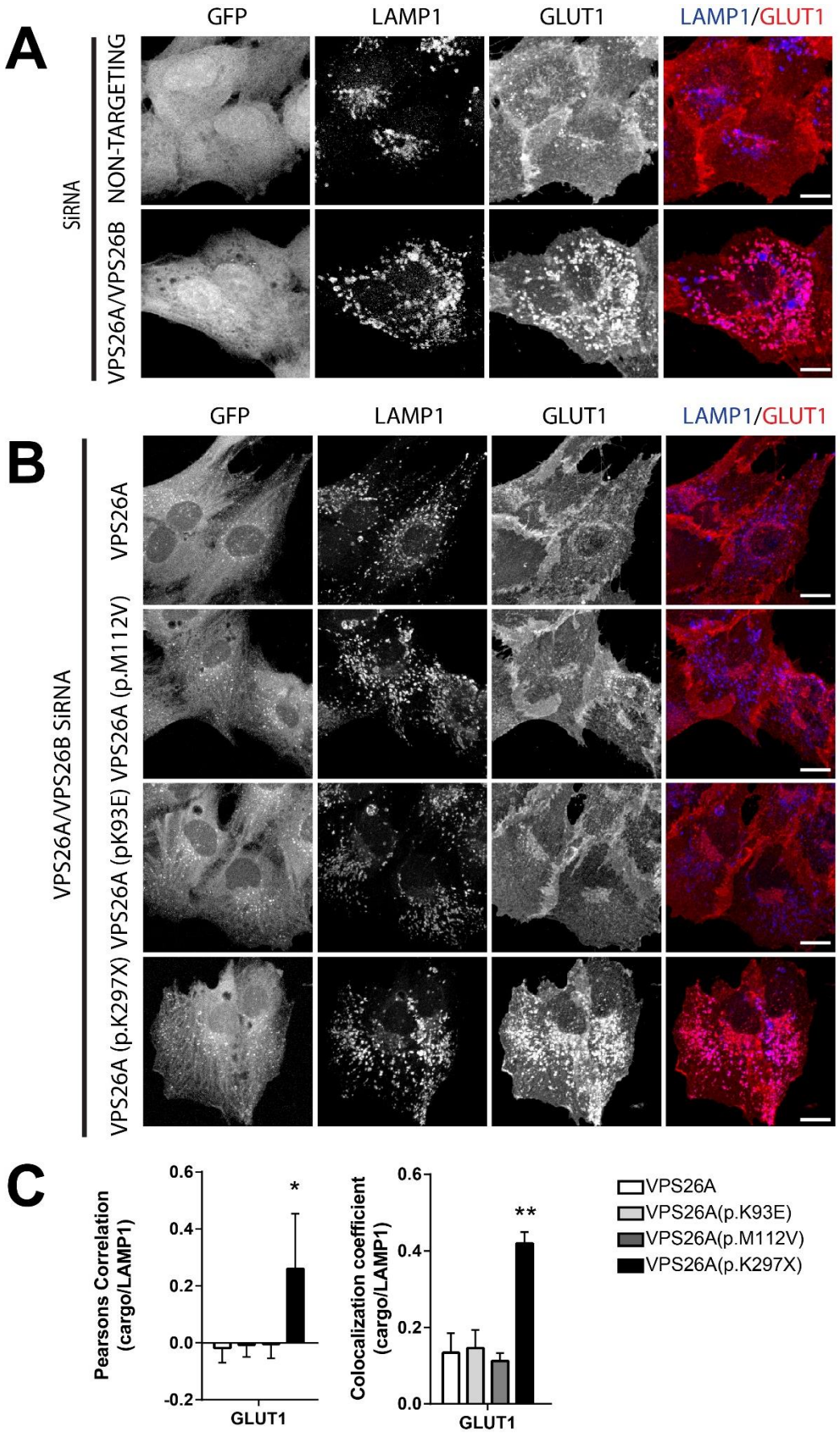

Figure 4.11 VPS26A(p.K297X) missorts the SNX27-dependent cargo GLUT1.

(A) RPE-1 cells transfected with GFP were suppressed with non-targeting or VPS26A and VPS26B siRNA. Cells were fixed using 4% paraformaldehyde and immuno-stained for endogenous LAMP1 and GLUT1. The cells were imaged on a confocal microscope. The scale bar indicates 10 µm. **(B)** RPE-1 cells, suppressed for VPS26A and VPS26B, stably expressing the indicated siRNA-resistant VPS26A-GFP constructs, were fixed with 4% paraformaldehyde. The cells were then immuno-stained with LAMP1 and GLUT1. The scale bar indicates 10 µm. **(C)** The Pearson's colocalisation coefficient and Overlap coefficient were quantified over 3 independent experiments. Error bars indicated standard error and data were analysed using a one-way ANOVA followed by a Dunnett's post hoc test; * P ≤ 0.05; ** P ≤ 0.01. Data from this figure was collected by Dr Kirsty McMillan.

was transfected into the HeLa cells under VPS26A/B suppression, GLUT1 retained its localisation at the cell surface, as did transfection of siRNA-resistant GFP-VPS26A(p.K93E) or GFP-VPS26A(p.M112V) **(Figure 4.11B-C)**. However, when Dr Kirsty McMillan transfected GFP-VPS26A(p.K297X), GLUT1 colocalised with the late endosomal/lysosomal marker LAMP1 **(Figure 4.11B-C)**.

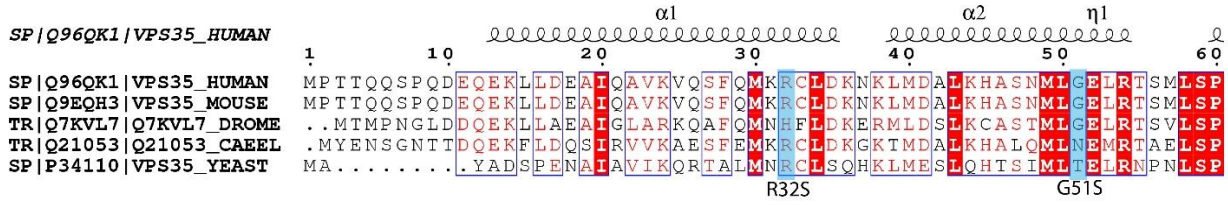

Figure 4.12 Bioinformatic alignment of VPS35 homologues, highlighting the N-terminal Parkinson's disease associated mutations.

Sequence alignment of the first 60 amino acids of VPS35 between *H. sapiens*, *M. musculus*, *D. melanogaster*, *C. elegans* and *S. cerevisiae* homologues. The positions of the R32S and G51S Parkinsonism-linked mutations are highlighted in blue.

4.2.7 Initial bioinformatic analysis of the VPS35 N-terminal Parkinsonism-linked mutations

VPS35 is the most commonly mutated protein in the retromer complex associated with Parkinsonism disorders (McMillan et al., 2017). The most common mutation in the retromer complex is VPS35(p.D620N) (McMillan et al., 2017). There have also been several other, much rarer mutations in VPS35, which have not been proven to be causative. Two mutations, clustering around the N-terminus of VPS35, have been linked to Parkinsonism disorders: VPS35(p.R32S) and VPS35(p.G51S). This region of VPS35 is known to bind to VPS26, SNX3 and Rab7 (Shi et al., 2006; Rojas et al., 2008; Harrison et al., 2014a). To determine the degree of conservation of these residues across species, I aligned various VPS35 homologues **(Figure 4.12)**. R32 is

highly conserved in all species compared except *D. melanogaster* and G51 is conserved except for in *C. elegans* and *S. cerevisiae* **(Figure 4.12)**.

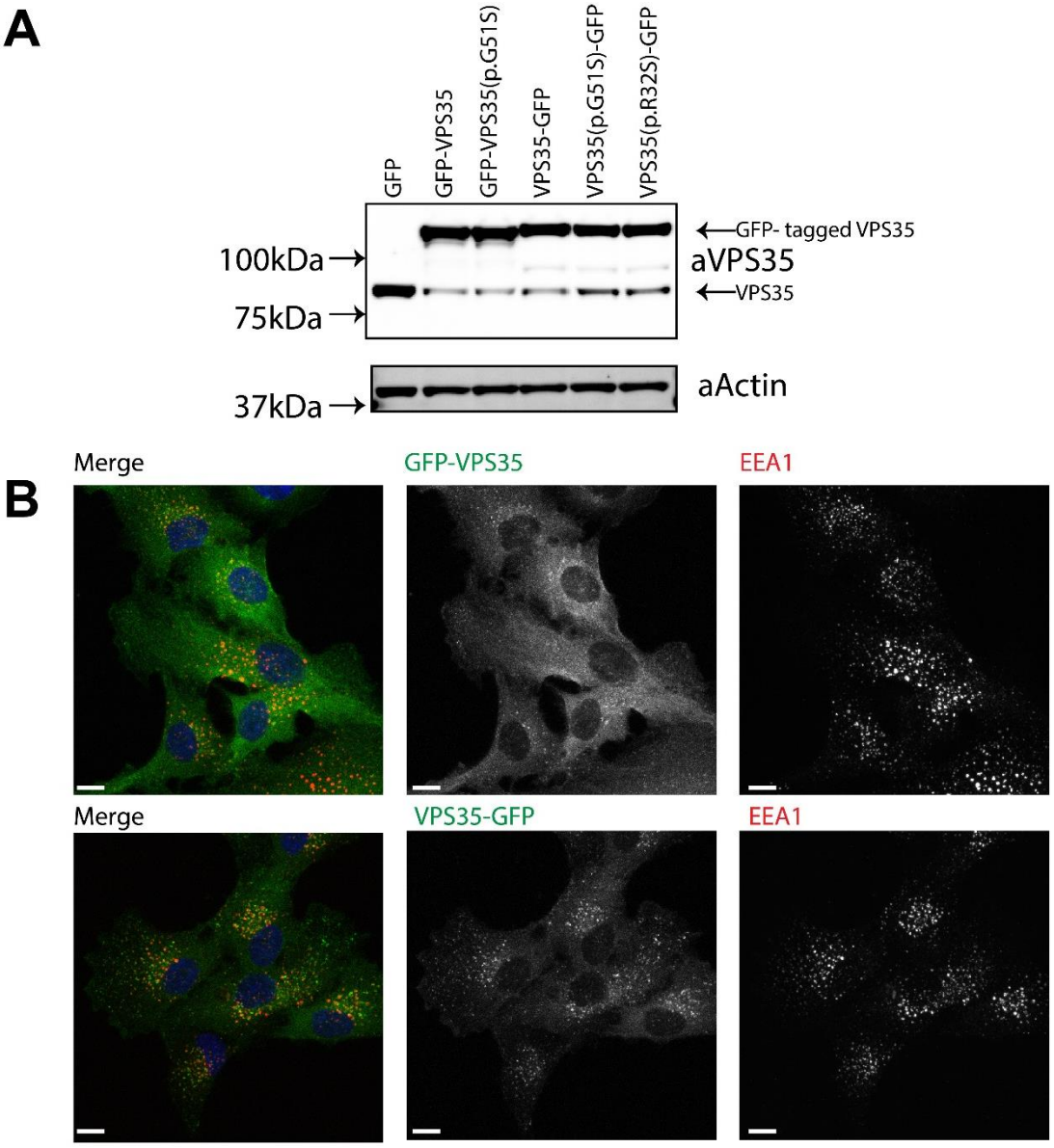

Figure 4.13 The VPS35-GFP construct is more endosomal compared to the GFP-VPS35 construct.

(A) RPE-1 cells were lentivirally transduced with the indicated GFP-tagged VPS35 construct. The cells were lysed, the lysate resolved by SDS-PAGE and immunoblotted for the indicated antibodies. **(B)** RPE-1 cells, transduced with VPS35-GFP or GFP-VPS35, were fixed using 4% paraformaldehyde and immuno-stained with EEA1. The cells were imaged on a confocal microscope. The scale bars indicate 11 µm.

4.2.8 Generation of C-terminal VPS35-GFP construct

Since the Parkinsonism linked mutations VPS35(p.R32S) and VPS35(p.G51S) are located at the N-terminus of VPS35, I created a C-terminal VPS35-GFP construct. To

compare the newly created VPS35-GFP chimera to GFP-VPS35, I cloned both constructs into XLG3 lentiviral vectors, packaged them into lentivirus and transduced RPE-1 cells. This resulted in stable RPE-1 lines which expressed either GFP-VPS35 or VPS35-GFP, both at similar levels and near to the endogenous level of expression **(Figure 4.13A)**. As seen in the transduction of GFP-VPS26A **(Figure 4.3)**, expressing GFP-tagged VPS35 caused the whole cell levels of the endogenous protein to decrease **(Figure 4.13A)**. Immunofluorescence analysis of the GFP-VPS35 and VPS35-GFP stable RPE-1 lines revealed that the GFP-VPS35 chimera had a more cytosolic localisation compared to the VPS35-GFP chimera **(Figure 4.13B)**.

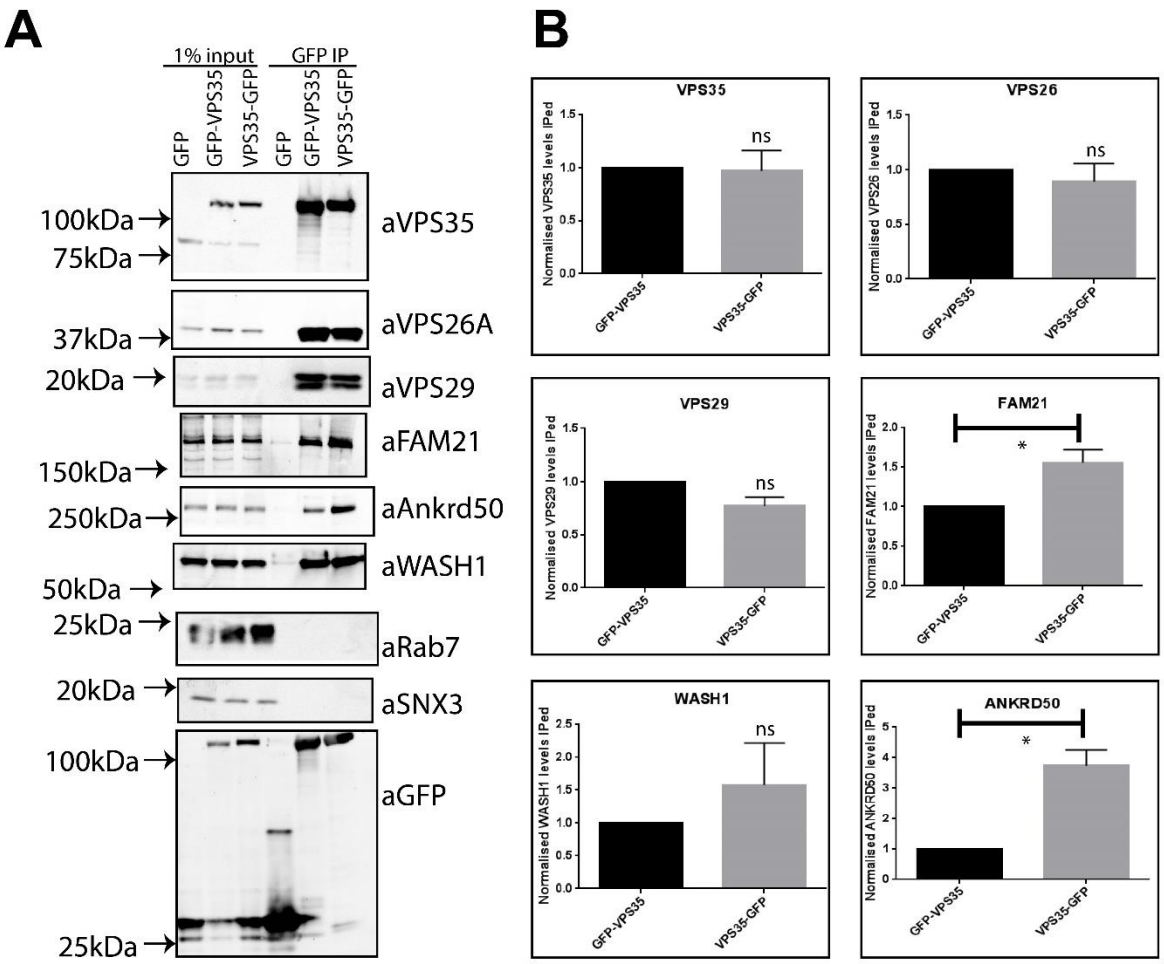

Figure 4.14 The C-terminal GFP tag enhances binding to the WASH complex and does not perturb retromer complex assembly.

(A) HEK293T cells were transfected with the indicated GFP-tagged construct and subjected to a GFP-trap. The immuno-precipitates were resolved using SDS-PAGE and immuno-blotted using the indicated antibodies. **(B)** Quantification of the relative binding between VPS35-GFP and the indicated proteins relative to the binding of GFP-VPS35. Quantification is representative of 3 experiments; significance was determined using a student's t-test; error bars indicate s.e.m.; * $P \leq 0.05$.

I then compared the ability of the two VPS35 chimeras to assemble into the retromer complex and to bind to known retromer interactors **(Figure 4.14A)**. Importantly, the retromer complex could still form **(Figure 4.14)**. Surprisingly, there was a trend towards increased WASH1 association and a significant increase in FAM21 association in the C-terminally tagged VPS35 construct compared to the N-terminally tagged VPS35 construct **(Figure 4.14)**. There was also a significant increase in association with Ankrd50 **(Figure 4.14)**, a WASH complex-associated protein (McGough et al., 2014a). As the C-terminus of VPS35 has been implicated in WASH-complex binding (Helfer et al., 2013) (see also Chapter 5), it is unlikely that the N-terminal GFP tag was occluding association with the WASH complex. I would speculate that it is the increase in endosomal association of the C-terminally tagged VPS35 construct that is causing the increased binding to the WASH complex components.

The interactome of GFP-VPS35 has been elucidated (McGough et al., 2014a), but GFP-tagging on one end of a protein can occlude some protein interactors (McNally et al., 2017). I therefore used SILAC-based proteomics coupled to a GFP-trap immuno-precipitation to generate the VPS35-GFP interactome to explore whether any other interactors could be identified. The VPS35-GFP interactome is shown in **Table 4.2** and **Figure 4.15**. Most of the GFP-VPS35 interactors: the other retromer components, WASH complex components, VARP, SDCCA3, TBC1D5, and polycystin-2, were identified in the VPS35-GFP interactome. In addition, other interactors were identified such as Aven [an inhibitor of caspase activation (Chau et al., 2000)] and LMO7 [a protein which contains PDZ, LIM and Calponin Homology domains and localises and contributes to the integrity of adherens junctions (te Velthuis and Bagowski, 2007)] . However, as suitable antibodies could not be validated I could not confirm these interactions through GFP-trap immunoprecipitations.

GFP-VPS35 interactors that are missing in the VPS35-GFP interactome are identified in **Table 4.3**. Notable validated retromer interactors that are absent in the VPS35-GFP interactome include: Ankrd50, FKBP15 and DNAJC15 (McGough et al., 2014a). The proteasome proteins in the GFP-VPS35 interactome were originally thought to be an artefact of the overexpression of GFP-VPS35; I may have avoided this by using a near endogenous level of VPS35-GFP expression **(Figure 4.13A)**. Using a near endogenous level of expression may have masked some lower affinity interactions, as the binding between VPS35-GFP and Ankrd50 has been validated through overexpression of VPS35-GFP in HEK293T cells coupled to a GFP-trap **(Figure 4.14)**.

Accession Number	Name	Average Score	Average Coverage	Average # Unique Peptides	Average # Peptides	Average # PSMs	Average Medium/Light ratio
A0A024R2H0	TBC1 domain family, member 5, isoform CRA	711.34	52.90	1.00	43.00	239.00	323.79
Q96NW4	Ankyrin repeat domain-containing protein 27 (VARP)	192.15	42.24	32	32	73	265.33
H7C331	Serologically defined colon cancer antigen 3	6.47	17.67	2.50	2.50	2.50	210.95
Q9UBQ0	VPS29	270.79	66.76	1.50	14.00	113.00	203.93
Q92609	TBC1 domain family member 5	726.68	52.90	1.00	43.00	243.00	176.24
Q53FR4	Vacuolar protein sorting 35 variant	1698.14	53.52	14.00	50.50	602.00	164.12
J3KP06	LIM domain only protein 7	37.18	8.96	11.50	12.50	17.00	162.28
Q4G0F5	VPS26B	406.84	56.25	20.00	23.00	151.00	161.72
B0QYK0	RNA-binding protein EWS	42.12	11.00	3.50	4.00	10.00	140.20
Q9NQS1	Cell death regulator Aven	23.22	19.48	4.50	4.50	8.00	136.38
Q5HYM2	VPS35	1474.94	55.19	2.50	39.00	496.50	117.73
O75436	VPS26A	1063.87	75.08	9.50	29.50	361.00	97.69
Q9Y4E1	WASH complex subunit FAM21C	287.95	30.13	3.00	34.50	100.50	78.31
K7EIY1	FAM32A	6.85	32.98	3.00	3.00	3.50	74.59
F8VXU5	VPS29	278.10	54.67	1.00	13.50	117.00	69.60
C4AMC7	WASH1	88.84	27.11	3.50	11.00	29.50	62.82
Q12768	Strumpellin	336.61	44.87	51.00	51.00	131.50	51.99
Q13563	Polycystin-2	120.24	23.66	19.50	19.50	46.50	41.92
A6H8X9	Centrosomal protein 170kDa	8.15	2.85	3.50	3.50	4.00	38.78
Q641Q2	FAM21A	308.13	32.75	6.00	35.00	103.50	29.84
B4DI81	Gap junction protein	33.10	25.07	5.50	5.50	10.00	28.43
A9QQ22	Actin nucleation promoting factor	104.81	28.42	2.00	9.50	33.50	27.12

Q8NDH0	WD repeat-containing protein 6	12.01	8.50	5.00	5.00	6.00	19.25
I6L9E8	Family with sequence similarity 98, member A	35.93	17.47	5.50	7.00	11.00	18.32
Q59H57	Fusion (Involved in t(12;16) in malignant liposarcoma) isoform a variant	125.59	31.84	6.50	10.50	49.50	17.19
B7ZKT9	KIAA1033 protein	209.91	26.92	31.50	32.00	89.50	15.31
O75190	DnaJ homolog subfamily B member 6	17.73	13.26	3.50	3.50	8.50	13.41
F5GWI9	CCDC53	24.75	24.31	3.50	3.50	7.50	12.04
R4GN98	Protein S100	35.62	35.89	6.50	6.50	23.00	11.65
Q8ND56	Protein LSM14 homolog A	1.78	3.89	2.00	2.00	3.00	10.45
Q14011	Cold-inducible RNA-binding protein	22.22	20.93	3.00	3.00	8.50	10.12
Q5VW36	Focadhesin	69.67	12.05	14.50	21.00	32.00	9.19
D9ZGF5	Fibroblast growth factor	20.40	26.13	4.50	4.50	9.50	8.62
A0A0U1RQH7	RNA-binding protein 39	26.22	26.13	5.00	5.00	11.50	6.71

Table 4.2 VPS35-GFP interactome

Highlighted in green are proteins in the retromer complex; in yellow are proteins in the WASH complex; in blue are other known retromer complex interactors. AA= amino acid; PSMs= peptide-to-spectrum matches (the total number of identified peptide sequences).

GFP-VPS35 interactor
Acetolactate synthase-like protein [ILVBL_HUMAN]
Proteasome (Prosome, macropain) 26S subunit, non-ATPase, 12, isoform CRA_c [A6NP15_HUMAN]
Uncharacterized protein [F5H0J6_HUMAN]
CDP-diacylglycerol--inositol 3-phosphatidyltransferase [CDIPT_HUMAN]
DnaJ homolog subfamily C member 13 [DJC13_HUMAN]
Proteasome subunit alpha type-2 [PSA2_HUMAN]
Proteasome subunit alpha type-4 [PSA4_HUMAN]
26S protease regulatory subunit 6B [PRS6B_HUMAN]
Fatty aldehyde dehydrogenase OS=Homo sapiens [AL3A2_HUMAN]
Uncharacterized protein [Q05DG7_HUMAN]
FK506-binding protein 15 [FKB15_HUMAN]
Ankyrin repeat domain-containing protein 13A [AN13A_HUMAN]
26S proteasome non-ATPase regulatory subunit 1 [PSMD1_HUMAN]
Ankyrin repeat domain-containing protein 50 [ANR50_HUMAN]

Table 4.3 GFP-VPS35 interactome members not present in VPS35-GFP interactome

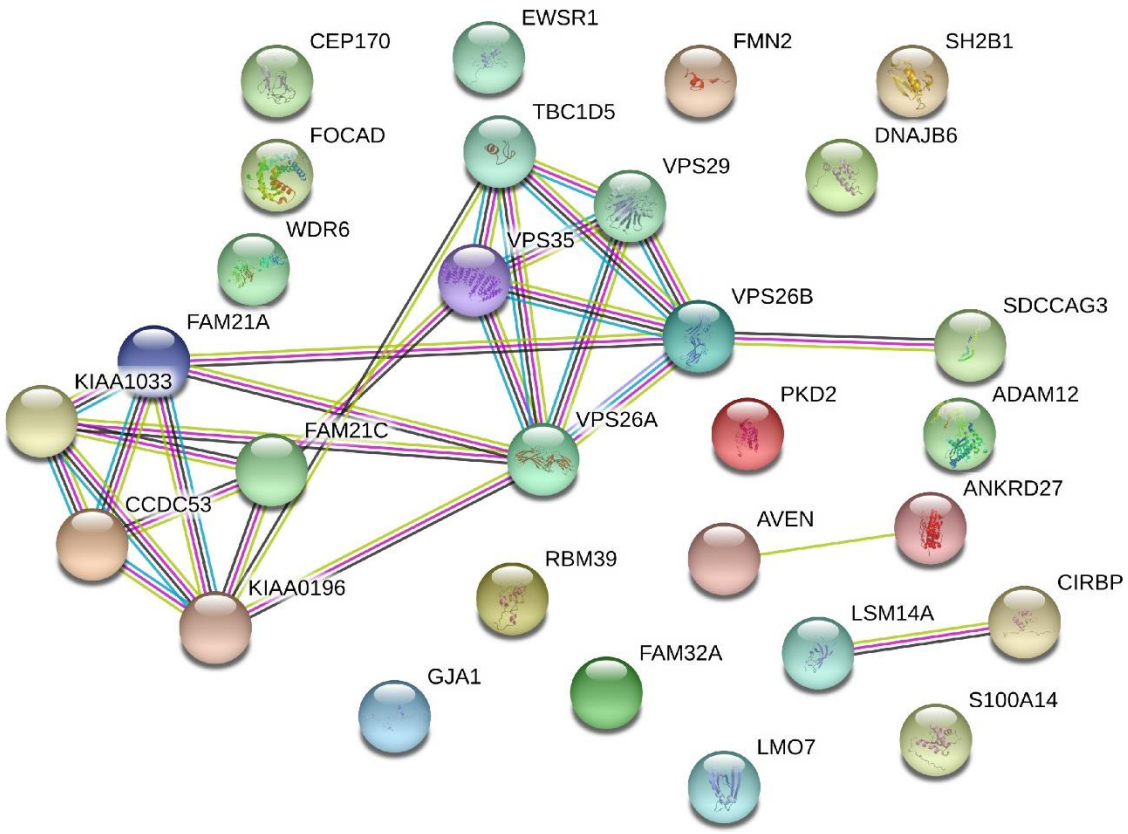

Figure 4.15 SILAC-based proteomics reveal the VPS35-GFP interactome.

STRING Analysis of the VPS35-GFP interactome, identifying connections between interactors in the dataset. RPE-1 cells, stably expressing GFP-only or VPS35-GFP, were grown in SILAC media supplemented with light (R0 K0) or medium (R6 K4) amino acids respectively, for 8 doublings. The

cells were then subjected to GFP-trap and the immuno-precipitates resolved using SDS-PAGE. The co-immunoprecipitated proteins were then identified using mass spectrometry.

4.2.9 The Parkinsonism-linked VPS35 mutations do not perturb retromer complex association

Having validated VPS35-GFP transduced cells as an appropriate model to investigate the N-terminal Parkinsonism-linked mutations, I undertook site-directed mutagenesis to introduce the R32S and G51S mutations. VPS26 binds to the N-terminus of VPS35 (Shi et al., 2006). I firstly tested whether the R32S or G51S mutations perturbed retromer complex assembly. I transfected HEK293T cells with the VPS35-GFP variants and performed a GFP-trap immunoprecipitation **(Figure 4.16A)**. There were no significant differences in the VPS35(p.R32S)-GFP and VPS35(p.G51S)-GFP variants' abilities to bind to VPS26 or VPS29 compared to VPS35-GFP **(Figure 4.16B)**.

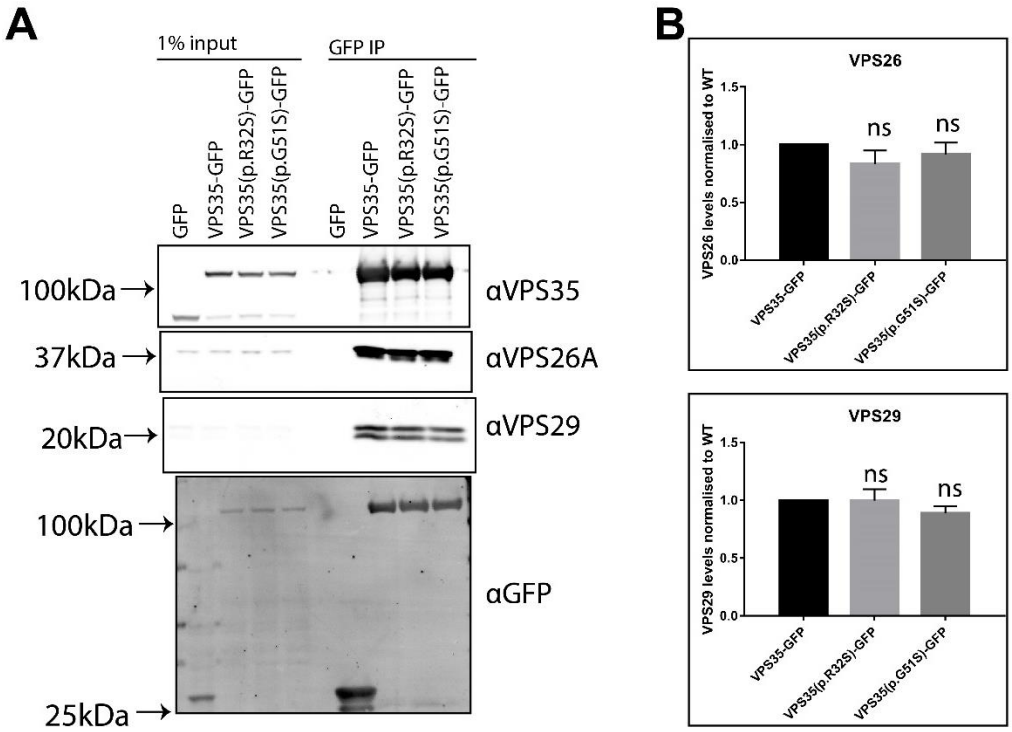

Figure 4.16 The Parkinsonism-linked VPS35(p.R32S) and VPS35(p.G51S) do not perturb retromer complex assembly.

(A) HEK293T cells were transfected with the indicated GFP-tagged construct and subjected to GFP-trap. The immuno-precipitates were resolved using SDS-PAGE and immuno-blotted for the indicated antibodies. **(B)** Quantification of the florescent bands, normalised to wild-type VPS35-GFP, using the Licor Odyssey Scanner from 3 independent experiments. Error bars indicate standard error. Data were analysed using a one-way ANOVA followed by a Dunnett's post-hoc test.

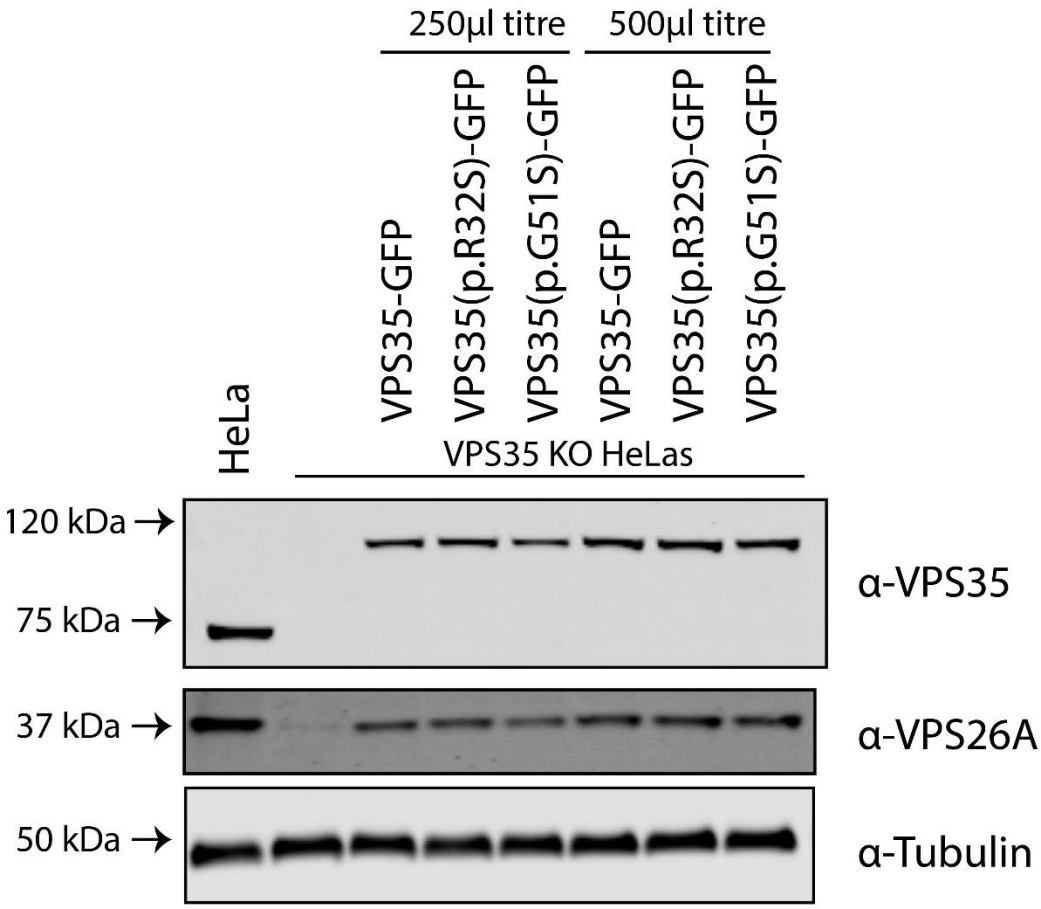

Figure 4.17 Creation of stably transduced VPS35-GFP lines in VPS35 knockout HeLa cells.

VPS35 knockout HeLa cells, obtained from Dr Florian Steinberg, were lentivirally transduced with titres (250µl or 500µl) of the indicated VPS35-GFP constructs. The cells were then lysed, the lysate resolved using SDS-PAGE, and immuno-stained for the indicated antibodies.

4.2.10 The Parkinsonism-linked VPS35 mutations do not perturb VPS35 localisation

Having gained access to CRISPR-Cas9 gene-edited VPS35 knockout HeLa cells from Dr Florian Steinberg, I transduced VPS35-GFP, VPS35(p.R32S)-GFP and VPS35(p.G51S)-GFP to near endogenous levels **(Figure 4.17)**. Like the siRNA-mediated knockdown of VPS35, knockout of VPS35 destabilises the entire retromer complex, causing the whole cell levels of VPS26 and VPS29 to decrease (McNally et al., 2017). When I transduced the VPS35 knockout cells with VPS35-GFP, the whole-cell levels of the retromer component VPS26 also increased **(Figure 4.17)**. Transducing the VPS35 knockout cells with VPS35-GFP allowed me to examine the localisation of the VPS35-GFP constructs without overexpression or an endogenous VPS35 background. Immunofluorescence analysis revealed no differences between the VPS35-GFP variants in their colocalisation with: SNX1

(Figure 4.18A-B); the early endosomal marker, EEA1 **(Figure 4.19A and C)**; the late endosomal marker, LAMP1 **(Figure 4.19B and C)**; or FAM21 **(Figure 4.20A-B)**. Furthermore, all the VPS35-GFP variants could rescue the localisation of FAM21 when reintroduced into the VPS35 knockout cells **(Figure 4.20 and C)**.

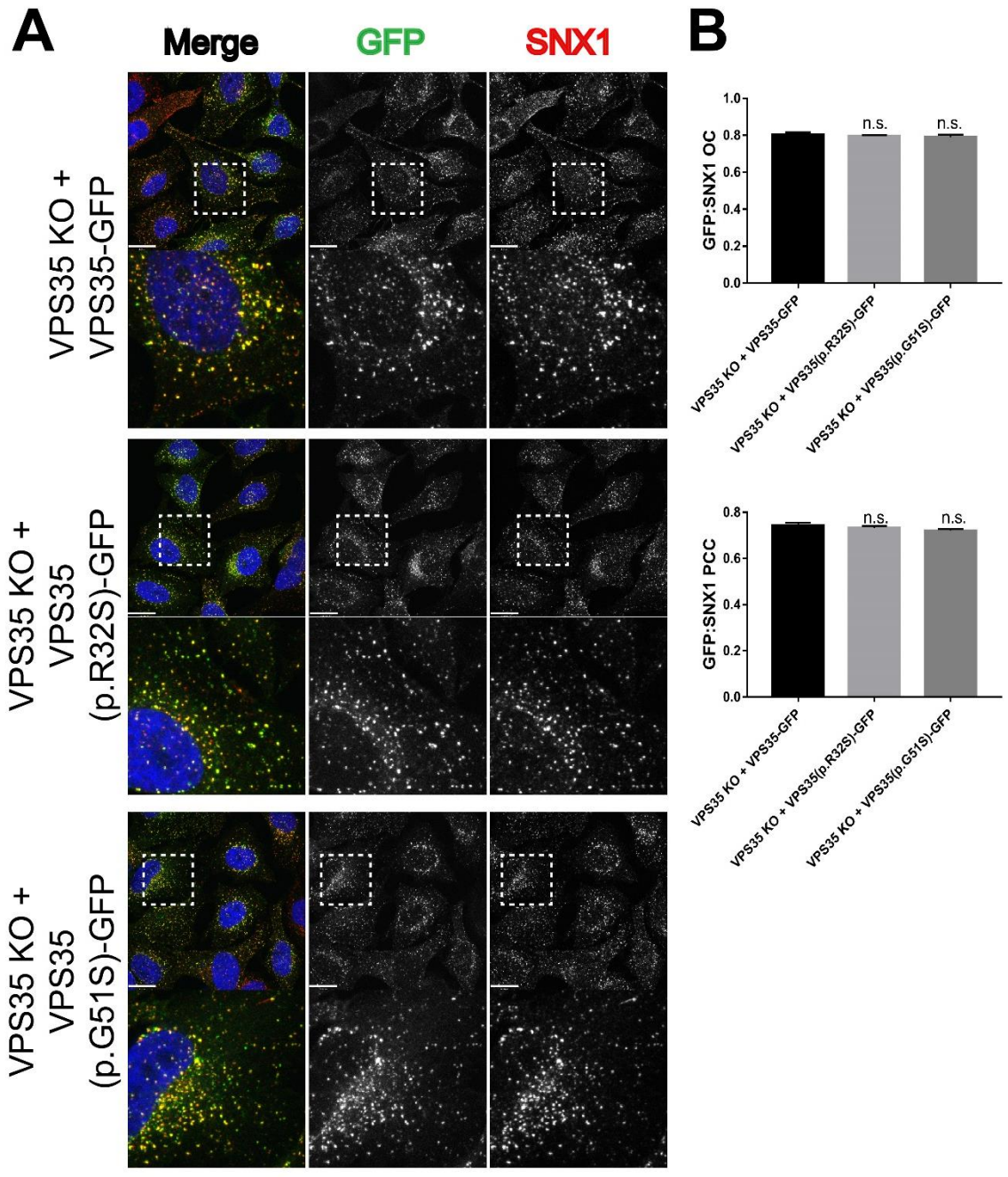

Figure 4.18 N-terminal VPS35 Parkinsonism-associated mutations do not perturb endosomal association.

(A) VPS35 knockout HeLa cells, transduced with VPS35-GFP constructs, were fixed with 4% paraformaldehyde and immuno-stained with endogenous SNX1. Cells were imaged using a confocal microscope. The scale bar indicates 19 µm. **(B)** Graphs showing the quantified Pearson's colocalisation coefficient (PCC) and Overlap coefficient (OC) from 3 independent experiments (at least 25 cells were quantified per experiment). Error bars indicate standard error; data were analysed

using a one-way ANOVA and a Dunnett's post-hoc test comparing the mutant constructs to the wild type VPS35-GFP construct.

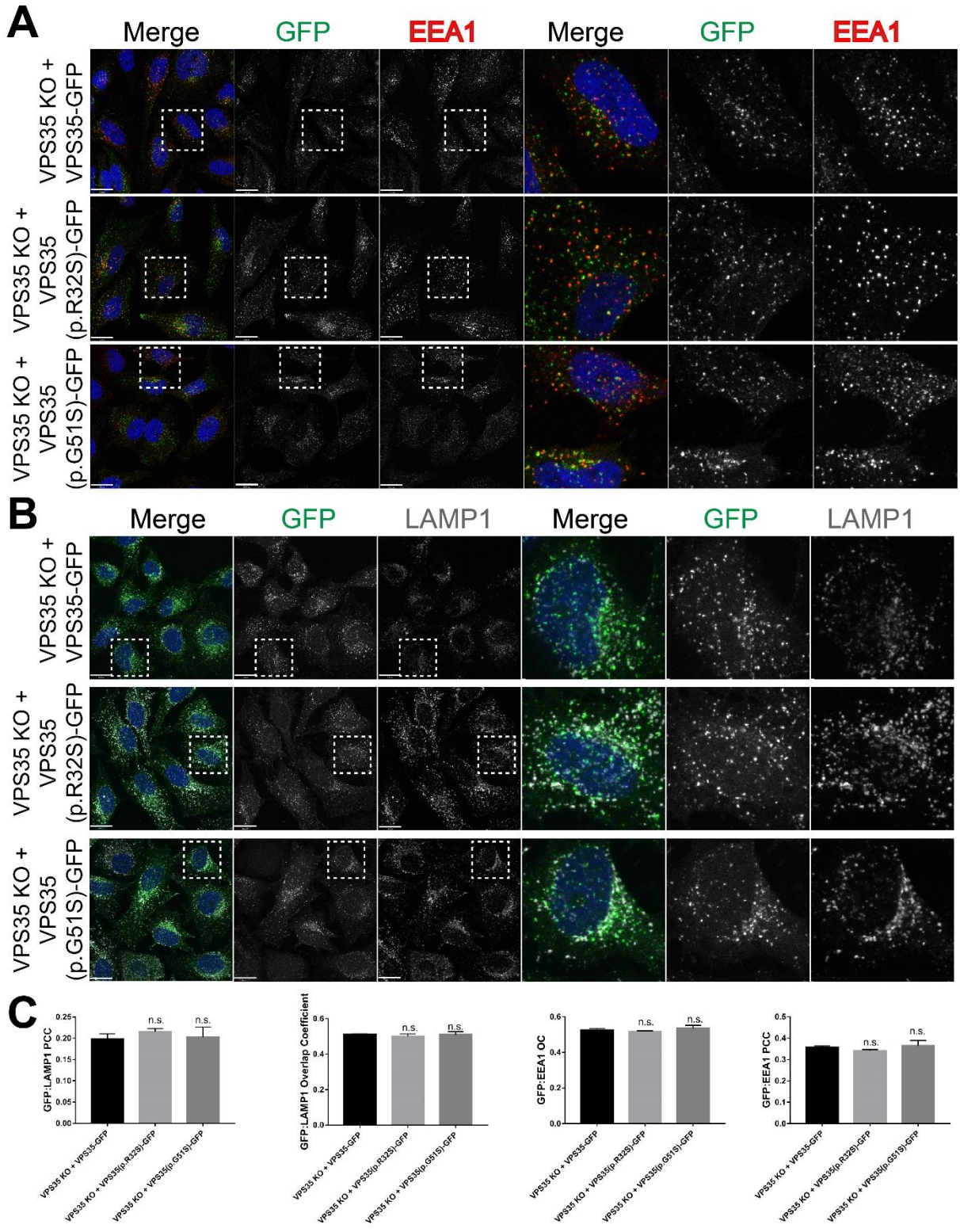

Figure 4.19 N-terminal VPS35 Parkinsonism-associated mutant constructs do not have altered early or late endosome localisation.

VPS35 knockout HeLa cells, transduced with VPS35-GFP constructs, were fixed with 4% paraformaldehyde and immuno-stained with endogenous **(A)** EEA1 or **(B)** LAMP1. Cells were

imaged using a confocal microscope. The scale bar indicates 19 µm. **(C)** Graphs showing the quantified Pearson's colocalisation coefficient (PCC) and Overlap coefficient (OC) from 3 independent experiments (at least 25 cells were quantified per experiment). Error bars indicate standard error; data were analysed using a one-way ANOVA and a Dunnett's post-hoc test comparing the mutant constructs to the wild type VPS35-GFP construct.

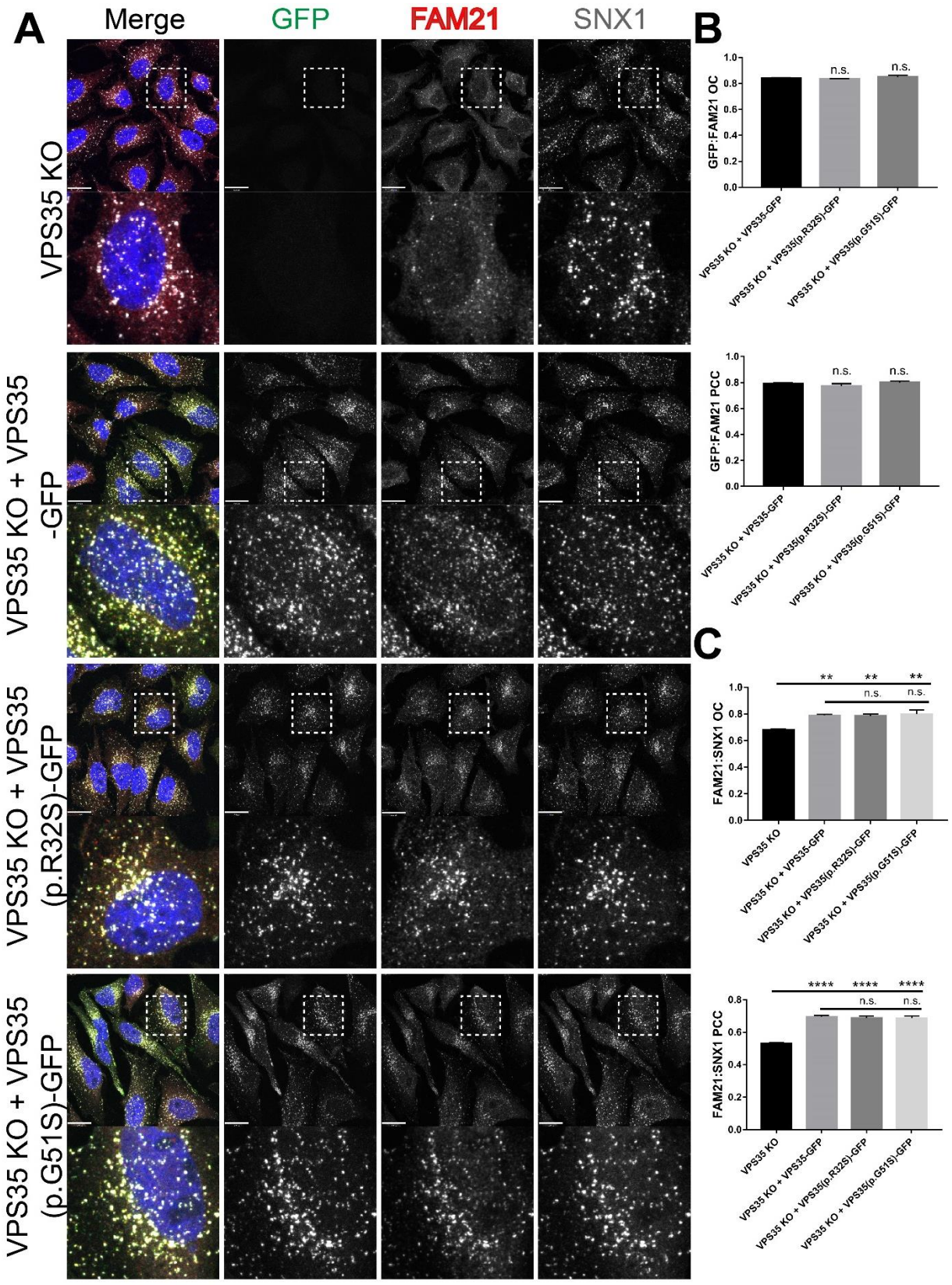

Figure 4.20 Parkinsonism-linked VPS35(p.R32S) and VPS35(p.G51S) rescue the localisation of FAM21 in VPS35 knockout HeLa cells.

(A) VPS35 knockout cells, stably expressing VPS35-GFP constructs from lentiviral transduction, were fixed with 4% paraformaldehyde and stained for endogenous FAM21 and SNX1. Cells were imaged using a confocal microscope. The scale bar indicates 19 µm. **(B)** Quantification, from 3 experiments with at least 20 cells per experiment, of Pearson's co-localisation coefficient (PCC) and overlap coefficient (OC). Data were analysed using one-way ANOVA followed by a Dunnett's test, comparing the rescue experiments to the VPS35 knockout values; ** P ≤ 0.01; **** P ≤ 0.0001.

4.2.11 The Parkinsonism-linked VPS35 mutations do not perturb the ability of VPS35 to bind to candidate proteins

I then tested the VPS35(p.R32S)-GFP and VPS35(p.G51S)-GFP variants for their ability to bind to known VPS35 interactors. I transiently transfected HEK293T cells with the VPS35-GFP variants and performed a GFP-trap immunoprecipitation experiment **(Figure 4.21A)**. No difference in binding to SNX27, Ankrd50, FAM21, strumpellin or WASH1 were identified between the VPS35-GFP variants **(Figure 4.21B)**.

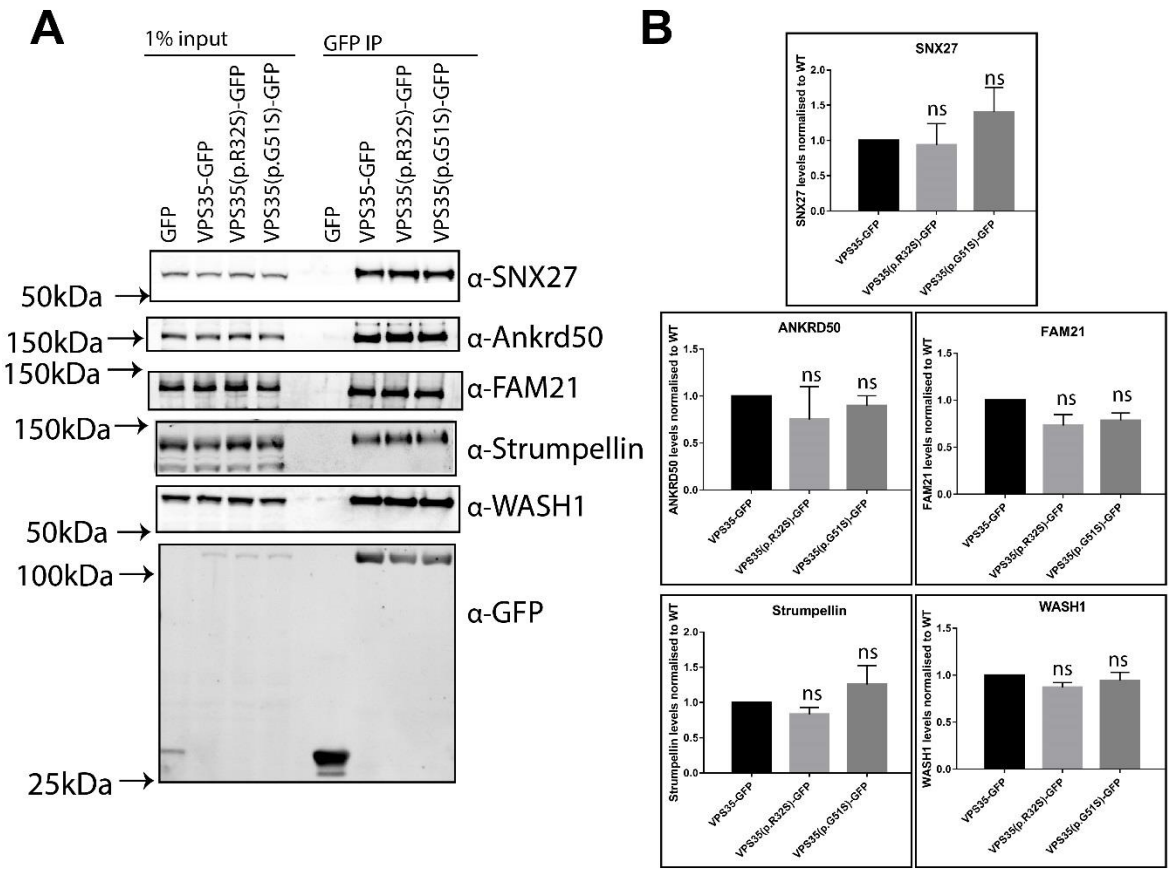

Figure 4.21 The Parkinsonism-linked VPS35(p.R32S) and VPS35(p.G51S) do not impair association with the WASH complex or SNX27.

(A) HEK293T cells were transfected with the indicated GFP-tagged constructs and subjected to a GFP-trap. The immuno-precipitates were resolved using SDS-PAGE and immuno-blotted for the indicated antibodies. **(B)** Quantification of the florescent bands, normalised to wild-type VPS35-GFP, using the Licor Odyssey Scanner from 3 independent experiments. Error bars indicate standard error. Data were analysed using a one-way ANOVA followed by a post-hoc Dunnett's test.

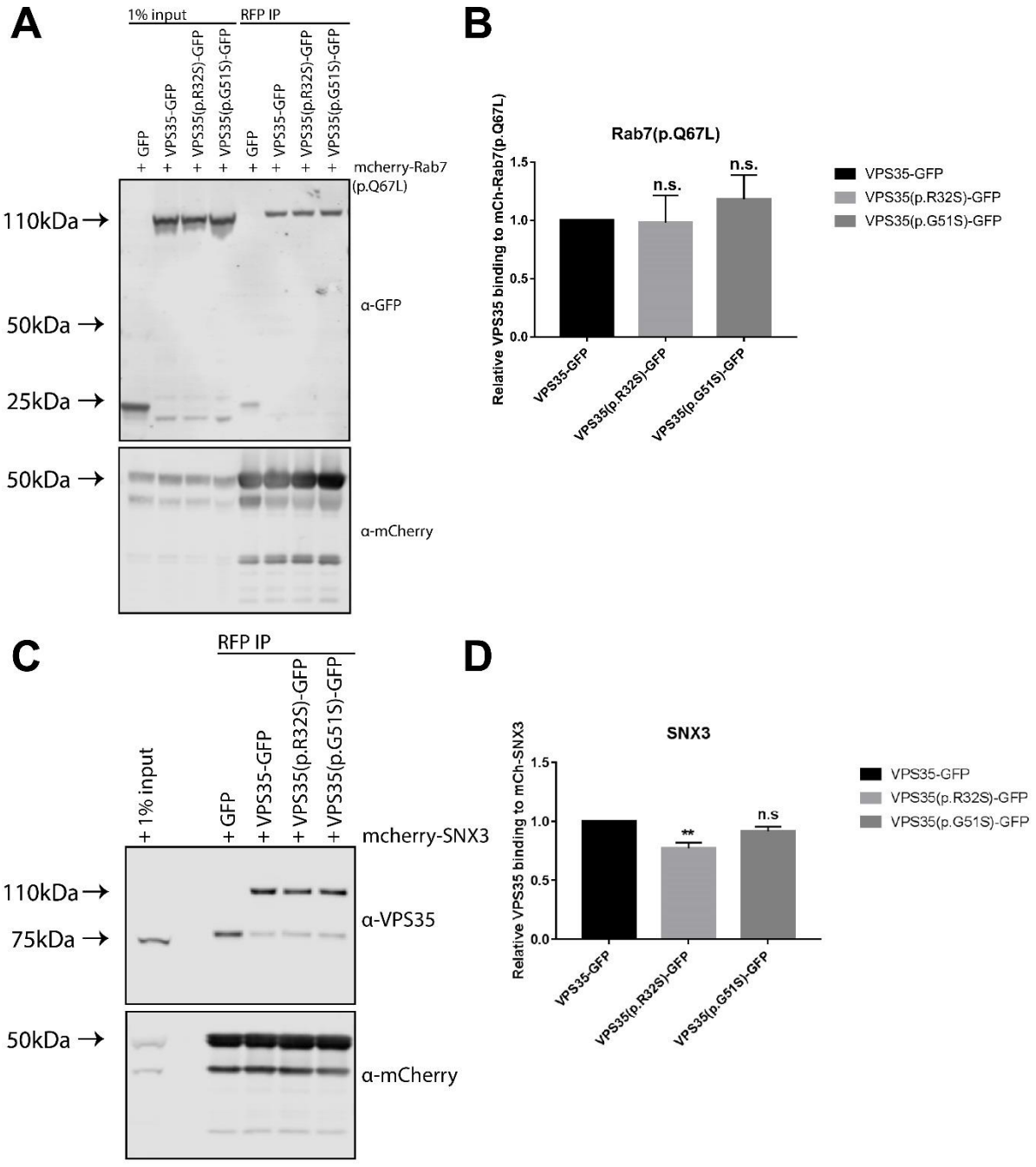

Figure 4.22 The Parkinsonism-linked VPS35(p.R32S) has a mild impairment in its ability to associate with SNX3.

HEK293T cells were transduced with lentivirus to stably express GFP-only or a VPS35-GFP construct. The HEK293T cells were then transiently transfected with constitutively active mcherry-Rab7(p.Q67L) **(A)** or mcherry-SNX3 **(C)** and subjected to an RFP-trap. The immuno-precipitates were

then resolved using SDS-PAGE and immunoblotted for the indicated antibodies. **(B and D)** Quantification of the relative amounts of immuno-precipitated VPS35-GFP constructs compared to wild-type VPS35-GFP from 3 independent experiments. Florescent bands were quantified using a Licor Odyssey Scanner; data were analysed through a one-way ANOVA followed by a post-hoc Dunnett's test. Error bars indicate standard error; **p=≤0.01.

As the N-terminal region of VPS35 is known to bind to SNX3 and Rab7 (Rojas et al., 2008; Harrison et al., 2014a), I then wished to test for association between those proteins and the Parkinsonism-linked VPS35 constructs. However, a GFP-trap of GFP-VPS35 or VPS35-GFP did not pull-down endogenous SNX3 or endogenous Rab7 **(Figure 4.14).** Previous studies have only shown the SNX3:VPS35 and the Rab7:VPS35 interaction through pulling down SNX3 or Rab7 (not from the opposite direction) (Rojas et al., 2008; Seaman et al., 2009; Balderhaar et al., 2010; Harrison et al., 2014a). I therefore transduced HEK293T cells with GFP, VPS35-GFP, VPS35(p.R32S)-GFP and VPS35(p.G51S)-GFP. Next, I transfected the stable HEK293T lines with mcherry-Rab7(p.Q67L), a constitutively-active Rab7 construct **(Figure 4.22A)**, lysed the cells and then performed an RFP-trap immunoprecipitation. There was not a significant difference in the co-immunoprecipitation of VPS35-GFP compared to VPS35(p.R32S)-GFP or VPS35(p.G51S)-GFP **(Figure 4.22B)**. I also transfected the stable HEK293T cells with mcherry-SNX3 **(Figure 4.22C)**, lysed the cells and then performed an RFP-trap immunoprecipitation. There was no difference in the co-immunoprecipitation of VPS35-GFP compared to VPS35(p.G51S)-GFP. However, there was a small, yet significant, decrease in the amount of VPS35(p.R32S)-GFP immunoprecipitated **(Figure 4.22D)**.

4.2.12 Tandem-mass tagging (TMT)-based proteomic analysis reveals no significant differences between the interactomes of VPS35-GFP compared to VPS35(p.R32S)-GFP or VPS35(p.G51S)-GFP

To more thoroughly investigate whether the G51S or R32S mutations affect the interactome of VPS35, I used an unbiased approach through tandem-mass tagging proteomics coupled to a GFP-trap immunoprecipitation. I took advantage of the near-endogenously expressed VPS35-GFP variants which had been transduced through lentiviral transduction in the VPS35 knockout HeLa cell lines **(Figure 4.17)**.

Once grown to confluency in a 15cm cell culture dish, I lysed the cells and performed GFP-trap immunoprecipitations. Dr Kate Heesom then digested the samples with trypsin and labelled them with Tandem Mass Tag ten plex reagents before pooling them. After preparation, the samples were fractionated into 5 fractions before nano-LC MS/MS analysis. The different labels added to the samples enabled the different peptides between conditions

to be distinguished on the mass spectrometer **(Figure 4.23A)**.

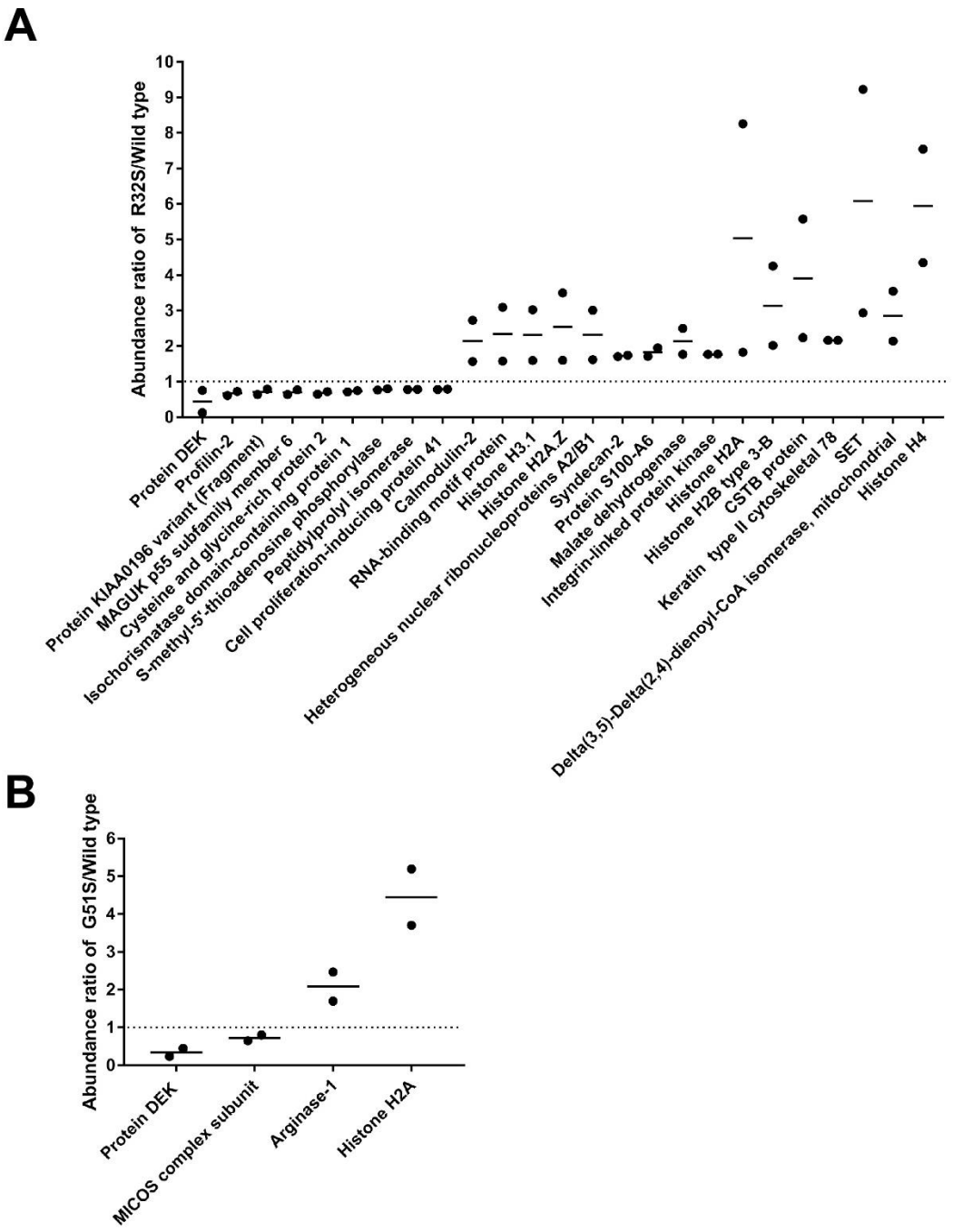

Figure 4.23 Proteomic analysis using tandem mass tag spectrometry reveals slight changes in the interactome of the Parkinsonism-linked VPS35(p.R32S) and VPS35(p.G51S) mutations.

VPS35 knockout HeLa cells, stably expressing wild-type VPS35-GFP, and VPS35(p.R32S)-GFP **(A)** or VPS35(p.G51S)-GFP **(B)** were subjected to a GFP-trap. The immuno-precipitates were then subjected to a GFP-trap experiment. The co-immunoprecipitated proteins were then labelled with tandem-mass tags, resolved using SDS-PAGE and identified using mass spectrometry. Data indicates two independent experiments. An abundance ratio of less than 1 indicates a loss of interaction. An abundance ratio of more than one indicates a gain of interaction. Data were filtered by excluding proteins with an interaction loss of less than 20% and excluding proteins with an interaction gain of less than 1.5-fold. Proteins averaging only 1 detected peptide were also excluded.

To determine to extent to which my TMT analysis worked, I examined whether the proteins identified in the SILAC-generated VPS35-GFP interactome were present **(Table 4.4)**. Many of the validated interactors identified through my SILAC-based analysis were also picked up in the TMT experiment, such as TBC1D5, other retromer complex components, VARP and some WASH complex components. TMT proteomics is less sensitive than SILAC which could explain why not all WASH complex components were detected. It should also be noted that the SILAC-based interactome analysis of VPS35-GFP was done in RPE-1 cells whereas the TMT analysis was done in the VPS35 knockout HeLa cells. This could explain some differences.

Table 4.5 show the differences in the interactome between the VPS35-GFP and the VPS35(p.R32S)-GFP interactome and **Table 4.6** shows the differences in the VPS35-GFP and VPS35(p.G51S)-GFP interactome.

Name of VPS35-GFP interactor identified through SILAC-based proteomics	Enrichment of interactor in TMT proteomics (N1)	Enrichment of interactor in TMT proteomics (N2)
TBC1 domain family, member 5, isoform CRA	100	100
Ankyrin repeat domain-containing protein 27	100	74.721
Serologically defined colon cancer antigen 3	N.D.	N.D.
VPS29	100	100
TBC1 domain family member 5	100	100
LIM domain only protein 7	22.423	N.D.
VPS26B	100	83.688
RNA-binding protein EWS	10.795	11.812
Cell death regulator Aven	N.D.	N.D.
VPS35	100	100
VPS26A	100	100
WASH complex subunit FAM21C	66.721	35.065
FAM32A	N.D.	N.D.
VPS29	100	100
WASH1	N.D.	N.D.
strumpellin	N.D.	N.D.
Polycystin-2	N.D.	N.D.
Centrosomal protein 170kDa	N.D.	N.D.
FAM21A	N.D.	N.D.
Gap junction protein	N.D.	N.D.
Actin nucleation promoting factor	N.D.	23.827
WD repeat-containing protein 61	13.684	13.653
Family with sequence similarity 98, member A	N.D.	N.D.

Fusion (Involved in t(12;16) in malignant liposarcoma) isoform a variant	N.D.	N.D.
KIAA1033 protein	44.174	14.203
DnaJ homolog subfamily B member 6	N.D.	N.D.
CCDC53	N.D.	12.85
Protein S100	16.347	7.362
Protein LSM14 homolog A	9.052	N.D.
Cold-inducible RNA-binding protein	N.D.	N.D.
Focadhesin	N.D.	N.D.
Fibroblast growth factor	N.D.	N.D.
RNA-binding protein 39	14.994	12.07

Table 4.4 Comparison of VPS35-GFP interactors identified through SILAC-based proteomics compared to two runs of TMT-based proteomics

Highlighted in green are retromer complex subunits and in yellow WASH complex subunits. 'N.D.' indicates 'not detected'. SILAC (stable isotope labelling with amino acids in cell culture). TMT (tandem mass tagging).

4.2.13 VPS35-GFP, VPS35(p.R32S)-GFP and VPS35(p.G51S)-GFP transduction rescues lysosomal GLUT1 degradation

Lastly, I tested whether the constructs could rescue the localisation of GLUT1 when re-expressed into VPS35 knockout HeLa cells. Indeed, when transduced at near endogenous levels **(Figure 4.17)**, the colocalisation between GLUT1 and LAMP1 was dramatically reduced when VPS35-GFP, VPS35(p.R32S)-GFP or VPS35(p.G51S)-GFP were expressed **(Figure 4.24)**. This indicates that the Parkinson's disease linked VPS35 variants do not perturb retromer-mediated endosome-to-plasma membrane trafficking.

Accession number	Description	Average Coverage	Average # Peptides	Average # PSMs	Average # Unique Peptides	# Average AAs	Average Abundance Ratio: [VPS35(p.R32S) / VPS35]
P62805	Histone H4 OS=Homo sapiens GN=HIST1H4A PE=1 SV=2	51.45631	6	33	6	103	5.9455
Q5VXV3	SET OS=Homo sapiens GN=SET PE=2 SV=1	29.13793	7	9	3.5	290	6.0805
A0A0U1RRH7	Histone H2A OS=Homo sapiens GN=HIST1H3D PE=3 SV=1	35.29412	5	10.5	2	170	5.041
Q76LA1	CSTB protein OS=Homo sapiens GN=CSTB PE=2 SV=1	55.10204	4.5	11	4.5	98	3.9075
Q8N257	Histone H2B type 3-B OS=Homo sapiens GN=HIST3H2BB PE=1 SV=3	45.63492	7	19.5	2	126	3.1355
Q13011	Delta(3,5)-Delta(2,4)-dienoyl-CoA isomerase, mitochondrial OS=Homo sapiens GN=ECH1 PE=1 SV=2	17.68293	5	5.5	5	328	2.843
P0C0S5	Histone H2A.Z OS=Homo sapiens GN=H2AFZ PE=1 SV=2	25.78125	3.5	7	1.5	128	2.5465
P38159	RNA-binding motif protein, X chromosome OS=Homo sapiens GN=RBMX PE=1 SV=3	7.800512	4	4.5	4	391	2.3365
P22626	Heterogeneous nuclear ribonucleoproteins A2/B1 OS=Homo sapiens GN=HNRNPA2B1 PE=1 SV=2	45.46742	14	21.5	12	353	2.314
P68431	Histone H3.1 OS=Homo sapiens GN=HIST1H3A PE=1 SV=2	29.77941	5.5	13.5	1	136	2.309
E7EMB3	Calmodulin-2 OS=Homo sapiens GN=CALM2 PE=1 SV=1	29.84694	5	6.5	5	196	2.145
Q8N1N4	Keratin, type II cytoskeletal 78 OS=Homo sapiens GN=KRT78 PE=1 SV=2	10.48077	6.5	12.5	3	520	2.1615

A0A024R4K3	Malate dehydrogenase OS=Homo sapiens GN=MDH2 PE=2 SV=1	37.42604	11	16.5	11	338	2.1325
A0A024RBB5	Cysteine and glycine-rich protein 2, isoform CRA_a OS=Homo sapiens GN=CSRP2 PE=4 SV=1	67.87565	12	44.5	12	193	0.683
P35080	Profilin-2 OS=Homo sapiens GN=PFN2 PE=1 SV=3	32.14286	4	7.5	2	140	0.666
P35659	Protein DEK OS=Homo sapiens GN=DEK PE=1 SV=1	4.533333	1.5	1.5	1.5	375	0.4375

Table 4.5 Changes in the VPS35(p.R32S)-GFP interactome compared to VPS35-GFP interactome

AA= amino acid; PSMs= peptide-to-spectrum matches (the total number of identified peptide sequences).

Accession number	Description	Average Coverage	Average # Peptides	Average # PSMs	Average # Unique Peptides	Average # AAs	Average Abundance Ratio: [VPS35(p.GS1S) / VPS35]
A0A0U1RRH7	Histone H2A OS=Homo sapiens GN=HIST1H3D PE=3 SV=1	24.35294	5	10.5	2	170	4.4465
P05089	Arginase-1 OS=Homo sapiens GN=ARG1 PE=1 SV=2	5.745342	1.5	2	1.5	322	2.083
C9JRZ6	MICOS complex subunit OS=Homo sapiens GN=CHCHD3 PE=1 SV=1	8.11722	2	2	2	236.5	0.723
P35659	Protein DEK OS=Homo sapiens GN=DEK PE=1 SV=1	4.533333	1.5	1.5	1.5	375	0.3395

Table 4.6 Changes in the VPS35(p.G51S)-GFP interactome compared to VPS35-GFP interactome

AA= amino acid; PSMs= peptide-to-spectrum matches (the total number of identified peptide sequences).

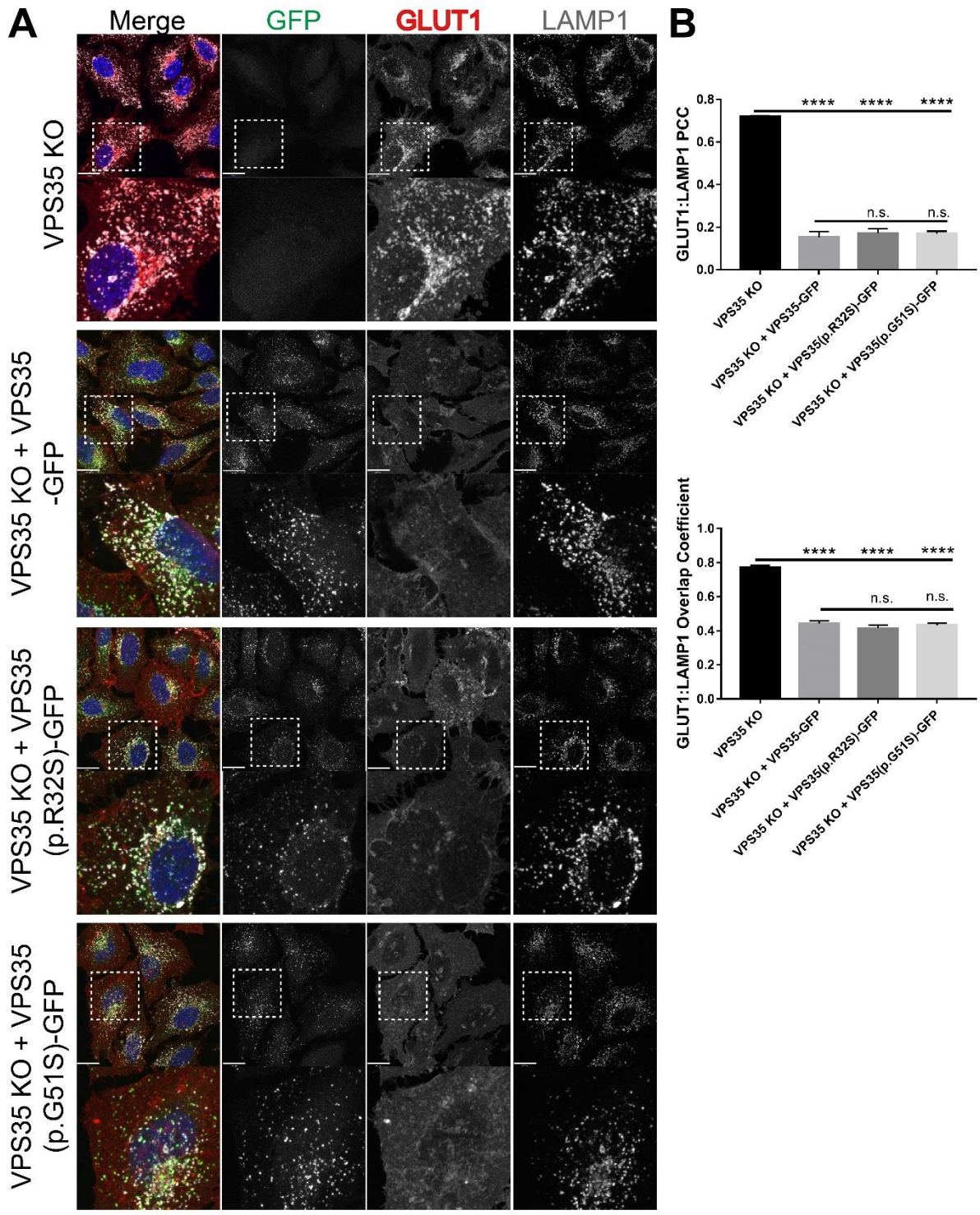

Figure 4.24 Parkinsonism-linked VPS35(p.R32S) and VPS35(p.G51S) rescue the localisation of GLUT1 in VPS35 knockout HeLa cells.

(A) VPS35 knockout cells, stably expressing VPS35-GFP constructs from lentiviral transduction, were fixed with 4% paraformaldehyde and stained for endogenous GLUT1 and LAMP1. Cells were imaged using a confocal microscope. The scale bar indicates 19 µm. **(B)** Quantification, from 3 experiments with at least 20 cells per experiment, of Pearson's co-localisation coefficient (PCC) and overlap coefficient (OC). Data were analysed using one-way ANOVA followed by a Dunnett's test, comparing the rescue experiments to the VPS35 knockout values; **** $P \leq 0.0001$.

4.3 Discussion

4.3.1 The VPS26A(p.K297X) truncation mutation uncouples SNX27 from the retromer complex

Proteomic and bioinformatic studies have identified hundreds of potential SNX27-retromer dependent cargoes which are dependent on SNX27-retromer for their endosomal sorting away from lysosomal degradation and have appropriate PDZ binding motifs for their association with SNX27 (Steinberg et al., 2013b; Clairfeuille et al., 2016). SNX27 is highly expressed in the brain (Kajii et al., 2003) and many neuronal receptors, such as NMDA (Wang et al., 2013) and AMPA receptors (Hussain et al., 2014; Loo et al., 2014), the β2-adrenergic receptor (Temkin et al., 2011) and 5-hydroxytryptamine type 4 receptors (Joubert et al., 2004), rely on SNX27-retromer for their cell-surface localisation. Homozygous loss of SNX27 in children leads to myoclonic epilepsy, defects in psychomotor development and death within 2 years of birth (Damseh et al., 2015) and the SNX27 knock-out mice display growth retardation, behaviour deficits and die within 4 weeks of birth (Cai et al., 2011). SNX27 dysfunction is also associated with Down's syndrome, where the overexpression of miR-155 negatively regulates the expression of SNX27 (Wang et al., 2013).

Cell culture-based experiments where a variant of SNX27 is used which cannot associate with the retromer complex display GLUT1 sorting defects (Gallon et al., 2014a) which are phenocopied in the context of VPS26A(p.K297X) **(Figure 4.11)**. Given the fairly drastic neurodevelopmental and childhood-onset symptoms in relation to the homozygous loss of SNX27 in mice and human children (Cai et al., 2011; Damseh et al., 2015), it might be thought that a patient harbouring this mutation would have developed symptoms sooner than an age of onset of 70 years old (Gustavsson et al., 2015). One explanation is the difference between a knock-out of SNX27 and a failure in SNX27-retromer complex assembly. SNX27 may have retromer-independent functions. Furthermore, the VPS26A(p.K297X) mutation was heterozygous – the patient had two wild-type copies of VPS26B and one wild-type copy of VPS26A. VPS26A is ubiquitously expressed, while VPS26B is more highly enriched in neuronal cells (Bugarcic et al., 2011). When knocked-out in mice, VPS26A is embryonic lethal, while VPS26B knockouts are viable (Kim et al., 2010), but there is little to distinguish the interactomes between VPS26A and VPS26B (McMillan et al., 2016). There is likely to be a large degree of redundancy between the two VPS26 paralogues.

The K297 and the subsequent residues on VPS26A may stabilise the linker region between the two β-sandwich domains of VPS26A, which forms direct contacts to the SNX27 PDZ domain (Gallon et al., 2014a). It is possible that the K297X truncation destabilises this linker region which perturbs SNX27 association. Since a truncated form, lacking residues 301-327 of VPS26A, was used in the Gallon et al., (2014) crystal structure, it is also possible that the C-terminal residues may play a greater role, which has been masked by the artificial environment in the crystal structure, in SNX27 binding *in vivo*. This investigation of the K297X truncation mutation has enhanced our understanding of how structurally, the C-terminus of VPS26A plays a scaffolding role not only in the recruitment of SNX27, but in the binding of DENND4C and PKD2.

The data presented here has focused on the severe reduction in association between VPS26A(p.K297X) and SNX27. However, VPS26A(p.K297X) also has an enhanced binding to PKD2 and DENND4C **(Figure 4.9B)**. PKD2 is a calcium-activated calcium channel (Koulen et al., 2002) which is associated with autosomal dominant polycystic kidney disease (Rossetti et al., 2007) and DENND4C is a guanine nucleotide exchange factor for Rab10 (Yoshimura et al., 2010). DENND4C and PKD2 were identified in the retromer interactome, but the functional significance of these interactors (in terms of regulating retromer function) is yet to be fully understood (McMillan et al., 2016; Tilley et al., 2018).

The retromer complex's interaction with DENND4C has not been shown to be direct but it is thought to directly interact with the amino-terminus of PKD2 (Feng et al., 2017; Tilley et al., 2018). Whether SNX27 and PKD2 compete for a similar binding site in VPS26A was investigated in Tilley et al. (2018). GFP-traps of VPS26A variants were performed under SNX27-suppressed conditions: this did not enhance the ability of VPS26A to immunoprecipitate PKD2 (Tilley et al., 2018). It is possible that VPS26A(p.K297X) causes structural changes in the architecture of the retromer complex which enhances PKD2 and DENND4C binding, independently of its effect on SNX27 binding.

4.3.2 Investigations of the other Parkinsonism-linked retromer mutations

The VPS26A(p.K93E) and VPS26A(p.M112V) variants of VPS26A have not proved to dramatically alter interactions with other proteins **(Figure 4.8)**. They also do not affect the endosome-to-plasma membrane sorting of GLUT1 **(Figure 4.11)** or the endosome-to-TGN sorting of CIMPR (personal communication from Dr Kirsty McMillan). It is possible that the K93E and M112V residues may cause effects on retromer function

that have not been investigated here. All three of these Parkinsonism-linked variants are extremely rare and have not been shown to be causally linked to disease, but have also not been found in healthy control databases (Gustavsson et al., 2015; McMillan et al., 2017). It is possible that the K93E and M112V mutations are not actually causing Parkinsonism disorders.

Co-expression of the VPS35-GFP variants and mCherry-SNX3 coupled with a GFP-trap revealed that introducing the R32S mutation in VPS35 causes a slight reduction in association with SNX3 **(Figure 4.22C-D)**. This reduction was not repeated in the interactome analysis **(Figure 4.23A)**, although SNX3 was not identified as an interactor in the GFP-VPS35 (McGough et al., 2014a) or VPS35-GFP interactomes **(Table 4.2)**. When highlighting the R32 and G51 residues of VPS35 on the Lucas et al., (2016) structure **(Figure 4.25)**, it is unclear why the R32S mutation may subtly affect SNX3's association with the retromer complex. It is possible that the loss of the basic arginine residue may cause a subtle structural reconfiguration of VPS35 which slightly impairs the interaction with SNX3.

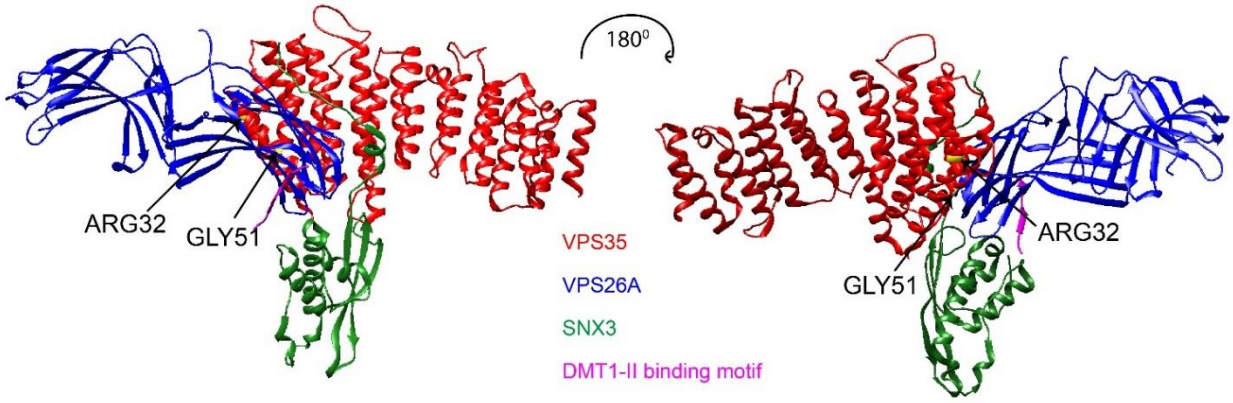

Figure 5.25 The VPS35 ARG32 and GLY51 residues are not in close proximity to the SNX3-retromer binding site

Model of the VPS35 (N-terminal) (red): VPS26A (blue): SNX3 (green): DMT1-II binding motif (magenta) crystal structure (Lucas et al., 2016). The VPS35 ARG32 and GLY51 residues are coloured in yellow and highlighted.

The same caveats discussed in relation to the VPS26A mutations also apply to the R32S and G51S VPS35 mutations – they are extremely rare mutations which have not been proven to be causative. The VPS35(p.R32S) mutation has not been found in healthy controls but the VPS35(p.G51S) mutation subsequently has (Sharma et al., 2012; Gustavsson et al., 2015; Bandres-Ciga et al., 2016; McMillan et al., 2017). Therefore, it is likely that the VPS35(p.G51S) variant is not causative of the

Parkinsonism symptoms but the case for VPS35(p.R32S) remains equivocal. Future studies may look at: possible post-translational functions of the affected residues (such as the ubiquitination of VPS26A LYS93 residue); the trafficking other retromer-dependent cargoes; cargo trafficking kinetics; and whether the Parkinsonism-linked retromer variants affect lysosomal health and α-synuclein degradation.

Chapter 5

FAM21 binds to areas of basic charge on the carboxyl-terminus of VPS35

5.1 Introduction

5.1.1 The WASH complex binds to retromer through a series of acidic motifs in FAM21

The WASH complex is an endosome-localised actin nucleation-promoting factor which promotes the polymerisation of branched networks through activating the Arp2/3 complex (Derivery et al., 2009; Gomez and Billadeau, 2009; Jia et al., 2010) **(Section 1.4.5)**. The WASH complex is a heteropentameric complex composed of: WASH1, FAM21, Strumpellin, CCDC53 and SWIP. A major factor in its endosomal targeting is the association of FAM21 to the retromer complex (Harbour et al., 2012; Jia et al., 2012; McNally et al., 2017). However, even in VPS35 knockout cells, there is a minority proportion of FAM21 which, through an unknown mechanism retains an endosomal localisation (McNally et al., 2017).

Little structural information concerning FAM21 is available, but the first 220 amino acids are predicted to form a globular 'head' domain and the proceeding ~1100 amino acids (the 'tail') are predicted to be unstructured and flexible (Derivery et al., 2009). The retromer:FAM21 interaction is mediated by a series of 21 acidic L-F-$[D/E]_{3-10}$-L-F (so-called LFa) motifs in the FAM21 tail (Jia et al., 2012). The mechanism by which these LFa motifs couple to retromer is unknown, but the interaction requires the carboxyl-terminal half of VPS35 (Helfer et al., 2013).

As described in **(Section 1.4.5)**, depletion of the WASH complex gives rise to several phenotypes, including a 'collapse' of the endosomal network, cargo trafficking defects and aberrant tubulation. The extent to which the retromer:WASH complex interaction is required for the normal functions of the WASH complex has not been determined. It is thought that the FAM21 tail can bind to multiple retromer complexes, which may promote the recruitment of the WASH complex to areas in which a high concentration of cargo is being retrieved, thereby coordinating cargo recognition with the polymerisation of branched actin (Harbour et al., 2012; Jia et al., 2012). Branched actin-polymerisation has also been proposed to contribute to the segregation of retrieval and degradative endosomal subdomains (Derivery et al., 2012; Cullen and Steinberg, 2018).

5.1.2 Aims

In this chapter, I sought to build upon the observation that acidic LFa motifs in the FAM21 tail mediate the retromer:WASH complex interaction. With the hypothesis that the FAM21:VPS35 interaction is mediated by electrostatic forces, I used bioinformatic-based analyses combined to a biochemical mutagenesis screen to identify evolutionary-conserved basic residues on VPS35 which are required for the interaction. Depletion of WASH complex components lead to pleiomorphic phenotypes **(Section 1.4.5)**. The model behind the significance of the retromer:WASH complex interaction requires further experimental evidence and the extent to which this interaction is required for the normal functions of these complexes remains unclear. I therefore introduced the VPS35 mutants with perturbed WASH complex association into cells to explore the functional consequence of uncoupling this interaction.

5.2 Results

5.2.1 Bioinformatic search to identify candidate residues in VPS35 that may mediate its interaction with FAM21

The extended and unstructured 'tail' of the FAM21 subunit of the WASH complex mediates its interaction with the retromer complex **(Figure 5.1)**. This is considered to occur via the C-terminus of VPS35 (Helfer et al., 2013) through a series of acidic LFa motifs in the FAM21 'tail' (Jia et al., 2012). To identify candidate residues in VPS35 which may mediate this interaction, I aligned VPS35 homologues from species which contain the WASH complex (*H. sapiens*, *M. musculus*, *D. melanogaster* and *C. elegans*) with *S. cerevisiae*, which does not express the WASH complex. This identified basic (arginine and lysine) residues which have been evolutionary maintained in species with the WASH complex but not in *S. cerevisiae* **(Figure 5.2)**. There were also several basic residues which were highly evolutionary conserved, even in *S. cerevisiae* **(Figure 5.2)**. Due to the discovery of the LFa repeat in the FAM21 tail (Jia et al., 2012), I hypothesised that a major factor in the nature of the interaction will be electrostatic binding.

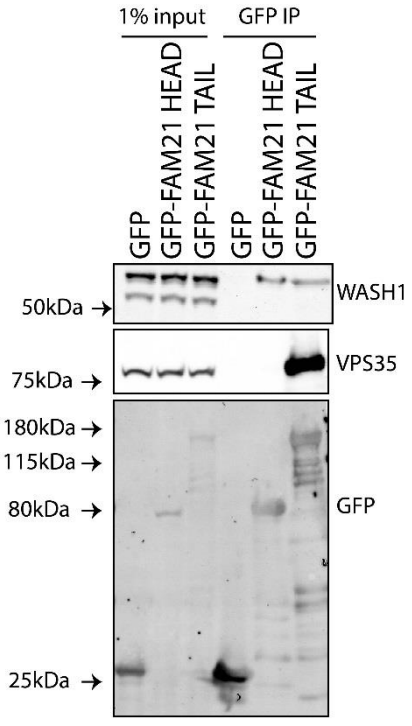

Figure 5.1 FAM21 binds to VPS35 through its extended carboxyl-terminus.

HEK293T cells were transiently transfected with the indicated GFP-tagged constructs and subjected to a GFP-trap. The immuno-precipitates were resolved using SDS-PAGE and immuno-blotted with the indicated antibodies. The globular 'head' of FAM21 is considered the first 220 amino acids; the unstructured tail is the remaining ~1100 amino acids.

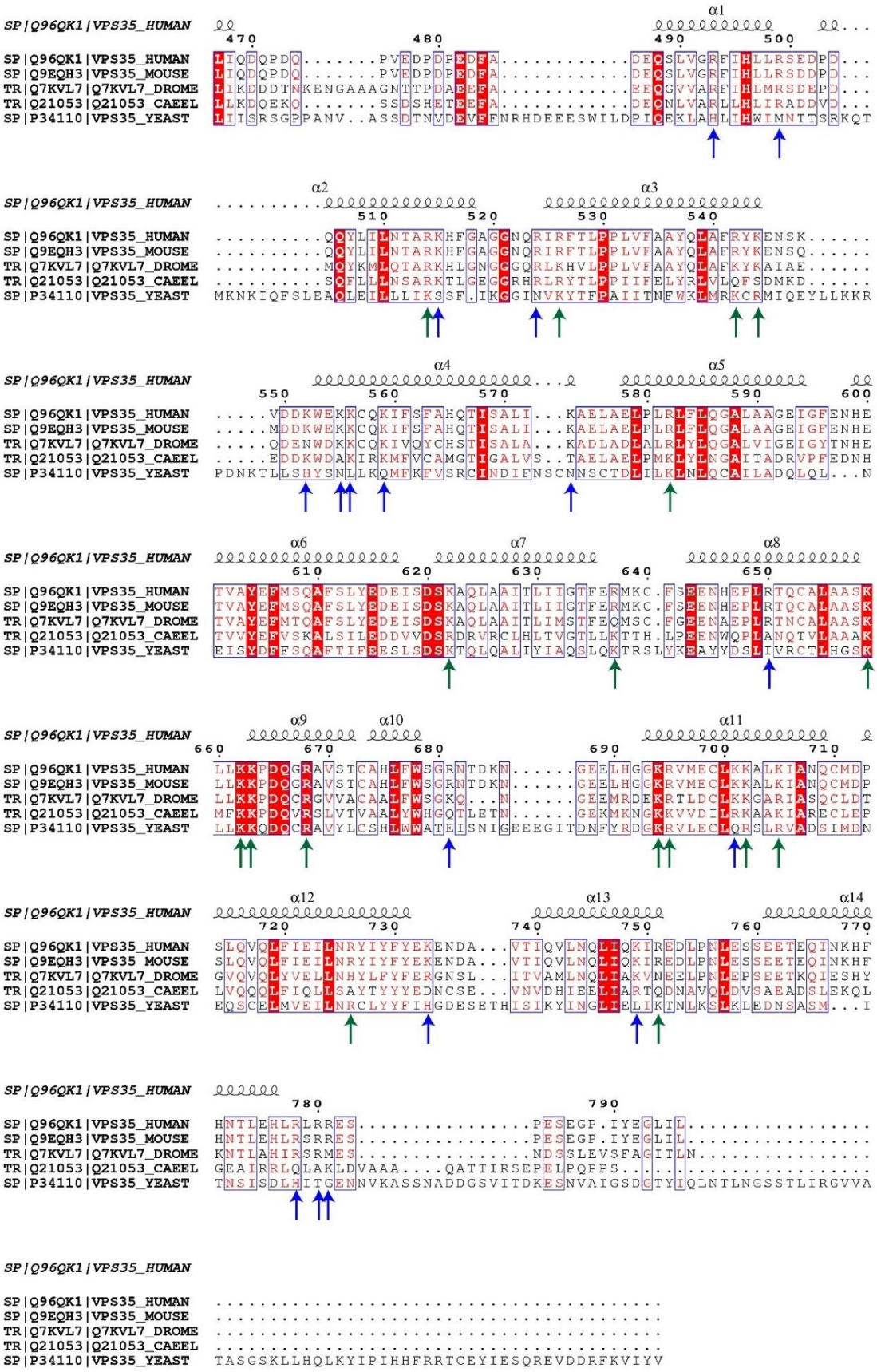

Figure 5.2 Bioinformatic analysis to identify candidate residues in VPS35 which may be important for FAM21 association.

Sequence alignment of the VPS35 homologues (starting at residue 467 of *H. sapiens* VPS35) whose species contain the WASH complex (*H. sapiens*, *M. musculus*, *D. melanogaster* and C. elegans) and *S. cerevisiae* (which does not have the WASH complex in its genome). Basic residues which are largely conserved in species containing the WASH complex, but not conserved in *S. cerevisiae* are highlighted by a blue arrow. Basic residues largely conserved the WASH complex-containing species and *S. cerevisiae* are highlighted by a green arrow.

To identify whether the basic residues highlighted in the bioinformatic sequence alignment may form a surface by which FAM21 could associate, I highlighted all the basic residues on VPS35 from the VPS35:VPS29 crystal structure (Hierro et al., 2007). Two patches of basic residues, located on two HEAT-repeat domains of VPS35, became apparent **(Figure 5.3A)**.

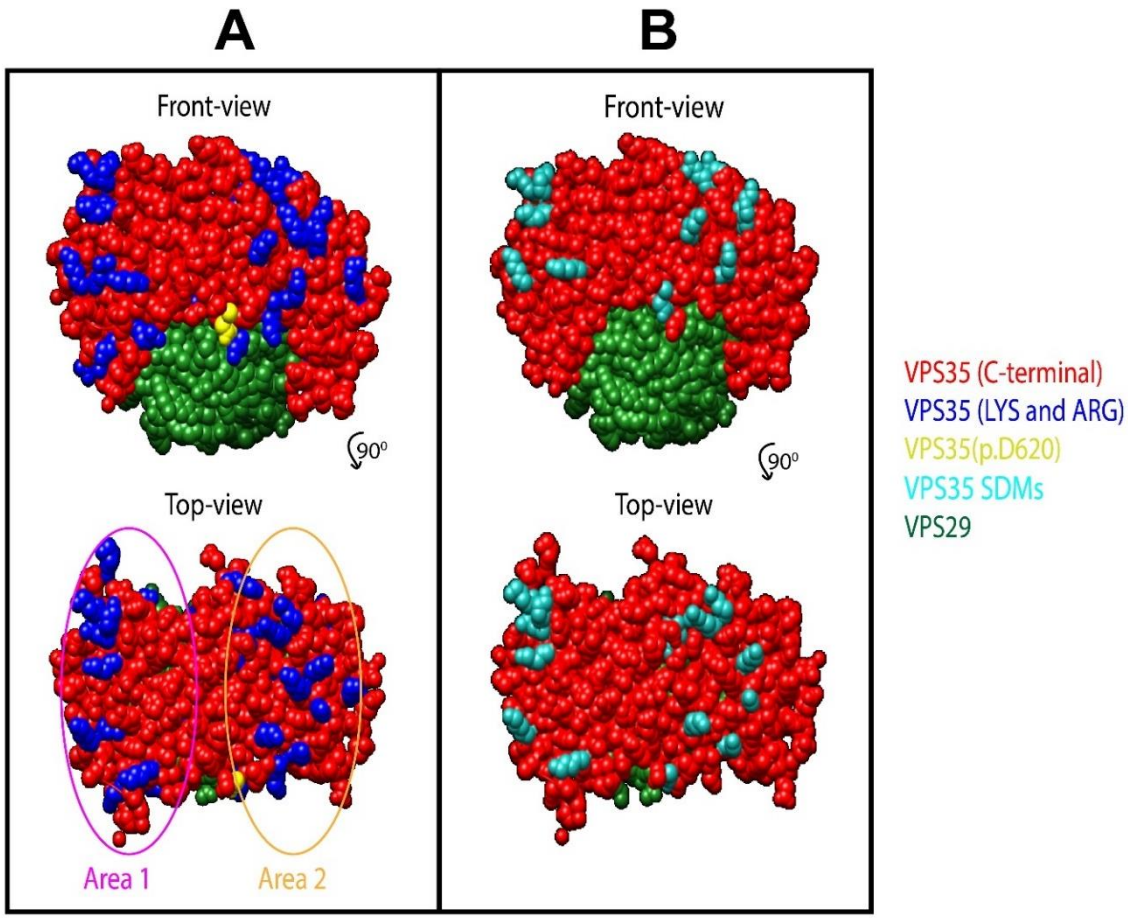

Figure 5.3 The C-terminal half of VPS35 contain two patches enriched in basic residues.

(A) Model of the crystal structure (Hierro et al., 2007) of C-terminal VPS35 (red) bound to VPS29 (green). All basic VPS35 residues are coloured in blue. The D620 residue is coloured in yellow. **(B)** model of the crystal structure of C-terminal VPS35 (red) bound to VPS29 (green). Residues mutated in VPS35-GFP constructs are coloured in cyan.

5.2.2 Immunoprecipitation screen to identify VPS35 mutations which perturb FAM21 binding

From the bioinformatic analysis, I identified candidate basic residues in VPS35 which may be important for FAM21 association. Two 'areas' had been identified when modelling all of the basic residues in the VPS35:VPS29 crystal structure (Hierro et al., 2007) **(Figure 5.3A)**. The first area contained basic residues that are not conserved in yeast. The second area contained basic residues that were conserved in yeast. I therefore introduced various point mutations in the VPS35-GFP construct: either human to yeast mutations, or charge swap mutations when the basic residues were conserved in the VPS35 *S. cerevisiae* homologue **(Table 5.1** and **Figure 5.3B)**.

I then used a GFP-trap experiment to test the ability of the VPS35-GFP variants to immuno-precipitate FAM21. From investigating the first 'area' in VPS35 **(Figure 5.4A)**, I identified several mutations which perturbed FAM21 binding **(Figure 5.4B-C)**. Importantly, these mutations did not cause a failure in retromer complex assembly **(Figure 5.4B-C)**. From investigating the second 'area' in VPS35 **(Figure 5.5A)**, I identified several mutations which also perturbed, but less severely than those identified in the first area, FAM21 binding **(Figure 5.5B)**. Again, the mutations did not cause a failure in retromer complex assembly **(Figure 5.5C)**. From these data, I have identified several residues in VPS35 that, when mutated, cause a significant reduction in FAM21 association **(Figure 5.6)**. Importantly, the VPS35(p.D620N) Parkinson's disease-linked mutation displays approximately 50% loss in FAM21 binding **(Figure 5.4** and **Figure 5.5)**, confirming previously published work (McGough et al., 2014b; Zavodszky et al., 2014).

VPS35-GFP variants			
D620N	K515S	K552H	K559Q
K573N	R650E	K659E	K663E
K694E	R695E	K701E	K705E
K552H, K555N, K556L		K555N, K556L, K559Q	

Table 5.1 VPS35-GFP variants created through site-directed mutagenesis

To extend my biochemical examination of the VPS35 mutations, I used immunofluorescence analysis to verify that the retromer complex was being uncoupled from the WASH complex. To avoid compensation from endogenous VPS35, I lentivirally transduced VPS35 knockout HeLa cells to create stable cell lines which

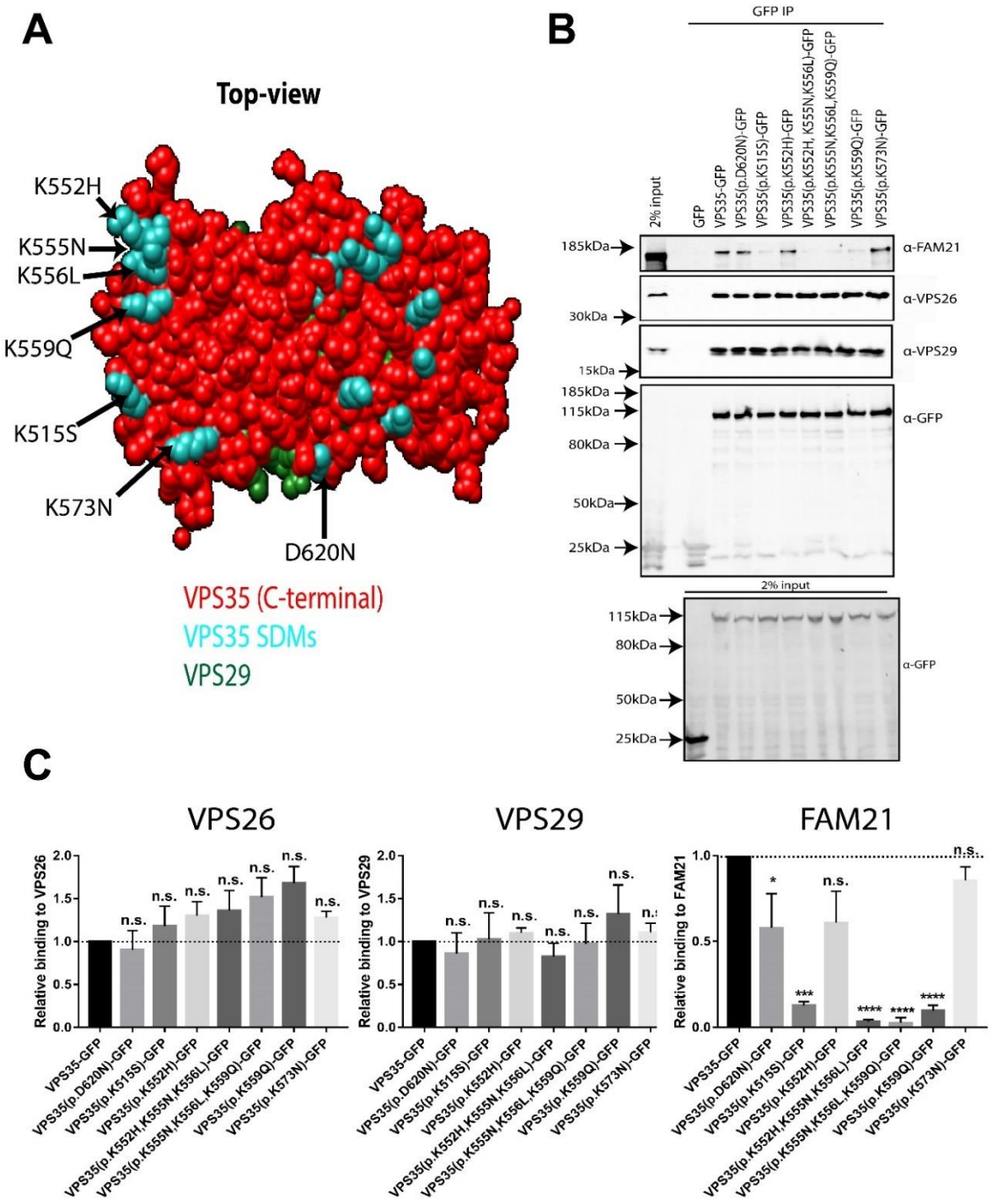

Figure 5.4 Screen of VPS35-GFP variants reveal residues important for FAM21 binding (area 1).

(A) Model identifying the mutants (highlighted in blue) created in VPS35 **(B)** HEK293T cells were transfected with the indicated VPS35-GFP constructs and subjected to a GFP-trap. The immuno-precipitates were resolved by SDS-PAGE and immuno-blotted for the indicated antibodies. **(C)** The florescent bands were quantified using a Licor Odyssey Scanner; quantification shown represents the mean of 3 experiments ± s.e.m; * P ≤ 0.05; ** P ≤ 0.01; ***P ≤ 0.001; **** P ≤ 0.0001. Immuno-precipitated bands were normalised to wild-type VPS35-GFP and analysed using a one-way ANOVA followed by a Dunnett's test.

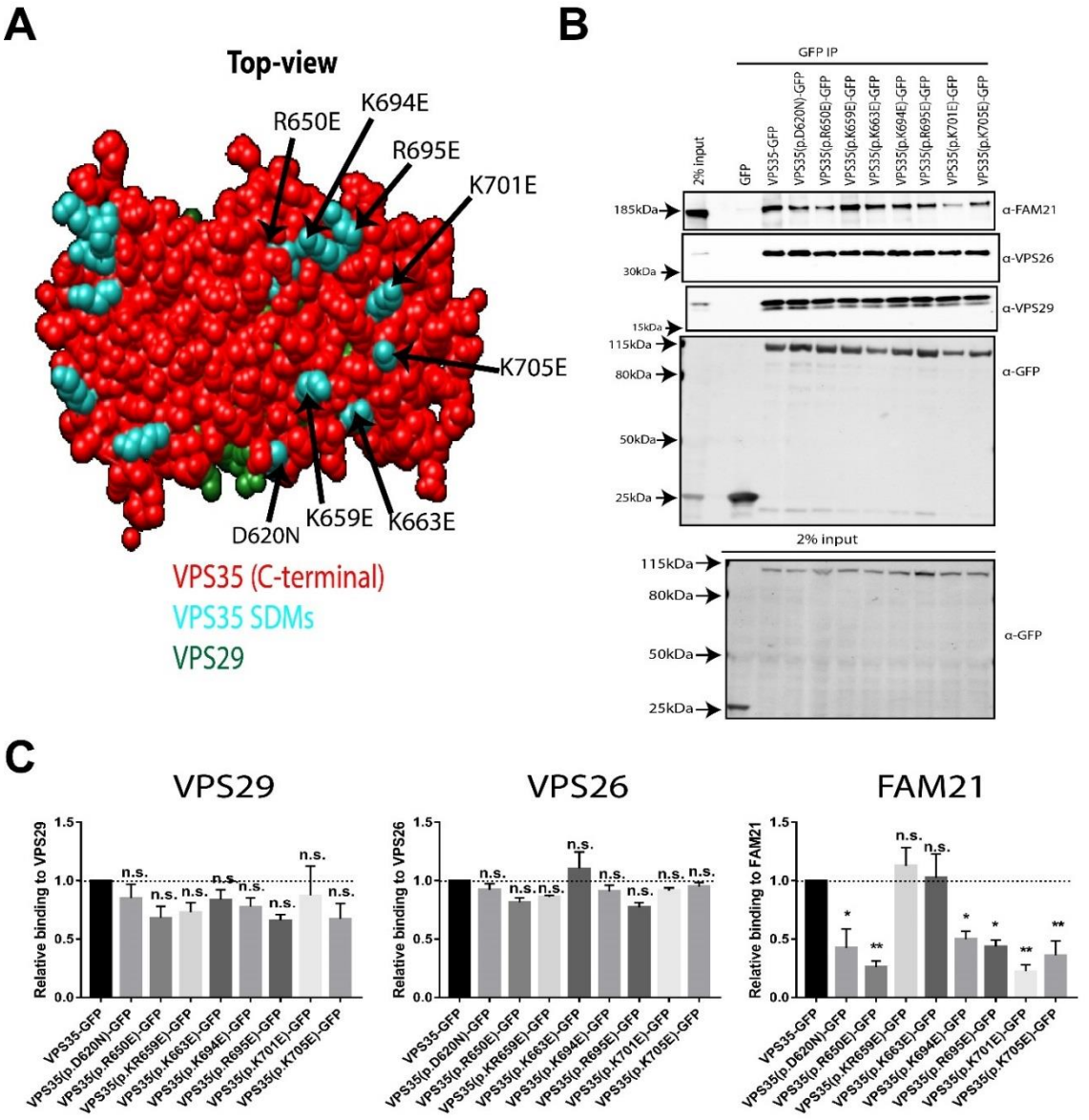

Figure 5.5 Screen of VPS35-GFP variants reveal residues important for FAM21 binding (area 2).

(A) (B) HEK293T cells were transfected with the indicated VPS35-GFP constructs and subjected to a GFP-trap. The immuno-precipitates were resolved by SDS-PAGE and immuno-blotted for the indicated antibodies. **(C)** The florescent bands were quantified using a Licor Odyssey Scanner; quantification shown represents the mean of 3 experiments ± s.e.m; * P ≤ 0.05; ** P ≤ 0.01; ***P ≤ 0.001; **** P ≤ 0.0001. Immuno-precipitated bands were normalised to wild-type VPS35-GFP and analysed using a one-way ANOVA followed by a Dunnett's test.

expressed endogenous levels of VPS35-GFP variants **(Figure 5.7)**. In VPS35 knockout cells, FAM21 has a reduced endosomal localisation (McNally et al., 2017). When wild-type VPS35-GFP was transduced into the VPS35 knock-out cells, the endosomal population of FAM21 was markedly increased; however, this rescue was repeated for all the VPS35-GFP variants tested **(Figure 5.8A)**. I measured the degree of rescue by

comparing the colocalisation between FAM21 and the endosomal marker SNX1 **(Figure 5.8B)**. This suggests that even though I could not biochemically identify an interaction between FAM21 and retromer in the verified mutants **(Figure 5.4 and Figure 5.5)**, FAM21 could still be recruited to endosomes by the VPS35-GFP variants.

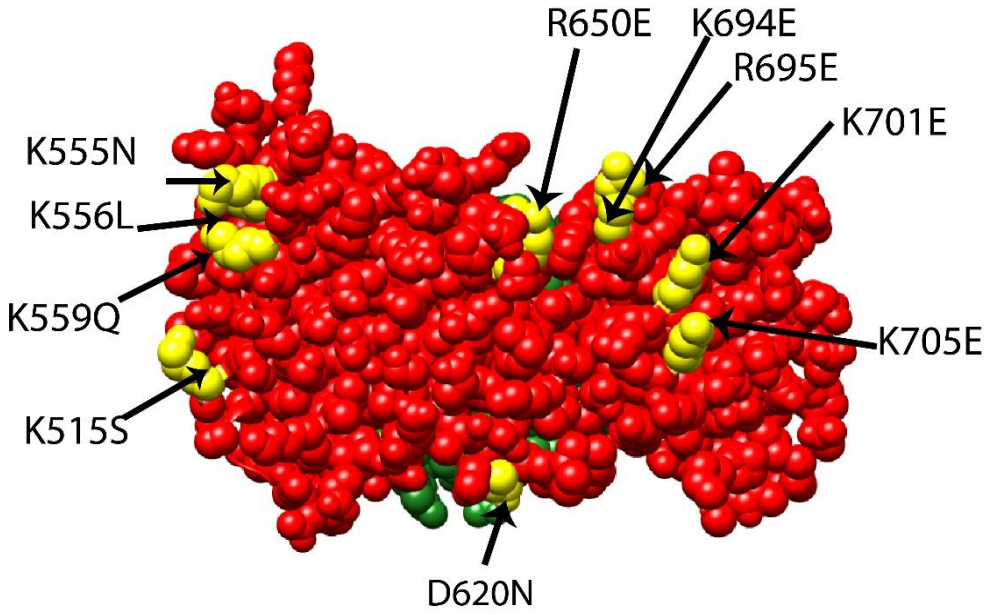

Figure 5.6 Model of residues in VPS35 that are implicated in FAM21 association.

Model of the C-terminal VPS35 (red) bound to VPS29 (green) crystal structure (Hierro et al., 2007). Residues that, when mutated, significantly perturb FAM21 binding are coloured in yellow.

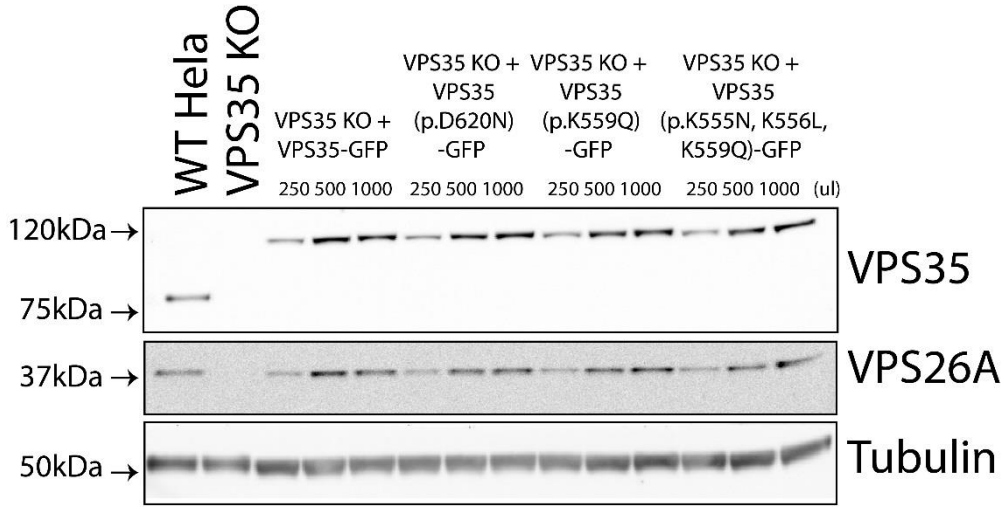

Figure 5.7 Lentiviral transduction of VPS35-GFP constructs into VPS35 knockout HeLa cells.

Various titres of lentivirus (250µl, 500µl and 1000µl) were added to transduce VPS35 knockout HeLa cells; the lysates were resolved using SDS-PAGE and subjected to immuno-blotting using the indicated antibodies.

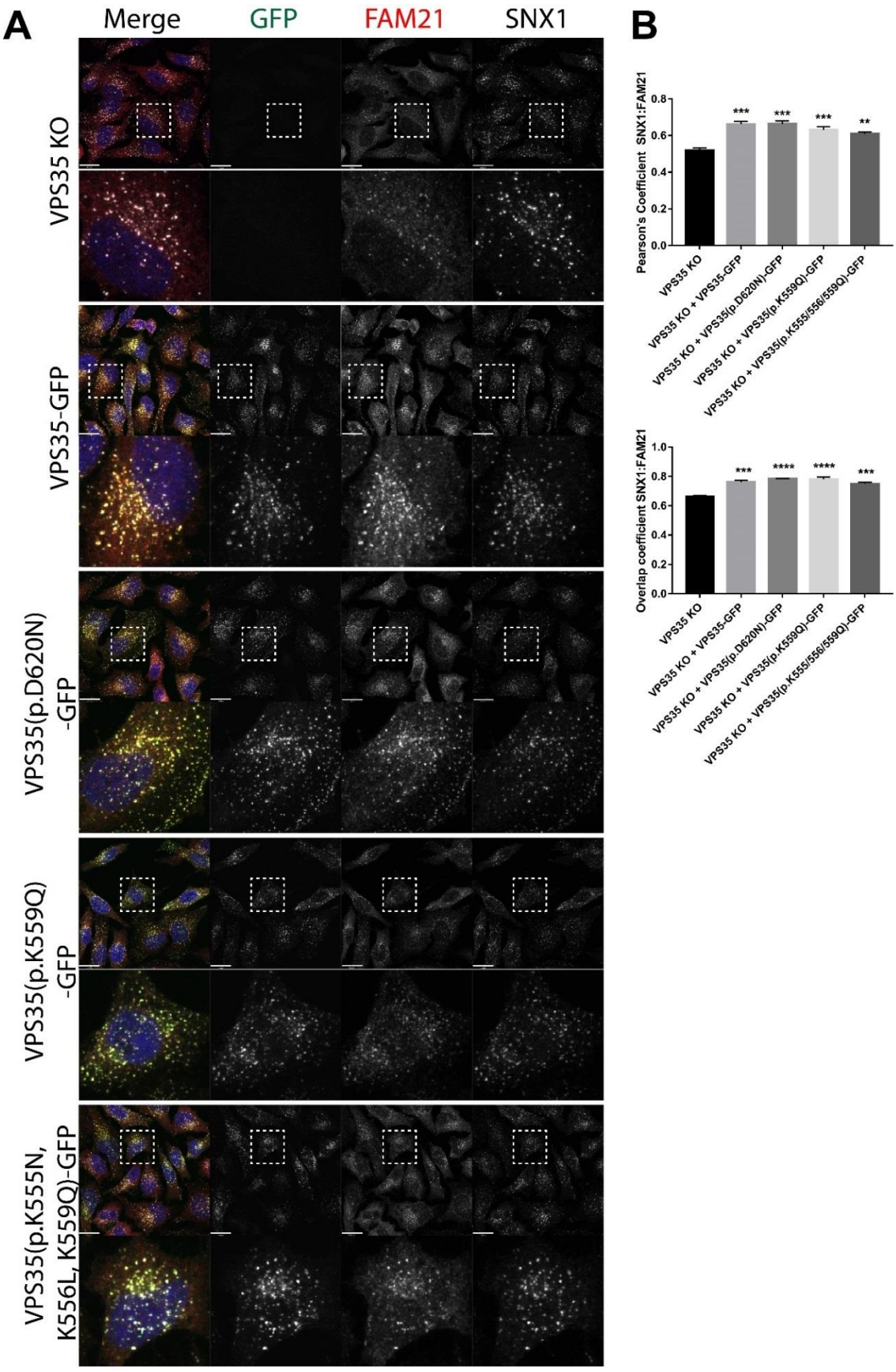

Figure 5.8 VPS35-GFP constructs with severely perturbed FAM21 association rescue the endosomal localisation of FAM21.

(A) VPS35 knockout HeLa cells, transduced with the indicated VPS35-GFP constructs, were fixed with 4% paraformaldehyde and immuno-stained with endogenous FAM21 and SNX1. Cells were imaged using a confocal microscope. The scale bar indicates 19 µm. **(B)** Graphs showing the quantified Pearson's colocalisation coefficient (PCC) and Overlap coefficient (OC) from 3 independent experiments (at least 25 cells were quantified per experiment). Error bars indicate standard error; data were analysed using a one-way ANOVA and a Dunnett's post-hoc test comparing the mutant constructs to the wild type VPS35-GFP construct. ** P ≤ 0.01; ***; P ≤ 0.001; **** P ≤ 0.0001.

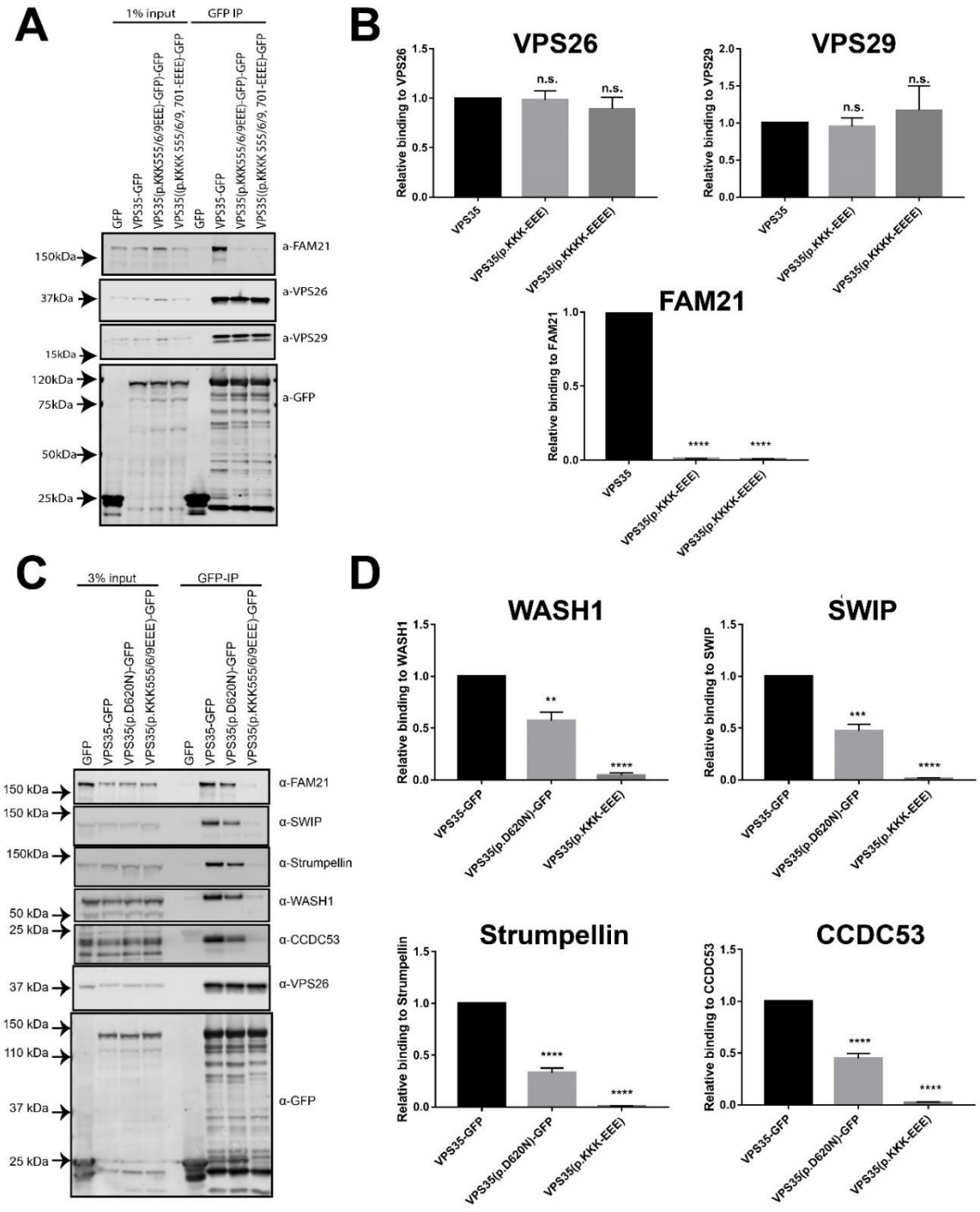

Figure 5.9 The VPS35(p.K555E, K556E, K559E)-GFP variant loses affinity for the WASH complex but retains the ability to assemble into the retromer complex.

(A and C) HEK293T cells were transfected with the indicated GFP-tag construct and subjected to a GFP-trap. The immuno-precipitates were resolved using SDS-PAGE and immuno-blotted with the indicated antibodies. **(B and D)** The florescent bands were quantified using a Licor Odyssey Scanner; quantification shown represents 3 experiments. Immuno-precipitated bands were normalised to wild-type VPS35-GFP and analysed using a one-way ANOVA followed by a Dunnett's test; ** P ≤ 0.01; *** P ≤ 0.001; **** P ≤ 0.0001.

5.2.3 Introduction of VPS35(p.K555E, K556E, K559E)-GFP causes a loss in endosomal WASH complex association

Unpublished results from the Cullen lab have identified that electrostatic interactions can require charge inversions to fully uncouple two interactions in cells and to see a functional phenotype. Considering this, I created, via site-directed mutagenesis, a VPS35(p.K555E, K556E, K559E)-GFP instead of VPS35(p.K555N, K556L, K559Q)-GFP. This mutant again, in GFP-nanotrap immunoprecipitations, displayed a greatly perturbated interaction with FAM21 but could still assemble into the retromer complex **(Figure 5.9A-B)**. Furthermore, this severe perturbation in association was also seen with the other WASH complex members (WASH1, SWIP, Strumpellin and CCDC53) **(Figure 5.9C-D)**, verifying that retromer associates with the WASH complex via FAM21.

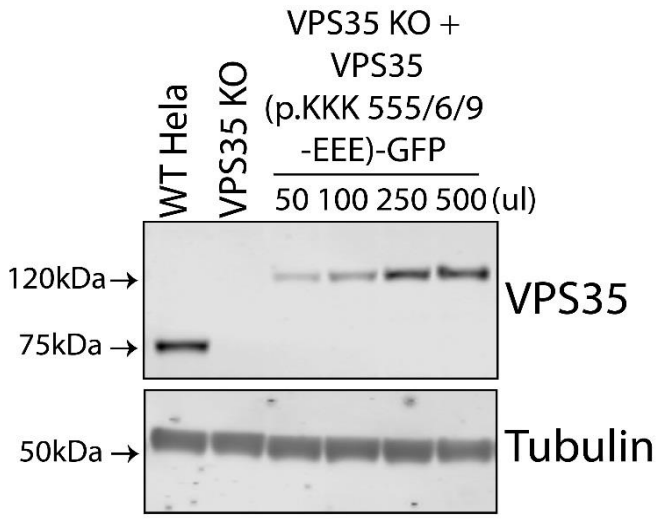

Figure 5.10 Lentiviral transduction of VPS35(p.K555E, K556E, K559E)-GFP into VPS35 knockout HeLa cells.

Lentiviral transduction of VPS35-GFP constructs into VPS35 knockout HeLa cells. Various titres of lentivirus (50µl, 100µl, 250µl and 500µl) added to transduce the cells; the lysates from these titres were resolved using SDS-PAGE and subjected to immuno-blotting using the indicated antibodies.

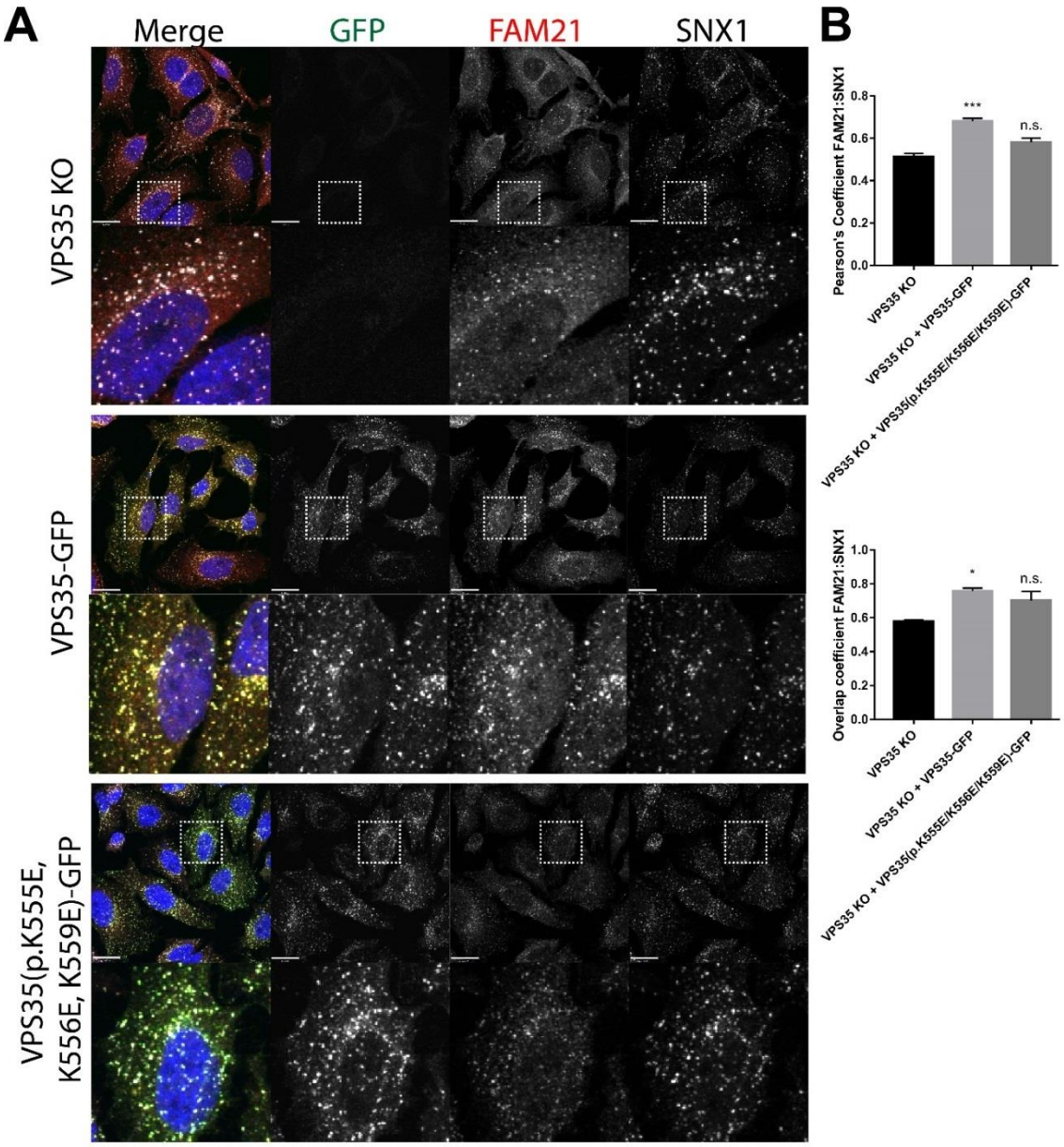

Figure 5.11 Introduction of VPS35(p.K555E, K556E, K559E)-GFP does not rescue the endosomal localisation of FAM21.

(A) VPS35 knockout HeLa cells, transduced with the indicated VPS35-GFP constructs, were fixed with 4% paraformaldehyde and immuno-stained with endogenous FAM21 and SNX1. Cells were imaged using a confocal microscope. The scale bar indicates 19 µm. **(B)** Graphs showing the quantified Pearson's colocalisation coefficient (PCC) and Overlap coefficient (OC) from 3 independent experiments (at least 25 cells were quantified per experiment). Error bars indicate standard error; data were analysed using a one-way ANOVA and a Dunnett's post-hoc test comparing the mutant constructs to the wild type VPS35-GFP construct; * $P \leq 0.05$; *** $P \leq 0.001$.

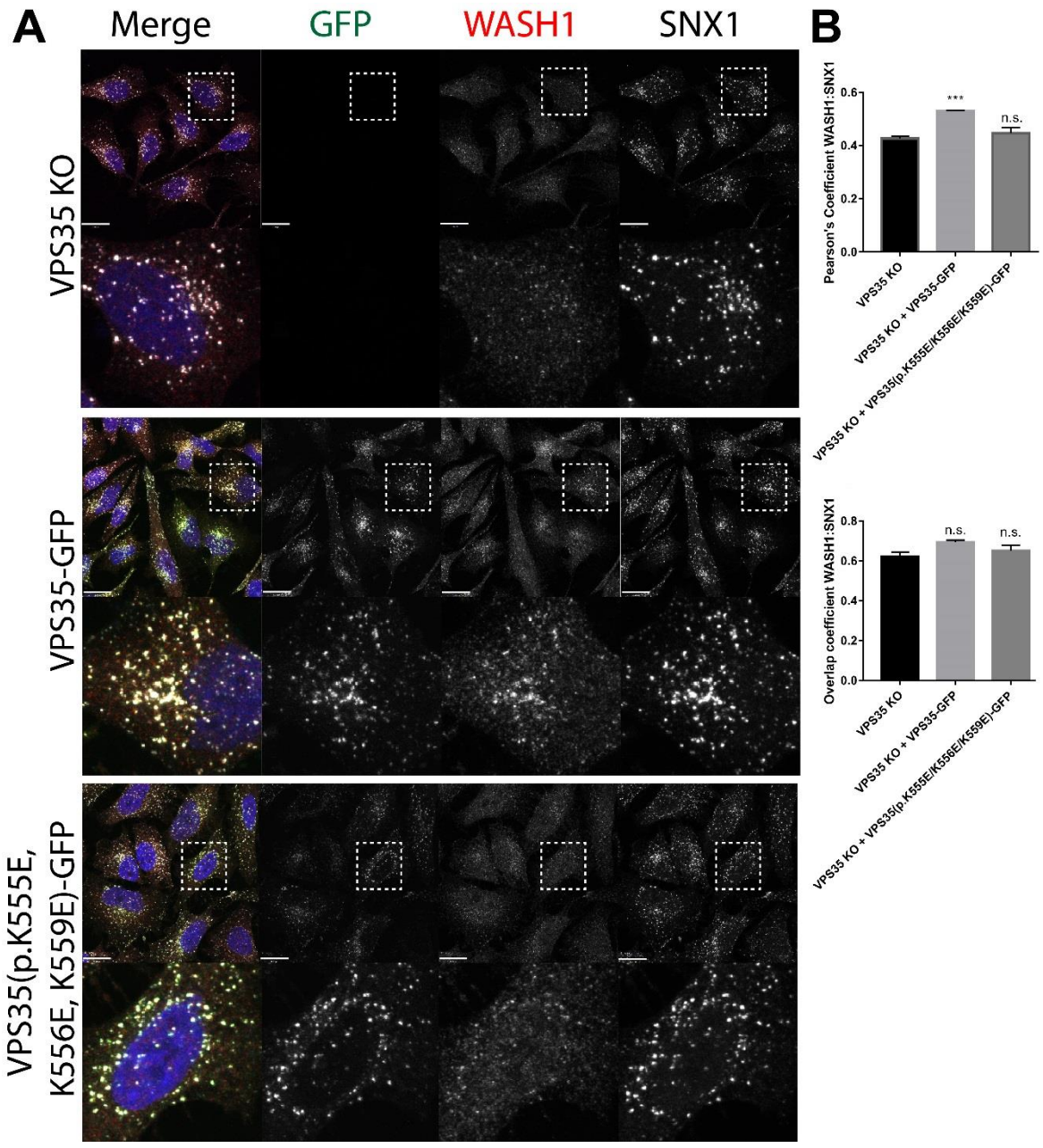

Figure 5.12 Introduction of VPS35(p.K555E, K556E, K559E)-GFP does not rescue the endosomal localisation of WASH1.

(A) VPS35 knockout HeLa cells, transduced with the indicated VPS35-GFP constructs, were fixed with 4% paraformaldehyde and immuno-stained with endogenous WASH1 and SNX1. Cells were imaged using a confocal microscope. The scale bar indicates 19 µm. **(B)** Graphs showing the quantified Pearson's colocalisation coefficient (PCC) and Overlap coefficient (OC) from 3 independent experiments (at least 25 cells were quantified per experiment). Error bars indicate standard error; data were analysed using a one-way ANOVA and a Dunnett's post-hoc test comparing the mutant constructs to the wild type VPS35-GFP construct; *** $P \leq 0.001$.

I then lentivirally transduced the charge-swap VPS35-GFP variants into VPS35 knockout HeLa cells to near endogenous levels **(Figure 5.10)** and analysed the localisation of FAM21 in these stably transduced cells **(Figure 5.11A)**. Comparing the

colocalisation between FAM21 and SNX1 between the VPS35-GFP variant-rescued cells, I found that the VPS35(p.K555E, K556E, K559E)-GFP transductions did not rescue the endosomal localisation of FAM21, whereas wild-type VPS35-GFP did **(Figure 5.11B)**. Additionally, when I analysed the localisation of another WASH complex member, WASH1 **(Figure 5.12A)**, the VPS35(p.K555E, K556E, K559E)-GFP transduced cells did not rescue the colocalisation between WASH1 and SNX1 **(Figure 5.12B)**.

5.2.4 Investigating the functional significance of the VPS35:FAM21 interaction

Having identified VPS35 mutations which dramatically perturb WASH complex binding and do not rescue the endosomal localisation of FAM21 in VPS35 knockout cells, I wished to examine the functional consequence of uncoupling the retromer complex from the WASH complex. For this, I utilised the endosome to plasma-membrane cargo, GLUT1. In VPS35 knockout cells, GLUT1 colocalises with LAMP1; when rescued with VPS35-GFP, GLUT1 re-localises to the cell surface **(Figure 5.13A)**. When VPS35(p.K555E,K556E,K559E)-GFP was introduced into the VPS35 knockout cells, GLUT1 also re-localised to the cell surface **(Figure 5.13A-B)**. There was also not an obvious GLUT1 re-localisation into other intracellular compartments, such as the TGN, following VPS35(p.K555E,K556E,K559E)-GFP transduction **(Figure 5.13A)**.

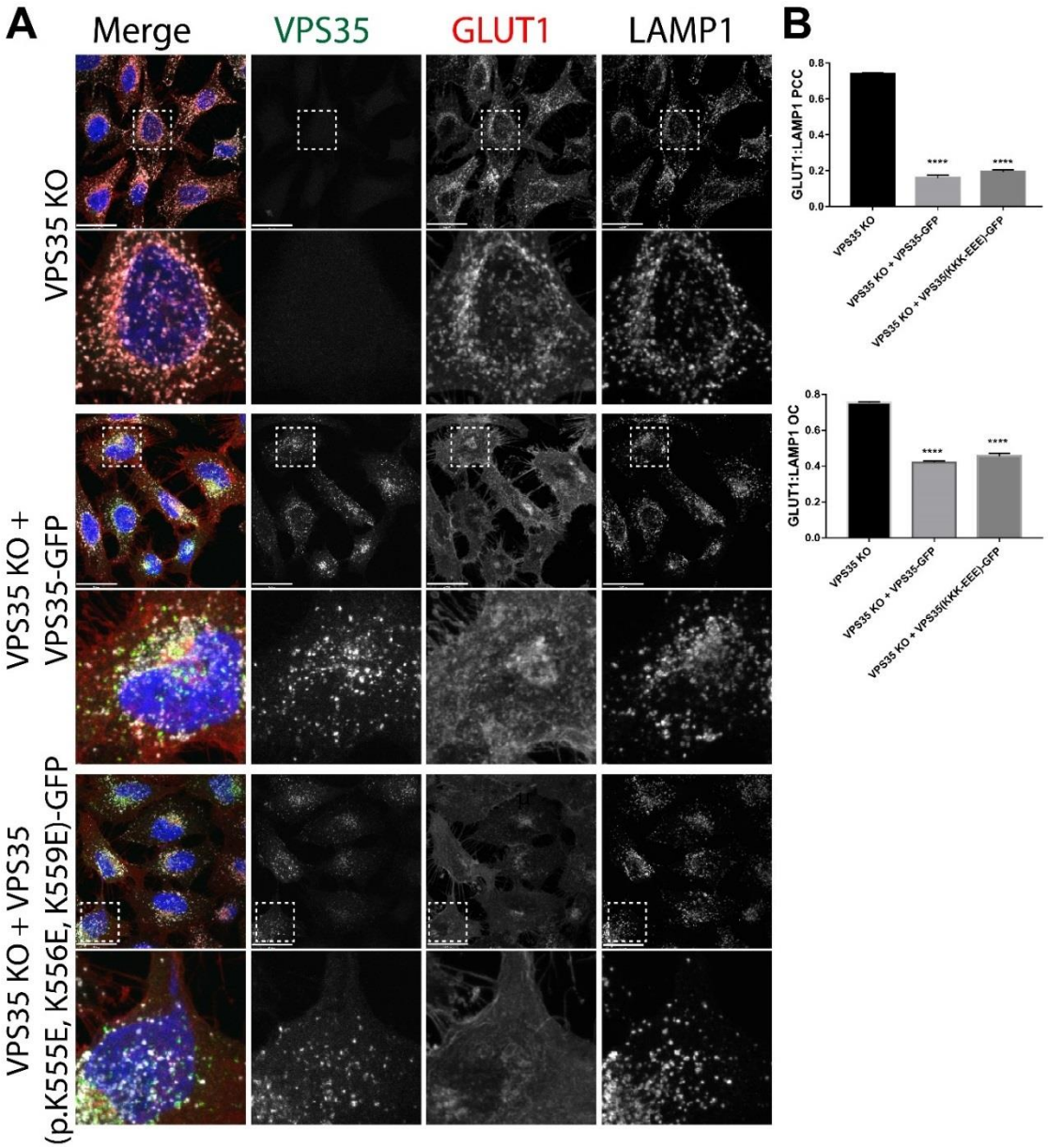

Figure 5.13 Introduction of VPS35(p.K555E, K556E, K559E)-GFP does rescue the GLUT1 trafficking defect.

(A) VPS35 knockout HeLa cells, transduced with the indicated VPS35-GFP constructs, were fixed with 4% paraformaldehyde and immuno-stained with endogenous GLUT1 and LAMP1. Cells were imaged using a confocal microscope. The scale bar indicates 19 µm. **(B)** Graphs showing the quantified Pearson's colocalisation coefficient (PCC) and Overlap coefficient (OC) from 3 independent experiments (at least 25 cells were quantified per experiment). Error bars indicate standard error; data were analysed using a one-way ANOVA and a Dunnett's post-hoc test comparing the mutant constructs to the wild-type VPS35-GFP construct; **** $P \leq 0.0001$.

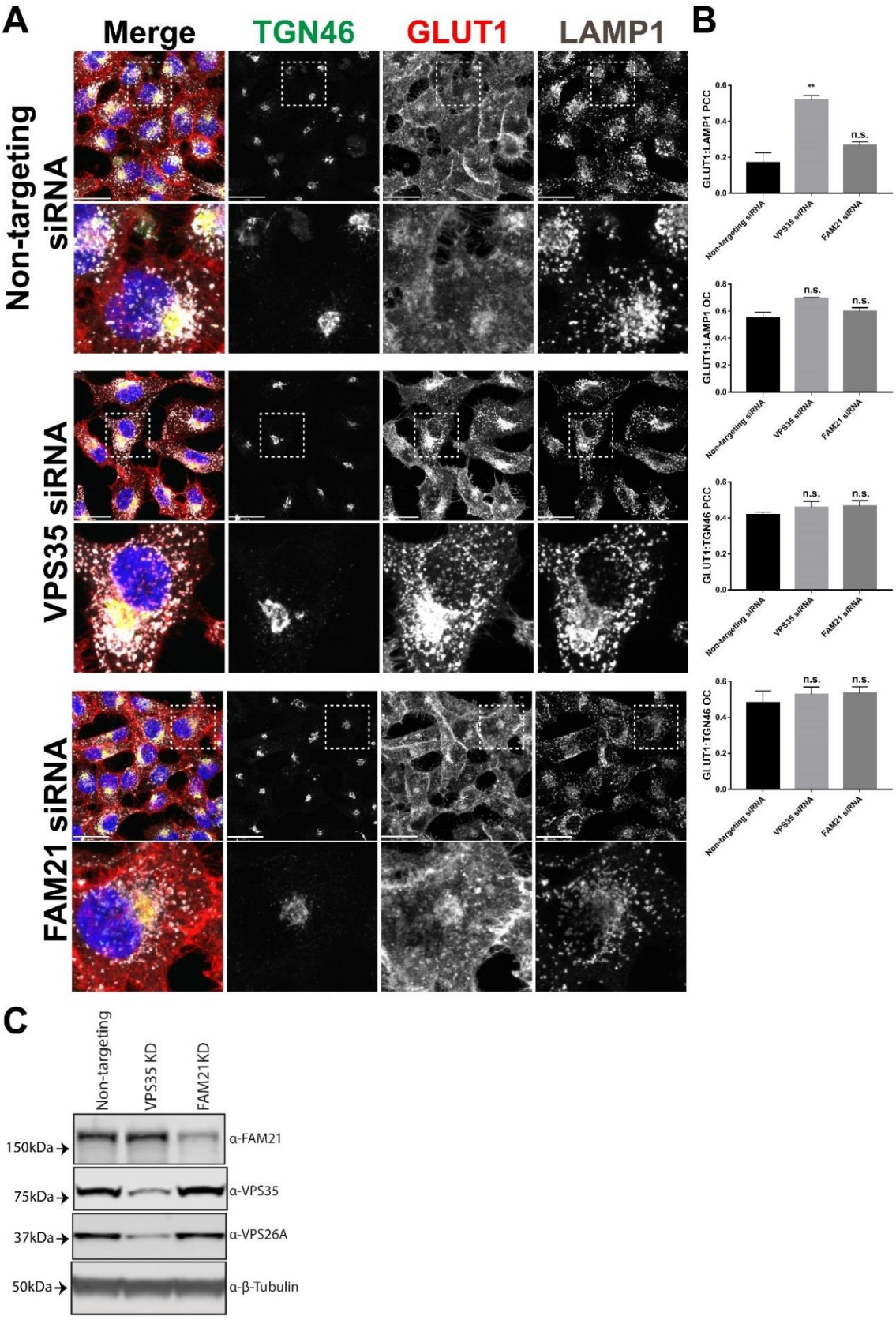

Figure 5.14 Knock-down of FAM21 in HeLa cells do not cause a significant increase in GLUT1 colocalisation with LAMP1 or TGN46.

(A) HeLa cells were suppressed using siRNA targeting VPS35 and FAM21. After adherence to coverslips, the cells were fixed using 4% paraformaldehyde and immuno-stained with

endogenous GLUT1, LAMP1 and TGN46. The scale bar indicates 29 µm. **(B)** Graphs showing the quantified Pearson's colocalisation coefficient (PCC) and Overlap coefficient (OC) from 3 independent experiments (at least 20 cells were quantified per experiment). Error bars indicate standard error; data were analysed using a one-way ANOVA and a Dunnett's post-hoc test comparing the mutant constructs to the wild type VPS35-GFP construct; ** $P \leq 0.01$. **(C)** HeLa cells, suppressed using the indicated siRNAs, were lysed and resolved using SDS-PAGE and immuno-blotted with the indicated antibody.

To take a step back, I investigated the functional consequence of FAM21 depletion on GLUT1 localisation. Recently, FAM21 knockdown has been shown to cause the TGN (Lee et al., 2016) or LAMP1 (Kvainickas et al., 2017b) re-localisation of GLUT1 (depending on the cell line utilised). When I treated HeLa cells with siRNA targeting VPS35, GLUT1 re-localised to a LAMP1-positive compartment, with no effect on GLUT1 re-localisation to the TGN **(Figure 5.14)**. In contrast, FAM21 depletion did not affect the localisation of GLUT1, either towards the LAMP1- or TGN46-positve compartments in HeLa cells **(Figure 5.14)**. The Lee et al. (2016) paper used RPE-1 cells to investigate the consequence of FAM21 depletion. I therefore repeated the experiment using RPE-1 cells. VPS35 suppression increased the colocalisation of GLUT1 with the LAMP1- and TGN46-postive compartments **(Figure 5.15)**. FAM21 suppression caused a less pronounced increase in GLUT1 colocalisation with LAMP1 and a more pronounced increase with TGN46 **(Figure 5.15)**.

As I could only see an effect of FAM21 suppression on GLUT1 localisation using RPE-1 cells (at the suppression levels achieved using siRNA), I sought to investigate whether VPS35(p.K555E,K556E,K559E)-GFP would affect the localisation of GLUT1 in RPE-1 cells. To do this, I overexpressed VPS35-GFP variants in RPE-1 cells to outcompete (an effect already seen in **Figure 4.3** and **Figure 4.13A**) endogenous VPS35 **(Figure 5.16)**. Overexpression of VPS35(p.K555E,K556E,K559E)-GFP caused a significant decrease in FAM21 colocalisation with the endosomal marker SNX1 **(Figure 5.17)**. Overexpression of VPS35-GFP did not cause a significant decrease in colocalisation of FAM21 with SNX1, although there was a consistent trend towards the colocalisation being lower.

I then investigated whether overexpressing VPS35-GFP or VPS35(p.K555E,K556E,K559E)-GFP has an effect on the localisation of GLUT1. The re-localisation of GLUT1 to a TGN46-postive compartment was the most striking phenotype seen in the FAM21 suppression experiments in RPE-1 cells **(Figure 5.15)**. I therefore quantified the colocalisation between GLUT1 and TGN46. However, no re-localisation of GLUT1 was seen in the context of VPS35(p.K555E,K556E,K559E)-GFP overexpression in RPE-1 cells **(Figure 5.18)**.

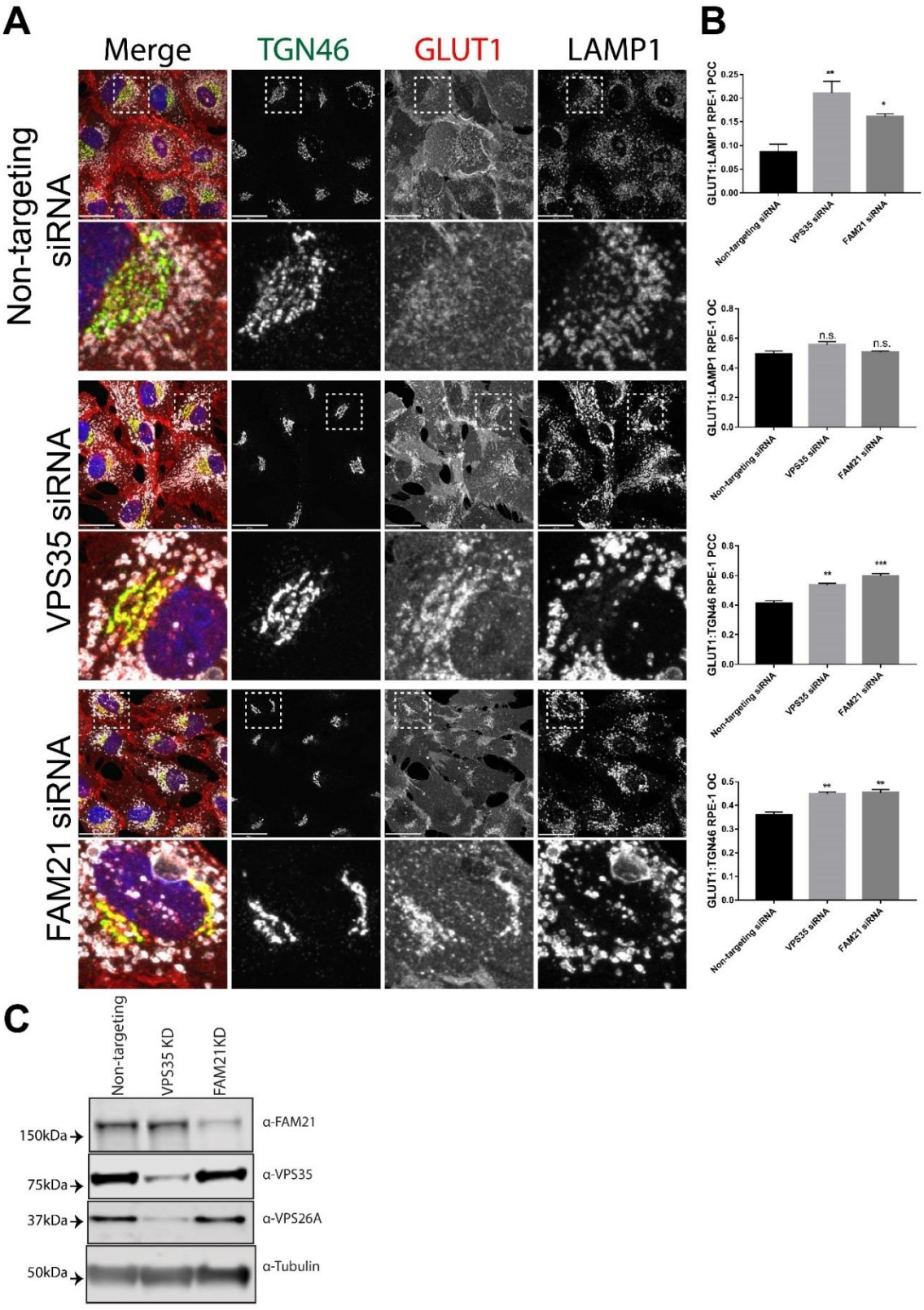

Figure 5.15 Knock-down of FAM21 in RPE-1 cells causes a significant increase in GLUT1 colocalisation with LAMP1 and TGN46.

(A) RPE-1 cells were suppressed using siRNA targeting VPS35 and FAM21. After adherence to coverslips, the cells were fixed using 4% paraformaldehyde and immuno-stained with endogenous GLUT1, LAMP1 and TGN46. Scale bar indicates 29 µm. **(B)** Graphs showing the

quantified Pearson's colocalisation coefficient (PCC) and Overlap coefficient (OC) from 3 independent experiments (at least 20 cells were quantified per experiment). Error bars indicate standard error; data were analysed using a one-way ANOVA and a Dunnett's post-hoc test comparing the mutant constructs to the wild-type VPS35-GFP construct; * P ≤ 0.05; ** P ≤ 0.01; *** P ≤ 0.001. **(C)** RPE-1 cells, suppressed using the indicated siRNAs, were lysed and resolved using SDS-PAGE and immuno-blotted with the indicated antibody.

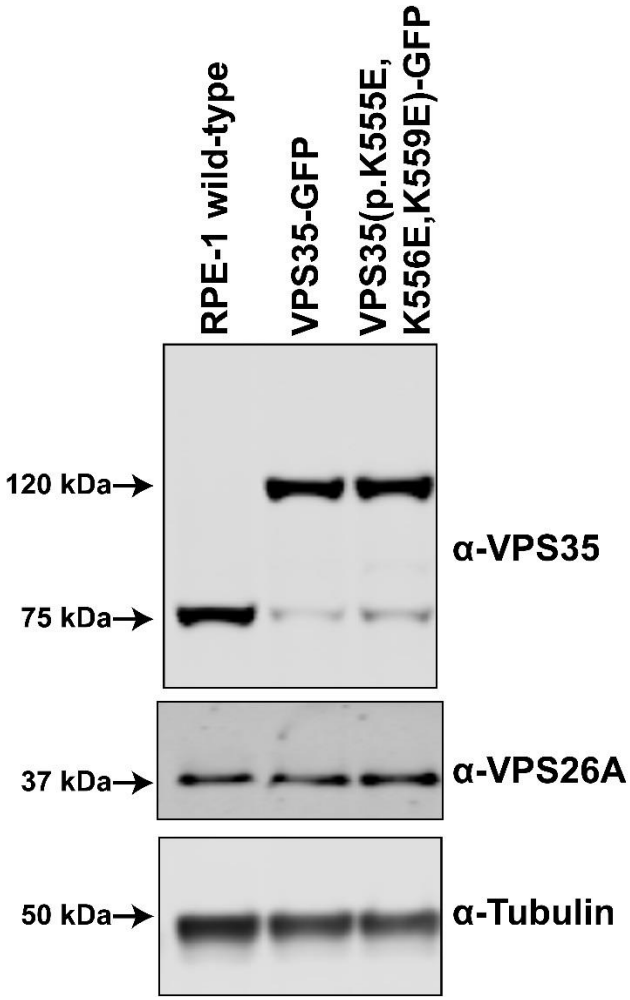

Figure 5.16 Overexpression of VPS35-GFP variants in RPE-1 cells outcompetes endogenous VPS35 for assembly into the retromer complex.

Lentivirus were added to RPE-1 cells to overexpress the VPS35-GFP variants; the lysates from these cells were resolved using SDS-PAGE and subjected to immuno-blotting using the indicated antibodies.

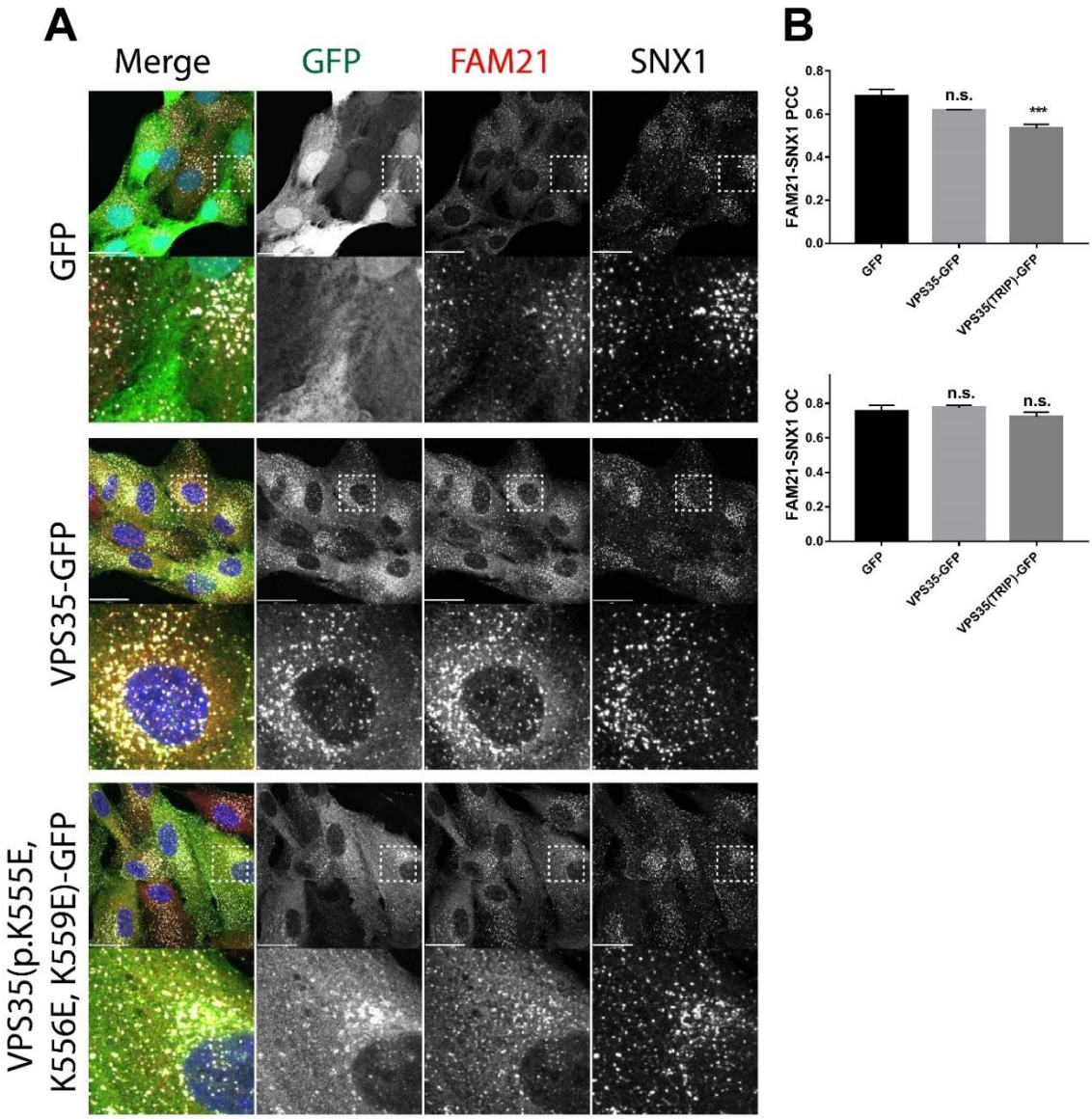

Figure 5.17 Overexpressing VPS35(p.K555E,K556E,K559E)-GFP in RPE-1 cells causes a decrease in endosomal association of FAM21.

(A) RPE-1 cells, stably overexpressing VPS35-GFP constructs through lentiviral transduction, were fixed with 4% paraformaldehyde and immuno-stained for endogenous FAM21 and SNX1. Scale bars indicate 29 µm. **(B)** Graphs showing the quantified Pearson's colocalisation coefficient (PCC) and Overlap coefficient (OC) from 3 independent experiments (at least 25 cells were quantified per experiment). Error bars indicate standard error; data were analysed using a one-way ANOVA and a Dunnett's post-hoc test comparing the mutant constructs to the wild type VPS35-GFP construct; *** $P \leq 0.001$.

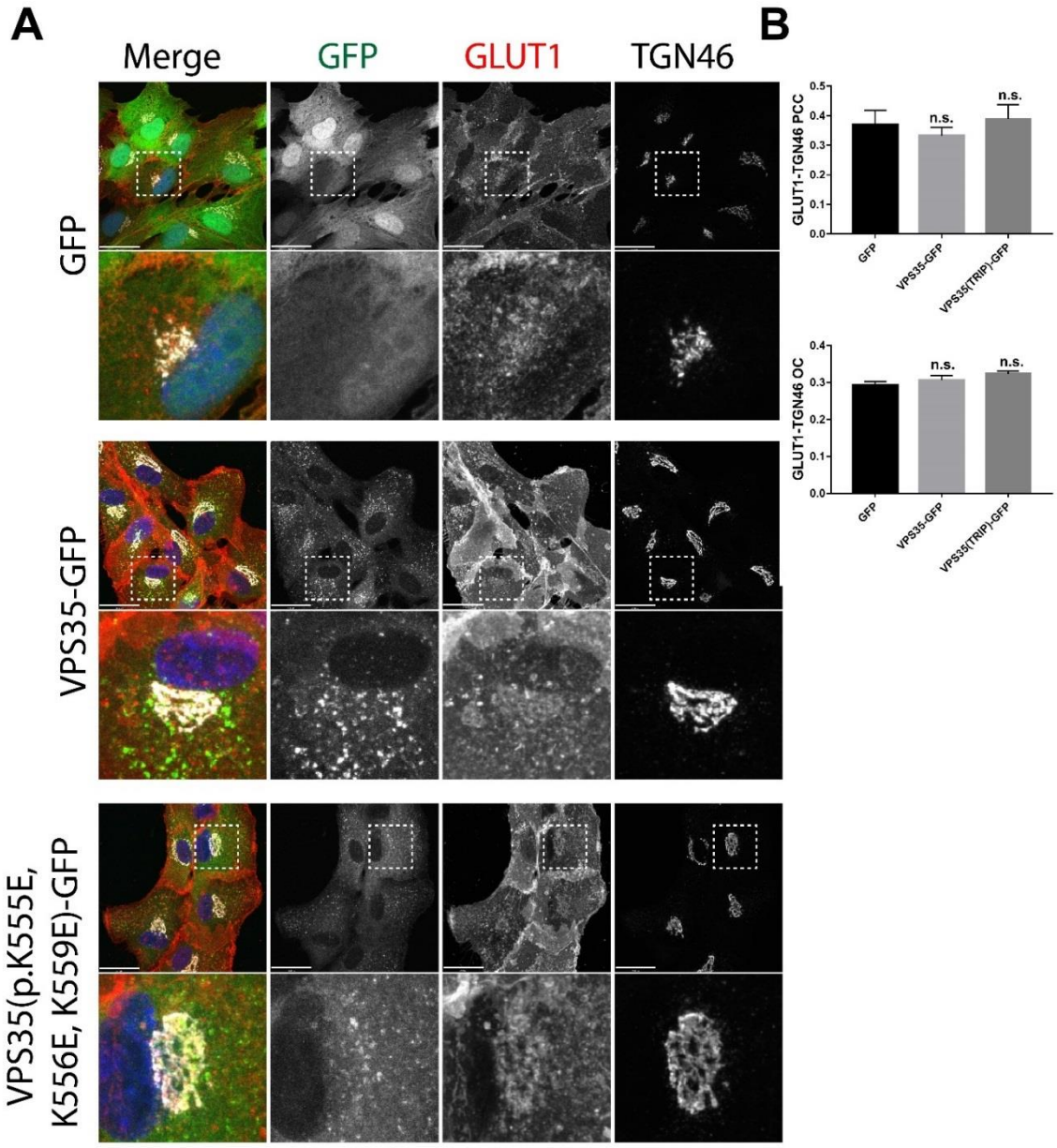

Figure 5.18 Overexpressing VPS35(p.K555E,K556E,K559E)-GFP in RPE-1 cells does not increase the TGN localisation of GLUT1.

(A) RPE-1 cells, stably overexpressing VPS35-GFP constructs through lentiviral transduction, were fixed with 4% paraformaldehyde and immuno-stained for endogenous GLUT1 and TGN46. Scale bars indicate 29 µm. **(B)** Graphs showing the quantified Pearson's colocalisation coefficient (PCC) and Overlap coefficient (OC) from 3 independent experiments (at least 25 cells were quantified per experiment). Error bars indicate standard error; data were analysed using a one-way ANOVA and a Dunnett's post-hoc test comparing the mutant constructs to the wild-type VPS35-GFP construct.

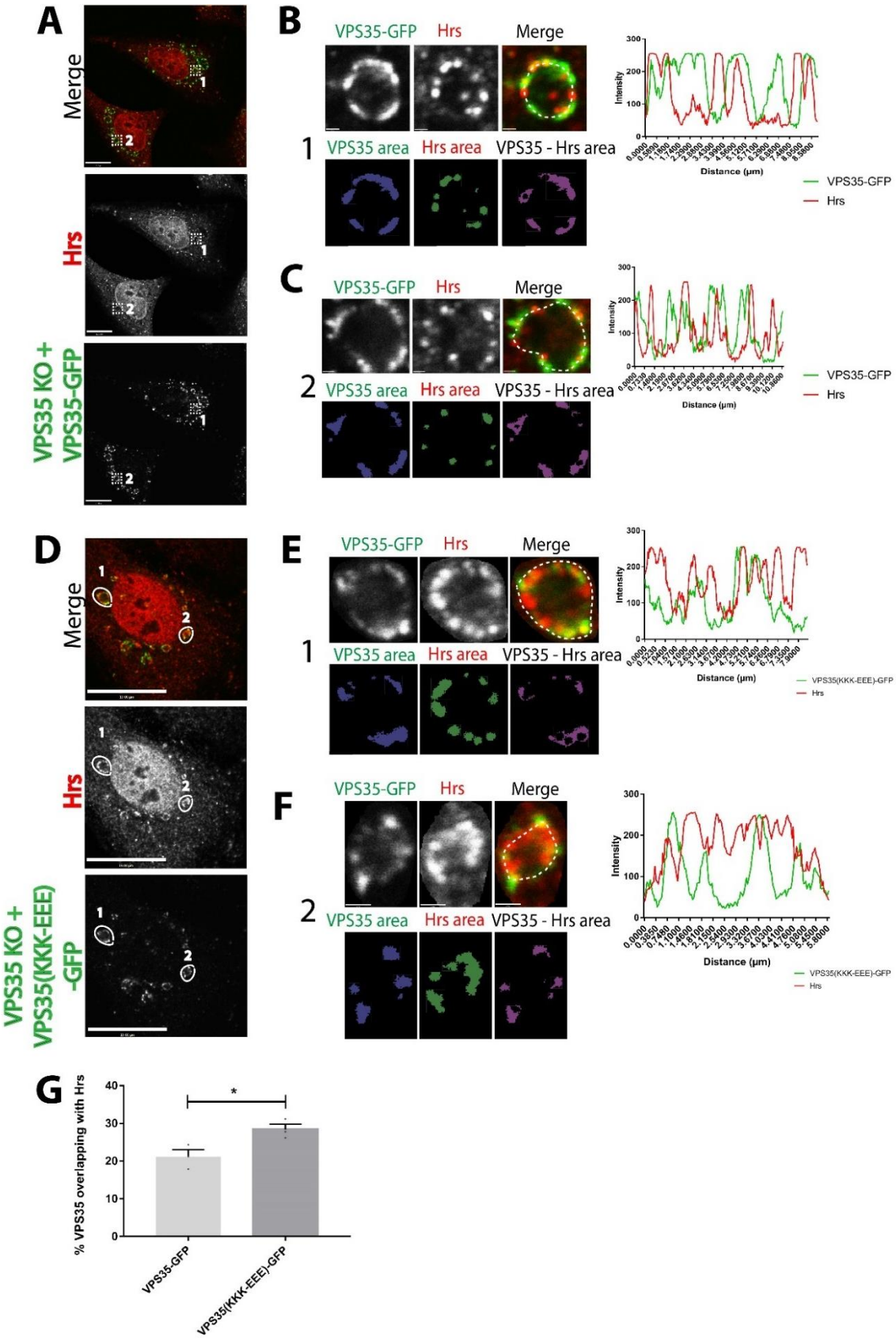

Figure 5.19 Reintroducing VPS35(p.K555E,K556E,K559E)-GFP into VPS35 knockout HeLa cells causes a mild enlargement of the overlap between retrieval and degradative subdomains on enlarged endosomes.

(A and D) VPS35 knockout HeLa cells, transduced with the indicated VPS35-GFP constructs, were transiently transfected with BFP-Rab5(p.Q79L) to enlarge endosomes. Cells were methanol fixed and immuno-stained for VPS35 and Hrs. Images were taken on a confocal microscope. Scale bars indicate 13 µm in A and 19 µm in D. **(B, C, E and F)** Areas of interest with line scans from A and D. Volocity software was used to measure the area of the different channels and to calculate the amount of overlap between the VPS35 and Hrs channels. **(G)** Quantification of the percentage overlap between the Hrs and VPS35 channels from 3 independent experiments. 40 enlarged vesicles were quantified per condition per experiment. Data were analysed using a students t-test and the error bars indicate s.e.m.; * $P \leq 0.05$.

5.2.5 The retromer-WASH complex interaction contributes to the maintenance of endosomal subdomains

The WASH complex and its actin-polymerisation ability has been proposed to maintain and regulate the formation of endosomal subdomains, possibly through binding to multiple retromer complexes (Jia et al., 2012; Cullen and Steinberg, 2018; Simonetti and Cullen, 2018a). I therefore examined whether the connection between retromer and the WASH complex is necessary for the segregation of the degradative and retrieval endosomal subdomains. Transfection of constitutively active Rab5(p.Q79L) creates enlarged, swollen endosomes, allowing the distinction between retrieval and degradative subdomains (Barbieri et al., 1996; McNally et al., 2017). Into VPS35 knockout HeLa cells transduced at endogenous levels with VPS35-GFP variants **(Figure 5.16)**, I transfected BFP-Rab5(p.Q79L) **(Figure 5.19)**. On enlarged endosomes, the Hrs and VPS35 channels could be segmented into apparent areas and the percentage overlap between VPS35 and Hrs could be measured **(Figure 5.19 B, C, E and F)**. When VPS35-GFP was transduced into the VPS35 knockout cells, an average of 21.14% ± 1.90% of VPS35 overlapped with Hrs in the enlarged vesicles **(Figure 5.19G)**. This compared to an average of 28.37% ± 1.46% of overlap when VPS35(p.K555E, K556E, K559E)-GFP was transduced, a significant increase **(Figure 5.19G)**.

I then examined whether this partial break-down in endosomal subdomain segregation could be phenocopied by FAM21 suppression. I therefore used siRNA-mediated suppression coupled to BFP-Rab5(p.Q79L) transfection to identify whether the overlap of endogenous VPS35 with Hrs is increased in the FAM21 suppressed HeLa cells **(Figure 5.20)**. Under non-targeting suppression, endogenous VPS35 averaged an overlap of 22.12% ± 1.03% with Hrs **(Figure 5.20G)**. Under FAM21 suppression, endogenous VPS35 had an overlap of 29.23% ± 1.92% with Hrs, again, a significant increase **(Figure 5.20G)**.

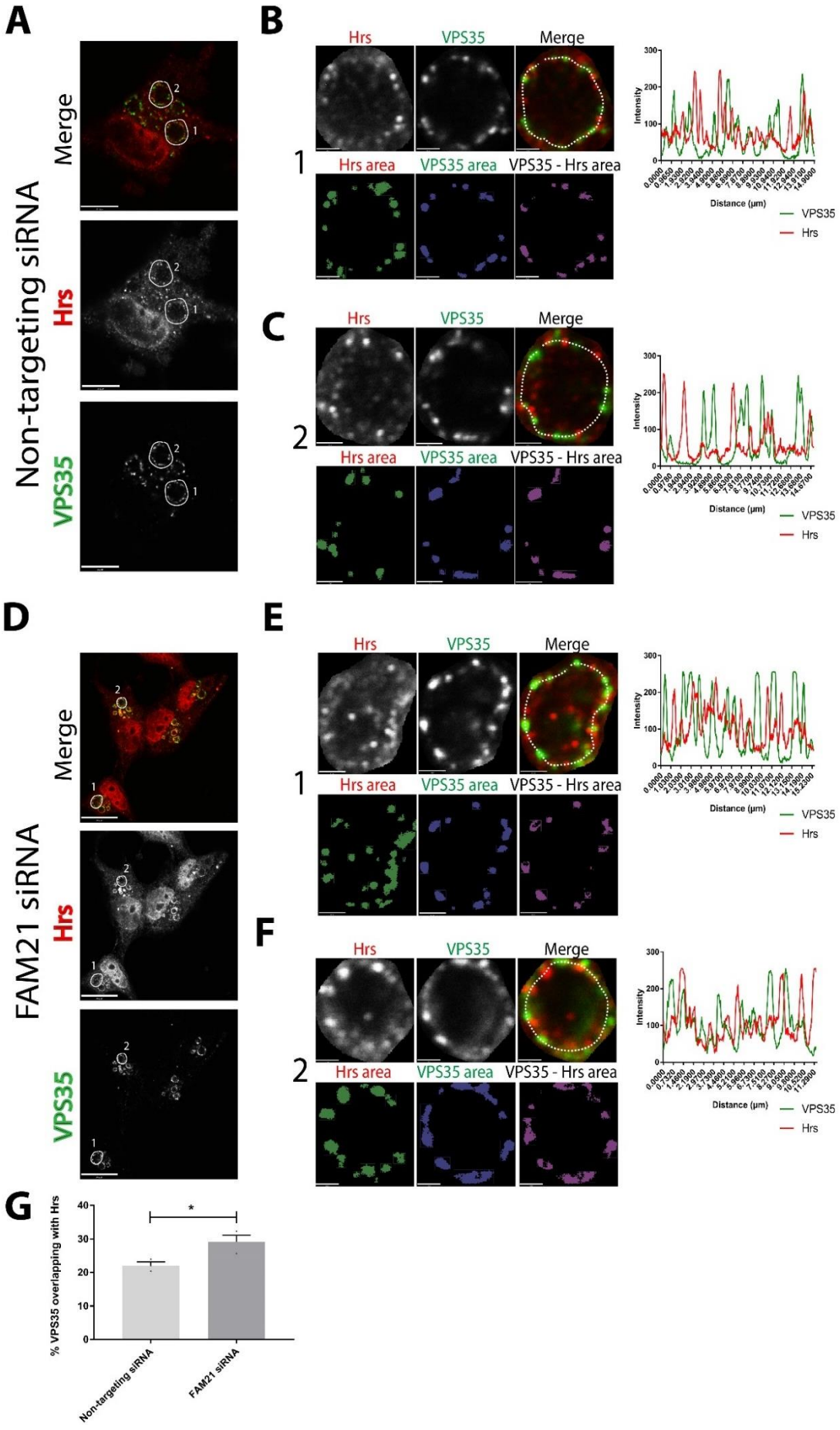
A
Non-targeting siRNA
Merge
Hrs
VPS35
B
Hrs
VPS35
Merge
Hrs area
VPS35 area
VPS35 - Hrs area
Intensity
Distance (μm)
VPS35
Hrs
C
D
FAM21 siRNA
E
F
G
% VPS35 overlapping with Hrs
Non-targeting siRNA
FAM21 siRNA
*

Figure 5.20 FAM21 suppression causes a mild enlargement of the overlap between retrieval and degradative subdomains on enlarged endosomes.

(A) HeLa cells, suppressed using either non-targeting or FAM21 siRNA, were transiently transfected with BFP-Rab5(p.Q79L) to create enlarged endosomes. The cells were methanol fixed and immuno-stained for VPS35 and Hrs. The images were taken on a confocal microscope and the scale bar indicates 10.3 µm in A and 19 µm in D. **(B, C, E and F)** Areas of interest with line scans from A and D. Volocity software was used to measure the area of the different channels and to calculate the amount of overlap between the VPS35 and Hrs channels. **(G)** Quantification of the percentage overlap between the Hrs and VPS35 channels from 3 independent experiments. 40 enlarged vesicles were quantified per condition per experiment. Data were analysed using a students t-test and the error bars indicate standard error; * $P \leq 0.05$.

5.2.6 TMT-based proteomics do not reveal novel changes in the VPS35(p.K555E, K556E, K559E)-GFP interactome

The K297X mutation in VPS26A caused not only severe perturbed binding to SNX27, but also intriguingly enhanced PKD2 and DENND4C binding (either directly or indirectly) **(Figure 4.9)**. To examine whether uncoupling the WASH complex from the retromer complex caused any unexpected changes in the VPS35 interactome, I turned to TMT-based proteomics combined with a GFP-trap immunoprecipitation. I compared the interactome of VPS35-GFP with VPS35(p.K555E, K556E, K559E)-GFP. The proteomics confirmed the decrease in association of the WASH complex components FAM21, SWIP and Strumpellin **(Table 5.2)**. The other WASH complex components were also decreased but were not identified in all 3 mass-spectrometry repeats and so were filtered out of the final dataset. The other consistent decreases in the VPS35(p.K555E, K556E, K559E)-GFP interactome are not thought to be true interactors of VPS35 as shown by the VPS35-GFP interactome **(Table 4.1)** or the previous GFP-VPS35 interactome (McGough et al., 2014a). The addition of the K555E, K556E and K559E mutations does not therefore appear to increase the association of VPS35 with other accessory proteins **(Table 5.2)**.

Accession Number	Description	Average Coverage	Average # Peptides	Average # PSMs	Average # Unique Peptides	Average # AAs	Average Abundance Ratio: (TRIP) / (WT)
P62805	Histone H4 OS=Homo sapiens GN=HIST1H4A PE=1 SV=2	51.45631	6	33	6	103	0.1105
A0A0U1RRH7	Histone H2A OS=Homo sapiens GN=HIST1H3D PE=3 SV=1	35.29412	5	10.5	2	170	0.1515
P51991	Heterogeneous nuclear ribonucleoprotein A3 OS=Homo sapiens GN=HNRNPA3 PE=1 SV=2	11.90476	4.5	7.5	3	378	0.225
A8K962	cDNA FLJ77827, highly similar to Human upstream binding factor (hUBF) OS=Homo sapiens PE=2 SV=1	5.693717	4.5	5	4.5	764	0.2395
P05204	Non-histone chromosomal protein HMG-17 OS=Homo sapiens GN=HMGN2 PE=1 SV=3	30	5.333333	4	5	90	0.247889
A0A096LPC5	WASH complex subunit 2C OS=Homo sapiens GN=WASHC2C PE=1 SV=1	3.355705	4	4	4	1341	0.25
A0A024R036	Disabled homolog 2, mitogen-responsive phosphoprotein (Drosophila), isoform CRA_a OS=Homo sapiens GN=DAB2 PE=4 SV=1	7.662338	4.5	5	4.5	770	0.271
A0A087X256	WASH complex subunit 4 OS=Homo sapiens GN=WASHC4 PE=1 SV=1	5.074572	6.5	7	6.5	825.5	0.329
A0A0S2Z4Z6	Serine/arginine repetitive matrix 1 isoform 2 (Fragment) OS=Homo sapiens GN=SRRM1 PE=2 SV=1	2.614379	2	2	2	918	0.332
P78406	mRNA export factor OS=Homo sapiens GN=RAE1 PE=1 SV=1	15.21739	5.5	5.5	5.5	368	0.3325
Q53EL1	Protein KIAA0196 variant (Fragment) OS=Homo sapiens PE=2 SV=1	10.56701	12	12.5	12	1164	0.3455

Table 5.2 Average change in the VPS35(p.K555E, K556E, K559E)-GFP interactome (TRIP) compared to the VPS35-GFP interactome (WT)

AA= amino acid; PSMs= peptide-to-spectrum matches (the total number of identified peptide sequences). Highlighted in yellow are WASH complex components.

5.2.7 The mechanism of VPS35-independent endosomal association of FAM21 is not dependent on VPS34

The interaction between VPS35 and FAM21 has been suggested to be essential for the endosomal recruitment of the WASH complex (Harbour et al., 2012; Jia et al., 2012). This view has been re-examined following the creation of VPS35 knockout HeLa cells, which still have a notable proportion of FAM21 remaining on endosomes **(Figure 5.8A)** (McNally et al., 2017). The retromer-independent mechanism of FAM21 endosomal recruitment is unknown but the WASH complex has been shown to directly interact with liposomes made from purified bovine brain lipids (Derivery et al., 2009). I therefore tested whether endosomal PI3P may be the mediator of retromer-independent FAM21 recruitment.

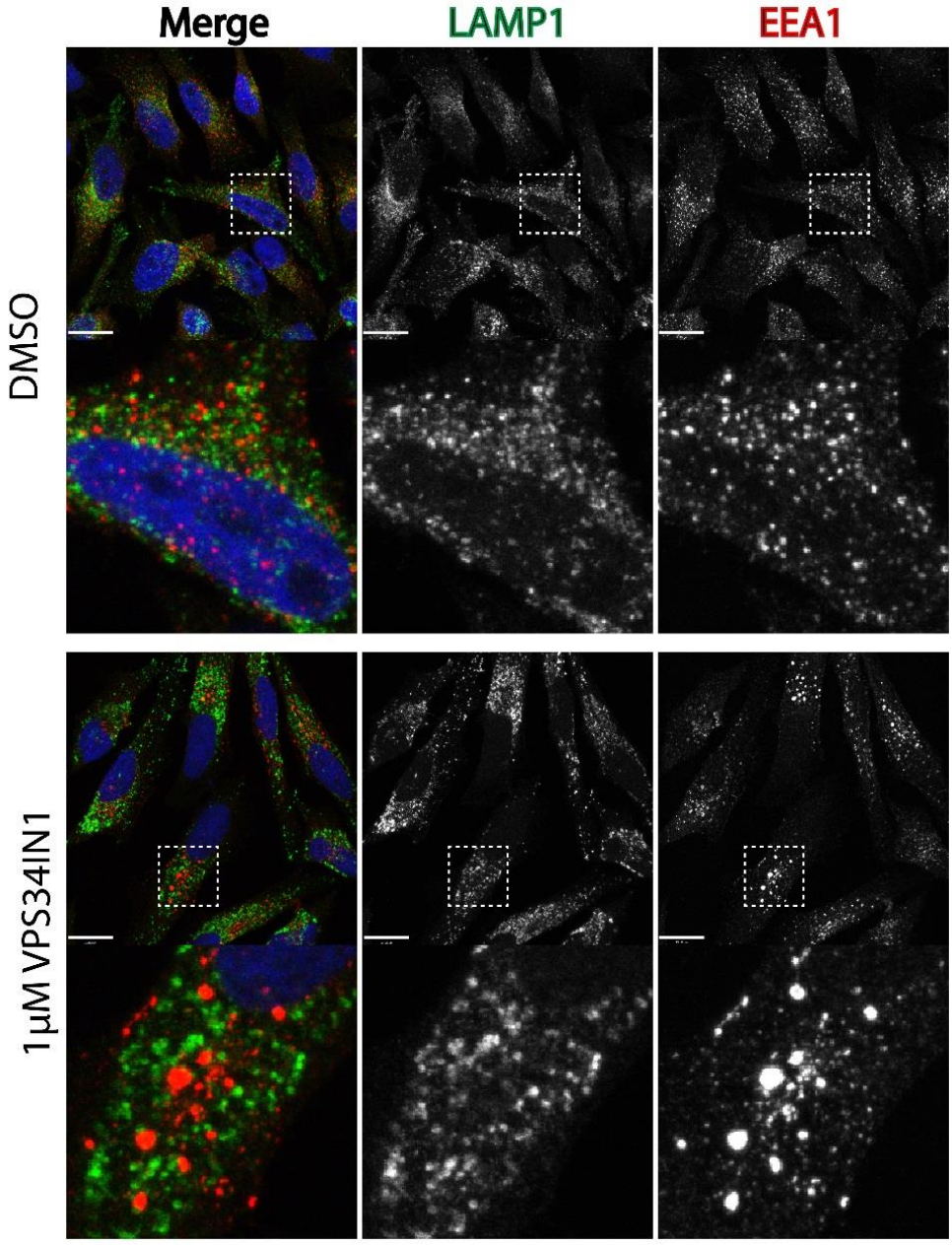

Figure 5.21 VPS34 inhibition causes swelling of the early endosomal compartment.

HeLa cells were treated with DMSO or 1µM VPS34IN1 (a VPS34 inhibitor) for 4 hours prior to 4% paraformaldehyde fixation and immuno-staining with endogenous LAMP1 and EEA1. The scale bars indicate 19 µm.

The synthesis of PI3P via the class III PI3-kinase VPS34 is fundamental in endosomal maturation and the recruitment of endosomal effector proteins (Raiborg et al., 2013; Jean and Kiger, 2014). I therefore utilised a VPS34-specific inhibitor, VPS34-IN1 (Bago et al., 2014). Unlike traditionally-used inhibitors, such as wortmannin, which are promiscuous in the inhibition of PI3-Kinases (Ferby et al., 1996), VPS34-IN1 is a selective and cell permeable VPS34 inhibitor (Bago et al., 2014).

VPS34-IN1 treatment has been shown to prevent the association of a FIVE-domain containing construct onto endosomes (Bago et al., 2014) but its effect on endosomal morphology hasn't been documented. I therefore treated HeLa cells with VPS34-IN1, which caused an enlargement of EEA1-positive endosomes but no striking difference in LAMP1 staining **(Figure 5.21)**. This phenotype is consistent with other studies, which suppressed VPS34 through RNAi (Johnson et al., 2006; Jaber et al., 2016). VPS34-IN1 treatment also decreased the endosomal population of the PI3P-binder SNX1 **(Figure 5.22A)**. The endosomal populations of FAM21 and VPS35 did not decrease; instead they localised around enlarged vesicles **(Figure 5.22A)**. The endosomal population of VPS35 is dependent on the PI3P-binder SNX3, and Rab7 (Rojas et al., 2008; Harterink et al., 2011; Harrison et al., 2014b). Rab7 may therefore be sufficient for the endosomal recruitment of VPS35 and the endosomal population of VPS35 is likely to be sufficient for the endosomal recruitment of FAM21. To determine whether the VPS35-independent mechanism of FAM21's association with endosomes via PI3P, I treated VPS35 knockout HeLa cells with VPS34IN1. SNX1 again largely lost its endosomal population **(Figure 5.22B)**. However, FAM21 retained its association around swollen, enlarged endosomes **(Figure 5.22B)**.

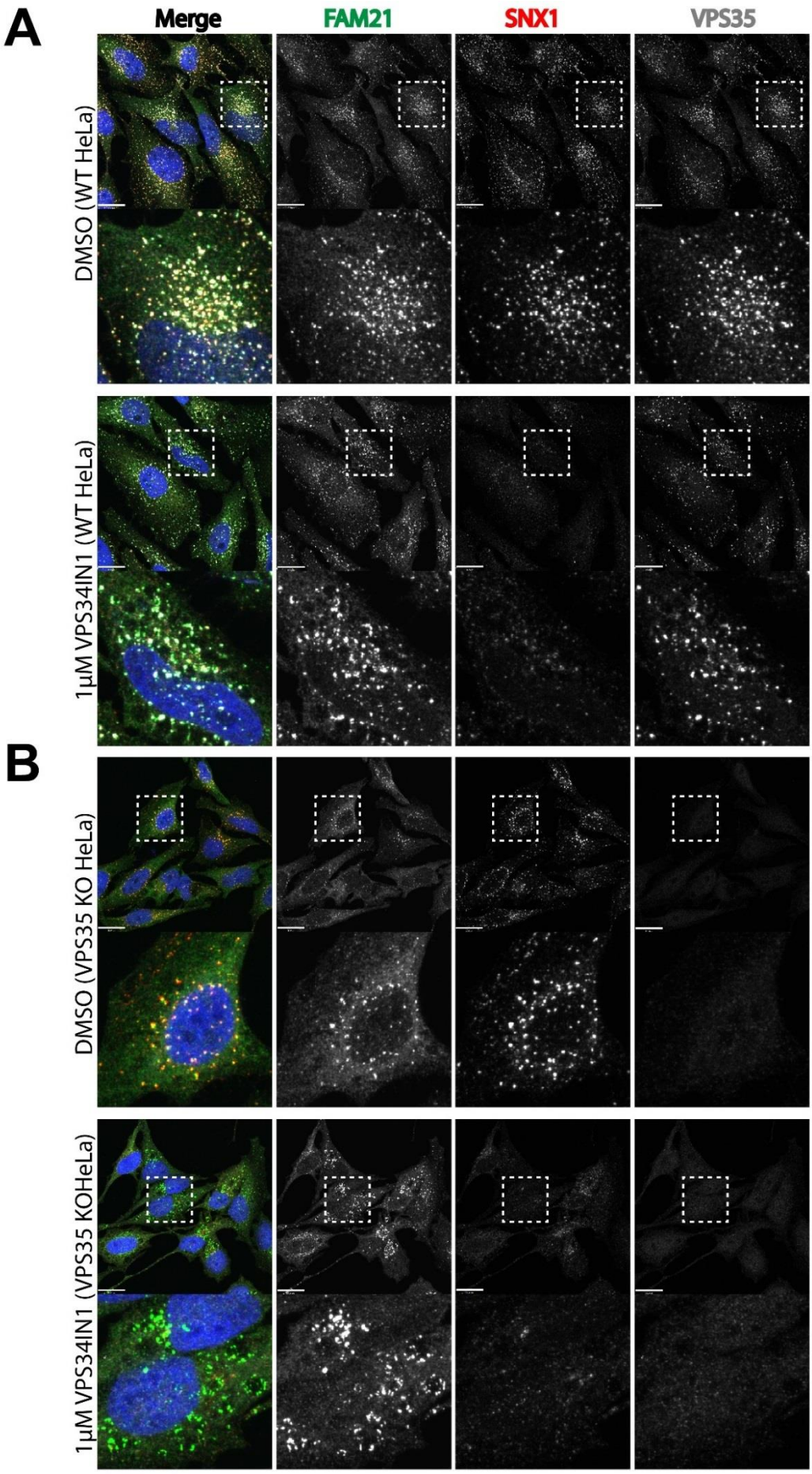
A
Merge
FAM21
SNX1
VPS35
DMSO (WT HeLa)
1μM VPS34IN1 (WT HeLa)
B
DMSO (VPS35 KO HeLa)
1μM VPS34IN1 (VPS35 KOHeLa)

Figure 5.22 VPS34 inhibition causes the dissociation of SNX1 from endosomes but not FAM21.

(A) HeLa cells were treated with DMSO or 1µM VPS34IN1 (a VPS34 inhibitor) for 4 hours prior to 4% paraformaldehyde fixation and immuno-staining with endogenous FAM21, SNX1 and VPS35. **(B)** VPS35 knockout HeLa cells were treated with DMSO or 1µM VPS34IN1 for 4 hours prior to 4% paraformaldehyde fixation and immuno-staining with endogenous FAM21, SNX1 and VPS35. The scale bars indicate 19 µm.

5.3 Discussion

5.3.1 Mechanism of endosomal WASH complex recruitment

VPS35 knockout HeLa cells have a decreased endosomal population of FAM21, but there is still a substantial population on endosomes (McNally et al., 2017). Therefore, contrary to the previous model, there is a retromer-independent mechanism of WASH complex recruitment. Depleting endosomes of PI3P through the inhibition of VPS34 did not displace the remaining FAM21 from endosomes **(Figure 5.22B)**. FAM21 has been shown to be promiscuous in its binding to phospholipids in a PIP-strip assay (Derivery et al., 2009), so it is possible that alternative lipids are mediating its endosomal association. Alternatively, the VPS34 inhibitor, VPS34-IN1, may not have removed a sufficient quantity of endosomal PI3P. This seems unlikely as the endosomal localisation of the PI3P-binding SNX1 was substantially decreased **(Figure 5.22B)**. The retromer-independent endosomal localisation of FAM21 may also be through a different protein:protein interaction. It is known to associate with multiple endosomal proteins, including RME-8 and SNX27, both of which have their own intrinsic membrane-binding properties (Steinberg et al., 2013a; Freeman et al., 2014). Recently, a paper was published which showed that knockdown of Hrs causes a decrease in endosomal association of WASH1 (MacDonald et al., 2018). It will be interesting to see whether a knockdown or knockout of Hrs in the VPS35 knockout HeLa cells displaces the remaining endosomal FAM21. It should be noted that Hrs binds to PI3P via its FYVE domain (Hayakawa et al., 2004) which may indicate that the VPS34-IN1 treatment should have affected the endosomal localisation of Hrs. However, a probe of GFP-4x-FYVE(Hrs) could still localise to endosomes in VPS34 knockout MEFs (Devereaux et al., 2013).

5.3.2 Mechanism of the VPS35:FAM21 association

The C-terminus of VPS35 and its interaction with VPS29 has been shown to be important for the VPS35 interaction with FAM21 (Helfer et al., 2013) through the acidic LFa repeats within the FAM21 tail (Jia et al., 2012). VPS29 binding may stabilise the C-terminus of VPS35 in a specific conformation, which may promote FAM21 association. In this chapter, I have identified several basic residues in VPS35, which I hypothesise interact with the acidic LFa repeats within the FAM21 tail, which are important for the retromer-WASH complex association **(Figures 5.4-5.6)**. Interestingly, a VPS35(p.R524W) Parkinson's disease linked mutation, which maps to the first basic

'area' in VPS35 **(Figure 5.3A)** has been reported to perturb FAM21 association (Follett et al., 2016).

I focused on the potential electrostatic interactions implied by the discovery of the acidic LFa repeats in the FAM21 tail (Jia et al., 2012). However, the hydrophobic leucine and phenylalanine elements of the LFa motifs have not been examined here. I therefore modelled the hydrophobicity of the VPS35 surface from the Hierro et al. (2007) structure **(Figure 5.23)**. This modelling revealed hydrophobic pockets (in red) in close proximity to the basic residues (in green) that I have identified to be important for FAM21 association **(Figure 5.23)**. The extent to which these hydrophobic pockets contribute to forming the VPS35-FAM21 association will need future examination. The definitive way to test the mechanism of binding will be through a structural approach. Expression and purification of the retromer components and the FAM21 tail, coupled to x-ray crystallography. However, the unstructured and flexible nature of the FAM21 tail makes a crystallography approach difficult.

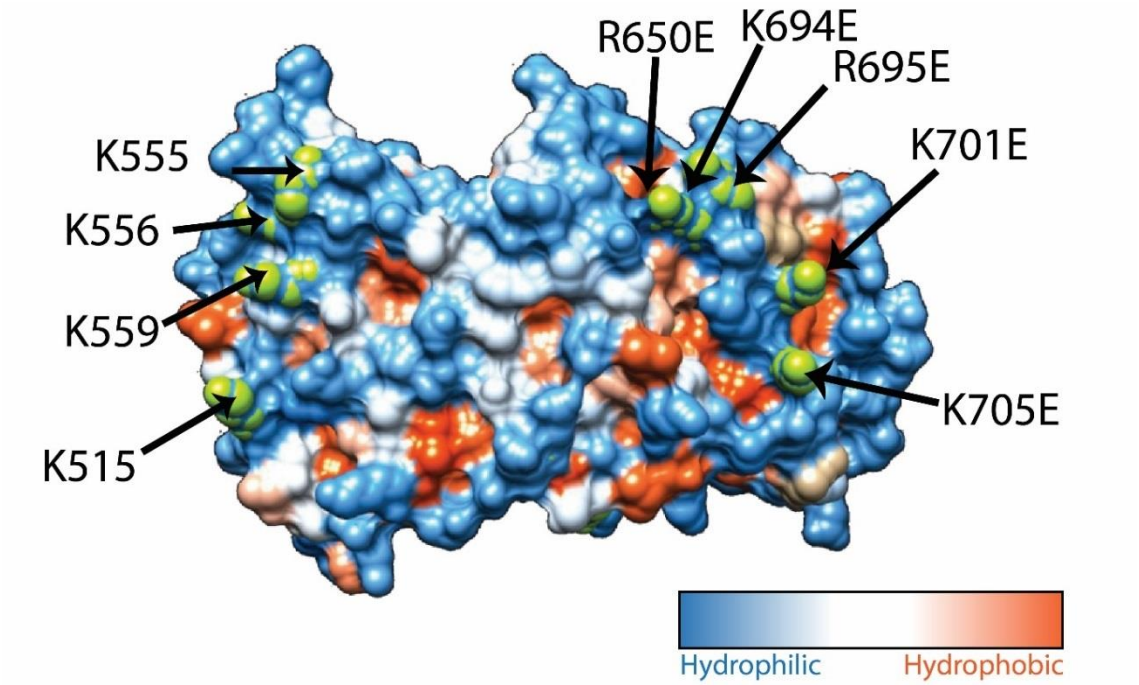

Figure 5.23 Modelling of the hydrophobicity surface of VPS35

Model of the hydrophobicity surface of the C-terminus of VPS35 onto the VPS35 crystal structure bound to VPS29 (Hierro et al., 2007). The basic residues identified to be important for FAM21 association are highlighted in green.

Interestingly, several of the lysine residues in VPS35 found to be important for FAM21 association, including K515, K555 and K701, were recently described to undergo

Parkin-mediated polyubiquitylation (Williams et al., 2018). This polyubiquitination did not promote proteasomal-mediated degradation of the retromer complex or influence its steady-state levels (Williams et al., 2018). The authors suggest that this ubiquitylation of VPS35 may regulate retromer-dependent endosomal sorting. It would be interesting to investigate whether the ubiquitylation of these lysine residues regulates the FAM21-retromer complex interaction. It is tempting to speculate that the addition of the polyubiquitin chains either mask the basic charges required for the electrostatic interaction or causes steric hindrance which prevents the interaction.

Recently, a cryo-electron tomography structure of the *C. thermophilium* pentameric retromer complex was solved (Kovtun et al., 2018). This provided definitive data, at least in yeast, that backed-up past studies suggesting that the trimeric retromer complex dimerises (Hierro et al., 2007; Lucas et al., 2016; Kovtun et al., 2018). In this arch-like dimer, the C-termini of the two VPS35 proteins form a dimerization interface, with VPS29 at the apex and VPS26 closest to the membrane **(Figure 5.24C)** (Kovtun et al., 2018). This dimerization region is in a similar area to the residues I found to be important for FAM21 association. I therefore modelled the cryo-electron tomography structure to highlight the locations of the residues I found to be important for FAM21 association. Firstly, I used bioinformatic software to align the *C. thermophilium VPS35 sequence* to others, including *H. sapiens* VPS35 **(Figure 5.24A)**. This allowed me to determine the *C. thermophilium* equivalent of the *H. sapiens* residues important for FAM21 association **(Figure 5.24B)**. There are some limitations to this analysis. Firstly, fungal retromer exists as a pentameric complex whereas *H. sapiens* retromer has diverged into two more loosely-associated complexes (Kvainickas et al., 2017a; Simonetti et al., 2017; Cullen and Steinberg, 2018). This may limit the comparisons that can be made between this structure and the *H. sapiens* equivalent. Secondly, *C. thermophilium*, like *S. cerevisiae*, does not contain a WASH complex and several of the equivalent *C. thermophilium* residues are not basic in charge. I am therefore making an assumption that the equivalent mammalian residues are broadly located in a similar position.

The residues I found to be most important for FAM21 association face away from the membrane, along the peak of the two retromer homodimers **(Figure 5.24C)**. This supports the notion that the FAM21 tail may straddle the interaction between the two retromers on the side facing away from the membrane. It is difficult to tell whether these residues are involved in retromer dimerization. Future computational or experimental studies may be able to answer this question. However, if the residues I

identified in human cells were critical for retromer complex dimerization, you might expect that they would be conserved to a greater degree between species.

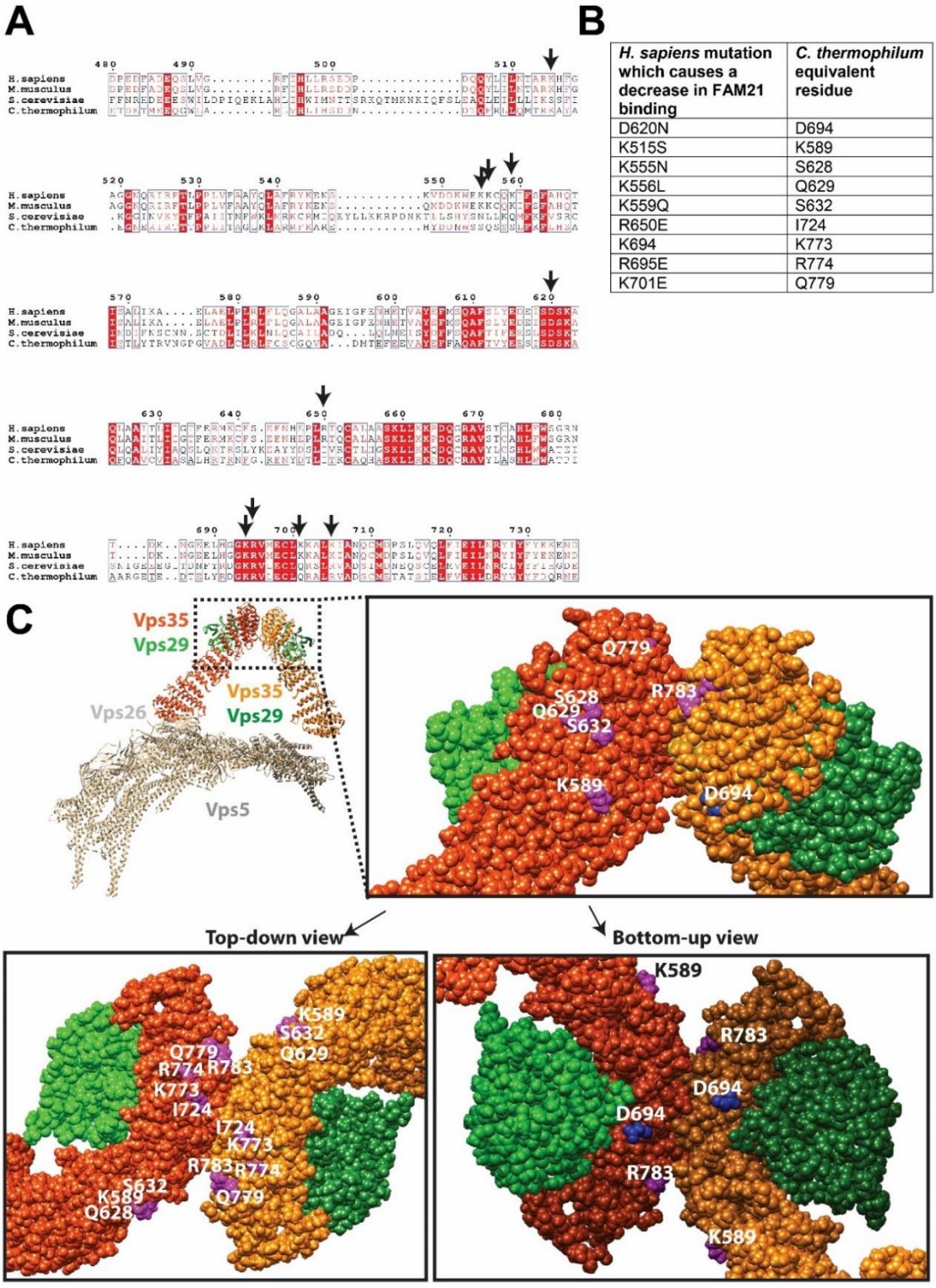

H. sapiens mutation which causes a decrease in FAM21 binding	*C. thermophilum* equivalent residue
D620N	D694
K515S	K589
K555N	S628
K556L	Q629
K559Q	S632
R650E	I724
K694	K773
R695E	R774
K701E	Q779

Figure 5.24 Modelling of the identified residues which affect FAM21 binding onto the retromer dimer interface

(A) Sequences of *H. sapiens*, M. musculus, *S. cerevisiae* and *C. thermophilium* VPS35 homologues were aligned using ESPript 3.0 online software (Robert and Gouet, 2014). The *H.*

sapiens residues which, when mutated, were found to decrease binding to FAM21 are indicated using arrows. **(B)** Table showing the *C. thermophilium* equivalent residues which in *H. sapiens* are important for FAM21 binding. **(C)** Modelling of the *C. thermophilium* retromer complex dimer bound to Vps5 which was solved using Cryo-Electron Tomography (Kovtun et al., 2018). The *C. thermophilium* equivalent residues which in *H. sapiens* are important for FAM21 binding are highlighted in purple and the equivalent D620 residue is highlighted in blue.

The VPS35(p.D620N) mutation causes a 50% decrease in the retromer-WASH complex interaction (McGough et al., 2014b; Zavodszky et al., 2014) **(Figure 5.9)**. This acidic aspartate residue does not fit my electrostatic model of interactions between the basic VPS35 residues and the acid clusters in the FAM21 tail. The *C. thermophilium* equivalent of the highly evolutionary-conserved D620 residue is located in the vicinity of the dimerization surface, facing towards the membrane **(Figure 5.24)**. Kovtun and colleagues speculate that the D620N mutation may perturb retromer dimerization; it is possible that the aspartate to asparagine change causes a conformational change which perturbs retromer dimerization. Again, future computational or experimental studies will need to test this.

My conclusions from the *in silico* modelling of the *C. thermophilium* cryo-electron tomography retromer structure is predicated on several assumptions and has its limitations. To definitively show the importance of the residues involved in the retromer-WASH complex interaction and the residues needed for retromer dimerization, a structural biology approach will be needed. The FAM21 tail is predicted to be flexible and unstructured which makes crystallisation difficult (Jia et al., 2010). The only structure (22 Å) that exists for the WASH complex, solved using electron microscopy, cut off the FAM21 tail (Jia et al., 2010). It is possible that its interaction with the retromer complex may stabilise the structure of the FAM21 tail, making crystallisation more feasible. However, it is likely that cryo-electron microscopy will be the most practical approach to achieving it. It would be especially interesting if a mammalian retromer version of the Kovtun et al. (2018) cryo-electron tomography structure, with the addition of FAM21 (or at least its retromer-binding tail region) was solved. The LFa repeats in the FAM21 tail are thought to enable FAM21 to bind to multiple retromer complexes (Jia et al., 2012). It is an intriguing possibility that a dimer of retromer complexes may be needed for the binding of the FAM21 tail.

5.3.3 Functional significance of the WASH-retromer complexes interaction

Protein:protein interactions are essential for endosomal retrieval and recycling (Cullen and Steinberg, 2018). Mutations in SNX27 that prevent retromer binding cause a

GLUT1 sorting defect (Gallon et al., 2014a). A mutation in VPS26A which prevents assembly with SNX27 cause a GLUT1 sorting defect **(Figure 4.11)**. Mutations in SNX3 which prevents its assembly into the SNX3-retromer causes a Wnt phenotype **(Figure 3.6)** and a defect in DMT1-II trafficking (Lucas et al., 2016). Therefore, I hypothesised that perturbing the retromer-WASH complex association may cause a defect in GLUT1 recycling. However, this was not the case **(Figure 5.13** and **Figure 5.18)**.

It has been reported that in RPE-1 cells, FAM21 suppression causes a GLUT1 trafficking defect where it accumulates in the TGN (and specifically not in LAMP1-postive vesicles) (Lee et al., 2016). It has also been reported that in U2OS cells, FAM21 suppression causes a GLUT1 trafficking defect where it accumulates in LAMP1-positive late endosomes/lysosomes (Kvainickas et al., 2017b). These phenotypes could be replicated (both at the same time) in RPE-1 cells **(Figure 5.15)** but not HeLa cells **(Figure 5.14)**. It is possible that the suppression levels achieved in HeLa cells were not enough to cause a GLUT1 trafficking defect. It is also possible that there are discrepancies between the phenotypes in different cell types. CRISPR-Cas9 mediated knockouts in HeLa cells and RPE-1 cells may provide some clarity on this issue. However, the suppression of FAM21 in HeLa cells causes the TGN-accumulation of β2-Adrenergic receptor, another endosome-to-plasma membrane SNX27-retromer cargo (Varandas et al., 2016). Other cargoes which could be followed up and have been reported to be dependent on the WASH complex include CIMPR (Gomez and Billadeau, 2009), α5 integrin (Zech et al., 2011) and the low-density lipoprotein receptor (Bartuzi et al., 2016).

To investigate whether uncoupling the WASH and retromer complexes cause a GLUT1 phenotype in RPE-1 cells, I overexpressed the VPS35-GFP variants to outcompete endogenous VPS35 for insertion into the retromer complex **(Figure 5.18)**. This overexpression experiment was crude compared to reintroducing the variants into VPS35 knockout cells. Ideally, a knockout VPS35 RPE-1 line would have been created where the VPS35-GFP variants could be expressed at endogenous levels with no endogenous level of VPS35 background.

Although there was no GLUT1 trafficking phenotype when retromer was uncoupled from the WASH complex, this association seems to contribute to the segregation of the retrieval and degradative endosomal subdomains **(Figure 5.19)**. The partial loss of subdomain segregation was also phenocopied by the suppression of FAM21 **(Figure 5.20)**. The data collected for this relies on the accuracy of the overlaps between channels which is limited by the resolution of confocal microscopy; super resolution

microscopy would provide a greater level of resolution. Electron microscopy has confirmed that these enlarged endosomes have only one vacuole and are formed through the fusion of several endosomes (Barbieri et al., 1996), but the extent to which the retrieval and degradative subdomains are maintained following the Rab5(p.Q79L) overexpression is difficult to measure. Nevertheless, an overlap between VPS35 and Hrs of 22.12% ± 1.03% **(Figure 5.20F)** is in agreement with a previous report examining the overlap between *C. elegans* VPS35 and HRS in naturally-large coelomocyte endosomes (Norris et al., 2017).

This is the first experimental evidence that the WASH complex as well as its interaction with retromer is linked to the segregation of endosomal subdomains. The WASH complex has been suggested to contribute to the architecture of the subdomains through its interaction with multiple retrieval complexes, including retromer, retriever (via the CCC complex), SNX27 and the SNX-BAR complex (via RME-8) (Simonetti and Cullen, 2018a). Secondly, it has been proposed to concentrate these retrieval complexes and transmembrane cargo through the creation of branched filamentous actin (Simonetti and Cullen, 2018a). It would be interesting for future studies to knock-in an actin-polymerisation-dead WASH1 mutant through CRISPR-Cas9 to investigate whether actin-polymerisation is required for the maintenance of endosomal subdomain segregation.

Chapter 6

General discussion

In this thesis, I have provided further insight into some of the molecular interactions of retromer and their functional significance. In **Chapter 3**, I defined residues within sorting nexin-3 (SNX3) which are critical for the formation of the SNX3-retromer. Through a collaboration with the Korswagen lab, the formation of SNX3-retromer was shown to be necessary for the formation of Wnt morphogenic gradients. I also established a model of how SNX3-retromer may couple to a membrane deformation complex (the MON2:DOPEY1/2:ATP9A flippase complex) to initiate membrane bending and promote carrier formation. In **Chapter 4**, I presented data showing that the Parkinsonism-associated retromer mutation, VPS26A(p.K297X), exhibits a severe perturbation in its assembly with SNX27. In **Chapter 5**, I identified a series of basic residues on the carboxyl-terminus of VPS35 which are required for the association between retromer and the WASH complex. Uncoupling retromer from the WASH complex, or suppressing the WASH complex subunit FAM21, resulted in an increase in the overlap between the retrieval and degradative endosomal subdomains. In this chapter, I expand upon some of the topics explored in my previous chapters and highlight some future questions I consider to be important for the field to address.

6.1 Cargo recognition by retromer

6.1.1 Retromer cargo adaptors

As discussed in **Section 1.4.3**, retromer can associate with cargo adaptors such as SNX27 and SNX3 to enable it to recognise a wider variety of cargoes. In contrast to the SNX27-retromer, which is required for the cell surface localisation of hundreds of cargoes (Steinberg et al., 2013b), only a handful of validated metazoan SNX3-retromer cargoes have been validated: Wntless (Belenkaya et al., 2008; Franch-Marro et al., 2008; Pan et al., 2008; Yang et al., 2008; Harterink et al., 2011; Zhang et al., 2011), transferrin receptor (Xu et al., 2001; Chen et al., 2013), DMT1-II (Lucas et al., 2016), polycystin-2 (Feng et al., 2017) and the *C. elegans* bone morphogenic protein type I receptor SMA-6 (Gleason et al., 2014). This is likely due to the lack of global proteomic studies investigating the SNX3-retromer. However, as the endosomal association of retromer is diminished upon knockdown or knockout of SNX3, or the uncoupling of SNX3 from retromer (Harterink et al., 2011; Lucas et al., 2016), it is likely that the SNX3-retromer is required for the endosomal sorting of various retromer cargoes. Furthermore, the SNX3 association with retromer causes a conformational change in VPS26 which reveals a binding pocket for cargoes with a Φ-X-[L/M/V] sorting motif (Φ

indicates an aromatic residue; x indicates any amino acid), which is present in several published retromer cargoes (Lucas et al., 2016).

6.1.2 Retromer dimerization and the formation of retromer coats

Recently published cryo-electron tomography data show that the fungal retromer can form dimers (Kovtun et al., 2018). This dimerization has also been previously suggested in the mammalian retromer (Hierro et al., 2007; Lucas et al., 2016). In the Kovtun et al. (2018) model, Vps26 form contacts with the SNX-BAR component Vps5 which is assembled on the membrane; retromers can dimerise via the homodimerization of the carboxyl-terminus of Vps35 **(Figure 5.24)**. As described in **Section 1.4.1**, the situation in yeast and in metazoans are different: metazoan retromer is not thought to form a stable complex with the SNX-BAR complex. However, if an equivalent higher metazoan retromer assembly is formed, how do the retromer cargo adaptors fit into this model?

The SNX27-retromer is assembled through direct contacts between VPS26 and the PDZ-domain of SNX27 (Gallon et al., 2014a) **(Section 4.3.1)**. If modelled into the Kovtun et al. (2018) yeast retromer (including the Vps5 component) coat, the cargo-binding ability of SNX27 is thought to be preserved (Simonetti and Cullen, 2018b). This is consistent with SNX27-retromer cargoes, such as GLUT1 and β2-adrenergic receptor, being dependent on the SNX-BAR complex for their endosomal sorting into tubular carriers (Temkin et al., 2011; Steinberg et al., 2013b), likely facilitated by an interaction between SNX27 and SNX1 (Steinberg et al., 2013b).

For SNX3-retromer, the cargo binding pocket induced by its assembly would be occluded if formed into a higher order assembly with the SNX-BAR complex (Simonetti and Cullen, 2018b). This suggests that SNX3-retromer-dependent cargoes could not be captured in the retromer coat as proposed by the Kovtun et al. (2018) model. This is consistent with the SNX3-retromer-dependent, SNX-BAR complex-independent, endosomal sorting of Wntless from the endosomes to the TGN **(Figure 3.11A)** (Harterink et al., 2011; Zhang et al., 2011). It is also consistent with the lack of Wntless enrichment in tubular carriers and the identified SNX3-postive, clathrin-decorated vesicular carriers (Harterink et al., 2011). In **Chapter 3**, I have proposed a model in which SNX3-retromer couples to a MON2:DOPEY1/2:ATP9A flippase complex which generates initial membrane curvature and may recruit a clathrin coat via the MON2 interaction with GGA adaptors **(Figure 3.18)**.

It is possible that the SNX3-retromer (or SNX27-retromer) may, through their PX domains, be able to assemble into analogous dimeric assemblies (to the Kovtun et al. model) on the endosomal membrane independently of the SNX-BAR complex (Simonetti and Cullen, 2018b). Equally, the SNX-BAR complex may be able to form a cargo-enriched coat without retromer cargo enrichment. The SNX-BAR complex can mediate cargo retrieval and recycling of the cargoes CIMPR and IGF1R independently of retromer (Kvainickas et al., 2017a; Simonetti et al., 2017). Recent experimental findings in the Cullen lab have now defined the structural mechanism for the SNX-BAR complex association with cargoes and identify a binding motif in the cytosolic-facing 'tail' of various cargoes (Boris Simonetti, unpublished).

6.2 Endosomal subdomains

6.2.1 The mechanism of cargo leakage into the degradative pathway following retrieval complex perturbation

In general, disrupting the function of endosomal retrieval complexes, either through knockdowns **(Figure 3.12A)**, knockouts **(Figure 4.24A)** or the perturbation of specific protein:protein interactions such as the formation of the SNX27-retromer **(Figure 4.11)**, results in cargo leakage into the degradative pathway. However, whether cargoes are targeted for degradation and sequestered within intralumenal vesicles is unclear.

In *S. cerevisiae*, the deletion of retrieval complexes has been coupled to the perturbation of ESCRT function (through the deletion of the *S. cerevisiae* equivalent of HRS: vps27; see **Section 1.3.1**). The double deletion strains: *vps27*Δ *snx3*Δ (Strochlic et al., 2008) and vps27Δ vps35Δ strains (Arcones et al., 2016) resulted in cargo (Frt1-GFP and Chs3-GFP respectively) accumulating on the limiting membrane of the vacuole (the yeast equivalent of the lysosome) and to the class E compartment (aberrant endosomes). These data are consistent with a model where deletion of ESCRT in the context of retrieval complex perturbation results in cargo accumulation in the endosomal network and the limiting membrane of lysosomes. This suggests that only the luminal-facing domain of cargoes would be degraded in this context. It will be interesting for future experiments to repeat a deletion analysis of ESCRT-0 in combination with retrieval complexes in a mammalian context.

An interesting experiment from the Fässler lab investigated the SNX17-dependent (See **Section 1.4.6**) retrieval of β1-integrin (Bottcher et al., 2012). The trafficking of a β1-

integrin mutant unable to bind to SNX17 resulted in its progression down the degradative pathway. When all the lysine residues of the β1-integrin tail were mutated into arginine residues (to prevent their ubiquitylation), the recycling of β1-integrin (which was unable to bind to SNX17) was rescued. The SNX17-dependent retrieval of β1-integrin has subsequently been shown to be dependent on the retriever complex **(Section 1.4.6)** (McNally et al., 2017). These data from the Fässler lab are consistent with the idea that without sequence-dependent retrieval or ubiquitylation-mediated inclusion into ILVs, β1-integrin will enter the recycling pathway through a 'bulk flow' mechanism. Whether this is a β1-integrin specific phenomenon requires further investigation.

6.2.2 Coordination of the endosomal retrieval complexes

As discussed in **Section 1.3.2.1**, the main retrieval complexes on endosomes are thought to be retromer, retriever, the CCC complex and the SNX-BAR complex. These are all thought to function on the same endosomal retrieval subdomains (McNally et al., 2017). Are the differential cargoes recognised by these complexes enriched in the same tubulovesicular carriers? The role of the WASH complex and actin polymerisation seems to be key in this discussion. All endosomal retrieval complexes so far directly or indirectly bind to the WASH complex (McNally and Cullen, 2018). Furthermore, the addition of an actin binding domain has been shown to be sufficient to promote cargo recycling (Puthenveedu et al., 2010; MacDonald et al., 2018). It is possible that the retrieval complexes link cargoes to the endosomal retrieval subdomain, where cargoes are corralled by branched actin filaments promoted by the WASH complex (Simonetti and Cullen, 2018a), until their recycling. This is a simplified view and it is possible that there are subtle differences in the localisation of these proteins: for example, the SNX3-retromer is thought to act in an earlier endosomal compartment compared to the SNX-BAR complex (Burd and Cullen, 2014b). Also, there are some cargoes, such as Wntless, which do not get enriched into tubular carriers (Harterink et al., 2011). The WASH complex also seems to contribute to the segregation of the endosomal retrieval and degradative subdomains **(Figure 5.19** and **Figure 5.20)**. The mechanism for this, as well as other phenotypes exhibited to the perturbation of the WASH complex, may lie in its promotion of branched-actin polymerisation, though more work is required to show this. The WASH complex is a heteropentameric assembly and there are hints in the literature, especially in the case of FAM21, which suggests that they may have

functions independent of the promotion of branched actin polymerisation (Lee et al., 2016; Shin et al., 2017). This will be an interesting avenue for future studies to explore.

Future work will be required to reconcile the cooperative and independent functions of endosomal retrieval and recycling complexes. For example, there are retromer cargoes (SNX27-retromer cargoes) which require the SNX-BAR complex for their recycling, but as discussed in **Section 6.1.2**, there are retromer cargoes which are independent of the SNX-BAR complex, and SNX-BAR complex cargoes independent of retromer. Furthermore, the retriever cargo β1-integrin has a mild trafficking defect in retromer knockouts (likely due to the decreased endosomal association of the WASH complex) and proteomic studies have identified cargoes which are lost from the cell surface dependent on both retromer and retriever (McNally et al., 2017). Potential cross-talk between retromer and retriever may be due to their cargo adaptors SNX27 and SNX17 (respectively) both containing FERM domains and therefore may potentially recognise some similar cargoes. Establishing the coordination of the different retrieval and recycling complexes is a fundamental question in the years to come.

6.3 Neuroprotection by retromer

6.3.1 Retromer promotes microglial health

Although much study has been focused on retromer's role in neuronal cells, there is increasing evidence that retromer activity may be essential for functional microglia. Overactivation of the microglial inflammatory response is thought to be a hallmark of neurodegenerative disorders (Hickman et al., 2018). As is the case in neuronal samples of patients with Alzheimer's disease (Small et al., 2005), VPS35 is downregulated in their microglial cells as well (Lucin et al., 2013). This decrease in retromer levels is thought to result in decreased phagocytic activity due to reduced surface localisation of microglial phagocytic receptors (Lucin et al., 2013). Retromer depletion is also thought to increase the inflammatory response mediated by microglial cells through the endosome to cell surface sorting of Trem2 (triggering receptor expressed on myeloid cells 2), an innate immune receptor which downregulates microglial activation (Yin et al., 2016). A recent paper used a mouse model which could conditionally deplete VPS35 in microglia (Appel et al., 2018). This resulted in an increase in hippocampal neural progenitor proliferation but a decrease in neuronal differentiation, suggesting a role for microglial VPS35 in promoting neurogenesis (Appel et al., 2018). This is interesting especially considering retromer's role in Wnt

signalling **(Section 6.3.2)**. These mice also displayed memory deficits and a depressive phenotype (Appel et al., 2018); all these phenotypes are consistent with Alzheimer's disease pathogenesis.

6.3.2 Neurodegeneration and aberrant Wnt signalling

As described in **Section 3.1**, Wnt signalling is a master controller of not just various developmental processes, but for adult tissue homeostasis too. In the nervous system, this includes axon pathfinding, dendritic development and assembly of the synapse (Salinas, 2012) as well as adult neurogenesis (Bengoa-Vergniory and Kypta, 2015). In Alzheimer's and Parkinson's disease, numerous studies have described the downregulation of the Wnt signalling pathway in their pathogenesis (Libro et al., 2016).

It is intriguing that both abnormal retromer function and aberrant Wnt signalling have both been linked to neurodegenerative disorders. Retromer has been connected to Wnt signalling via three different routes: Wnt secretion through the trafficking of the Wnt chaperone Wntless (SNX3-retromer) **(Section 3.1)**, modulating the surface localisation and activity of the Wnt-activated polycystin channel complex (SNX3-retromer) (Feng et al., 2017), and in modulating the surface localisation and function of receptors of the planar cell polarity non-canonical Wnt pathway (SNX27-retromer) (Cullen and Strutt labs, unpublished). The trafficking of Wntless is the best characterised link that retromer has to Wnt signalling and it is interesting to note that mice with conditional (homozygous nulls are embryonic lethal) Wntless knockouts display severe abnormalities of the midbrain and hindbrain (Carpenter et al., 2010). It would be interesting for future studies to investigate the Parkinson's disease-causing retromer mutation, VPS35(p.D620N), in the context of aberrant Wnt secretion or downstream signalling. As the protein levels of retromer components are thought to be decreased in Alzheimer's and Parkinson's disease, it would also be interesting to investigate Wnt signalling in the context of VPS35 heterozygous nulls as well.

Chapter 7

References

Ando, M., Funayama, M., Li, Y., Kashihara, K., Murakami, Y., Ishizu, N., Toyoda, C., Noguchi, K., Hashimoto, T., Nakano, N.*, et al.* (2012). VPS35 mutation in Japanese patients with typical Parkinson's disease. Movement disorders : official journal of the Movement Disorder Society *27*, 1413-1417.

Ansari, I.U.H., Longacre, M.J., Paulusma, C.C., Stoker, S.W., Kendrick, M.A., and MacDonald, M.J. (2015). Characterization of P4 ATPase Phospholipid Translocases (Flippases) in Human and Rat Pancreatic Beta Cells THEIR GENE SILENCING INHIBITS INSULIN SECRETION. Journal of Biological Chemistry *290*, 23110-23123.

Antonny, B., Burd, C., De Camilli, P., Chen, E., Daumke, O., Faelber, K., Ford, M., Frolov, V.A., Frost, A., Hinshaw, J.E.*, et al.* (2016). Membrane fission by dynamin: what we know and what we need to know. The EMBO journal *35*, 2270-2284.

Appel, J.R., Ye, S., Tang, F., Sun, D., Zhang, H., Mei, L., and Xiong, W.C. (2018). Increased Microglial Activity, Impaired Adult Hippocampal Neurogenesis, and Depressive-like Behavior in Microglial VPS35-Depleted Mice. The Journal of neuroscience : the official journal of the Society for Neuroscience *38*, 5949-5968.

Arcones, I., Sacristan, C., and Roncero, C. (2016). Maintaining protein homeostasis: early and late endosomal dual recycling for the maintenance of intracellular pools of the plasma membrane protein Chs3. Mol Biol Cell *27*, 4021-4032.

Avaro, S., Belgareh-Touze, N., Sibella-Arguelles, C., Volland, C., and Haguenauer-Tsapis, R. (2002). Mutants defective in secretory/vacuolar pathways in the EUROFAN collection of yeast disruptants. Yeast *19*, 351-371.

Babst, M., Wendland, B., Estepa, E.J., and Emr, S.D. (1998). The Vps4p AAA ATPase regulates membrane association of a Vps protein complex required for normal endosome function. The EMBO journal *17*, 2982-2993.

Bache, K.G., Raiborg, C., Mehlum, A., and Stenmark, H. (2003). STAM and Hrs are subunits of a multivalent ubiquitin-binding complex on early endosomes. J Biol Chem *278*, 12513-12521.

Bago, R., Malik, N., Munson, M.J., Prescott, A.R., Davies, P., Sommer, E., Shpiro, N., Ward, R., Cross, D., Ganley, I.G.*, et al.* (2014). Characterization of VPS34-IN1, a selective inhibitor of Vps34, reveals that the phosphatidylinositol 3-phosphate-binding

SGK3 protein kinase is a downstream target of class Ill phosphoinositide 3-kinase. Biochem J *463*, 413-427.

Balana, B., Maslennikov, I., Kwiatkowski, W., Stern, K.M., Bahima, L., Choe, S., and Slesinger, P.A. (2011). Mechanism underlying selective regulation of G protein-gated inwardly rectifying potassium channels by the psychostimulant-sensitive sorting nexin 27. Proc Natl Acad Sci U S A *108*, 5831-5836.

Balderhaar, H.J., Lachmann, J., Yavavli, E., Brocker, C., Lurick, A., and Ungermann, C. (2013). The CORVET complex promotes tethering and fusion of Rab5/Vps21-positive membranes. Proc Natl Acad Sci U S A *110*, 3823-3828.

Balderhaar, H.J.K., Arlt, H., Ostrowicz, C., Brocker, C., Sundermann, F., Brandt, R., Babst, M., and Ungermann, C. (2010). The Rab GTPase Ypt7 is linked to retromer-mediated receptor recycling and fusion at the yeast late endosome. Journal of Cell Science *123*, 4085-4094.

Bandres-Ciga, S., Mencacci, N.E., Duran, R., Barrero, F.J., Escamilla-Sevilla, F., Morgan, S., Hehir, J., Vives, F., Hardy, J., and Pittman, A.M. (2016). Analysis of the genetic variability in Parkinson's disease from Southern Spain. Neurobiol Aging *37*, 210 e211-210 e215.

Bankaitis, V.A., Johnson, L.M., and Emr, S.D. (1986). Isolation of yeast mutants defective in protein targeting to the vacuole. Proc Natl Acad Sci U S A *83*, 9075-9079.

Banziger, C., Soldini, D., Schutt, C., Zipperlen, P., Hausmann, G., and Basler, K. (2006). Wntless, a conserved membrane protein dedicated to the secretion of Wnt proteins from signaling cells. Cell *125*, 509-522.

Barbieri, M.A., Li, G., Mayorga, L.S., and Stahl, P.D. (1996). Characterization of Rab5:Q79L-stimulated endosome fusion. Arch Biochem Biophys *326*, 64-72.

Barbosa, S., Pratte, D., Schwarz, H., Pipkorn, R., and Singer-Kruger, B. (2010). Oligomeric Dop1p is Part of the Endosomal Neo1p-Ysl2p-Arl1p Membrane Remodeling Complex. Traffic *11*, 1092-1106.

Baron, R., and Kneissel, M. (2013). WNT signaling in bone homeostasis and disease: from human mutations to treatments. Nature medicine *19*, 179-192.

Barr, F.A. (2013). Review series: Rab GTPases and membrane identity: causal or inconsequential? The Journal of cell biology *202*, 191-199.

Bartscherer, K., Pelte, N., Ingelfinger, D., and Boutros, M. (2006). Secretion of Wnt Ligands requires Evi, a conserved transmembrane protein. Cell *125*, 523-533.

Bartuzi, P., Billadeau, D.D., Favier, R., Rong, S., Dekker, D., Fedoseienko, A., Fieten, H., Wijers, M., Levels, J.H., Huijkman, N.*, et al.* (2016). CCC- and WASH-mediated endosomal sorting of LDLR is required for normal clearance of circulating LDL. Nature communications *7*, 10961.

Beer, K.B., Rivas-Castillo, J., Kuhn, K., Fazeli, G., Karmann, B., Nance, J.F., Stigloher, C., and Wehman, A.M. (2018). Extracellular vesicle budding is inhibited by redundant regulators of TAT-5 flippase localization and phospholipid asymmetry. Proceedings of the National Academy of Sciences of the United States of America *115*, E1127-E1136.

Behnia, R., and Munro, S. (2005). Organelle identity and the signposts for membrane traffic. Nature *438*, 597-604.

Belenkaya, T.Y., Wu, Y.H., Tang, X.F., Zhou, B., Cheng, L.Q., Sharma, Y.V., Yan, D., Selva, E.M., and Lin, X.H. (2008). The retromer complex influences Wnt secretion by recycling Wntless from endosomes to the trans-Golgi network. Developmental Cell *14*, 120-131.

Bell, R.M., Ballas, L.M., and Coleman, R.A. (1981). Lipid topogenesis. J Lipid Res *22*, 391-403.

Bengoa-Vergniory, N., and Kypta, R.M. (2015). Canonical and noncanonical Wnt signaling in neural stem/progenitor cells. Cellular and molecular life sciences : CMLS *72*, 4157-4172.

Bentley, S.R., Bortnick, S., Guella, I., Fowdar, J.Y., Silburn, P.A., Wood, S.A., Farrer, M.J., and Mellick, G.D. (2018). Pipeline to gene discovery - Analysing familial Parkinsonism in the Queensland Parkinson's Project. Parkinsonism & related disorders *49*, 34-41.

Bettencourt, C., Morris, H.R., Singleton, A.B., Hardy, J., and Houlden, H. (2013). Exome sequencing expands the mutational spectrum of SPG8 in a family with spasticity responsive to L-DOPA treatment. J Neurol *260*, 2414-2416.

Bhalla, A., Vetanovetz, C.P., Morel, E., Chamoun, Z., Di Paolo, G., and Small, S.A. (2012). The location and trafficking routes of the neuronal retromer and its role in amyloid precursor protein transport. Neurobiology of disease *47*, 126-134.

Bhatia, V.K., Madsen, K.L., Bolinger, P.Y., Kunding, A., Hedegard, P., Gether, U., and Stamou, D. (2009). Amphipathic motifs in BAR domains are essential for membrane curvature sensing. The EMBO journal *28*, 3303-3314.

Bi, F., Li, F., Huang, C., and Zhou, H. (2013). Pathogenic mutation in VPS35 impairs its protection against MPP(+) cytotoxicity. International journal of biological sciences *9*, 149-155.

Bishop, N., Horman, A., and Woodman, P. (2002). Mammalian class E vps proteins recognize ubiquitin and act in the removal of endosomal protein-ubiquitin conjugates. The Journal of cell biology *157*, 91-101.

Bishop, N., and Woodman, P. (2000). ATPase-defective mammalian VPS4 localizes to aberrant endosomes and impairs cholesterol trafficking. Mol Biol Cell *11*, 227-239.

Bitsikas, V., Correa, I.R., Jr., and Nichols, B.J. (2014). Clathrin-independent pathways do not contribute significantly to endocytic flux. Elife *3*, e03970.

Blom, T., Somerharju, P., and Ikonen, E. (2011). Synthesis and biosynthetic trafficking of membrane lipids. Cold Spring Harb Perspect Biol *3*, a004713.

Blumental-Perry, A., Haney, C.J., Weixel, K.M., Watkins, S.C., Weisz, O.A., and Aridor, M. (2006). Phosphatidylinositol 4-phosphate formation at ER exit sites regulates ER export. Dev Cell *11*, 671-682.

Bodnar, A.G., Ouellette, M., Frolkis, M., Holt, S.E., Chiu, C.P., Morin, G.B., Harley, C.B., Shay, J.W., Lichtsteiner, S., and Wright, W.E. (1998). Extension of life-span by introduction of telomerase into normal human cells. Science *279*, 349-352.

Bonangelino, C.J., Chavez, E.M., and Bonifacino, J.S. (2002). Genomic screen for vacuolar protein sorting genes in Saccharomyces cerevisiae. Mol Biol Cell *13*, 2486-2501.

Bottcher, R.T., Stremmel, C., Meves, A., Meyer, H., Widmaier, M., Tseng, H.Y., and Fassler, R. (2012). Sorting nexin 17 prevents lysosomal degradation of beta1 integrins by binding to the beta1-integrin tail. Nat Cell Biol *14*, 584-592.

Boucrot, E., Ferreira, A.P., Almeida-Souza, L., Debard, S., Vallis, Y., Howard, G., Bertot, L., Sauvonnet, N., and McMahon, H.T. (2015). Endophilin marks and controls a clathrin-independent endocytic pathway. Nature *517*, 460-465.

Bright, N.A., Davis, L.J., and Luzio, J.P. (2016). Endolysosomes Are the Principal Intracellular Sites of Acid Hydrolase Activity. Current biology : CB *26*, 2233-2245.

Bugarcic, A., Zhe, Y., Kerr, M.C., Griffin, J., Collins, B.M., and Teasdale, R.D. (2011). Vps26A and Vps26B subunits define distinct retromer complexes. Traffic *12*, 1759-1773.

Burd, C., and Cullen, P.J. (2014a). Retromer: A Master Conductor of Endosome Sorting. Cold Spring Harbor Perspectives in Biology *6*.

Burd, C., and Cullen, P.J. (2014b). Retromer: a master conductor of endosome sorting. Cold Spring Harb Perspect Biol *6*.

Burstein, E., Hoberg, J.E., Wilkinson, A.S., Rumble, J.M., Csomos, R.A., Komarck, C.M., Maine, G.N., Wilkinson, J.C., Mayo, M.W., and Duckett, C.S. (2005). COMMD proteins, a novel family of structural and functional homologs of MURR1. J Biol Chem *280*, 22222-22232.

Cai, L., Loo, L.S., Atlashkin, V., Hanson, B.J., and Hong, W. (2011). Deficiency of sorting nexin 27 (SNX27) leads to growth retardation and elevated levels of N-methyl-D-aspartate receptor 2C (NR2C). Mol Cell Biol *31*, 1734-1747.

Campa, C.C., Margaria, J.P., Derle, A., Del Giudice, M., De Santis, M.C., Gozzelino, L., Copperi, F., Bosia, C., and Hirsch, E. (2018). Rab11 activity and PtdIns(3)P turnover removes recycling cargo from endosomes. Nature chemical biology *14*, 801-810.

Campelo, F., and Malhotra, V. (2012). Membrane fission: the biogenesis of transport carriers. Annu Rev Biochem *81*, 407-427.

Carlton, J., Bujny, M., Peter, B.J., Oorschot, V.M.J., Rutherford, A., Mellor, H., Klumperman, J., McMahon, H.T., and Cullen, P.J. (2004). Sorting nexin-1 mediates tubular endosome-to-TGN transport through coincidence sensing of high-curvature membranes and 3-phosphoinositides. Current Biology *14*, 1791-1800.

Carpenter, A.C., Rao, S., Wells, J.M., Campbell, K., and Lang, R.A. (2010). Generation of mice with a conditional null allele for Wntless. Genesis *48*, 554-558.

Cataldi, S., Follett, J., Fox, J.D., Tatarnikov, I., Kadgien, C., Gustavsson, E.K., Khinda, J., Milnerwood, A.J., and Farrer, M.J. (2018). Altered dopamine release and monoamine transporters in Vps35 p.D620N knock-in mice. NPJ Parkinsons Dis *4*, 27.

Chan, A.S., Clairfeuille, T., Landao-Bassonga, E., Kinna, G., Ng, P.Y., Loo, L.S., Cheng, T.S., Zheng, M., Hong, W., Teasdale, R.D.*, et al.* (2016). Sorting nexin 27 couples PTHR trafficking to retromer for signal regulation in osteoblasts during bone growth. Mol Biol Cell *27*, 1367-1382.

Chau, B.N., Cheng, E.H., Kerr, D.A., and Hardwick, J.M. (2000). Aven, a novel inhibitor of caspase activation, binds Bcl-xL and Apaf-1. Mol Cell *6*, 31-40.

Chen, C.Y., Garcia-Santos, D., Ishikawa, Y., Seguin, A., Li, L.T., Fegan, K.H., Hildick-Smith, G.J., Shah, D.I., Cooney, J.D., Chen, W.*, et al.* (2013). Snx3 Regulates Recycling of the Transferrin Receptor and Iron Assimilation. Cell Metabolism *17*, 343-352.

Chen, S., Wang, J., Muthusamy, B.P., Liu, K., Zare, S., Andersen, R.J., and Graham, T.R. (2006). Roles for the Drs2p-Cdc50p complex in protein transport and phosphatidylserine asymmetry of the yeast plasma membrane. Traffic *7*, 1503-1517.

Chen, Y.F., Chang, Y.Y., Lan, M.Y., Chen, P.L., and Lin, C.H. (2017). Identification of VPS35 p.D620N mutation-related Parkinson's disease in a Taiwanese family with successful bilateral subthalamic nucleus deep brain stimulation: a case report and literature review. BMC Neurol *17*, 191.

Chiaruttini, N., and Roux, A. (2017). Dynamic and elastic shape transitions in curved ESCRT-III filaments. Current opinion in cell biology *47*, 126-135.

Chu, J., and Pratico, D. (2017). The retromer complex system in a transgenic mouse model of AD: influence of age. Neurobiol Aging *52*, 32-38.

Clairfeuille, T., Mas, C., Chan, A.S., Yang, Z., Tello-Lafoz, M., Chandra, M., Widagdo, J., Kerr, M.C., Paul, B., Merida, I.*, et al.* (2016). A molecular code for endosomal recycling of phosphorylated cargos by the SNX27-retromer complex. Nat Struct Mol Biol *23*, 921-932.

Coleman, J.A., Kwok, M.C., and Molday, R.S. (2009). Localization, purification, and functional reconstitution of the P4-ATPase Atp8a2, a phosphatidylserine flippase in photoreceptor disc membranes. J Biol Chem *284*, 32670-32679.

Coleman, J.A., Vestergaard, A.L., Molday, R.S., Vilsen, B., and Andersen, J.P. (2012). Critical role of a transmembrane lysine in aminophospholipid transport by mammalian photoreceptor P4-ATPase ATP8A2. Proc Natl Acad Sci U S A *109*, 1449-1454.

Collawn, J.F., Stangel, M., Kuhn, L.A., Esekogwu, V., Jing, S.Q., Trowbridge, I.S., and Tainer, J.A. (1990). Transferrin receptor internalization sequence YXRF implicates a tight turn as the structural recognition motif for endocytosis. Cell *63*, 1061-1072.

Collins, B.M., Norwood, S.J., Kerr, M.C., Mahony, D., Seaman, M.N., Teasdale, R.D., and Owen, D.J. (2008). Structure of Vps26B and mapping of its interaction with the retromer protein complex. Traffic *9*, 366-379.

Collins, B.M., Skinner, C.F., Watson, P.J., Seaman, M.N., and Owen, D.J. (2005). Vps29 has a phosphoesterase fold that acts as a protein interaction scaffold for retromer assembly. Nat Struct Mol Biol *12*, 594-602.

Costes, S.V., Daelemans, D., Cho, E.H., Dobbin, Z., Pavlakis, G., and Lockett, S. (2004). Automatic and quantitative measurement of protein-protein colocalization in live cells. Biophys J *86*, 3993-4003.

Coudreuse, D.Y., Roel, G., Betist, M.C., Destree, O., and Korswagen, H.C. (2006). Wnt gradient formation requires retromer function in Wnt-producing cells. Science *312*, 921-924.

Cozier, G.E., Carlton, J., McGregor, A.H., Gleeson, P.A., Teasdale, B.D., Mellor, H., and Cullen, P.J. (2002). The Phox Homology (PX) domain-dependent, 3-phosphoinositide-mediated association of sorting nexin-1 with an early sorting endosomal compartment is required for its ability to regulate epidermal growth factor receptor degradation. Journal of Biological Chemistry *277*, 48730-48736.

Cui, T.Z., Peterson, T.A., and Burd, C.G. (2017). A CDC25 family protein phosphatase gates cargo recognition by the Vps26 retromer subunit. Elife *6*.

Cullen, P.J. (2008). Endosomal sorting and signalling: an emerging role for sorting nexins. Nat Rev Mol Cell Biol *9*, 574-582.

Cullen, P.J. (2011). Phosphoinositides and the regulation of tubular-based endosomal sorting. Biochemical Society transactions *39*, 839-850.

Cullen, P.J., and Korswagen, H.C. (2012). Sorting nexins provide diversity for retromer-dependent trafficking events. Nature Cell Biology *14*, 29-37.

Cullen, P.J., and Steinberg, F. (2018). To degrade or not to degrade: mechanisms and significance of endocytic recycling. Nat Rev Mol Cell Biol.

Dai, J., Li, J., Bos, E., Porcionatto, M., Premont, R.T., Bourgoin, S., Peters, P.J., and Hsu, V.W. (2004). ACAP1 promotes endocytic recycling by recognizing recycling sorting signals. Dev Cell *7*, 771-776.

Dalton, L.E., Bean, B.D.M., Davey, M., and Conibear, E. (2017). Quantitative high-content imaging identifies novel regulators of Neo1 trafficking at endosomes. Molecular Biology of the Cell *28*, 1539-1550.

Damseh, N., Danson, C.M., Al-Ashhab, M., Abu-Libdeh, B., Gallon, M., Sharma, K., Yaacov, B., Coulthard, E., Caldwell, M.A., Edvardson, S.*, et al.* (2015). A defect in the retromer accessory protein, SNX27, manifests by infantile myoclonic epilepsy and neurodegeneration. Neurogenetics *16*, 215-221.

de Bot, S.T., Vermeer, S., Buijsman, W., Heister, A., Voorendt, M., Verrips, A., Scheffer, H., Kremer, H.P., van de Warrenburg, B.P., and Kamsteeg, E.J. (2013). Pure adult-onset spastic paraplegia caused by a novel mutation in the KIAA0196 (SPG8) gene. J Neurol *260*, 1765-1769.

Demaison, C., Parsley, K., Brouns, G., Scherr, M., Battmer, K., Kinnon, C., Grez, M., and Thrasher, A.J. (2002). High-level transduction and gene expression in hematopoietic repopulating cells using a human immunodeficiency [correction of imunodeficiency] virus type 1-based lentiviral vector containing an internal spleen focus forming virus promoter. Hum Gene Ther *13*, 803-813.

Deng, Y., Rivera-Molina, F.E., Toomre, D.K., and Burd, C.G. (2016). Sphingomyelin is sorted at the trans Golgi network into a distinct class of secretory vesicle. Proc Natl Acad Sci U S A *113*, 6677-6682.

Derivery, E., Helfer, E., Henriot, V., and Gautreau, A. (2012). Actin polymerization controls the organization of WASH domains at the surface of endosomes. PloS one *7*, e39774.

Derivery, E., Sousa, C., Gautier, J.J., Lombard, B., Loew, D., and Gautreau, A. (2009). The Arp2/3 Activator WASH Controls the Fission of Endosomes through a Large Multiprotein Complex. Developmental Cell *17*, 712-723.

Devereaux, K., Dall'Armi, C., Alcazar-Roman, A., Ogasawara, Y., Zhou, X., Wang, F., Yamamoto, A., De Camilli, P., and Di Paolo, G. (2013). Regulation of mammalian autophagy by class II and III PI 3-kinases through PI3P synthesis. PloS one *8*, e76405.

Dhungel, N., Eleuteri, S., Li, L.B., Kramer, N.J., Chartron, J.W., Spencer, B., Kosberg, K., Fields, J.A., Stafa, K., Adame, A.*, et al.* (2015). Parkinson's Disease Genes VPS35 and EIF4G1 Interact Genetically and Converge on alpha-Synuclein. Neuron *85*, 76-87.

Dickson, D.W. (2012). Parkinson's disease and parkinsonism: neuropathology. Cold Spring Harb Perspect Med *2*.

Ding, L., Han, L., Dube, J., and Billadeau, D.D. (2018). WASH Regulates Glucose Homeostasis by Facilitating Glut2 Receptor Recycling in Pancreatic Beta Cells. Diabetes.

Dirac-Svejstrup, A.B., Sumizawa, T., and Pfeffer, S.R. (1997). Identification of a GDI displacement factor that releases endosomal Rab GTPases from Rab-GDI. The EMBO journal *16*, 465-472.

Dislich, B., Than, M.E., and Lichtenthaler, S.F. (2011). Specific amino acids in the BAR domain allow homodimerization and prevent heterodimerization of sorting nexin 33. Biochem J *433*, 75-83.

Dong, X.P., Shen, D., Wang, X., Dawson, T., Li, X., Zhang, Q., Cheng, X., Zhang, Y., Weisman, L.S., Delling, M.*, et al.* (2010). PI(3,5)P(2) controls membrane trafficking by direct activation of mucolipin Ca(2+) release channels in the endolysosome. Nature communications *1*, 38.

Dores, M.R., Chen, B., Lin, H., Soh, U.J., Paing, M.M., Montagne, W.A., Meerloo, T., and Trejo, J. (2012). ALIX binds a YPX(3)L motif of the GPCR PAR1 and mediates ubiquitin-independent ESCRT-III/MVB sorting. The Journal of cell biology *197*, 407-419.

Dores, M.R., Grimsey, N.J., Mendez, F., and Trejo, J. (2016). ALIX Regulates the Ubiquitin-Independent Lysosomal Sorting of the P2Y1 Purinergic Receptor via a YPX3L Motif. PloS one *11*, e0157587.

Dowlatshahi, D.P., Sandrin, V., Vivona, S., Shaler, T.A., Kaiser, S.E., Melandri, F., Sundquist, W.I., and Kopito, R.R. (2012). ALIX is a Lys63-specific polyubiquitin binding protein that functions in retrovirus budding. Dev Cell *23*, 1247-1254.

Duleh, S.N., and Welch, M.D. (2010). WASH and the Arp2/3 complex regulate endosome shape and trafficking. Cytoskeleton (Hoboken) *67*, 193-206.

Efe, J.A., Plattner, F., Hulo, N., Kressler, D., Emr, S.D., and Deloche, O. (2005). Yeast Mon2p is a highly conserved protein that functions in the cytoplasm-to-vacuole transport pathway and is required for Golgi homeostasis. Journal of Cell Science *118*, 4751-4764.

Ehrlich, M., Boll, W., Van Oijen, A., Hariharan, R., Chandran, K., Nibert, M.L., and Kirchhausen, T. (2004). Endocytosis by random initiation and stabilization of clathrin-coated pits. Cell *118*, 591-605.

Elliott, A.M., Simard, L.R., Coghlan, G., Chudley, A.E., Chodirker, B.N., Greenberg, C.R., Burch, T., Ly, V., Hatch, G.M., and Zelinski, T. (2013). A novel mutation in KIAA0196: identification of a gene involved in Ritscher-Schinzel/3C syndrome in a First Nations cohort. J Med Genet *50*, 819-822.

Fadok, V.A., de Cathelineau, A., Daleke, D.L., Henson, P.M., and Bratton, D.L. (2001). Loss of phospholipid asymmetry and surface exposure of phosphatidylserine is required for phagocytosis of apoptotic cells by macrophages and fibroblasts. J Biol Chem *276*, 1071-1077.

Farge, E., Ojcius, D.M., Subtil, A., and Dautry-Varsat, A. (1999). Enhancement of endocytosis due to aminophospholipid transport across the plasma membrane of living cells. Am J Physiol *276*, C725-733.

Feng, S., Streets, A.J., Nesin, V., Tran, U., Nie, H., Onopiuk, M., Wessely, O., Tsiokas, L., and Ong, A.C.M. (2017). The Sorting Nexin 3 Retromer Pathway Regulates the Cell Surface Localization and Activity of a Wnt-Activated Polycystin Channel Complex. J Am Soc Nephrol *28*, 2973-2984.

Ferby, I., Waga, I., Kume, K., Sakanaka, C., and Shimizu, T. (1996). PAF-induced MAPK activation is inhibited by Wortmannin in neutrophils and macrophages. Adv Exp Med Biol *416*, 321-326.

Ferreira, A.P.A., and Boucrot, E. (2018). Mechanisms of Carrier Formation during Clathrin-Independent Endocytosis. Trends Cell Biol *28*, 188-200.

Ferrer, I., Martinez, A., Blanco, R., Dalfo, E., and Carmona, M. (2011). Neuropathology of sporadic Parkinson disease before the appearance of parkinsonism: preclinical Parkinson disease. J Neural Transm (Vienna) *118*, 821-839.

Fjorback, A.W., Seaman, M., Gustafsen, C., Mehmedbasic, A., Gokool, S., Wu, C., Militz, D., Schmidt, V., Madsen, P., Nyengaard, J.R.*, et al.* (2012). Retromer binds the FANSHY sorting motif in SorLA to regulate amyloid precursor protein sorting and processing. The Journal of neuroscience : the official journal of the Society for Neuroscience *32*, 1467-1480.

Florian, V., Schluter, T., and Bohnensack, R. (2001). A new member of the sorting nexin family interacts with the C-terminus of P-selectin. Biochem Biophys Res Commun *281*, 1045-1050.

Follett, J., Bugarcic, A., Yang, Z., Ariotti, N., Norwood, S.J., Collins, B.M., Parton, R.G., and Teasdale, R.D. (2016). Parkinson Disease-linked Vps35 R524W Mutation Impairs the Endosomal Association of Retromer and Induces alpha-Synuclein Aggregation. J Biol Chem *291*, 18283-18298.

Follett, J., Norwood, S.J., Hamilton, N.A., Mohan, M., Kovtun, O., Tay, S., Zhe, Y., Wood, S.A., Mellick, G.D., Silburn, P.A.*, et al.* (2014). The Vps35 D620N mutation linked to Parkinson's disease disrupts the cargo sorting function of retromer. Traffic *15*, 230-244.

Forsburg, S.L. (2001). The art and design of genetic screens: yeast. Nat Rev Genet *2*, 659-668.

Franch-Marro, X., Wendler, F., Guidato, S., Griffith, J., Baena-Lopez, A., Itasaki, N., Maurice, M.M., and Vincent, J.P. (2008). Wingless secretion requires endosome-to-Golgi retrieval of Wntless/Evi/Sprinter by the retromer complex. Nature Cell Biology *10*, 170-U140.

Frankel, E.B., and Audhya, A. (2018). ESCRT-dependent cargo sorting at multivesicular endosomes. Seminars in cell & developmental biology *74*, 4-10.

Freeman, C.L., Hesketh, G., and Seaman, M.N. (2014). RME-8 coordinates the activity of the WASH complex with the function of the retromer SNX dimer to control endosomal tubulation. J Cell Sci *127*, 2053-2070.

Frost, A., Perera, R., Roux, A., Spasov, K., Destaing, O., Egelman, E.H., De Camilli, P., and Unger, V.M. (2008). Structural basis of membrane invagination by F-BAR domains. Cell *132*, 807-817.

Gall, W.E., Geething, N.C., Hua, Z., Ingram, M.F., Liu, K., Chen, S.I., and Graham, T.R. (2002). Drs2p-dependent formation of exocytic clathrin-coated vesicles in vivo. Current biology : CB *12*, 1623-1627.

Gallon, M., Clairfeuille, T., Steinberg, F., Mas, C., Ghai, R., Sessions, R.B., Teasdale, R.D., Collins, B.M., and Cullen, P.J. (2014a). A unique PDZ domain and arrestin-like fold interaction reveals mechanistic details of endocytic recycling by SNX27-retromer. Proc Natl Acad Sci U S A *111*, E3604-3613.

Gallon, M., Clairfeuille, T., Steinberg, F., Mas, C., Ghai, R., Sessions, R.B., Teasdale, R.D., Collins, B.M., and Cullen, P.J. (2014b). A unique PDZ domain and arrestin-like fold interaction reveals mechanistic details of endocytic recycling by SNX27-retromer. Proceedings of the National Academy of Sciences of the United States of America *111*, E3604-E3613.

Gallop, J.L., and McMahon, H.T. (2005). BAR domains and membrane curvature: bringing your curves to the BAR. Biochem Soc Symp, 223-231.

Gasnereau, I., Herr, P., Chia, P.Z.C., Basler, K., and Gleeson, P.A. (2011). Identification of an Endocytosis Motif in an Intracellular Loop of Wntless Protein, Essential for Its Recycling and the Control of Wnt Protein Signaling. Journal of Biological Chemistry *286*, 43324-43333.

Gautreau, A., Oguievetskaia, K., and Ungermann, C. (2014). Function and regulation of the endosomal fusion and fission machineries. Cold Spring Harb Perspect Biol *6*.

Gershlick, D.C., and Lucas, M. (2017). Endosomal Trafficking: Retromer and Retriever Are Relatives in Recycling. Current biology : CB *27*, R1233-R1236.

Geuze, H.J., Slot, J.W., Strous, G.J., and Schwartz, A.L. (1983). The pathway of the asialoglycoprotein-ligand during receptor-mediated endocytosis: a morphological study

with colloidal gold/ligand in the human hepatoma cell line, Hep G2. Eur J Cell Biol *32*, 38-44.

Ghai, R., Bugarcic, A., Liu, H., Norwood, S.J., Skeldal, S., Coulson, E.J., Li, S.S., Teasdale, R.D., and Collins, B.M. (2013). Structural basis for endosomal trafficking of diverse transmembrane cargos by PX-FERM proteins. Proc Natl Acad Sci U S A *110*, E643-652.

Ghai, R., Mobli, M., Norwood, S.J., Bugarcic, A., Teasdale, R.D., King, G.F., and Collins, B.M. (2011). Phox homology band 4.1/ezrin/radixin/moesin-like proteins function as molecular scaffolds that interact with cargo receptors and Ras GTPases. Proc Natl Acad Sci U S A *108*, 7763-7768.

Gillingham, A.K., Whyte, J.R.C., Panic, B., and Munro, S. (2006). Mon2, a relative of large Arf exchange factors, recruits Dop1 to the Golgi apparatus. Journal of Biological Chemistry *281*, 2273-2280.

Gleason, R.J., Akintobi, A.M., Grant, B.D., and Padgett, R.W. (2014). BMP signaling requires retromer-dependent recycling of the type I receptor. Proceedings of the National Academy of Sciences of the United States of America *111*, 2578-2583.

Goley, E.D., and Welch, M.D. (2006). The ARP2/3 complex: an actin nucleator comes of age. Nat Rev Mol Cell Biol *7*, 713-726.

Gomez, T.S., and Billadeau, D.D. (2009). A FAM21-containing WASH complex regulates retromer-dependent sorting. Dev Cell *17*, 699-711.

Gomez, T.S., Gorman, J.A., de Narvajas, A.A., Koenig, A.O., and Billadeau, D.D. (2012). Trafficking defects in WASH-knockout fibroblasts originate from collapsed endosomal and lysosomal networks. Mol Biol Cell *23*, 3215-3228.

Goodman, R.M., Thombre, S., Firtina, Z., Gray, D., Betts, D., Roebuck, J., Spana, E.P., and Selva, E.M. (2006). Sprinter: a novel transmembrane protein required for Wg secretion and signaling. Development *133*, 4901-4911.

Goren, M.A., Morizumi, T., Menon, I., Joseph, J.S., Dittman, J.S., Cherezov, V., Stevens, R.C., Ernst, O.P., and Menon, A.K. (2014). Constitutive phospholipid scramblase activity of a G protein-coupled receptor. Nature communications *5*, 5115.

Graham, F.L., Smiley, J., Russell, W.C., and Nairn, R. (1977). Characteristics of a human cell line transformed by DNA from human adenovirus type 5. J Gen Virol *36*, 59-74.

Guipponi, M., Brunschwig, K., Chamoun, Z., Scott, H.S., Shibuya, K., Kudoh, J., Delezoide, A.L., El Samadi, S., Chettouh, Z., Rossier, C.*, et al.* (2000). C21orf5, a novel human chromosome 21 gene, has a Caenorhabditis elegans ortholog (pad-1) required for embryonic patterning. Genomics *68*, 30-40.

Gustavsson, E.K., Guella, I., Trinh, J., Szu-Tu, C., Rajput, A., Rajput, A.H., Steele, J.C., McKeown, M., Jeon, B.S., Aasly, J.O.*, et al.* (2015). Genetic Variability of the Retromer Cargo Recognition Complex in Parkinsonism. Movement Disord *30*, 580-584.

Haas, A.K., Fuchs, E., Kopajtich, R., and Barr, F.A. (2005). A GTPase-activating protein controls Rab5 function in endocytic trafficking. Nat Cell Biol *7*, 887-893.

Haft, C.R., de la Luz Sierra, M., Bafford, R., Lesniak, M.A., Barr, V.A., and Taylor, S.I. (2000). Human orthologs of yeast vacuolar protein sorting proteins Vps26, 29, and 35: assembly into multimeric complexes. Mol Biol Cell *11*, 4105-4116.

Haft, C.R., de la Luz Sierra, M., Barr, V.A., Haft, D.H., and Taylor, S.I. (1998). Identification of a family of sorting nexin molecules and characterization of their association with receptors. Mol Cell Biol *18*, 7278-7287.

Han, J., Pluhackova, K., and Bockmann, R.A. (2017). The Multifaceted Role of SNARE Proteins in Membrane Fusion. Front Physiol *8*, 5.

Harbour, M.E., Breusegem, S.Y., and Seaman, M.N.J. (2012). Recruitment of the endosomal WASH complex is mediated by the extended 'tail' of Fam21 binding to the retromer protein Vps35. Biochem J *442*, 209-220.

Harrison, M.S., Hung, C.S., Liu, T.T., Christiano, R., Walther, T.C., and Burd, C.G. (2014a). A mechanism for retromer endosomal coat complex assembly with cargo. Proc Natl Acad Sci U S A *111*, 267-272.

Harrison, M.S., Hung, C.S., Liu, T.T., Christiano, R., Walther, T.C., and Burd, C.G. (2014b). A mechanism for retromer endosomal coat complex assembly with cargo. Proceedings of the National Academy of Sciences of the United States of America *111*, 267-272.

Harterink, M., Port, F., Lorenowicz, M.J., McGough, I.J., Silhankova, M., Betist, M.C., van Weering, J.R.T., van Heesbeen, R., Middelkoop, T.C., Basler, K.*, et al.* (2011). A SNX3-dependent retromer pathway mediates retrograde transport of the Wnt sorting receptor Wntless and is required for Wnt secretion. Nature Cell Biology *13*, 914-U358.

Hayakawa, A., Hayes, S.J., Lawe, D.C., Sudharshan, E., Tuft, R., Fogarty, K., Lambright, D., and Corvera, S. (2004). Structural basis for endosomal targeting by FYVE domains. J Biol Chem *279*, 5958-5966.

Helfer, E., Harbour, M.E., Henriot, V., Lakisic, G., Sousa-Blin, C., Volceanov, L., Seaman, M.N.J., and Gautreau, A. (2013). Endosomal recruitment of the WASH complex: Active sequences and mutations impairing interaction with the retromer. Biol Cell *105*, 191-207.

Henry, A.G., Hislop, J.N., Grove, J., Thorn, K., Marsh, M., and von Zastrow, M. (2012). Regulation of endocytic clathrin dynamics by cargo ubiquitination. Dev Cell *23*, 519-532.

Herr, P., and Basler, K. (2012). Porcupine-mediated lipidation is required for Wnt recognition by Wls. Dev Biol *361*, 392-402.

Hickman, S., Izzy, S., Sen, P., Morsett, L., and El Khoury, J. (2018). Microglia in neurodegeneration. Nat Neurosci *21*, 1359-1369.

Hierro, A., Rojas, A.L., Rojas, R., Murthy, N., Effantin, G., Kajava, A.V., Steven, A.C., Bonifacino, J.S., and Hurley, J.H. (2007). Functional architecture of the retromer cargo-recognition complex. Nature *449*, 1063-U1068.

Hinshaw, J.E., and Schmid, S.L. (1995). Dynamin self-assembles into rings suggesting a mechanism for coated vesicle budding. Nature *374*, 190-192.

Hirsch, L., Jette, N., Frolkis, A., Steeves, T., and Pringsheim, T. (2016). The Incidence of Parkinson's Disease: A Systematic Review and Meta-Analysis. Neuroepidemiology *46*, 292-300.

Horazdovsky, B.F., Davies, B.A., Seaman, M.N., McLaughlin, S.A., Yoon, S., and Emr, S.D. (1997). A sorting nexin-1 homologue, Vps5p, forms a complex with Vps17p and is required for recycling the vacuolar protein-sorting receptor. Mol Biol Cell *8*, 1529-1541.

Hua, Z.L., Fatheddin, P., and Graham, T.R. (2002). An essential subfamily of Drs2p-related P-type ATPases is required for protein trafficking between Golgi complex and endosomal/vacuolar system. Molecular Biology of the Cell *13*, 3162-3177.

Hua, Z.L., and Graham, T.R. (2003). Requirement for Neo1p in retrograde transport from the Golgi complex to the endoplasmic reticulum. Molecular Biology of the Cell *14*, 4971-4983.

Hung, A.Y., and Sheng, M. (2002). PDZ domains: structural modules for protein complex assembly. J Biol Chem *277*, 5699-5702.

Huotari, J., and Helenius, A. (2011). Endosome maturation. The EMBO journal *30*, 3481-3500.

Hurley, J.H., Boura, E., Carlson, L.A., and Rozycki, B. (2010). Membrane budding. Cell *143*, 875-887.

Hussain, N.K., Diering, G.H., Sole, J., Anggono, V., and Huganir, R.L. (2014). Sorting Nexin 27 regulates basal and activity-dependent trafficking of AMPARs. Proc Natl Acad Sci U S A *111*, 11840-11845.

Ichinose, Y., Koh, K., Fukumoto, M., Yamashiro, N., Kobayashi, F., Miwa, M., Nagasaka, T., Shindo, K., Ishiura, H., Tsuji, S.*, et al.* (2016). Exome sequencing reveals a novel missense mutation in the KIAA0196 gene in a Japanese patient with SPG8. Clin Neurol Neurosurg *144*, 36-38.

Ingolfsson, H.I., Melo, M.N., van Eerden, F.J., Arnarez, C., Lopez, C.A., Wassenaar, T.A., Periole, X., de Vries, A.H., Tieleman, D.P., and Marrink, S.J. (2014). Lipid organization of the plasma membrane. J Am Chem Soc *136*, 14554-14559.

Ishiura, H., Takahashi, Y., Hayashi, T., Saito, K., Furuya, H., Watanabe, M., Murata, M., Suzuki, M., Sugiura, A., Sawai, S.*, et al.* (2014). Molecular epidemiology and clinical spectrum of hereditary spastic paraplegia in the Japanese population based on comprehensive mutational analyses. J Hum Genet *59*, 163-172.

Ishizu, N., Yui, D., Hebisawa, A., Aizawa, H., Cui, W., Fujita, Y., Hashimoto, K., Ajioka, I., Mizusawa, H., Yokota, T.*, et al.* (2016). Impaired striatal dopamine release in homozygous Vps35 D620N knock-in mice. Human molecular genetics *25*, 4507-4517.

Jaber, N., Mohd-Naim, N., Wang, Z.Q., DeLeon, J.L., Kim, S., Zhong, H., Sheshadri, N., Dou, Z.X., Edinger, A.L., Du, G.W.*, et al.* (2016). Vps34 regulates Rab7 and late endocytic trafficking through recruitment of the GTPase-activating protein Armus. Journal of Cell Science *129*, 4424-4435.

Jahic, A., Khundadze, M., Jaenisch, N., Schule, R., Klimpe, S., Klebe, S., Frahm, C., Kassubek, J., Stevanin, G., Schols, L.*, et al.* (2015). The spectrum of KIAA0196 variants, and characterization of a murine knockout: implications for the mutational mechanism in hereditary spastic paraplegia type SPG8. Orphanet J Rare Dis *10*, 147.

Jean, S., and Kiger, A.A. (2014). Classes of phosphoinositide 3-kinases at a glance. Journal of Cell Science *127*, 923-928.

Jia, D., Gomez, T.S., Billadeau, D.D., and Rosen, M.K. (2012). Multiple repeat elements within the FAM21 tail link the WASH actin regulatory complex to the retromer. Molecular Biology of the Cell *23*, 2352-2361.

Jia, D., Gomez, T.S., Metlagel, Z., Umetani, J., Otwinowski, Z., Rosen, M.K., and Billadeau, D.D. (2010). WASH and WAVE actin regulators of the Wiskott-Aldrich syndrome protein (WASP) family are controlled by analogous structurally related complexes. Proc Natl Acad Sci U S A *107*, 10442-10447.

Jia, D., Zhang, J.S., Li, F., Wang, J., Deng, Z., White, M.A., Osborne, D.G., Phillips-Krawczak, C., Gomez, T.S., Li, H.*, et al.* (2016). Structural and mechanistic insights into regulation of the retromer coat by TBC1d5. Nature communications *7*, 13305.

Jimenez-Orgaz, A., Kvainickas, A., Nagele, H., Denner, J., Eimer, S., Dengjel, J., and Steinberg, F. (2018). Control of RAB7 activity and localization through the retromer-TBC1D5 complex enables RAB7-dependent mitophagy. The EMBO journal *37*, 235-254.

Jin, E.J., Kiral, F.R., and Hiesinger, P.R. (2018). The where, what, and when of membrane protein degradation in neurons. Dev Neurobiol *78*, 283-297.

Johnson, E.E., Overmeyer, J.H., Gunning, W.T., and Maltese, W.A. (2006). Gene silencing reveals a specific function of hVps34 phosphatidylinositol 3-kinase in late versus early endosomes. Journal of Cell Science *119*, 1219-1232.

Joubert, L., Hanson, B., Barthet, G., Sebben, M., Claeysen, S., Hong, W., Marin, P., Dumuis, A., and Bockaert, J. (2004). New sorting nexin (SNX27) and NHERF

specifically interact with the 5-HT4a receptor splice variant: roles in receptor targeting. J Cell Sci *117*, 5367-5379.

Kadlecova, Z., Spielman, S.J., Loerke, D., Mohanakrishnan, A., Reed, D.K., and Schmid, S.L. (2017). Regulation of clathrin-mediated endocytosis by hierarchical allosteric activation of AP2. The Journal of cell biology *216*, 167-179.

Kajii, Y., Muraoka, S., Hiraoka, S., Fujiyama, K., Umino, A., and Nishikawa, T. (2003). A developmentally regulated and psychostimulant-inducible novel rat gene mrt1 encoding PDZ-PX proteins isolated in the neocortex. Mol Psychiatry *8*, 434-444.

Kaksonen, M., and Roux, A. (2018). Mechanisms of clathrin-mediated endocytosis. Nat Rev Mol Cell Biol *19*, 313-326.

Kalin, S., Buser, D.P., and Spiess, M. (2016). A fresh look at the function of Rabaptin5 on endosomes. Small GTPases *7*, 34-37.

Kanamori, T., Inoue, T., Sakamoto, T., Gengyo-Ando, K., Tsujimoto, M., Mitani, S., Sawa, H., Aoki, J., and Arai, H. (2008). beta-catenin asymmetry is regulated by PLA(1) and retrograde traffic in C-elegans stem cell divisions. Embo Journal *27*, 1647-1657.

Katzmann, D.J., Babst, M., and Emr, S.D. (2001). Ubiquitin-dependent sorting into the multivesicular body pathway requires the function of a conserved endosomal protein sorting complex, ESCRT-I. Cell *106*, 145-155.

Kelly, B.T., Graham, S.C., Liska, N., Dannhauser, P.N., Honing, S., Ungewickell, E.J., and Owen, D.J. (2014). Clathrin adaptors. AP2 controls clathrin polymerization with a membrane-activated switch. Science *345*, 459-463.

Kelly, B.T., McCoy, A.J., Spate, K., Miller, S.E., Evans, P.R., Honing, S., and Owen, D.J. (2008). A structural explanation for the binding of endocytic dileucine motifs by the AP2 complex. Nature *456*, 976-979.

Keren-Kaplan, T., Attali, I., Estrin, M., Kuo, L.S., Farkash, E., Jerabek-Willemsen, M., Blutraich, N., Artzi, S., Peri, A., Freed, E.O.*, et al.* (2013). Structure-based in silico identification of ubiquitin-binding domains provides insights into the ALIX-V:ubiquitin complex and retrovirus budding. The EMBO journal *32*, 538-551.

Ketel, K., Krauss, M., Nicot, A.S., Puchkov, D., Wieffer, M., Muller, R., Subramanian, D., Schultz, C., Laporte, J., and Haucke, V. (2016). A phosphoinositide conversion mechanism for exit from endosomes. Nature *529*, 408-412.

Kim, E., Lee, Y., Lee, H.J., Kim, J.S., Song, B.S., Huh, J.W., Lee, S.R., Kim, S.U., Kim, S.H., Hong, Y.*, et al.* (2010). Implication of mouse Vps26b-Vps29-Vps35 retromer complex in sortilin trafficking. Biochem Biophys Res Commun *403*, 167-171.

Kim, G.H., Dayam, R.M., Prashar, A., Terebiznik, M., and Botelho, R.J. (2014). PIKfyve inhibition interferes with phagosome and endosome maturation in macrophages. Traffic *15*, 1143-1163.

Kirchhausen, T., Owen, D., and Harrison, S.C. (2014). Molecular structure, function, and dynamics of clathrin-mediated membrane traffic. Cold Spring Harb Perspect Biol *6*, a016725.

Klemm, R.W., Ejsing, C.S., Surma, M.A., Kaiser, H.J., Gerl, M.J., Sampaio, J.L., de Robillard, Q., Ferguson, C., Proszynski, T.J., Shevchenko, A.*, et al.* (2009). Segregation of sphingolipids and sterols during formation of secretory vesicles at the trans-Golgi network. The Journal of cell biology *185*, 601-612.

Klumperman, J., and Raposo, G. (2014). The complex ultrastructure of the endolysosomal system. Cold Spring Harb Perspect Biol *6*, a016857.

Knutson, B.A. (2010). Insights into the domain and repeat architecture of target of rapamycin. J Struct Biol *170*, 354-363.

Kolanczyk, M., Krawitz, P., Hecht, J., Hupalowska, A., Miaczynska, M., Marschner, K., Schlack, C., Emmerich, D., Kobus, K., Kornak, U.*, et al.* (2015). Missense variant in CCDC22 causes X-linked recessive intellectual disability with features of Ritscher-Schinzel/3C syndrome. Eur J Hum Genet *23*, 720.

Koulen, P., Cai, Y., Geng, L., Maeda, Y., Nishimura, S., Witzgall, R., Ehrlich, B.E., and Somlo, S. (2002). Polycystin-2 is an intracellular calcium release channel. Nat Cell Biol *4*, 191-197.

Koumandou, V.L., Klute, M.J., Herman, E.K., Nunez-Miguel, R., Dacks, J.B., and Field, M.C. (2011). Evolutionary reconstruction of the retromer complex and its function in Trypanosoma brucei. J Cell Sci *124*, 1496-1509.

Kovtun, O., Leneva, N., Bykov, Y.S., Ariotti, N., Teasdale, R.D., Schaffer, M., Engel, B.D., Owen, D.J., Briggs, J.A.G., and Collins, B.M. (2018). Structure of the membrane-assembled retromer coat determined by cryo-electron tomography. Nature *561*, 561-564.

Kulak, N.A., Pichler, G., Paron, I., Nagaraj, N., and Mann, M. (2014). Minimal, encapsulated proteomic-sample processing applied to copy-number estimation in eukaryotic cells. Nat Methods *11*, 319-324.

Kulkarni, V.V., and Maday, S. (2018). Neuronal endosomes to lysosomes: A journey to the soma. The Journal of cell biology *217*, 2977-2979.

Kumar, K.R., Weissbach, A., Heldmann, M., Kasten, M., Tunc, S., Sue, C.M., Svetel, M., Kostic, V.S., Segura-Aguilar, J., Ramirez, A.*, et al.* (2012). Frequency of the D620N mutation in VPS35 in Parkinson disease. Arch Neurol *69*, 1360-1364.

Kummel, D., and Ungermann, C. (2014). Principles of membrane tethering and fusion in endosome and lysosome biogenesis. Current opinion in cell biology *29*, 61-66.

Kvainickas, A., Jimenez-Orgaz, A., Nagele, H., Hu, Z., Dengjel, J., and Steinberg, F. (2017a). Cargo-selective SNX-BAR proteins mediate retromer trimer independent retrograde transport. The Journal of cell biology *216*, 3677-3693.

Kvainickas, A., Orgaz, A.J., Nagele, H., Diedrich, B., Heesom, K.J., Dengjel, J., Cullen, P.J., and Steinberg, F. (2017b). Retromer- and WASH-dependent sorting of nutrient transporters requires a multivalent interaction network with ANKRD50. J Cell Sci *130*, 382-395.

Kyuuma, M., Kikuchi, K., Kojima, K., Sugawara, Y., Sato, M., Mano, N., Goto, J., Takeshita, T., Yamamoto, A., Sugamura, K.*, et al.* (2007). AMSH, an ESCRT-III associated enzyme, deubiquitinates cargo on MVB/late endosomes. Cell Struct Funct *31*, 159-172.

Lane, R.F., Raines, S.M., Steele, J.W., Ehrlich, M.E., Lah, J.A., Small, S.A., Tanzi, R.E., Attie, A.D., and Gandy, S. (2010). Diabetes-associated SorCS1 regulates Alzheimer's amyloid-beta metabolism: evidence for involvement of SorL1 and the retromer complex. The Journal of neuroscience : the official journal of the Society for Neuroscience *30*, 13110-13115.

Langemeyer, L., Frohlich, F., and Ungermann, C. (2018). Rab GTPase Function in Endosome and Lysosome Biogenesis. Trends Cell Biol *28*, 957-970.

Langton, P.F., Kakugawa, S., and Vincent, J.P. (2016). Making, Exporting, and Modulating Wnts. Trends in Cell Biology *26*, 756-765.

Lau, W.C., Li, Y., Liu, Z., Gao, Y., Zhang, Q., and Huen, M.S. (2016). Structure of the human dimeric ATM kinase. Cell Cycle *15*, 1117-1124.

Law, F., and Rocheleau, C.E. (2017). Vps34 and the Armus/TBC-2 Rab GAPs: Putting the brakes on the endosomal Rab5 and Rab7 GTPases. Cell Logist *7*, e1403530.

Lee, J.J., Radice, G., Perkins, C.P., and Costantini, F. (1992). Identification and characterization of a novel, evolutionarily conserved gene disrupted by the murine H beta 58 embryonic lethal transgene insertion. Development *115*, 277-288.

Lee, S., Chang, J., and Blackstone, C. (2016). FAM21 directs SNX27-retromer cargoes to the plasma membrane by preventing transport to the Golgi apparatus. Nature communications *7*, 10939.

Lee, S., Uchida, Y., Wang, J., Matsudaira, T., Nakagawa, T., Kishimoto, T., Mukai, K., Inaba, T., Kobayashi, T., Molday, R.S.*, et al.* (2015). Transport through recycling endosomes requires EHD1 recruitment by a phosphatidylserine translocase. The EMBO journal *34*, 669-688.

Lend, A.K., Kazantseva, A., Kivil, A., Valvere, V., and Palm, K. (2015). Diagnostic significance of alternative splice variants of REST and DOPEY1 in the peripheral blood of patients with breast cancer. Tumour Biol *36*, 2473-2480.

Lenoir, G., Williamson, P., Puts, C.F., and Holthuis, J.C.M. (2009). Cdc50p Plays a Vital Role in the ATPase Reaction Cycle of the Putative Aminophospholipid Transporter Drs2p. Journal of Biological Chemistry *284*, 17956-17967.

Lenoir, M., Ustunel, C., Rajesh, S., Kaur, J., Moreau, D., Gruenberg, J., and Overduin, M. (2018). Phosphorylation of conserved phosphoinositide binding pocket regulates sorting nexin membrane targeting. Nature communications *9*, 993.

Lesage, S., Condroyer, C., Klebe, S., Honore, A., Tison, F., Brefel-Courbon, C., Durr, A., Brice, A., and French Parkinson's Disease Genetics Study, G. (2012). Identification

of VPS35 mutations replicated in French families with Parkinson disease. Neurology *78*, 1449-1450.

Letourneur, F., and Klausner, R.D. (1992). A novel di-leucine motif and a tyrosine-based motif independently mediate lysosomal targeting and endocytosis of CD3 chains. Cell *69*, 1143-1157.

Li, H., Koo, Y., Mao, X., Sifuentes-Dominguez, L., Morris, L.L., Jia, D., Miyata, N., Faulkner, R.A., van Deursen, J.M., Vooijs, M.*, et al.* (2015). Endosomal sorting of Notch receptors through COMMD9-dependent pathways modulates Notch signaling. The Journal of cell biology *211*, 605-617.

Li, S.C., Diakov, T.T., Xu, T., Tarsio, M., Zhu, W., Couoh-Cardel, S., Weisman, L.S., and Kane, P.M. (2014). The signaling lipid PI(3,5)P(2) stabilizes V(1)-V(o) sector interactions and activates the V-ATPase. Mol Biol Cell *25*, 1251-1262.

Libro, R., Bramanti, P., and Mazzon, E. (2016). The role of the Wnt canonical signaling in neurodegenerative diseases. Life Sci *158*, 78-88.

Lin, M.K., and Farrer, M.J. (2014). Genetics and genomics of Parkinson's disease. Genome Med *6*, 48.

Linhart, R., Wong, S.A., Cao, J., Tran, M., Huynh, A., Ardrey, C., Park, J.M., Hsu, C., Taha, S., Peterson, R.*, et al.* (2014). Vacuolar protein sorting 35 (Vps35) rescues locomotor deficits and shortened lifespan in Drosophila expressing a Parkinson's disease mutant of Leucine-Rich Repeat Kinase 2 (LRRK2). Molecular neurodegeneration *9*, 23.

Lippe, R., Miaczynska, M., Rybin, V., Runge, A., and Zerial, M. (2001). Functional synergy between Rab5 effector Rabaptin-5 and exchange factor Rabex-5 when physically associated in a complex. Mol Biol Cell *12*, 2219-2228.

Liu, A.P., Aguet, F., Danuser, G., and Schmid, S.L. (2010). Local clustering of transferrin receptors promotes clathrin-coated pit initiation. The Journal of cell biology *191*, 1381-1393.

Liu, K., Xing, R., Jian, Y., Gao, Z., Ma, X., Sun, X., Li, Y., Xu, M., Wang, X., Jing, Y.*, et al.* (2017). WDR91 is a Rab7 effector required for neuronal development. The Journal of cell biology *216*, 3307-3321.

Loo, L.S., Tang, N., Al-Haddawi, M., Dawe, G.S., and Hong, W. (2014). A role for sorting nexin 27 in AMPA receptor trafficking. Nature communications *5*, 3176.

Lorenowicz, M.J., Macurkova, M., Middelkoop, T.C., de Groot, R., Betist, M.C., and Korswagen, H.C. (2014). Inhibition of late endosomal maturation restores Wnt secretion in Caenorhabditis elegans vps-29 retromer mutants. Cellular Signalling *26*, 19-31.

Lorente-Rodriguez, A., and Barlowe, C. (2011). Requirement for Golgi-localized PI(4)P in fusion of COPII vesicles with Golgi compartments. Mol Biol Cell *22*, 216-229.

Lucas, M., Gershlick, D.C., Vidaurrazaga, A., Rojas, A.L., Bonifacino, J.S., and Hierro, A. (2016). Structural Mechanism for Cargo Recognition by the Retromer Complex. Cell *167*, 1623-+.

Lucin, K.M., O'Brien, C.E., Bieri, G., Czirr, E., Mosher, K.I., Abbey, R.J., Mastroeni, D.F., Rogers, J., Spencer, B., Masliah, E.*, et al.* (2013). Microglial beclin 1 regulates retromer trafficking and phagocytosis and is impaired in Alzheimer's disease. Neuron *79*, 873-886.

Lundmark, R., and Carlsson, S.R. (2004). Regulated membrane recruitment of dynamin-2 mediated by sorting nexin 9. J Biol Chem *279*, 42694-42702.

Lyssenko, N.N., Miteva, Y., Gilroy, S., Hanna-Rose, W., and Schlegel, R.A. (2008). An unexpectedly high degree of specialization and a widespread involvement in sterol metabolism among the C. elegans putative aminophospholipid translocases. BMC Dev Biol *8*, 96.

MacDonald, E., Brown, L., Selvais, A., Liu, H., Waring, T., Newman, D., Bithell, J., Grimes, D., Urbe, S., Clague, M.J.*, et al.* (2018). HRS-WASH axis governs actin-mediated endosomal recycling and cell invasion. The Journal of cell biology *217*, 2549-2564.

MacLeod, D.A., Rhinn, H., Kuwahara, T., Zolin, A., Di Paolo, G., McCabe, B.D., Marder, K.S., Honig, L.S., Clark, L.N., Small, S.A.*, et al.* (2013). RAB7L1 interacts with LRRK2 to modify intraneuronal protein sorting and Parkinson's disease risk. Neuron *77*, 425-439.

Mahajan, D., Boh, B.K., Zhou, Y., Chen, L., Cornvik, T.C., Hong, W., and Lu, L. (2013). Mammalian Mon2/Ysl2 regulates endosome-to-Golgi trafficking but possesses no guanine nucleotide exchange activity toward Arl1 GTPase. Sci Rep *3*, 3362.

Maloof, J.N., Whangbo, J., Harris, J.M., Jongeward, G.D., and Kenyon, C. (1999). A Wnt signaling pathway controls Hox gene expression and neuroblast migration in C-elegans. Development *126*, 37-49.

Mari, M., Bujny, M.V., Zeuschner, D., Geerts, W.J., Griffith, J., Petersen, C.M., Cullen, P.J., Klumperman, J., and Geuze, H.J. (2008). SNX1 defines an early endosomal recycling exit for sortilin and mannose 6-phosphate receptors. Traffic *9*, 380-393.

Mattera, R., and Bonifacino, J.S. (2008). Ubiquitin binding and conjugation regulate the recruitment of Rabex-5 to early endosomes. The EMBO journal *27*, 2484-2494.

Maxfield, F.R., and McGraw, T.E. (2004). Endocytic recycling. Nat Rev Mol Cell Biol *5*, 121-132.

Maxfield, F.R., and Yamashiro, D.J. (1987). Endosome acidification and the pathways of receptor-mediated endocytosis. Adv Exp Med Biol *225*, 189-198.

Mayor, S., Parton, R.G., and Donaldson, J.G. (2014). Clathrin-independent pathways of endocytosis. Cold Spring Harb Perspect Biol *6*.

Mayor, S., Presley, J.F., and Maxfield, F.R. (1993). Sorting of membrane components from endosomes and subsequent recycling to the cell surface occurs by a bulk flow process. The Journal of cell biology *121*, 1257-1269.

McCullough, J., Row, P.E., Lorenzo, O., Doherty, M., Beynon, R., Clague, M.J., and Urbe, S. (2006). Activation of the endosome-associated ubiquitin isopeptidase AMSH by STAM, a component of the multivesicular body-sorting machinery. Current biology : CB *16*, 160-165.

McGough, I.J., de Groot, R.E.A., Jellett, A.P., Betist, M.C., Varandas, K.C., Danson, C.M., Heesom, K.J., Korswagen, H.C., and Cullen, P.J. (2018). SNX3-retromer requires an evolutionary conserved MON2:DOPEY2:ATP9A complex to mediate Wntless sorting and Wnt secretion. Nature communications *9*, 3737.

McGough, I.J., Steinberg, F., Gallon, M., Yatsu, A., Ohbayashi, N., Heesom, K.J., Fukuda, M., and Cullen, P.J. (2014a). Identification of molecular heterogeneity in

SNX27-retromer-mediated endosome-to-plasma-membrane recycling. Journal of Cell Science *127*, 4940-4953.

McGough, I.J., Steinberg, F., Jia, D., Barbuti, P.A., McMillan, K.J., Heesom, K.J., Whone, A.L., Caldwell, M.A., Billadeau, D.D., Rosen, M.K.*, et al.* (2014b). Retromer Binding to FAM21 and the WASH Complex Is Perturbed by the Parkinson Disease-Linked VPS35(D620N) Mutation. Current Biology *24*, 1670-1676.

McMillan, K.J., Gallon, M., Jellett, A.P., Clairfeuille, T., Tilley, F.C., McGough, I., Danson, C.M., Heesom, K.J., Wilkinson, K.A., Collins, B.M.*, et al.* (2016). Atypical parkinsonism-associated retromer mutant alters endosomal sorting of specific cargo proteins. Journal of Cell Biology *214*, 389-399.

McMillan, K.J., Korswagen, H.C., and Cullen, P.J. (2017). The emerging role of retromer in neuroprotection. Current opinion in cell biology *47*, 72-82.

McNally, K.E., and Cullen, P.J. (2018). Endosomal Retrieval of Cargo: Retromer Is Not Alone. Trends Cell Biol *28*, 807-822.

McNally, K.E., Faulkner, R., Steinberg, F., Gallon, M., Ghai, R., Pim, D., Langton, P., Pearson, N., Danson, C.M., Nagele, H.*, et al.* (2017). Retriever is a multiprotein complex for retromer-independent endosomal cargo recycling. Nature Cell Biology *19*, 1214-+.

Mecozzi, V.J., Berman, D.E., Simoes, S., Vetanovetz, C., Awal, M.R., Patel, V.M., Schneider, R.T., Petsko, G.A., Ringe, D., and Small, S.A. (2014). Pharmacological chaperones stabilize retromer to limit APP processing. Nature chemical biology *10*, 443-449.

Menon, I., Huber, T., Sanyal, S., Banerjee, S., Barre, P., Canis, S., Warren, J.D., Hwa, J., Sakmar, T.P., and Menon, A.K. (2011). Opsin is a phospholipid flippase. Current biology : CB *21*, 149-153.

Mierzwa, B.E., Chiaruttini, N., Redondo-Morata, L., von Filseck, J.M., Konig, J., Larios, J., Poser, I., Muller-Reichert, T., Scheuring, S., Roux, A.*, et al.* (2017). Dynamic subunit turnover in ESCRT-III assemblies is regulated by Vps4 to mediate membrane remodelling during cytokinesis. Nat Cell Biol *19*, 787-798.

Mim, C., Cui, H., Gawronski-Salerno, J.A., Frost, A., Lyman, E., Voth, G.A., and Unger, V.M. (2012). Structural basis of membrane bending by the N-BAR protein endophilin. Cell *149*, 137-145.

Miura, E., Hasegawa, T., Konno, M., Suzuki, M., Sugeno, N., Fujikake, N., Geisler, S., Tabuchi, M., Oshima, R., Kikuchi, A.*, et al.* (2014). VPS35 dysfunction impairs lysosomal degradation of alpha-synuclein and exacerbates neurotoxicity in a Drosophila model of Parkinson's disease. Neurobiology of disease *71*, 1-13.

Mohan, M., and Mellick, G.D. (2017). Role of the VPS35 D620N mutation in Parkinson's disease. Parkinsonism & related disorders *36*, 10-18.

Muhammad, A., Flores, I., Zhang, H., Yu, R., Staniszewski, A., Planel, E., Herman, M., Ho, L., Kreber, R., Honig, L.S.*, et al.* (2008). Retromer deficiency observed in Alzheimer's disease causes hippocampal dysfunction, neurodegeneration, and Abeta accumulation. Proc Natl Acad Sci U S A *105*, 7327-7332.

Muller, M.P., and Goody, R.S. (2018). Molecular control of Rab activity by GEFs, GAPs and GDI. Small GTPases *9*, 5-21.

Munsie, L.N., Milnerwood, A.J., Seibler, P., Beccano-Kelly, D.A., Tatarnikov, I., Khinda, J., Volta, M., Kadgien, C., Cao, L.P., Tapia, L.*, et al.* (2014). Retromer-dependent neurotransmitter receptor trafficking to synapses is altered by the Parkinson's Disease VPS35 mutation p.D620N. Human molecular genetics.

Murk, J.L., Humbel, B.M., Ziese, U., Griffith, J.M., Posthuma, G., Slot, J.W., Koster, A.J., Verkleij, A.J., Geuze, H.J., and Kleijmeer, M.J. (2003). Endosomal compartmentalization in three dimensions: implications for membrane fusion. Proc Natl Acad Sci U S A *100*, 13332-13337.

Murray, D.H., Jahnel, M., Lauer, J., Avellaneda, M.J., Brouilly, N., Cezanne, A., Morales-Navarrete, H., Perini, E.D., Ferguson, C., Lupas, A.N.*, et al.* (2016). An endosomal tether undergoes an entropic collapse to bring vesicles together. Nature *537*, 107-111.

Murray, J.T., Panaretou, C., Stenmark, H., Miaczynska, M., and Backer, J.M. (2002). Role of Rab5 in the recruitment of hVps34/p150 to the early endosome. Traffic *3*, 416-427.

Muthusamy, B.P., Natarajan, P., Zhou, X., and Graham, T.R. (2009). Linking phospholipid flippases to vesicle-mediated protein transport. Biochimica et biophysica acta *1791*, 612-619.

Nakada-Tsukui, K., Saito-Nakano, Y., Ali, V., and Nozaki, T. (2005). A retromerlike complex is a novel Rab7 effector that is involved in the transport of the virulence factor cysteine protease in the enteric protozoan parasite Entamoeba histolytica. Mol Biol Cell *16*, 5294-5303.

Natarajan, P., Wang, J., Hua, Z., and Graham, T.R. (2004). Drs2p-coupled aminophospholipid translocase activity in yeast Golgi membranes and relationship to in vivo function. Proc Natl Acad Sci U S A *101*, 10614-10619.

Nielsen, E., Christoforidis, S., Uttenweiler-Joseph, S., Miaczynska, M., Dewitte, F., Wilm, M., Hoflack, B., and Zerial, M. (2000). Rabenosyn-5, a novel Rab5 effector, is complexed with hVPS45 and recruited to endosomes through a FYVE finger domain. The Journal of cell biology *151*, 601-612.

Norris, A., Tammineni, P., Wang, S., Gerdes, J., Murr, A., Kwan, K.Y., Cai, Q., and Grant, B.D. (2017). SNX-1 and RME-8 oppose the assembly of HGRS-1/ESCRT-0 degradative microdomains on endosomes. Proc Natl Acad Sci U S A *114*, E307-E316.

Norwood, S.J., Shaw, D.J., Cowieson, N.P., Owen, D.J., Teasdale, R.D., and Collins, B.M. (2011). Assembly and solution structure of the core retromer protein complex. Traffic *12*, 56-71.

Nothwehr, S.F., Bryant, N.J., and Stevens, T.H. (1996). The newly identified yeast GRD genes are required for retention of late-Golgi membrane proteins. Mol Cell Biol *16*, 2700-2707.

Nunez, D., Antonescu, C., Mettlen, M., Liu, A., Schmid, S.L., Loerke, D., and Danuser, G. (2011). Hotspots organize clathrin-mediated endocytosis by efficient recruitment and retention of nucleating resources. Traffic *12*, 1868-1878.

Nuytemans, K., Bademci, G., Inchausti, V., Dressen, A., Kinnamon, D.D., Mehta, A., Wang, L., Zuchner, S., Beecham, G.W., Martin, E.R.*, et al.* (2013). Whole exome sequencing of rare variants in EIF4G1 and VPS35 in Parkinson disease. Neurology *80*, 982-989.

Odorizzi, G., Babst, M., and Emr, S.D. (1998). Fab1p PtdIns(3)P 5-kinase function essential for protein sorting in the multivesicular body. Cell *95*, 847-858.

Ohashi, E., Tanabe, K., Henmi, Y., Mesaki, K., Kobayashi, Y., and Takei, K. (2011). Receptor sorting within endosomal trafficking pathway is facilitated by dynamic actin filaments. PloS one *6*, e19942.

Ory, D.S., Neugeboren, B.A., and Mulligan, R.C. (1996). A stable human-derived packaging cell line for production of high titer retrovirus/vesicular stomatitis virus G pseudotypes. Proc Natl Acad Sci U S A *93*, 11400-11406.

Overduin, M., Rajesh, S., Gruenberg, J., and Lenoir, M. (2015). Secondary structure and H-1, C-13, N-15 resonance assignments of the endosomal sorting protein sorting nexin 3. Biomolecular Nmr Assignments *9*, 355-358.

Owen, D.J., and Evans, P.R. (1998). A structural explanation for the recognition of tyrosine-based endocytotic signals. Science *282*, 1327-1332.

Pan, C.L., Baum, P.D., Gu, M.Y., Jorgensen, E.M., Clark, S.G., and Garriga, G. (2008). C-elegans AP-2 and retromer control Wnt signaling by regulating MIG-14/Wntless. Developmental Cell *14*, 132-139.

Parachoniak, C.A., Luo, Y., Abella, J.V., Keen, J.H., and Park, M. (2011). GGA3 functions as a switch to promote Met receptor recycling, essential for sustained ERK and cell migration. Dev Cell *20*, 751-763.

Pashkova, N., Gakhar, L., Winistorfer, S.C., Sunshine, A.B., Rich, M., Dunham, M.J., Yu, L., and Piper, R.C. (2013). The yeast Alix homolog Bro1 functions as a ubiquitin receptor for protein sorting into multivesicular endosomes. Dev Cell *25*, 520-533.

Phillips-Krawczak, C.A., Singla, A., Starokadomskyy, P., Deng, Z., Osborne, D.G., Li, H., Dick, C.J., Gomez, T.S., Koenecke, M., Zhang, J.S.*, et al.* (2015). COMMD1 is linked to the WASH complex and regulates endosomal trafficking of the copper transporter ATP7A. Mol Biol Cell *26*, 91-103.

Piotrowski, J.T., Gomez, T.S., Schoon, R.A., Mangalam, A.K., and Billadeau, D.D. (2013). WASH knockout T cells demonstrate defective receptor trafficking, proliferation, and effector function. Mol Cell Biol *33*, 958-973.

Pomorski, T., Lombardi, R., Riezman, H., Devaux, P.F., van Meer, G., and Holthuis, J.C. (2003). Drs2p-related P-type ATPases Dnf1p and Dnf2p are required for phospholipid translocation across the yeast plasma membrane and serve a role in endocytosis. Mol Biol Cell *14*, 1240-1254.

Pons, V., Ustunel, C., Rolland, C., Torti, E., Parton, R.G., and Gruenberg, J. (2012). SNX12 role in endosome membrane transport. PloS one *7*, e38949.

Ponting, C.P. (1996). Novel domains in NADPH oxidase subunits, sorting nexins, and PtdIns 3-kinases: binding partners of SH3 domains? Protein Sci *5*, 2353-2357.

Port, F., Kuster, M., Herr, P., Furger, E., Banziger, C., Hausmann, G., and Basler, K. (2008). Wingless secretion promotes and requires retromer-dependent cycling of Wntless. Nature Cell Biology *10*, 178-U148.

Poteryaev, D., Datta, S., Ackema, K., Zerial, M., and Spang, A. (2010). Identification of the switch in early-to-late endosome transition. Cell *141*, 497-508.

Prasad, B.C., and Clark, S.G. (2006). Wnt signaling establishes anteroposterior neuronal polarity and requires retromer in C-elegans. Development *133*, 1757-1766.

Puthenveedu, M.A., Lauffer, B., Temkin, P., Vistein, R., Carlton, P., Thorn, K., Taunton, J., Weiner, O.D., Parton, R.G., and von Zastrow, M. (2010). Sequence-dependent sorting of recycling proteins by actin-stabilized endosomal microdomains. Cell *143*, 761-773.

Pylypenko, O., Lundmark, R., Rasmuson, E., Carlsson, S.R., and Rak, A. (2007). The PX-BAR membrane-remodeling unit of sorting nexin 9. The EMBO journal *26*, 4788-4800.

Pylypenko, O., Rak, A., Durek, T., Kushnir, S., Dursina, B.E., Thomae, N.H., Constantinescu, A.T., Brunsveld, L., Watzke, A., Waldmann, H*., et al.* (2006). Structure of doubly prenylated Ypt1:GDI complex and the mechanism of GDI-mediated Rab recycling. The EMBO journal *25*, 13-23.

Rachidi, M., Delezoide, A.L., Delabar, J.M., and Lopes, C. (2009). A quantitative assessment of gene expression (QAGE) reveals differential overexpression of DOPEY2, a candidate gene for mental retardation, in Down syndrome brain regions. Int J Dev Neurosci *27*, 393-398.

Raiborg, C., Bache, K.G., Gillooly, D.J., Madshus, I.H., Stang, E., and Stenmark, H. (2002). Hrs sorts ubiquitinated proteins into clathrin-coated microdomains of early endosomes. Nat Cell Biol *4*, 394-398.

Raiborg, C., Bache, K.G., Mehlum, A., Stang, E., and Stenmark, H. (2001a). Hrs recruits clathrin to early endosomes. The EMBO journal *20*, 5008-5021.

Raiborg, C., Bremnes, B., Mehlum, A., Gillooly, D.J., D'Arrigo, A., Stang, E., and Stenmark, H. (2001b). FYVE and coiled-coil domains determine the specific localisation of Hrs to early endosomes. J Cell Sci *114*, 2255-2263.

Raiborg, C., Schink, K.O., and Stenmark, H. (2013). ClassIII phosphatidylinositol 3-kinase and its catalytic product PtdIns3P in regulation of endocytic membrane traffic. Febs J *280*, 2730-2742.

Rakesh, R., Krishnan, R., Sattlegger, E., and Srinivasan, N. (2017). Recognition of a structural domain (RWDBD) in Gcn1 proteins that interacts with the RWD domain containing proteins. Biol Direct *12*, 12.

Ratcliffe, C.D., Sahgal, P., Parachoniak, C.A., Ivaska, J., and Park, M. (2016). Regulation of Cell Migration and beta1 Integrin Trafficking by the Endosomal Adaptor GGA3. Traffic *17*, 670-688.

Robert, X., and Gouet, P. (2014). Deciphering key features in protein structures with the new ENDscript server. Nucleic Acids Research *42*, W320-W324.

Robinson, J.S., Klionsky, D.J., Banta, L.M., and Emr, S.D. (1988). Protein sorting in Saccharomyces cerevisiae: isolation of mutants defective in the delivery and processing of multiple vacuolar hydrolases. Mol Cell Biol *8*, 4936-4948.

Rojas, R., van Vlijmen, T., Mardones, G.A., Prabhu, Y., Rojas, A.L., Mohammed, S., Heck, A.J.R., Raposo, G., van der Sluijs, P., and Bonifacino, J.S. (2008). Regulation of retromer recruitment to endosomes by sequential action of Rab5 and Rab7. Journal of Cell Biology *183*, 513-526.

Ropers, F., Derivery, E., Hu, H., Garshasbi, M., Karbasiyan, M., Herold, M., Nurnberg, G., Ullmann, R., Gautreau, A., Sperling, K.*, et al.* (2011). Identification of a novel candidate gene for non-syndromic autosomal recessive intellectual disability: the WASH complex member SWIP. Human molecular genetics *20*, 2585-2590.

Ross, J.L., Ali, M.Y., and Warshaw, D.M. (2008). Cargo transport: molecular motors navigate a complex cytoskeleton. Current opinion in cell biology *20*, 41-47.

Rossetti, S., Consugar, M.B., Chapman, A.B., Torres, V.E., Guay-Woodford, L.M., Grantham, J.J., Bennett, W.M., Meyers, C.M., Walker, D.L., Bae, K.*, et al.* (2007). Comprehensive molecular diagnostics in autosomal dominant polycystic kidney disease. J Am Soc Nephrol *18*, 2143-2160.

Rothman, J.H., and Stevens, T.H. (1986). Protein sorting in yeast: mutants defective in vacuole biogenesis mislocalize vacuolar proteins into the late secretory pathway. Cell *47*, 1041-1051.

Rovelet-Lecrux, A., Charbonnier, C., Wallon, D., Nicolas, G., Seaman, M.N., Pottier, C., Breusegem, S.Y., Mathur, P.P., Jenardhanan, P., Le Guennec, K.*, et al.* (2015). De novo deleterious genetic variations target a biological network centered on Abeta peptide in early-onset Alzheimer disease. Mol Psychiatry *20*, 1046-1056.

Saito, K., Fujimura-Kamada, K., Furuta, N., Kato, U., Umeda, M., and Tanaka, K. (2004). Cdc50p, a protein required for polarized growth, associates with the Drs2p P-type ATPase implicated in phospholipid translocation in Saccharomyces cerevisiae. Mol Biol Cell *15*, 3418-3432.

Salinas, P.C. (2012). Wnt signaling in the vertebrate central nervous system: from axon guidance to synaptic function. Cold Spring Harb Perspect Biol *4*.

Santos, A.L., and Preta, G. (2018). Lipids in the cell: organisation regulates function. Cellular and molecular life sciences : CMLS *75*, 1909-1927.

Sasaki, T., Kikuchi, A., Araki, S., Hata, Y., Isomura, M., Kuroda, S., and Takai, Y. (1990). Purification and characterization from bovine brain cytosol of a protein that inhibits the dissociation of GDP from and the subsequent binding of GTP to smg p25A, a ras p21-like GTP-binding protein. J Biol Chem *265*, 2333-2337.

Sbrissa, D., Ikonomov, O.C., and Shisheva, A. (2002). Phosphatidylinositol 3-phosphate-interacting domains in PIKfyve. Binding specificity and role in PIKfyve. Endomenbrane localization. J Biol Chem *277*, 6073-6079.

Scherer, W.F., Syverton, J.T., and Gey, G.O. (1953). Studies on the propagation in vitro of poliomyelitis viruses. IV. Viral multiplication in a stable strain of human

malignant epithelial cells (strain HeLa) derived from an epidermoid carcinoma of the cervix. J Exp Med *97*, 695-710.

Schink, K.O., Tan, K.W., and Stenmark, H. (2016). Phosphoinositides in Control of Membrane Dynamics. Annu Rev Cell Dev Biol *32*, 143-171.

Schoneberg, J., Lee, I.H., Iwasa, J.H., and Hurley, J.H. (2017). Reverse-topology membrane scission by the ESCRT proteins. Nat Rev Mol Cell Biol *18*, 5-17.

Schreij, A.M., Fon, E.A., and McPherson, P.S. (2016). Endocytic membrane trafficking and neurodegenerative disease. Cellular and molecular life sciences : CMLS *73*, 1529-1545.

Schu, P.V., Takegawa, K., Fry, M.J., Stack, J.H., Waterfield, M.D., and Emr, S.D. (1993). Phosphatidylinositol 3-kinase encoded by yeast VPS34 gene essential for protein sorting. Science *260*, 88-91.

Schwarz, D.G., Griffin, C.T., Schneider, E.A., Yee, D., and Magnuson, T. (2002). Genetic analysis of sorting nexins 1 and 2 reveals a redundant and essential function in mice. Mol Biol Cell *13*, 3588-3600.

Seaman, M.N. (2007). Identification of a novel conserved sorting motif required for retromer-mediated endosome-to-TGN retrieval. J Cell Sci *120*, 2378-2389.

Seaman, M.N., Marcusson, E.G., Cereghino, J.L., and Emr, S.D. (1997). Endosome to Golgi retrieval of the vacuolar protein sorting receptor, Vps10p, requires the function of the VPS29, VPS30, and VPS35 gene products. The Journal of cell biology *137*, 79-92.

Seaman, M.N., McCaffery, J.M., and Emr, S.D. (1998). A membrane coat complex essential for endosome-to-Golgi retrograde transport in yeast. The Journal of cell biology *142*, 665-681.

Seaman, M.N.J., Harbour, M.E., Tattersall, D., Read, E., and Bright, N. (2009). Membrane recruitment of the cargo-selective retromer subcomplex is catalysed by the small GTPase Rab7 and inhibited by the Rab-GAP TBC1D5. Journal of Cell Science *122*, 2371-2382.

Shannon, B., Soto-Ortolaza, A., Rayaprolu, S., Cannon, H.D., Labbe, C., Benitez, B.A., Choi, J., Lynch, T., Boczarska-Jedynak, M., Opala, G.*, et al.* (2014). Genetic variation

of the retromer subunits VPS26A/B-VPS29 in Parkinson's disease. Neurobiol Aging *35*, 1958 e1951-1952.

Sharma, M., Ioannidis, J.P., Aasly, J.O., Annesi, G., Brice, A., Bertram, L., Bozi, M., Barcikowska, M., Crosiers, D., Clarke, C.E.*, et al.* (2012). A multi-centre clinico-genetic analysis of the VPS35 gene in Parkinson disease indicates reduced penetrance for disease-associated variants. J Med Genet *49*, 721-726.

Sheerin, U.M., Charlesworth, G., Bras, J., Guerreiro, R., Bhatia, K., Foltynie, T., Limousin, P., Silveira-Moriyama, L., Lees, A., and Wood, N. (2012). Screening for VPS35 mutations in Parkinson's disease. Neurobiol Aging *33*, 838 e831-835.

Shi, A., Sun, L., Banerjee, R., Tobin, M., Zhang, Y., and Grant, B.D. (2009). Regulation of endosomal clathrin and retromer-mediated endosome to Golgi retrograde transport by the J-domain protein RME-8. The EMBO journal *28*, 3290-3302.

Shi, H., Rojas, R., Bonifacino, J.S., and Hurley, J.H. (2006). The retromer subunit Vps26 has an arrestin fold and binds Vps35 through its C-terminal domain. Nat Struct Mol Biol *13*, 540-548.

Shin, H.W., Takatsu, H., and Nakayama, K. (2012). Mechanisms of membrane curvature generation in membrane traffic. Membranes (Basel) *2*, 118-133.

Shin, J.J.H., Gillingham, A.K., Begum, F., Chadwick, J., and Munro, S. (2017). TBC1D23 is a bridging factor for endosomal vesicle capture by golgins at the trans-Golgi. Nat Cell Biol *19*, 1424-1432.

Simonetti, B., and Cullen, P.J. (2018a). Actin-dependent endosomal receptor recycling. Current opinion in cell biology *56*, 22-33.

Simonetti, B., and Cullen, P.J. (2018b). Endosomal Sorting: Architecture of the Retromer Coat. Current biology : CB *28*, R1350-R1352.

Simonetti, B., Danson, C.M., Heesom, K.J., and Cullen, P.J. (2017). Sequence-dependent cargo recognition by SNX-BARs mediates retromer-independent transport of CI-MPR. The Journal of cell biology *216*, 3695-3712.

Singer-Kruger, B., Lasic, M., Burger, A.M., Hausser, A., Pipkorn, R., and Wang, Y. (2008). Yeast and human Ysl2p/hMon2 interact with Gga adaptors and mediate their subcellular distribution. Embo Journal *27*, 1423-1435.

Singer, S.J., and Nicolson, G.L. (1972). The fluid mosaic model of the structure of cell membranes. Science *175*, 720-731.

Small, S.A., Kent, K., Pierce, A., Leung, C., Kang, M.S., Okada, H., Honig, L., Vonsattel, J.P., and Kim, T.W. (2005). Model-guided microarray implicates the retromer complex in Alzheimer's disease. Annals of neurology *58*, 909-919.

Small, S.A., and Petsko, G.A. (2015). Retromer in Alzheimer disease, Parkinson disease and other neurological disorders. Nature reviews Neuroscience *16*, 126-132.

Sokol, S.Y. (2015). Spatial and temporal aspects of Wnt signaling and planar cell polarity during vertebrate embryonic development. Seminars in cell & developmental biology *42*, 78-85.

Starokadomskyy, P., Gluck, N., Li, H., Chen, B., Wallis, M., Maine, G.N., Mao, X., Zaidi, I.W., Hein, M.Y., McDonald, F.J.*, et al.* (2013). CCDC22 deficiency in humans blunts activation of proinflammatory NF-kappaB signaling. J Clin Invest *123*, 2244-2256.

Steinberg, F., Gallon, M., Winfield, M., Thomas, E.C., Bell, A.J., Heesom, K.J., Tavare, J.M., and Cullen, P.J. (2013a). A global analysis of SNX27-retromer assembly and cargo specificity reveals a function in glucose and metal ion transport. Nature Cell Biology *15*, 461-+.

Steinberg, F., Gallon, M., Winfield, M., Thomas, E.C., Bell, A.J., Heesom, K.J., Tavare, J.M., and Cullen, P.J. (2013b). A global analysis of SNX27-retromer assembly and cargo specificity reveals a function in glucose and metal ion transport. Nat Cell Biol *15*, 461-471.

Steinberg, F., Heesom, K.J., Bass, M.D., and Cullen, P.J. (2012). SNX17 protects integrins from degradation by sorting between lysosomal and recycling pathways. Journal of Cell Biology *197*, 219-230.

Steinhart, Z., and Angers, S. (2018). Wnt signaling in development and tissue homeostasis. Development *145*.

Strochlic, T.I., Schmiedekamp, B.C., Lee, J., Katzmann, D.J., and Burd, C.G. (2008). Opposing activities of the Snx3-retromer complex and ESCRT proteins mediate regulated cargo sorting at a common endosome. Mol Biol Cell *19*, 4694-4706.

Strochlic, T.I., Setty, T.G., Sitaram, A., and Burd, C.G. (2007). Grd19/Snx3p functions as a cargo-specific adapter for retromer-dependent endocytic recycling. The Journal of cell biology *177*, 115-125.

Subramanian, S., Woolford, C.A., and Jones, E.W. (2004). The Sec1/Munc18 protein, Vps33p, functions at the endosome and the vacuole of Saccharomyces cerevisiae. Mol Biol Cell *15*, 2593-2605.

Sun, Q., Westphal, W., Wong, K.N., Tan, I., and Zhong, Q. (2010). Rubicon controls endosome maturation as a Rab7 effector. Proc Natl Acad Sci U S A *107*, 19338-19343.

Swaminathan, S., Huentelman, M.J., Corneveaux, J.J., Myers, A.J., Faber, K.M., Foroud, T., Mayeux, R., Shen, L., Kim, S., Turk, M.*, et al.* (2012). Analysis of copy number variation in Alzheimer's disease in a cohort of clinically characterized and neuropathologically verified individuals. PloS one *7*, e50640.

Swarbrick, J.D., Shaw, D.J., Chhabra, S., Ghai, R., Valkov, E., Norwood, S.J., Seaman, M.N., and Collins, B.M. (2011). VPS29 is not an active metallo-phosphatase but is a rigid scaffold required for retromer interaction with accessory proteins. PloS one *6*, e20420.

Tabuchi, M., Yanatori, I., Kawai, Y., and Kishi, F. (2010). Retromer-mediated direct sorting is required for proper endosomal recycling of the mammalian iron transporter DMT1. Journal of Cell Science *123*, 756-766.

Takada, N., Naito, T., Inoue, T., Nakayama, K., Takatsu, H., and Shin, H.W. (2018). Phospholipid-flipping activity of P4-ATPase drives membrane curvature. The EMBO journal *37*.

Takar, M., Wu, Y.T., and Graham, T.R. (2016). The Essential Neo1 Protein from Budding Yeast Plays a Role in Establishing Aminophospholipid Asymmetry of the Plasma Membrane. Journal of Biological Chemistry *291*, 15727-15739.

Takatsu, H., Baba, K., Shima, T., Umino, H., Kato, U., Umeda, M., Nakayama, K., and Shin, H.W. (2011). ATP9B, a P4-ATPase (a Putative Aminophospholipid Translocase), Localizes to the trans-Golgi Network in a CDC50 Protein-independent Manner. Journal of Biological Chemistry *286*, 38159-38167.

Takatsu, H., Tanaka, G., Segawa, K., Suzuki, J., Nagata, S., Nakayama, K., and Shin, H.W. (2014). Phospholipid flippase activities and substrate specificities of human type IV P-type ATPases localized to the plasma membrane. J Biol Chem *289*, 33543-33556.

Tanaka, Y., Ono, N., Shima, T., Tanaka, G., Katoh, Y., Nakayama, K., Takatsu, H., and Shin, H.W. (2016). The phospholipid flippase ATP9A is required for the recycling pathway from the endosomes to the plasma membrane. Molecular Biology of the Cell *27*, 3883-3893.

Tang, F.L., Erion, J.R., Tian, Y., Liu, W., Yin, D.M., Ye, J., Tang, B., Mei, L., and Xiong, W.C. (2015a). VPS35 in Dopamine Neurons Is Required for Endosome-to-Golgi Retrieval of Lamp2a, a Receptor of Chaperone-Mediated Autophagy That Is Critical for alpha-Synuclein Degradation and Prevention of Pathogenesis of Parkinson's Disease. The Journal of neuroscience : the official journal of the Society for Neuroscience *35*, 10613-10628.

Tang, F.L., Liu, W., Hu, J.X., Erion, J.R., Ye, J., Mei, L., and Xiong, W.C. (2015b). VPS35 Deficiency or Mutation Causes Dopaminergic Neuronal Loss by Impairing Mitochondrial Fusion and Function. Cell reports *12*, 1631-1643.

te Velthuis, A.J., and Bagowski, C.P. (2007). PDZ and LIM domain-encoding genes: molecular interactions and their role in development. ScientificWorldJournal *7*, 1470-1492.

Temkin, P., Lauffer, B., Jager, S., Cimermancic, P., Krogan, N.J., and von Zastrow, M. (2011). SNX27 mediates retromer tubule entry and endosome-to-plasma membrane trafficking of signalling receptors. Nature Cell Biology *13*, 715-U199.

Thomas, B., and Beal, M.F. (2007). Parkinson's disease. Human molecular genetics *16 Spec No. 2*, R183-194.

Tilley, F.C., Gallon, M., Luo, C., Danson, C.M., Zhou, J., and Cullen, P.J. (2018). Retromer associates with the cytoplasmic amino-terminus of polycystin-2. J Cell Sci *131*.

Toh, W.H., Chia, P.Z.C., Hossain, M.I., and Gleeson, P.A. (2018). GGA1 regulates signal-dependent sorting of BACE1 to recycling endosomes, which moderates Abeta production. Mol Biol Cell *29*, 191-208.

Tomita, Y., Noda, T., Fujii, K., Watanabe, T., Morikawa, Y., and Kawaoka, Y. (2011). The cellular factors Vps18 and Mon2 are required for efficient production of infectious HIV-1 particles. J Virol *85*, 5618-5627.

Traub, L.M. (2009). Tickets to ride: selecting cargo for clathrin-regulated internalization. Nat Rev Mol Cell Biol *10*, 583-596.

Traut, T.W. (1994). Physiological concentrations of purines and pyrimidines. Mol Cell Biochem *140*, 1-22.

Tyrrell, B.J., Woodham, E.F., Spence, H.J., Strathdee, D., Insall, R.H., and Machesky, L.M. (2016). Loss of strumpellin in the melanocytic lineage impairs the WASH Complex but does not affect coat colour. Pigment Cell Melanoma Res *29*, 559-571.

Valdmanis, P.N., Meijer, I.A., Reynolds, A., Lei, A., MacLeod, P., Schlesinger, D., Zatz, M., Reid, E., Dion, P.A., Drapeau, P.*, et al.* (2007). Mutations in the KIAA0196 gene at the SPG8 locus cause hereditary spastic paraplegia. American journal of human genetics *80*, 152-161.

van de Sluis, B., Muller, P., Duran, K., Chen, A., Groot, A.J., Klomp, L.W., Liu, P.P., and Wijmenga, C. (2007). Increased activity of hypoxia-inducible factor 1 is associated with early embryonic lethality in Commd1 null mice. Mol Cell Biol *27*, 4142-4156.

van Kerkhof, P., Lee, J., McCormick, L., Tetrault, E., Lu, W., Schoenfish, M., Oorschot, V., Strous, G.J., Klumperman, J., and Bu, G. (2005). Sorting nexin 17 facilitates LRP recycling in the early endosome. The EMBO journal *24*, 2851-2861.

van Weering, J.R., Verkade, P., and Cullen, P.J. (2010). SNX-BAR proteins in phosphoinositide-mediated, tubular-based endosomal sorting. Seminars in cell & developmental biology *21*, 371-380.

van Weering, J.R.T., Sessions, R.B., Traer, C.J., Kloer, D.P., Bhatia, V.K., Stamou, D., Carlsson, S.R., Hurley, J.H., and Cullen, P.J. (2012). Molecular basis for SNX-BAR-mediated assembly of distinct endosomal sorting tubules. Embo Journal *31*, 4466-4480.

Varandas, K.C., Irannejad, R., and von Zastrow, M. (2016). Retromer Endosome Exit Domains Serve Multiple Trafficking Destinations and Regulate Local G Protein Activation by GPCRs. Current Biology *26*, 3129-3142.

Vardarajan, B.N., Bruesegem, S.Y., Harbour, M.E., St George-Hyslop, P., Seaman, M.N.J., and Farrer, L.A. (2012). Identification of Alzheimer disease-associated variants in genes that regulate retromer function. Neurobiology of Aging *33*.

Verstraeten, A., Wauters, E., Crosiers, D., Meeus, B., Corsmit, E., Elinck, E., Mattheijssens, M., Peeters, K., Cras, P., Pickut, B.*, et al.* (2012). Contribution of VPS35 genetic variability to LBD in the Flanders-Belgian population. Neurobiol Aging *33*, 1844 e1811-1843.

Vetter, I.R., and Wittinghofer, A. (2001). The guanine nucleotide-binding switch in three dimensions. Science *294*, 1299-1304.

Vieira, S.I., Rebelo, S., Esselmann, H., Wiltfang, J., Lah, J., Lane, R., Small, S.A., Gandy, S., da Cruz, E.S.E.F., and da Cruz, E.S.O.A. (2010). Retrieval of the Alzheimer's amyloid precursor protein from the endosome to the TGN is S655 phosphorylation state-dependent and retromer-mediated. Molecular neurodegeneration *5*, 40.

Vilarino-Guell, C., Wider, C., Ross, O.A., Dachsel, J.C., Kachergus, J.M., Lincoln, S.J., Soto-Ortolaza, A.I., Cobb, S.A., Wilhoite, G.J., Bacon, J.A.*, et al.* (2011). VPS35 mutations in Parkinson disease. American journal of human genetics *89*, 162-167.

Voos, W., and Stevens, T.H. (1998). Retrieval of resident late-Golgi membrane proteins from the prevacuolar compartment of Saccharomyces cerevisiae is dependent on the function of Grd19p. The Journal of cell biology *140*, 577-590.

Wang, C., Niu, M., Zhou, Z., Zheng, X., Zhang, L., Tian, Y., Yu, X., Bu, G., Xu, H., Ma, Q.*, et al.* (2016a). VPS35 regulates cell surface recycling and signaling of dopamine receptor D1. Neurobiol Aging *46*, 22-31.

Wang, W., Ma, X., Zhou, L., Liu, J., and Zhu, X. (2017). A conserved retromer sorting motif is essential for mitochondrial DLP1 recycling by VPS35 in Parkinson's disease model. Human molecular genetics *26*, 781-789.

Wang, W., Wang, X., Fujioka, H., Hoppel, C., Whone, A.L., Caldwell, M.A., Cullen, P.J., Liu, J., and Zhu, X. (2016b). Parkinson's disease-associated mutant VPS35 causes mitochondrial dysfunction by recycling DLP1 complexes. Nature medicine *22*, 54-63.

Wang, X., Yang, Y., Wang, X., Li, C., and Jia, J. (2014). A novel KIAA0196 (SPG8) mutation in a Chinese family with spastic paraplegia. Chin Med J (Engl) *127*, 1987-1989.

Wang, X., Zhao, Y., Zhang, X., Badie, H., Zhou, Y., Mu, Y., Loo, L.S., Cai, L., Thompson, R.C., Yang, B.*, et al.* (2013). Loss of sorting nexin 27 contributes to excitatory synaptic dysfunction by modulating glutamate receptor recycling in Down's syndrome. Nature medicine *19*, 473-480.

Wassmer, T., Attar, N., Bujny, M.V., Oakley, J., Traer, C.J., and Cullen, P.J. (2007). A loss-of-function screen reveals SNX5 and SNX6 as potential components of the mammalian retromer. Journal of Cell Science *120*, 45-54.

Wassmer, T., Attar, N., Harterink, M., van Weering, J.R.T., Traer, C.J., Oakley, J., Goud, B., Stephens, D.J., Verkade, P., Korswagen, H.C.*, et al.* (2009). The Retromer Coat Complex Coordinates Endosomal Sorting and Dynein-Mediated Transport, with Carrier Recognition by the trans-Golgi Network. Developmental Cell *17*, 110-122.

Wehman, A.M., Poggioli, C., Schweinsberg, P., Grant, B.D., and Nance, J. (2011). The P4-ATPase TAT-5 Inhibits the Budding of Extracellular Vesicles in C. elegans Embryos. Current Biology *21*, 1951-1959.

Wen, L., Tang, F.L., Hong, Y., Luo, S.W., Wang, C.L., He, W., Shen, C., Jung, J.U., Xiong, F., Lee, D.H.*, et al.* (2011). VPS35 haploinsufficiency increases Alzheimer's disease neuropathology. The Journal of cell biology *195*, 765-779.

Wicky, S., Schwarz, H., and Singer-Kruger, B. (2004). Molecular interactions of yeast Neo1p, an essential member of the Drs2 family of aminophospholipid translocases, and its role in membrane trafficking within the endomembrane system. Molecular and Cellular Biology *24*, 7402-7418.

Williams, D.R., and Litvan, I. (2013). Parkinsonian syndromes. Continuum (Minneap Minn) *19*, 1189-1212.

Williams, E.T., Glauser, L., Tsika, E., Jiang, H., Islam, S., and Moore, D.J. (2018). Parkin mediates the ubiquitination of VPS35 and modulates retromer-dependent endosomal sorting. Human molecular genetics *27*, 3189-3205.

Wu, S., Fagan, R.R., Uttamapinant, C., Lifshitz, L.M., Fogarty, K.E., Ting, A.Y., and Melikian, H.E. (2017). The Dopamine Transporter Recycles via a Retromer-Dependent

Postendocytic Mechanism: Tracking Studies Using a Novel Fluorophore-Coupling Approach. The Journal of neuroscience : the official journal of the Society for Neuroscience *37*, 9438-9452.

Wu, Y., Takar, M., Cuentas-Condori, A.A., and Graham, T.R. (2016). Neo1 and phosphatidylethanolamine contribute to vacuole membrane fusion in Saccharomyces cerevisiae. Cell Logist *6*, e1228791.

Xu, P., Baldridge, R.D., Chi, R.J., Burd, C.G., and Graham, T.R. (2013). Phosphatidylserine flipping enhances membrane curvature and negative charge required for vesicular transport. The Journal of cell biology *202*, 875-886.

Xu, Y., Hortsman, H., Seet, L., Wong, S.H., and Hong, W. (2001). SNX3 regulates endosomal function through its PX-domain-mediated interaction with PtdIns(3)P. Nat Cell Biol *3*, 658-666.

Yabas, M., Jing, W., Shafik, S., Broer, S., and Enders, A. (2016). ATP11C Facilitates Phospholipid Translocation across the Plasma Membrane of All Leukocytes. PloS one *11*, e0146774.

Yang, P.T., Lorenowicz, M.J., Silhankova, M., Coudreuse, D.Y.M., Betist, M.C., and Korswagen, H.C. (2008). Wnt signaling requires retromer-dependent recycling of MIG-14/Wntless in Wnt-producing cells. Developmental Cell *14*, 140-147.

Yasuda, S., Morishita, S., Fujita, A., Nanao, T., Wada, N., Waguri, S., Schiavo, G., Fukuda, M., and Nakamura, T. (2016). Mon1-Ccz1 activates Rab7 only on late endosomes and dissociates from the lysosome in mammalian cells. J Cell Sci *129*, 329-340.

Yin, J., Liu, X., He, Q., Zhou, L., Yuan, Z., and Zhao, S. (2016). Vps35-dependent recycling of Trem2 regulates microglial function. Traffic *17*, 1286-1296.

Yoshimori, T., Yamamoto, A., Moriyama, Y., Futai, M., and Tashiro, Y. (1991). Bafilomycin A1, a specific inhibitor of vacuolar-type H(+)-ATPase, inhibits acidification and protein degradation in lysosomes of cultured cells. J Biol Chem *266*, 17707-17712.

Yoshimura, S., Gerondopoulos, A., Linford, A., Rigden, D.J., and Barr, F.A. (2010). Family-wide characterization of the DENN domain Rab GDP-GTP exchange factors. The Journal of cell biology *191*, 367-381.

Yu, J., Chia, J., Canning, C.A., Jones, C.M., Bard, F.A., and Virshup, D.M. (2014). WLS Retrograde Transport to the Endoplasmic Reticulum during Wnt Secretion. Developmental Cell *29*, 277-291.

Zavodszky, E., Seaman, M.N., Moreau, K., Jimenez-Sanchez, M., Breusegem, S.Y., Harbour, M.E., and Rubinsztein, D.C. (2014). Mutation in VPS35 associated with Parkinson's disease impairs WASH complex association and inhibits autophagy. Nature communications *5*, 3828.

Zech, T., Calaminus, S.D., Caswell, P., Spence, H.J., Carnell, M., Insall, R.H., Norman, J., and Machesky, L.M. (2011). The Arp2/3 activator WASH regulates alpha5beta1-integrin-mediated invasive migration. J Cell Sci *124*, 3753-3759.

Zhan, T., Rindtorff, N., and Boutros, M. (2017). Wnt signaling in cancer. Oncogene *36*, 1461-1473.

Zhang, P., Wu, Y.H., Belenkaya, T.Y., and Lin, X.H. (2011). SNX3 controls Wingless/Wnt secretion through regulating retromer-dependent recycling of Wntless. Cell Research *21*, 1677-1690.

Zhang, P.L., Chen, Y., Zhang, C.H., Wang, Y.X., and Fernandez-Funez, P. (2018). Genetics of Parkinson's disease and related disorders. J Med Genet *55*, 73-80.

Zhao, Y., and Keen, J.H. (2008). Gyrating clathrin: highly dynamic clathrin structures involved in rapid receptor recycling. Traffic *9*, 2253-2264.

Zhou, C.Z., de La Sierra-Gallay, I.L., Quevillon-Cheruel, S., Collinet, B., Minard, P., Blondeau, K., Henckes, G., Aufrere, R., Leulliot, N., Graille, M.*, et al.* (2003). Crystal structure of the yeast Phox homology (PX) domain protein Grd19p complexed to phosphatidylinositol-3-phosphate. Journal of Biological Chemistry *278*, 50371-50376.

Zhou, X.M., and Graham, T.R. (2009). Reconstitution of phospholipid translocase activity with purified Drs2p, a type-IV P-type ATPase from budding yeast. Proceedings of the National Academy of Sciences of the United States of America *106*, 16586-16591.

Zimprich, A., Benet-Pages, A., Struhal, W., Graf, E., Eck, S.H., Offman, M.N., Haubenberger, D., Spielberger, S., Schulte, E.C., Lichtner, P.*, et al.* (2011). A mutation in VPS35, encoding a subunit of the retromer complex, causes late-onset Parkinson disease. American journal of human genetics *89*, 168-175.

Zufferey, R., Nagy, D., Mandel, R.J., Naldini, L., and Trono, D. (1997). Multiply attenuated lentiviral vector achieves efficient gene delivery in vivo. Nat Biotechnol *15*, 871-875.